

**Investigation into Some Metal-Organic
Frameworks: Synthesis, Structural Studies
and Exploration of Catalytic Property**

A Thesis

**Submitted for the Degree of
Doctor of Philosophy (Science)**

By

Pameli Ghosh



**Department of Chemistry
Jadavpur University
Jadavpur, Kolkata - 700 032
India
April, 2023**

DEDICATED
TO
MY PARENTS & BOROMA

যাদবপুর বিশ্ববিদ্যালয়
কলকাতা-৭০০০৩২, ভারত



*JADAVPUR UNIVERSITY
KOLKATA-700 032, INDIA

FACULTY OF SCIENCE: DEPARTMENT OF CHEMISTRY : INORGANIC CHEMISTRY SECTION

CERTIFICATE FROM THE SUPERVISOR

This is to certify that thesis entitled “Investigation into Some Metal-Organic Frameworks: Synthesis, Structural Studies and Exploration of Catalytic Property” submitted by Smt. Pamei Ghosh, who got her name registered on 16/02/2018 for the award of Ph.D. (Science) degree of Jadavpur University, is absolutely based upon her own work under my supervision and that neither this thesis nor any part of it has been submitted for either any degree/diploma or any other academic award anywhere before.

Subrata nath Koner 11/04/2023
(Signature of the Supervisor, date with official seal)

Dr. SUBRATA NATH KONER
Professor in Chemistry
Jadavpur University
Kolkata - 700 032

* Established on and from 24th December, 1955 vide Notification No.10986-Edn.IU-42/55 dated 6th December, 1955 under Jadavpur University Act, 1955 (West Bengal Act XXXIII of 1955) followed by Jadavpur University Act, 1981 (West Bengal Act XXIV of 1981)

দূরত্বসং: ২৪১৪-৩৩৩৩/৩১৩৩/৩৩৩৩/৩৩৩৩/৩৩৩৩ প্রসারণ: ২৪১৩ Website: www.jadavpur.edu Phone: 2414-6666/6194/6643/6495/6443 Extn.2469
দলকাতা: (৩১)-৩০০-৩৪৩৪-৩৪৩৪/৩৪৩৩/৩৪৩৩-৭১২৩ E-mail : hod@chemistry.jdvu.ac.in Fax: (91)-033-2414-6414/6210/2413-7121

Acknowledgements

The past five years have become one of the most important and memorable chapters in my life. By that time, there are so many people those deserve my heartfelt gratitude. At the outset, I am happy to take the opportunity to express my deepest sense of gratitude and regards to my supervisor, **Prof. Subratanath Koner** for his constant guidance, advice and valuable suggestions. Above all and the most needed, he provided me unflinching encouragement and support in various ways. His truly scientist intuition has made him as a constant oasis of ideas and passions in science, which exceptionally inspire and enrich my growth as a researcher want to be.

I express my sincere gratitude to Prof. Subenoy Chakraborty, Dean of the Faculty of Science, Prof. Subratanath Koner, Head of the Department of Chemistry, and Prof. Sourav Das, Section-in-Charge, Inorganic Chemistry Section, Jadavpur University, for their keen interest and constant encouragement.

I am thankful to Prof. Amrita Saha, Prof. Mahammad Ali, Prof. Kajal Krishna Rajak, Prof. Shouvik Chattopadhyay, Prof. Kaushikishankar Pramanik, Prof. Sujoy K. Baitalik, Prof. Jnan Prakash Naskar, Prof. Chittaranjan Sinha for their various academic help and encouragement.

I would like to thank all the faculty members of Chemistry department, The University of Burdwan for their continuous support.

I am grateful to Prof. Partha Mahata, Department of Chemistry, Jadavpur University, for his assistance regarding the X-ray crystallography during the investigation.

I am also thankful to Prof. Amitava Patra and his scholars, Department of Materials Science, IACS, for their prompt assistance in finishing my job within time.

I am also thankful to Prof. Ashis Battacharyya and his scholars, Department of Chemistry, Viswa Bharati University, for their continuous help.

I am also thankful to my friends Priyanka, Anita, Janagaseeni, Rajnandini, Atasi, Tamasi, Saraswati, Sunanda and Tamanna for their constant encouragement.

I owe to my lab mates Dr. Santu Ghosh, Rakesh Debnath, Dr. Dasarath Mal, Dr. Sandip Saha, Dr. Rupam Sen, Dr. Rajesh Bera, Dr. Satyajit Halder, Dr. Debraj Saha, Dr. Soma Das, Dr. Saikat Gayen for rendering valuable suggestions, cooperation and help. It is also a pleasure for me to convey my gratefulness to Dr. Debopom Sinha, Dr. Tapasi Das, Dr. Soumitra Dinda, Dr. Tapas Gharui, Dr. Sima Das, Dr. Pranab Saha, Dr. Snehya Nandi, Dr. Asit Saha, Mrs. Mitali Mazumdar, Mr. Debasish Jana, Mr. Ayon Mukherjee, Mr. Rabi Shankar Das, Mrs. Srijita Naskar, Mr. Supriya Debnath, Mr. Sourav Saha, Miss Debjani Maity, Dr. Pravat Ghorui, Mr. Jayanta Saha, Dr. Amit Maity, Dr. Tanmoy Saha, Miss Roumi Patra, and Dr. Basudev Dutta for their ungrudging suggestions, cooperation and help in many ways.

I wish to thank Department of Science and Technology for funds granted to the Department of Chemistry, Jadavpur University, for procuring a single-crystal X-ray, high resolution mass spectrometer, powder X-ray diffractometer and NMR facility.

I must sincerely acknowledge University Grants Commission for awarding me JRF and SRF which have enabled me to carry out my research work successfully.

I would also like to express my deep gratitude and regards to my dadamoni (Sukanata Ghosh) who has supported me unconditionally during this journey.

Finally, and most importantly, my deepest sense of gratitude goes to my beloved parents, who mean a world to me, for their

unflagging love, patience, encouragement, understanding and continual support throughout my life. Completion of this Ph.D. would have been impossible without them. I have no enough words to acknowledge them. Thank you for keeping faith in me and giving liberty to choose the life I desired. I want to thank my elder sisters, Sonali, Mitali and brother in law, Utpal Ghosh and Uday Chand Ghosh for their kind, unconditional support and love. I am glad to remember my nephew (Basudeb, Sayan, Soumyadeep) and niece (Supriti) in this pleasant moment. A Special thanks to Shymoli and Sankar for their encouragement over the years. I am sure this thesis will make them happier than me.

Department of Chemistry,
Inorganic Chemistry Section,
Jadavpur University,
Kolkata - 700032,
India,
April, 2023

Pameli Ghosh
11/04/23

(Pameli Ghosh)

(Senior Research Fellow)

Table of Contents

	Page No.
List of Abbreviations	
CHAPTER 1: Introduction and brief review	1
1.1 General.....	3
1.2 Metal organic frameworks.....	4
1.2.1 Synthetic procedure of MOFs.....	7
1.2.2 MOFs:terms and different linker for design.....	9
1.2.3 MOFs based on carboxylate linker.....	16
1.3 Application of MOFs.....	22
1.3.1 Catalysis	22
1.3.1.1 C–C coupling reactions.....	24
1.3.1.2 C-heteroatom bond formation reactions.....	27
1.3.1.3 Decarboxylative coupling reaction.....	31
1.3.2 Use of lanthanide-MOF in catalysis.....	33
1.3.3 Gas adsorption and separation studies.....	38
1.3.4 MOF in photoluminescence sensing.....	40
1.3.5 Proton conductivity in MOFs.....	42
1.4 Scope and objective of the present thesis.....	45
1.5 Summary.....	46
1.6 References.....	49

	Page No.
CHAPTER 2: Robust Gd-MOF for heterogeneous catalytic O-arylation reaction.....	67
2.1 Introduction.....	69
2.2 Experimental.....	70
2.2.1 Materials.....	70
2.2.2 Physical measurements.....	71
2.2.3 Synthesis of {[Gd ₄ (NDC) ₆ (H ₂ O) ₆]·2H ₂ O} _n (MOF-1).....	71
2.2.4 X-ray crystallography.....	72
2.2.5 General procedure for catalytic reactions.....	74
2.3 Results and discussion.....	75
2.3.1 Description of the X-ray crystal structure of MOF-1.....	75
2.3.2 PXRD study.....	82
2.3.3 Catalytic activity study.....	84
2.3.4 Separation, catalyst reuse and heterogeneity test.....	90
2.4 Conclusion.....	93
2.5 References.....	94
CHAPTER 3: Aromatic N-arylation reaction catalyzed by 2D paddle-wheel Dy-MOF under heterogeneous condition	97
3.1 Introduction.....	99
3.2 Experimental.....	100
3.2.1 Materials.....	100
3.2.2 Physical measurements.....	100
3.2.3 Synthesis of [Dy(NDC)(NO ₃)(DMA) ₂] _n (MOF- 2).....	101
3.2.4 X-ray crystallography.....	102
3.2.5 General procedure for catalytic reactions.....	104
3.3 Results and discussion.....	104
3.3.1 Description of crystal structure of MOF-2.....	104
3.3.2 Hirshfeld surface analysis for MOF-2.....	110

	Page No.
3.3.3 Thermal study of MOF-2	113
3.3.4 Catalytic activity studies	114
3.3.5 Separation, stability and recycling of the catalyst (MOF-2)	122
3.3.6 Heterogeneity of the catalyst.....	124
3.4 Conclusion	124
3.5 References	124
CHAPTER 4: Synthesis of two isostructural lanthanide paddle-wheel based 2D MOF and exploration of catalytic O-arylation reaction.....	127
4.1 Introduction.....	129
4.2 Experimental.....	131
4.2.1 Materials.....	131
4.2.2 Physical measurements.....	131
4.2.3 Synthesis of [Tb(NDC)(NO ₃)(DMA) ₂] _n (MOF-3).....	131
4.2.4 Synthesis of [Ho(NDC)(NO ₃)(DMA) ₂] _n (MOF-4).....	132
4.2.5 X-ray crystallography.....	132
4.2.6 General procedure for catalytic O-arylation reactions.....	134
4.3 Results and discussion.....	135
4.3.1 X-ray structural description of [Tb(NDC)(NO ₃)(DMA) ₂] _n (MOF-3) and [Ho(NDC)(NO ₃)(DMA) ₂] _n (MOF-4).....	135
4.3.2 Phase identification for MOF-3 and MOF-4.....	141
4.3.3 Hirshfeld surface analysis for MOF-3 and MOF-4.....	142
4.3.4 Thermal study of MOF-3 and MOF-4.....	145
4.3.5 Catalytic activity studies.....	146
4.3.6 Heterogeneity of the catalysts.....	152
4.3.7 Separation and stability of the two catalysts (MOF-3 and MOF-4)	153
4.4 Conclusion.....	154
4.5 References.....	155

	Page No.
CHAPTER 5: In situ decarboxylation hydroxylation of 3-hydroxy-2-quinoxaline carboxylic acid assisted by lanthanide metal in autoclave.....	159
5.1 Introduction.....	161
5.2 Experimental Section.....	164
5.2.1 Materials.....	164
5.2.2 Physical measurements.....	164
5.2.3 Synthesis of MOF-5 {[Gd(NDC) ₅ (DQD)]·H ₂ O} _n , MOF-6 {[Ho(NDC) ₅ (DQD)]·H ₂ O} _n , MOF-7 {[Er(NDC) ₅ (DQD)]·H ₂ O} _n , MOF-8 {[Yb(NDC) ₅ (DQD)]·H ₂ O} _n and DQD.....	164
5.2.4 X-ray crystallography.....	166
5.3 Results and discussion.....	168
5.3.1 Synthesis.....	168
5.3.2 Characterization.....	174
5.3.3 Description of crystal structure of 1,4-dihydro-quinoxaline-2,3-dione (DQD).....	175
5.3.4 Description of crystal structure of MOF-(5-8).....	176
5.4 Conclusion.....	179
5.5 References.....	179
 CHEPTEr 6: Highlights.....	 183
6.1 Highlights.....	185
 Appendix I.....	 189
 List of Publications.....	 191
 Appendix II.....	 193
 Selective ¹H-NMR spectra and bond-length, bond-angle data	 195

List of Abbreviations

1D	One- dimensional
2D	Two- dimensional
3D	Three- dimensional
Å	Angstrom
OAc	Acetoxy group
Anal.	Elemental analysis
BDC	1,4-Benzenedicarboxylate
BET	Brunauer– Emmett–Teller
bpym	2,2'-Bipyrimidine
BTB	1,3,5-Benzenetricarboxylic acid
BTC	1,3,5-benzenetricarboxylate
BTT	1,3,5-benzenetristetrazolate
CN	Coordination Network
°C	Degree Centigrade
Calcd.	Calculated
DABCO	1,4-Diazabicyclo [2.2.2] octane
DMA	Dimethylacetamide
DMF	Dimethylformamide
DMSO	Dimethylsulfoxide
DMSO- <i>d</i> 6	Deuterated Dimethylsulfoxide
DTA	Differential Thermal Analysis
DHQ	2,3-Dihydroxyquinoxaline
DQD	1,4-Dihydroquinoxaline-2,3-dione
EtOH	Ethanol
FTIR	Fourier Transform Infrared
FW	Formula Weight
H ₂ bdda	4,4-[benzene-1,4-diylbis(methylidenenitrilo)] dibenzoic acid
HKUST	Hong Kong University

HRMS	High Resolution Mass Spectrometer
HQC	3-Hydroxy-2-quinoxaline carboxylic acid
HS	Hirshfeld Surface
INA	Isonicotinate Ion
IR	Infrared
IRMOF	Isorecticular Metal-Organic Framework
LMCT	Ligand to Metal Charge Transfer
Ln-MOF	Lanthanide Metal Organic Framework
Ln-PF1	Lanthanide Polymeric Framework
Ln-TM-MOFs	Lanthanide-Transition Metal Organic Framework
MeCN	Acetonitrile
MeOH	Methanol
MIL	Materials of Institute Lavoisier
MIm	Melamine
MLCT	Metal to Ligand Charge Transfer
MOF	Metal Organic Framework
MOM	Metal Organic Material
MOP	Metal Organic Polyhedra
MPC	6-Mercapto pyridine-3-carboxylic acid
2,6-NDC	2,6-Naphthalenedicarboxylic acid
2,6-NDC ²⁻	2,6-Naphthalenedicarboxylate
NDS	Naphthalenedisulfonic acid
NMR	Nuclear Magnetic Resonance
NP	Nano Particle
PCP	Porous Coordination Polymer
POM	Polyoxometalate
PSM	Post-Synthetic Modification
PW	Paddle Wheel
PXRD	Powder X-ray Diffraction

pzdc	Pyrazole-3,5-dicarboxylate
SALH	Salicylate hydroxylase
SBU	Secondary Building Unit
SC-XRD	Single Crystal X-Ray Diffraction
TDPAT	2,4,6-Tris (3,5-Dicarboxylphenylamino) 1,3,5-Triazine
TGA	Thermogravimetric Analysis
THF	Tetrahydrofuran
TLC	Thin Layered Chromatography
TOF	Turn Over Frequency
TON	Turn Over Number
XRD	X-Ray Diffraction
ZIF	ZeoliticImidazolate Frameworks

Chapter 1

Introduction

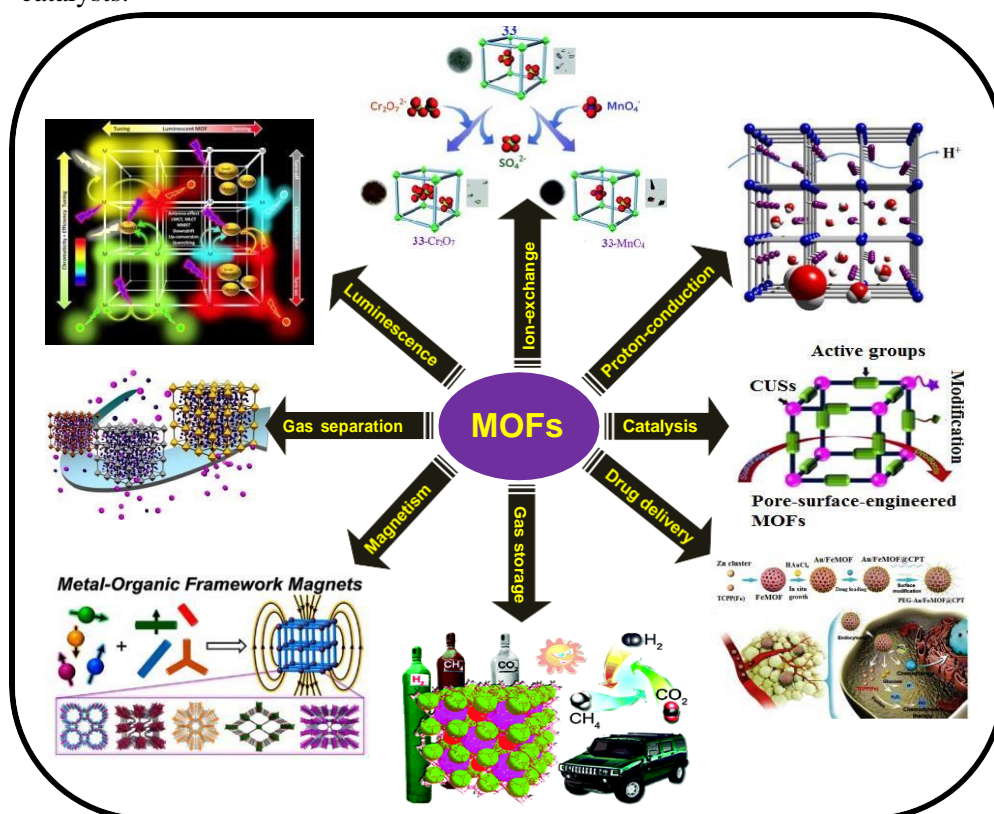
&

Brief Review

1.1 General

In the late 1990s, the invention of metal-organic frameworks (MOFs) was an exceptional success that enticed many researchers because of the elegant structures of MOF with tunable pore size, variety of composition, high surface area etc. MOFs are crystalline coordination compounds produced through self-assembly of metal ions or clusters with organic ligands. These crystalline porous materials generally built up from inorganic and organic building blocks, having (1) well-ordered porous structures, (2) flexible and dynamic behaviors in response to guest molecules, and (3) designable channel surface functionalities, with much elegance than the classical inorganic porous materials [1]. MOFs with various surface functionalities, particle shapes, and porosities can be prepared easily through limitless combinations of inorganic and organic constituents [2]. They exhibit high permanent porosity, abundant active sites and large specific surface areas. Unlike zeolites, activated carbon or silica, MOFs offer unique structural tunability [3,4]. Recently, the new types of hybrid materials have received tremendous attention as a functional material also. The design and synthesis of such materials are important to researchers because of their manifestation in a variety of fascinating topological architectures and immensely potential applications such as, selective gas storage [5] and separation [6], ion exchange [7], electrical and proton conduction [8], magnetism [9], photoluminescence [10], drug delivery [11], catalysis [12] and so forth (**Scheme-1.1**). Last few decades witnessed a great evolution towards configuring of catalytic schemes which cover the entire applicable range of distinctive methods, in heterogeneous catalysis (zeolites, nanocrystallites etc.), homogeneous catalysis (well-defined local environment of the active center) and engineering (reactor internals, structured catalyst bodies, microreactors etc.). The synthetic versatility and robustness of solid catalytic materials are of great boon for fabrication of heterogeneous catalysts. Metal incorporated micro/meso-porous solids bear prospects for designing of new

heterogeneous catalysts that are spatially accessible for directing the reactions to occur in the site-isolated and structurally well-defined active centers like enzymatic catalysts [13]. Metal inorganic/organic framework compounds being porous, play key roles in the same way like zeolites or aluminosilicate-based catalysts.



Scheme-1.1 MOFs as functional material in different fields

1.2 Metal organic frameworks

Metal-organic frameworks (MOFs) are constructed from organic linkers and metal-containing nodes (also known as secondary building units, or SBUs). These are a new class of crystalline solid materials with one- (1D), two- (2D) or three-

dimensional (3D) structures. The components, metals and organic ligands or building blocks of MOFs, are linked through coordination bonds and other weak chemical interactions such as hydrogen bonding and van der Waals interactions in a periodic manner (**Figure 1.1**). The resulting crystalline solids are composed of rigid frameworks of molecules with coordinated metal ions in two or three dimensions that render the crystalline structure highly porous. Structure and properties of MOFs exclusively depend on the nature of the metal ion(s) and linker(s) present in MOFs. A variety of coordination numbers may be achieved depending on size of metal ions and stereo-, chemical, electronic properties of metals and ligands. The coordination preference of the metal site dictates the number of linkers that can attach to the metal site and their orientation in the space. It has been noticed that subtle changes in reaction conditions, such as changes in temperature, concentrations, reaction time and pH may reduce crystallinity, yield or form phases which are not expected. Therefore, it may be inferred that reaction conditions play a vital role in determining the final structure of MOF. Solvents used as the reaction medium, may play major roles in controlling the topology of the resultant framework as solvent molecules can co-crystallize into the final structure and also occupy the void space as guest molecules. These guest solvent molecules may be eliminated when the structural network has formed allowing porosity to be attained provided the framework does not breakdown on desolvation. Consequently, the solvent can play as a template while porous phases are formed [14].

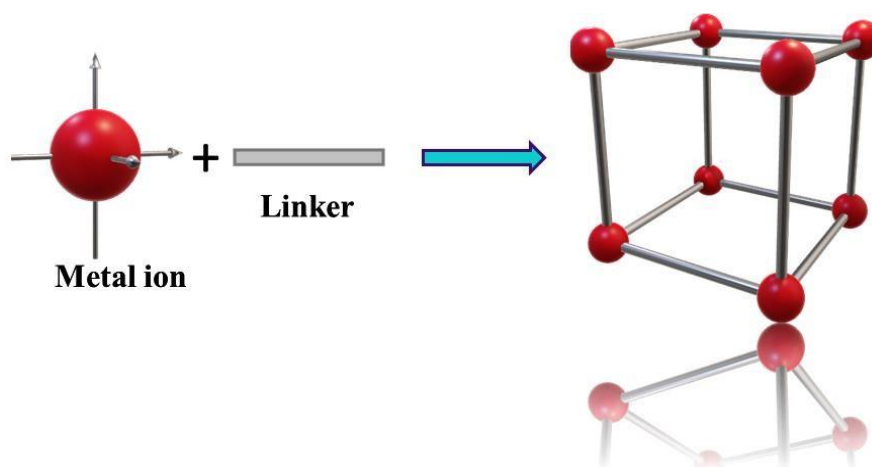


Figure 1.1 Periodic linking of metal ions by linkers to form a MOF.

In 1990, R. Robson and B. F. Hoskins proposed the possibility of a new class of scaffolding like material with broader scope. They reported the synthesis and structure of a three-dimensional material made from copper(I) metal ion and 4,4',4'',4'''-tetracyanotetraphenylmethane as linker with tetrafluoroborate as the counter anion. They speculated about some exciting features of their newly proposed materials which are common to zeolites. It is proposed that the new materials would have greater number of active sites, bigger cavities, facile access of guest molecules, and more widely variable functionalization of the matrix than cross-linked polymers or zeolites [15]. The report of first iconic “MOF”, denoted as MOF-5, was synthesized by the research group of Omar M. Yaghi [16]. Although the term “coordination polymer” was used in a paper published in 1916 [17], however, at that time there was no means of demonstrating infinite frameworks, without single-crystal X-ray crystallographic measurement. In 1936, the well-known Prussian-Blue compounds, based on Fe-CN-Fe linkages, were introduced which had a three-dimensional coordination framework [18]. However, it was not till the early 1990 that research into materials with polymeric and in particular porous structures based on metal ions and organic bridging ligands

undertaken extensively [19]. Early publications by Robson [20], Moore [21], Yaghi [22], and Zawarotko [23] contributed significantly to the field of MOFs, which today witnessed an exponential growth as can be seen from literature. Presently development of metal-organic materials, namely MOMs, continues with the seminal work of A. F. Wells who pioneered the simple and practically suitable “node and spacer” understanding of inorganic crystal structures. Inorganic crystal structures thus can be identified as metal ions (nodes) connected together through bonds (spacer or edge) [24].

1.2.1 Synthetic procedure of MOFs

There are several synthetic procedures (**Figure 1.2**) that employed in isolation of crystalline hybrid compounds, for example, diffusion-based crystallization, hydrothermal or solvothermal, and ionothermal synthesis. Usually, MOFs are synthesized by using solvothermal or hydrothermal process, wherein the reactions are carried out in an organic solvent or in water, respectively, at high temperature under autogenous pressure.

Hydrothermal synthesis depends on the principle that the precursors used in microporous framework formation are insoluble under ambient conditions, but are more soluble at elevated temperatures (100–260°C) and pressures [25]. Most of the reported MOF materials have been synthesized using solvothermal and hydrothermal synthesis conditions, often by using sealed autoclaves. The autoclave is a thick-walled sealed steel reaction vessel with a Teflon-lined insert and the temperature of the reaction media is capable to increase above the boiling point of the solvent used. The pressure within the reaction vessel increases dramatically with rising of temperature although is dependent on the fill of the vessel and also the amount of reagents used in the reaction [26]. The increased pressure and temperature allow the dissolution of reagents which would otherwise be insoluble under ambient

conditions [27]. The reduced viscosity of water under these conditions enhances diffusion processes so that crystal growth from solution is favored allowing retention of the structural elements of the reactants in the final product [28]. This “soft-chemistry” approach enables the formation of polymeric units through molecular building blocks [29]. Other solvents can also be utilized in this reaction technique changing the synthesis to solvothermal synthesis. The hydrothermal and solvothermal routes have been used to synthesize new materials, for the development of new processes for the preparation of new functional materials and also in the shaping of new materials *i.e.* crystal growth [30]. Compared to the solution reactions hydrothermal techniques play an important role in preparing robust and stable MOF compounds [31]. Small changes in one or more of the reaction variables, such as; temperature, time, pH or the solvent type can have a profound influence on the topology of the resulting framework also. A major disadvantage would be that it may be impossible to watch the crystal growth. However, it is possible to deduce the mechanism of formation of crystalline phases produced via the use of the *in-situ* energy dispersive X-ray diffraction technique [32]. In some cases, organic amines or alkylammonium cations are used as templates in the crystallization process [33]. The disadvantage of this approach is that these templates tend to block the pores of the resulting framework. Recently it is understood that this technique can also be used in preparation of MOFs which undergo *in situ* ligand synthesis [34]. Apart from solvo/hydrothermal synthesis, alternative synthesis methods were attempted afterward in an effort to shorten the synthesis time and to produce smaller and uniform crystals, such as microwave-assisted [35], sonochemical [36–38], electrochemical [39,37], ionothermal method and mechanochemical methods [40]. Limited synthesis scale-up for industrial applications was also conducted [41,42] sometimes, detailed investigations on the optimization of MOF synthesis conditions in these studies were carried out in order to obtain high yields of solid products for industrial applications.

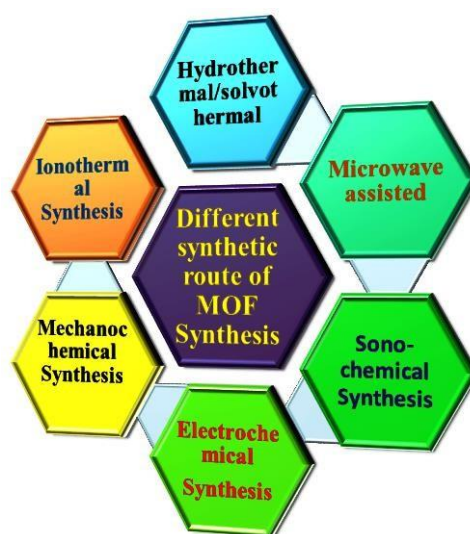


Figure 1.2 Different synthetic procedures for MOF synthesis.

1.2.2 MOFs: Terms and different linker for design

MOFs are also termed as reticular because it has the form of a net (usually periodic). For this reason, sometimes MOF chemistry is ascribed as reticular chemistry. An isoreticular MOF has same net (with the same topology) throughout its structure. During the growth of MOF, the mutual intergrowth of two or more networks with same or different topology in a structure where the networks are physically but not chemically linked, the phenomenon is known as interpenetration. Expansion is the process of using of longer linker to increase the space between vertices of a network to replace a bond by a sequence of bonds. For example, oxalic acid, terephthalic acid and 2,6-naphthalenedicarboxylic acid linker have two carboxylate moieties but as a linker, the last one is longer in length (**Figure 1.3**). Decoration is the process involving replacement of a vertex with a group of vertices. **Figure 1.4** shows an illustrative example of decoration where a metal–carboxylate clusters with a group of atoms representing the vertex

in a primitive cubic network instead of a single atom. In reticular chemistry, secondary building units (SBUs) are polyatomic groups, which may be similar to molecular metal complexes known in coordination chemistry. They are connected through their points of extension to give a framework structure. For example, in **Figure 1.4**, the metal–carboxylate clusters are SBUs linked by phenylene rings through their points of extension.

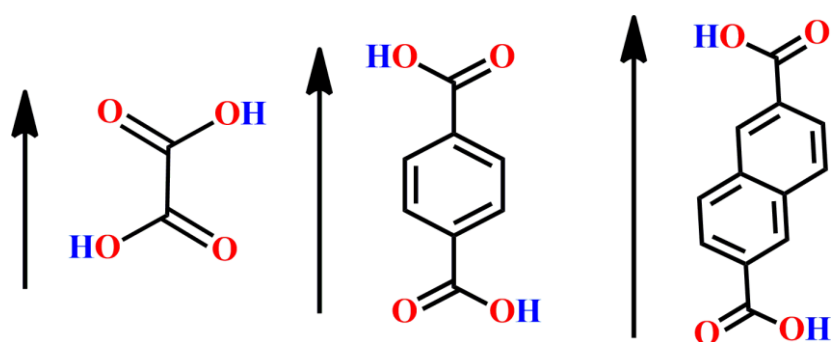


Figure 1.3 Replacement of a bond by a sequence of bonds increases the length of the linker.

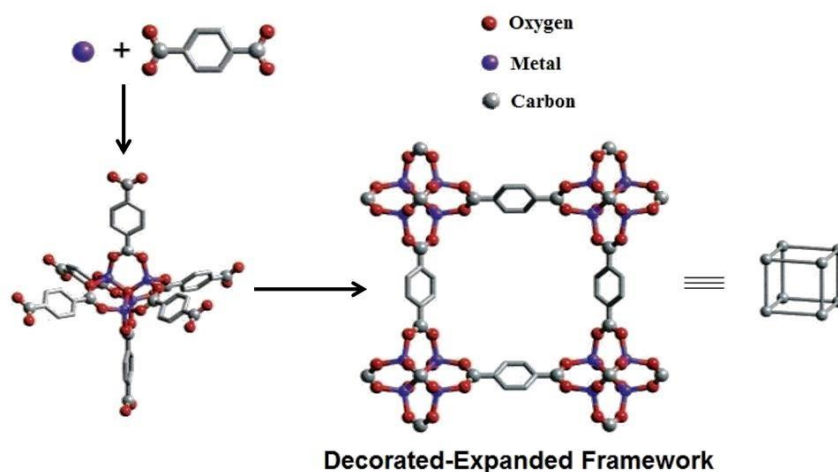


Figure 1.4 Rigid metal-carboxylate clusters are linked by benzene “struts” to form a rigid extended framework in which the M-O-C core (SBU) of each cluster acts as a large octahedron decorating a 6-connected vertex in a cube.

Secondary building units (SBUs), formed in a MOFs structure, are defined as the inorganic clusters or coordination spheres, connected together by the organic components. SBUs are not introduced directly in a synthesis but are formed *in-situ* under specific reaction conditions. To construct a MOF, the first step is to identify a discrete di-, tri- or tetra-nuclear metal cluster as symmetrical module for polymerization involving multidentate linker. The metal clusters can act as SBUs and can be linked by linkers to give a network with a particular topology depending on the geometry of SBU and linker. Some examples of SBUs that are found in MOFs are shown in **Figure 1.5**. Branched organic linkers, with more than two coordinating functionalities, for example square tetrakis (4-carboxyphenyl) porphyrin (**Figure 1.6a**), tetrahedral adamantane-1,3,5,7-tetracarboxylic acid (**Figure 1.6b**), and trigonal 1,3,5-tris(4-carboxyphenyl) benzene (**Figure 1.6c**), are also known SBUs but they are pre-formed before synthesis [43]. The inscribe of SBUs which have been formed in the synthesis of MOFs possess one to predict if certain SBUs will be formed using specific organic ligands and metals. That is why it may be possible, in certain cases, to predict the topology which will be manifested in the final structure. The index of SBUs which have been designed in the synthesis of MOFs permits one to guess if certain SBUs will be fastened by some specific metals and organic linkers in synthesis.

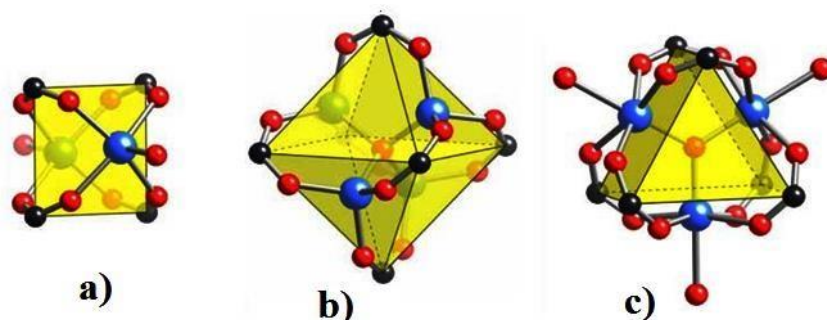


Figure 1.5 Inorganic secondary building units (SBUs) commonly occurring in metal carboxylates include a) the square “paddlewheel” with two terminal ligand sites; b) the octahedral “basic zinc acetate” cluster; and c) the trigonal prismatic oxo-centered trimer, with three terminal ligand sites [43].

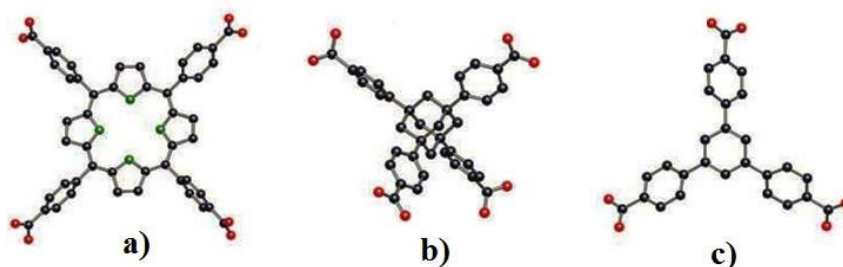


Figure 1.6 Some carboxylate SBUs which are pre-formed before synthesis of MOFs a) square tetrakis(4-carboxyphenyl) porphyrin; b) tetrahedral adamantane-1,3,5,7-tetracarboxylic acid; and c) trigonal 1,3,5-tris(4-carboxyphenyl) benzene [43].

Further for construction of MOF, the first step is to choose a discrete di-, tri- or tetra-nuclear metal cluster as symmetrical module for polymerization involving multidentate linker. The metal clusters can act as SBUs and can be connected by linkers to give a network with a particular topology depending on the geometry of SBU and linker. A metal cluster serves as an inorganic SBU. Its

shape is defined by atoms representing its points of extension to other SBUs. Those atoms define the underlying geometry of the SBU and geometry of the SBU is important to predict the overall topology of the network. For example, polymerization of paddle-wheel copper acetate (SBU) and multidentate linker 1,3,5,7-adamentanetetracarboxylate generate MOF-11. For the construction of MOF-11, the carboxylate carbon atoms of paddle-wheel copper acetate define its square geometry which is shown in **Figure 1.7** [44].

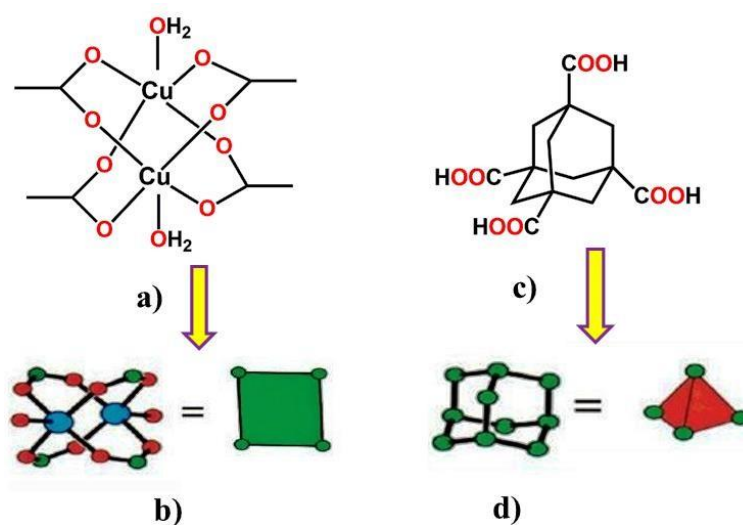


Figure 1.7 a) Paddle-wheel copper acetate SBU with square geometry; b) Copper acetate in ball-and-stick model, representing a square grid (green) (Cu, blue; O, red; C, green); c) 1,3,5,7-adamentanetetracarboxylic acid; d) Adamentane in ball-and-stick model, representing a tetrahedron (red) with four points of linking (green balls) [44].

For construction of MOF, there are an extensive variety of choices for the organic linker as well. Rigid backbones type ligands are regularly favored, since it is easier to predict the network geometry prior to synthesis, and even after the removal of the guest solvents, the rigidity helps to maintain the open-pore

structure of MOF compound. Basically, the linkers are cationic, anionic or electrically neutral, (**Figure 1.8**) [45]. In particular, these linkers are efficient for construction of pillared-layer in 3D networks [46]. Carboxylates ligands are most commonly used anionic linkers [47] since they have the capability to accumulate metal ions into clusters and thus form more stable frameworks. Conversely, cationic organic ligands are comparatively less used due to lower affinities for cationic metal ions, [48]. The most commonly used neutral organic ligands are pyrazine and 4,4'-bipyridine (bpy) [49]. The organic linkers also play a vital role in the construction of porous MOFs, such as long bridging ligands. This type of ligands can create some troubles within a framework like interpenetration, while large voids are created with longer ligands which permit a second polymer network to interpenetrate the first created network, consequently infusing potential cavities that led to diminished or total elimination of porosity. The proper selection of metal ion and organic linker are known to influence the topology of framework and hence, the size and shape of the pores.

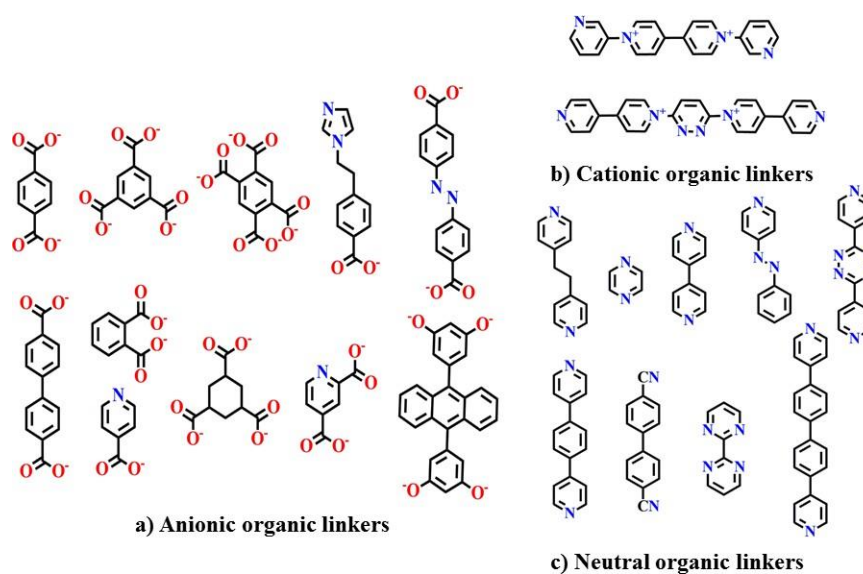


Figure 1.8 Examples of linkers used in MOFs [45].

Same functional groups containing ligands may have a different organic connectivity, such as linear dicarboxylates (like benzene-1,4-dicarboxylate, biphenyl-4,4'-dicarboxylate etc.) be able to form a series of isorecticular materials which are topologically indistinguishable however the organic linking molecule is extended [50]. This is represented by the MOF-5 [51] (also designated as IRMOF-1) and successively linked frameworks IRMOFs 2-16, where the identical

$Zn_4O(COO)_6$ clusters afford the inorganic core, whereas the ligand among the carboxylate groups is diverse with maintenance of the cubic network of channels (**Figure 1.9**). Reticular synthesis is a strategy which exploits previously formed SBUs [52]. In some cases, utilization of reticular synthesis encompasses the construction of carboxylate MOFs derived via MOF-5 as a prototype. These kinds of MOFs are recognized as isorecticular metal-organic frameworks (IRMOFs), wherein they are created on the same net and topology as in MOF-5. The organic ligands employed different functionality of the pendant groups in IRMOFs 1-7, as they have the additional functional groups such as bromo (2), amino (3), n-propoxy (4), n-pentaoxy (5), cyclobutyl (6) and fused benzene functional groups (7), and in length by substituting 1,4-benzenedicarboxylate producing IRMOFs 8-16, by 2,6-naphthalenedicarboxylate (8), biphenyl-4,4'-dicarboxylate (10), pyrene-2,7-dicarboxylate (14) and terphenyl-4"-dicarboxylate (16) [53,54]. Each structure comprises of the same SBUs i.e., $Zn_4O(COO)_6$ as well as in MOF-5, consequently the topology of the structure remains identical, even though the pore size and their functionalities differ.

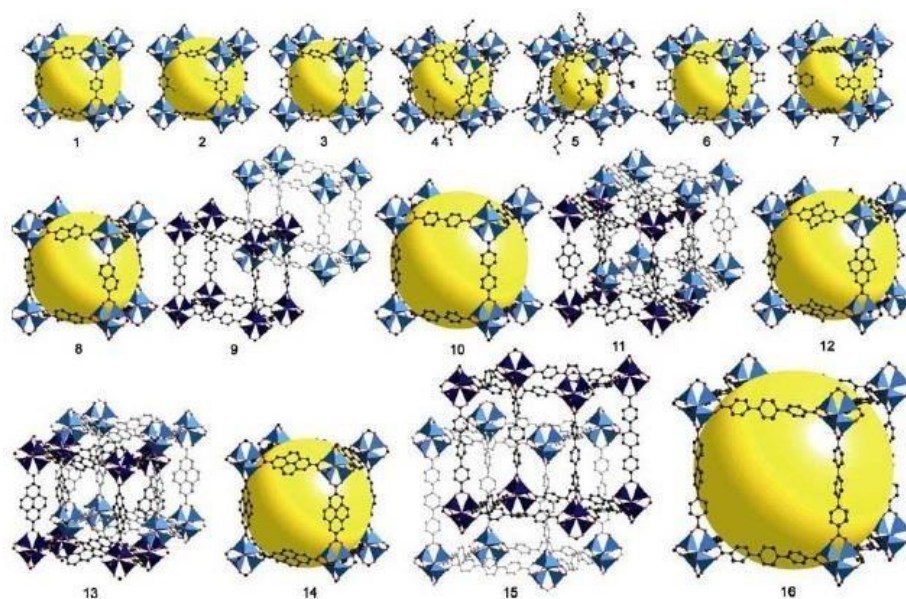


Figure 1.9 Structures of isoreticular MOFs (IRMOFs 1–16) using MOF–5 as the prototype [43].

1.2.3 MOFs based on carboxylate linker

For designing of MOFs, various kinds of organic ligands have been used strategically. Organic carboxylates are the most demanding candidate due to its various binding modes (**Figure 1.10**), which facilitate to form numerous kinds of frameworks with functional properties.

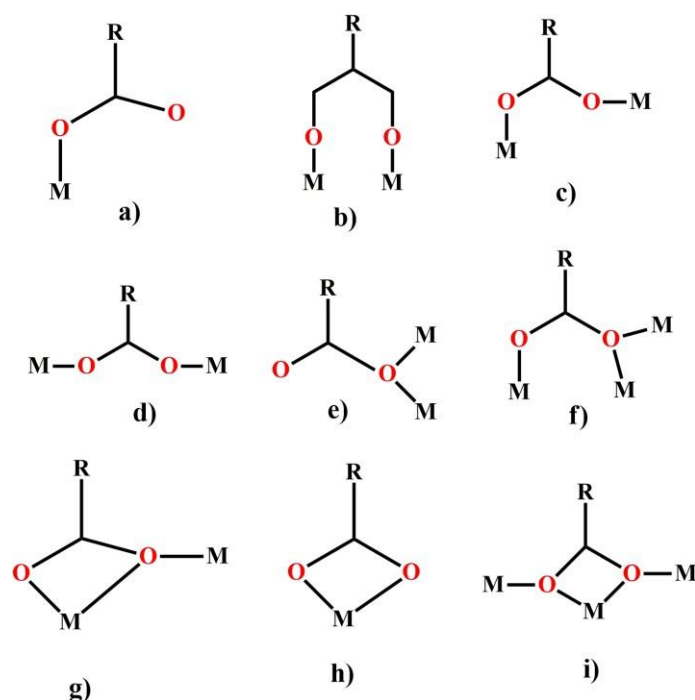


Figure 1.10 Coordination modes of carboxylate; a) unidentate b) *syn-syn* bridging c) *syn-anti* bridging d) *anti-anti* bridging e) $\mu_{1,1}$ -bridging f) unidentate with $\mu_{1,1}$ -bridging g) chelation with $\mu_{1,1}$ -bridging h) chelating bidentate i) chelation with $\mu_{1,2}$ -bridging.

Continued and targeted research has been commenced into MOF system that culminated in the synthesis of different porous structures [55]. Most interesting frameworks have been synthesized in the metal carboxylate system, where di- and trivalent metals have been combined with di- and tricarboxylic acids, resulting in high symmetry structures. The M–O–C bonds are strong, giving the frameworks high thermal stabilities, while the carboxylate linkers are not prone to self-condensation. A variation of metal surroundings has been reported, for example four zinc atoms cluster in MOF-5 [56], chain of vanadium atoms in MIL-47 [57] and MIL-68 [58] and clusters of three chromium atoms connecting to the identical μ_3 oxygen atom in MIL-100 [59] and MIL-101 [60]. Research group

of O. M. Yaghi discovered the structure of MOF-5 in 1999, it was the first three-dimensional porous metal-organic framework structure reported in the literature, which is stable to solvent elimination, representing permanent and reversible nitrogen adsorption at 77 K and 1 atm. pressure. As described previously, a complete family of associated reticular MOF structure has been delineated with the similar primary structure as MOF-5, however, by a variety of dissimilar dicarboxylate ligands (namely IRMOF-n series) [61]. By using varieties of dicarboxylic acid linkers (Figure 1.11) the topology and features of the frameworks can be altered and improved in predictable manner.

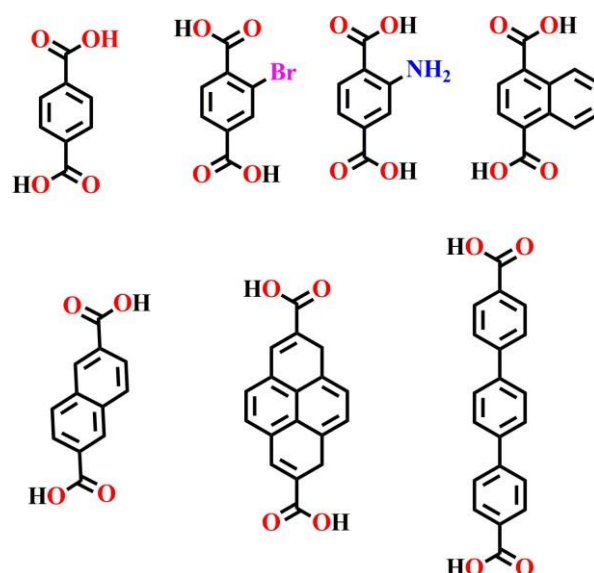


Figure 1.11 Examples of dicarboxylic acid linkers used in the IRMOF-n series of structures [43].

Apart from MOF-5, another interesting porous carboxylate MOF material was synthesized termed HKUST-1 (named after Hong Kong University of Science and Technology) [62]. The structure was synthesized from 1,3,5-benzenetricarboxylic acid (trimesic acid) and copper nitrate that contains dinuclear copper units with a short Cu-Cu distance of 2.63 Å. The structure contains 1-D

square shaped channels when viewed down the crystallographic [100] direction, with *ca.* 10 Å in diameter. These 1-D channels are present in all three crystallographic directions, which upon the intersections resulted in large hexagonal shaped windows of 10 Å in diameter. Physically adsorbed waters present in the channels, and chemically adsorbed water is coordinated to the dinuclear copper species. The chemically adsorbed water can be eliminated by thermal activation, resulting in empty coordination sites on the copper cations. These empty sites act as Lewis acids, resulting in favorable adsorption and catalysis.

Another example of an amazing structural feature in a carboxylate MOF with empty metal sites is the helical octahedral chain in CPO-27 generated after activation. CPO-27 exists in Co [63] and Ni [64] forms, and is isostructural with MOF-74 [65] (synthesized using Zn). The MOF is synthesized by the linker 2,5-dihydroxyterephthalic acid, and the framework has a super rhombohedral symmetry. The framework is composed of helical chains of metal octahedra along the direction of the crystallographic *c*-axis connected together by the 2,5-dihydroxyterephthalate linkers, generating large *ca.* 10 Å diameter hexagonal 1-D channels.

Besides the most important carboxylates linker, many other types of organic molecules that have been used to synthesize MOF frameworks, are bipyridyl [66], imidazole (ZIF-n series) (**Figure 1.12**) [67] and phosphonate [68] based ligands. Use of these linkers results in an innumerable inventory of reported structures, which is flourishing in number all the time.

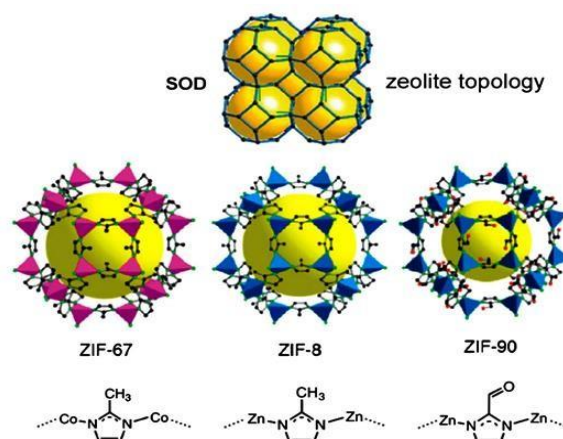


Figure 1.12 Imidazolate linker used for construction of ZIF series [69].

Now-a-days, lanthanide-MOFs (Ln-MOFs)/ rare-earth MOF (RE-MOF) have attracted significant attention as a brilliant candidate for different field of applications like in electronic devices [70], controllable luminescence [71], clean energy technologies [72], medical imaging [73] and catalysis [74] (**Figure 1.13**). A number of Ln-MOFs have been formed from benzene-1,4-dicarboxylate (1,4-bdc) and Ln (Ln = La, Ce, Pr, Nd, Sm, Eu, Gd, Tb, Dy, Ho, Er, and Tm) in water, that have a general formula of $\text{Ln}_2(1,4\text{-bdc})_3(\text{H}_2\text{O})_4$ [75]. Recently, the combination of lanthanides and transition metals has enticed immense attraction to construct 3D lanthanide-transition metal MOFs (Ln-TM MOFs). Benzene-carboxylates are generally rigid and suitable to coordinate with metal in abundant coordination fashion. Reactions between 2,2'-bipyridine, isophthalic acid, and copper and lanthanide salts generated a series of Ln-Cu MOF based on rod-shaped metal units and 2D sheets [76]. However, benzene-carboxylate oxygen has a strong affinity to coordinate to lanthanides over transition metals. Therefore, an addition of N donor-ligand will assist the introduction of transition metal into the

final product [77]. One class of satisfactory ligands is the pyrazine carboxylic acids, which contain multiple O- and N-donors.

Ln-MOFs benefit from the inherent properties of lanthanide metal ions that provide unique coordination and electronic properties. Many lanthanide-based metal-organic framework (Ln-MOF) compounds have been synthesized mainly to study their magnetic and photoluminescence property, but, their catalytic efficacy is not so well explored till date [78]. However, apart from transition metals, the f-electrons of lanthanides make those elements capable of having abundant coordination geometry and large coordination number that in principle facilitates Ln-MOFs to be active in catalysis [79–81]. Based on the hard–soft acid–base consideration [82], the lanthanides have strong affinity in relatively hard oxygen-containing linkers over other type of functional groups. By virtue of variable coordination ability Ln ions bring about greater number of solvent molecules assembled in the coordination sphere of Ln sites. Upon removal of the solvent molecules, unsaturated metal centers served as active site for catalyzed reactions [83, 84]. Consequently, lanthanides are emerging as attractive Lewis acid catalysts in various organic transformations [85, 86].

MOF-based catalysts have been successfully employed in many organic transformations such as Suzuki cross-coupling [87], Sonogashira reaction [88] and epoxide ring opening reaction [89] *etc.* Use of different porous MOFs are tested as heterogeneous catalysts in a variety of organic reactions such as C–C, C–N, C–O coupling reactions, aldol condensation, hydrogenation, epoxidation [90] *etc.* But Ln-based MOF catalysts that are used for this organic reaction are rarely explored [91]. So, use of Ln-MOF as catalyst for these types of organic transformations is quite interesting and gives valuable prospects for organic chemistry.

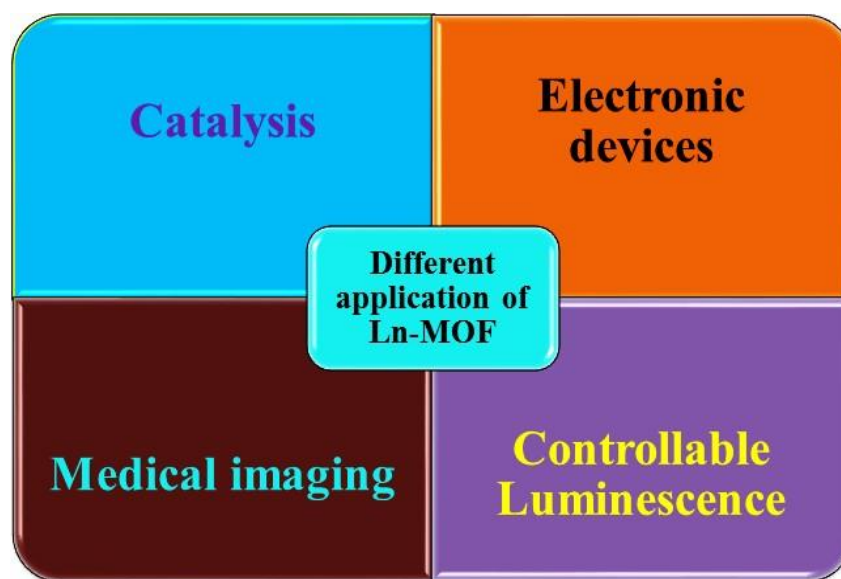


Figure 1.13 Application of lanthanide-based MOF in different fields.

1.3 Application of MOFs

1.3.1 Catalysis

The term catalysis was first coined by Jöns Jakob Berzelius in 1835 to describe changes in substances when they were brought in contact with small amount of certain species called “ferments”. Many years later in 1895 Ostwald came up with the definition of catalyst after his work where he explained the rates can be used to determine the strengths of acids and bases for acid/base catalyzed reaction. For his work, Ostwald was awarded the 1909 Nobel Prize in chemistry. Catalysis plays a key role in the industrial (large scale) production of liquid fuels and bulk chemicals.

Formation of carbon–carbon and carbon–heteroatom bond is important tools in synthetic organic chemistry. These coupling reactions have numerous industrial applications, including the synthesis of intermediates as well as

synthetic targets for the natural products, pharmaceutical agents, polymers etc. [86,92]. In this domain, various catalytic methods have been developed that played vital roles in the formation of carbon–heteroatom bonds. Copper–mediated arylation of amines [93], phenols [94] (Ullmann condensations), amides, carbamates [95] (Ullmann–Goldberg condensations), and activated methylene compounds [96] (Ullmann–Hurtley condensations) are well documented even before the palladium or nickel–catalyzed procedures have been attempted. Nevertheless, the challenge is still on to devise even more effective, selective and environment friendly synthetic procedures for carbon–heteroatom coupling reaction.

Classically, these types of coupling involved nucleophilic aromatic substitution reactions (Ullmann), which requires the use of electron–deficient aryl halides. However, Ullmann–type coupling has not been employed to its full potential for a long time. The synthetic scope of these transformations was restricted because of access to limited range of suitable substrates and harsh reaction conditions that lead to moderate yield of products. Condensations were usually carried out in high–boiling polar solvents such as nitrobenzene, or dimethylformamide (DMF), at temperatures as high as 210 °C, employing stoichiometric amounts of copper reagent in many cases. Aryl halides activated by electron–withdrawing groups were preferentially used [97]. Some reports revealed rate enhancement of arylations in the presence of ligands for copper or other additives [98]. Ligands or additives were thought to increase the solubility or stability of catalyst and/or prevent aggregation of the metal, however, their exact role was not established unequivocally. Finally, in 2001, one research group achieved important breakthrough [99] with the discovery of versatile and very efficient new copper/ligand systems for the formation of C–C, C–N, C–S and C–O bonds that enabled the use of only catalytic amounts of metal under much milder conditions (90–110 °C). These important discoveries, with their promise of being

able to use a catalytic amount of copper in place of the more toxic and expensive palladium, led to spectacular resurgence of interest in Ullmann-type reactions. The challenge was on to devise even more effective synthetic procedures. Many researchers have been involved in the development of more efficient copper/ligand combinations to widen the scope of such reactions in terms of substrate tolerance, copper loading, milder reaction conditions, enhanced chemoselectivity, and enantioselectivity.

1.3.1.1 C–C coupling reactions

❖ Cross–Coupling reaction

Transition metal-catalyzed cross coupling reactions have attracted tremendous importance for the construction of C–C, C–N and C–S bonds via combination of electrophilic and nucleophilic segments. Construction of these bonds is important for preparation of biologically active organic compounds [100] (**Figure 1.14**). Suzuki reactions have potential for forming C–C bonds, synthesizing a variety of compounds, including heterocycles, in the electronics industry to cover chips, as herbicides and natural products, as well as in engineering materials such as molecular wires, conducting polymers and liquid crystals [101, 102]. Metal plays a major role in carbon-carbon bond forming reactions and have a long history in organic synthesis. Among these, Cu-catalyzed carbon-carbon bond forming reactions have been widely used in synthesis. Cu in particular performs the coupling of two aromatic rings with a large number of organic compounds of metals and aryl halides. Biaryls are valuable organic compounds with applications in polymer and life science related products as well as chemical industry [103, 104], a number of them displaying special biological and pharmacological activities [105–107]. Due to their significance, efficient methods for their synthesis are still an active area of research and they have captured the interests of researchers for a long time. Among the various protocols reported to date, copper-

based catalysts are the most general pathway to generate these compounds with Pd- or Cu-catalyzed Suzuki cross-coupling [108–110].

Recently, a new Cu complex based metal-organic framework has been synthesized by using 2,2'-bipyrimidine linker (bpym) ($[\text{Cu}(\text{bpym})\cdot 2\text{H}_2\text{O}]_n$) and used as a recyclable metal-organic framework (MOF). It is investigated as catalyst for preparation of biaryl derivatives through Suzuki reactions using aryl halides with arylboronic acids and K_2CO_3 in DMSO solvent [111].

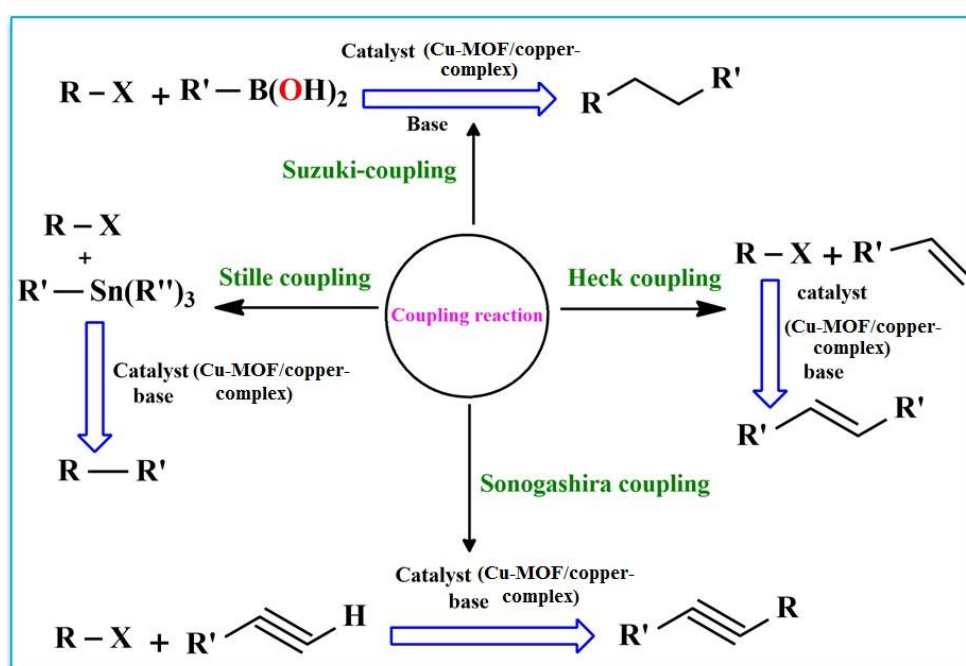


Figure 1.14 Various C–C cross-coupling reactions.

❖ Henry reaction

The Henry reaction is another type of important classic carbon–carbon bond formation reaction in organic chemistry. In 1895, Belgian chemist Louis Henry first invented the Henry reaction between a nitroalkane and an aldehyde/ketone in

the presence of a base. The reaction is used for the preparation of most important building blocks of natural products or pharmaceuticals [112]. This type of reaction is commonly known as nitroaldol reaction due to the similarity with aldol reaction. This interesting organic reaction is used to convert a nitroalkane with an α -hydrogen to a β -nitro alcohol upon condensation with an aldehyde or ketone (Figure 1.15). Among the different chiral transition metal complexes used as catalysts, chiral copper complexes play an important role for asymmetric Henry reaction [113,114]. A novel chiral Cu(II) complex that was synthesized by a tetradentate chiral Schiff-base ligand, N,N'-bis(2-pyridylmethylidene)-(R,R)-1,2-cyclohexanediamine, was employed for its catalytic efficacy in asymmetric Henry reaction between benzaldehyde and nitromethane [115]. Recently, a report on novel cobalt containing metal-organic framework with the formula $\text{Co}_2(\text{bdda})_{1.5}(\text{OAc})\cdot\text{H}_2\text{O}$ {H₂bdda = 4,4-[benzene-1,4-diylbis(methylidene)nitro]dibenzoic acid}, OAc = acetoxy group) [116]. The MOF was tested for catalytic Henry reaction by using various aromatic aldehydes with a variety of nitroalkanes. Wang et al. synthesized Mn(II) complexes with triazole ring containing Schiff bases. The complex was examined as catalyst in the catalytic Henry reaction [117]. The result shows that the MOF is capable to catalyze the Henry reaction that generates β -hydroxynitroalkanes in high yield.

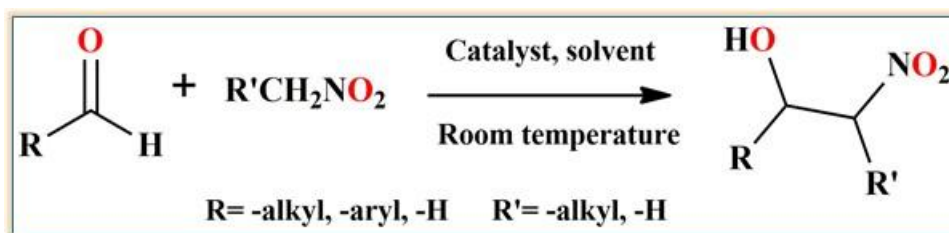


Figure 1.15 Henry reaction of aldehyde.

1.3.1.2 C–heteroatom bond formation reactions**❖ C–O coupling reaction**

Transition metal-catalyzed chemical transformation of organometallic reagents and organic electrophiles associated to the most important cross coupling reaction in organic synthesis. The biaryl ether (**Figure 1.16**) moiety is not only present in synthetic pharmaceuticals and natural products but also extensively found in many pesticides, polymers, and ligands. Copper, being one of the earth-abundant elements, has received ever increasing attention due to its low toxicity and low cost. In the early 20th century, Ullmann and Goldberg have reported O-arylation reaction involving cleavage of an aromatic carbon-halide bond in the presence of a stoichiometric amount of copper as catalyst [118,119]. In this reaction, two moles of aryl halides are coupled in the presence of a stoichiometric amount of copper salt to afford the homocoupling product at 210–260°C [119,120]. Although this reaction received immense attention from the chemical industries, however, the reaction requires harsh conditions, which include strong base, high temperature, large amount of copper catalyst, limited substrate scope etc. [121]. Later, Sharma et al. also reported a copper-catalyzed C-N [122]. X. Ribas et al. published Ullmann type C-O and C-N coupling reaction by using Cu-based catalysts for the chemo selective arylation with aryl iodides and bromides [123]. A major breakthrough was eventually reported by Chan,[124] Lam,[125] and Evans,[126] who developed milder conditions for the synthesis of diaryl ethers using boronic acids and stoichiometric amount of copper(II) acetate at room temperature. To modernize this classical Ullmann reaction, it is required to establish a novel composition and morphology of catalyst, and reducing agents and suitable solvents. Among different types of metal-based catalysts nickel, palladium, and gold are mostly employed in Ullmann's reaction [127-129]. However, palladium and nickel were found to be the best catalyst for Ullmann type reaction in respect of their high regioselectivity and activity. But unfortunately, metal catalysts have

several drawbacks, such as highly toxic, high cost, and generally required poisonous organic phosphines as a stabilizing ligand [130]. Besides these, silver [131], and rhodium [132] were also employed as catalyst in Ullmann coupling reaction.

Last few decades metal-organic framework (MOF) based catalytic reaction have received an ever-growing attention for their fascinating architectures, variable dimensionality, tunable pore size and readily available internal surface which facilitate the efficacy of catalytic reaction. Porous MOFs are used in various types of catalytic reactions, including coupling reactions, such as C–O, C–N coupling reaction. In 2017, Sadeghi et al. reported UiO-66-NH₂ MOF that acts as a heterogeneous catalyst for C–O coupling reaction. Initially, UiO-66-NH₂ is modified by a post-synthesis modification with melamine (Mlm) for the impregnation of copper NPs on the surface of modified UiO-66-NH₂. Copper oxide was doped on MOF surface through free amine group and π -electron interaction of melamine (Mlm) and ligand; UiO-66-NH₂-Mlm/CuO NPs composite. It was used as a heterogeneous catalyst in the Ullmann etherification reaction which efficiently promoted C–O bond formation reaction [133]. Later on, H. Q. Ha's team synthesized copper–MOF based catalyst, Cu₂(BDC)₂(DABCO). The MOF was prepared by using benzene-1,4-dicarboxylate (BDC) and 1,4-diazabicyclo [2.2.2] octane (DABCO) as ligand in dimethylformamide solvent medium. This Cu-MOF is efficient for the synthesis of diphenyl ethers [134].

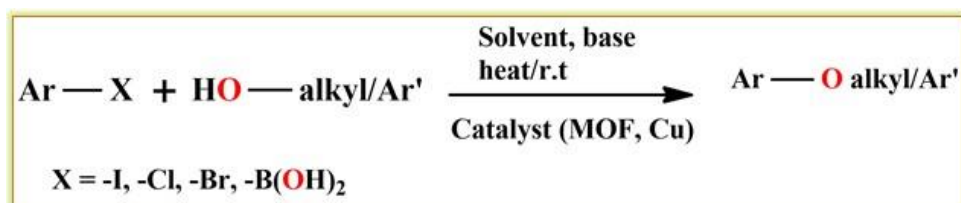


Figure 1.16 C–O cross-coupling reaction of different aromatic electrophile.

❖ C–N coupling reaction

The nitrogen-containing compound has received the utmost importance as it serves as a key building block in different types of pharmaceuticals, natural products, organic materials and catalysts and also in basic studies of medicinal chemistry. To introduce nitrogen into organic molecules through C–N bond formation, the metal-catalyzed cross-coupling reaction is a versatile method (**Figure 1.17**) [135]. It has shortened the synthetic procedure of retrosynthesis by employing mild reaction conditions [136–137]. In 1903 and 1906 Ullmann [93] and Goldberg [95] reported the C–N coupling reaction of amine with cheap and low-cost copper-catalyst. However, the classic Ullmann and Goldberg coupling reactions require strong bases, high temperature, stoichiometric copper reagents, and a longer reaction time. In 1983, Kosugi et al. reported for the first time the introduction of the C–N bond formation reaction in palladium-catalyzed aromatic amination [138]. However, the scope of reaction was restricted to electron-neutral aryl halides and dialkyl amides. Thus, it remained dormant for decades owing to its several limitations. In 1998, independent publications by Chan [124] and Lam [125] reported the development copper-mediated N-arylation in a generally applicable protocol of amines using stoichiometric copper(II) acetate and boronic acids at room temperature with an impressive range of nucleophiles. In last one decade, the arylation of *N*-nucleophiles with arylboronic acids has become a standard protocol for C–N coupling reaction. The topic has been reviewed in 2003 by Thomas and Ley [139]. Over the years, different modifications in the C–N bond formation reaction were carried out. Amongst them, the works by Buchwald and Hartwig are worth mentioning [140]. They developed an important and new process of N-arylation of amines catalyzed by palladium replacing the traditional Ullmann coupling. Needless to say, here also drawbacks like cost of catalyst, air sensitivity, difficulties to separate products and recycling the catalyst limits in the applications of the catalyst. Buchwald and Hartwig's methods suffered from

functional group tolerance and substrate scope limitations [141]. These major drawbacks concerned into account and intense research was carried out that includes the use of various ligands such as amino acids [142], diamines [143], diols [144], amino alcohols [145], diethylamine [146], phenanthrolines [147], etc. which facilitate the copper-based C–N bond formation to a greater extent.

MOFs in the solid state evolved as efficient heterogeneous catalysts towards Ullmann type C–N bond formation. Use of MOF as catalysts facilitated ligand-free protocols, easy separation, and less reaction time. Early reports by Long et al. and Truong et al. demonstrated efficacy of Cu-based MOF in C–N coupling reactions; MOFs like, Cu-TDPAT ($H_6TDPAT = 2,4,6\text{-tris}(3,5\text{-dicarboxylphenylamino})\text{-}1,3,5\text{-triazine}$) [148] and $[Cu(INA)_2]$ (INA = isonicotinate ion) [149], catalyzed the Ullmann type C–N coupling reactions between aryl halide and N-heterocycles. The C–N bond formation was carried out between imidazole and iodobenzene with Cu-TDPAT MOF which was active in polar solvent DMSO in presence of base K_2CO_3 at $120^\circ C$ temperature. Furthermore, Dai et al. published the use of copper-based MOF-199 [150] and amorphous Cu-MOF-74 (Cu-MOF-74) [151] as effective and recyclable heterogeneous catalysts for direct N-arylation of heterocycles with aryl halides. MOF-199 which is identical to MOF HKUST-1 possesses an exposed copper site. The reaction was performed with 10 mol% of MOF-199, NaOH as a base in DMSO at $120^\circ C$. At the optimized reaction condition, a maximum yield of 97% was obtained for C–N bond formation between pyrrole and p-methoxyiodobenzene. Koner et al. reported the use of zinc-based porous IRMOF-3 as a host [152]. IRMOF-3 was synthesized from $Zn(NO_3)_2 \cdot 4H_2O$ and 2-amino-1,4-benzene dicarboxylic acid [153]. The bidentate Schiff base moiety was generated inside the pores of IRMOF-3 availing post-synthetic modification (PSM) technique, where the amine group is condensed with the pyridine-2 aldehyde. Thereafter, Cu(II) ion was introduced to anchor these moieties so that it

can act as an active catalyst (IRMOF-PI-Cu). The post synthetically prepared IRMOF-PI-Cu was then employed as a catalyst toward C–N bond formation. The optimized condition used pyrazole and phenyl bromide as a coupling partner with catalyst, Cs₂CO₃ as a base in DMSO solvent under the N₂ atmosphere.

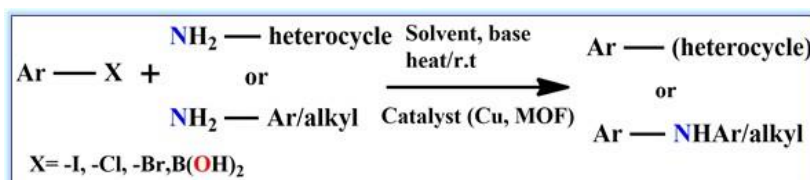


Figure 1.17 Transition metal catalyzed N-arylation reactions.

1.3.1.3 Decarboxylative coupling reaction

The development of useful procedure for the regio-, chemo-, and stereoselective cleavage and formation of chemical bonds for the building of functional materials has employed chemists for more than a century. Recent progress of selective carbon-hydrogen and carbon-carbon bond activation provides hope for revolutionary approaches for direct introduction of the desired functionality in non-functionalized substrates. This would have an immense influence on both of our economics and environment.

Recently, carboxylate groups have dedicated as versatile connection points for construction of carbon frameworks. The attractiveness of the use of carboxylic acids is attributed due to its wide abundance. Carboxylic acid groups are generally stable in air and moisture, easy to store and handle [154,155]. They can also be synthesized in laboratory scale by a wide range of well-established method. The last decade, in particular, witnessed the development of a wealth of catalytic transformations of carboxylic acids, which produces various important product classes along with multifaceted reaction pathways [156]. The importance of this reaction is that they can react with metal with generation of either acyl

metal species or metal carboxylate which can be utilized in catalytic reaction. Carbon monoxide gas can be released from acyl metal intermediates and carbon dioxide gas from carboxylate complexes when different organometallic species is formed in each case. One of the most attractive transformations of carboxylic acids is decarboxylation reaction [157,158]. These reactions can roughly be classified into five categories with respect to the position and polarity of the bond formation: (1) redox neutral cross-coupling reactions with aryl, vinyl or allyl electrophiles, (2) Heck-type vinylation reactions, (3) direct arylation processes, (4) conjugate additions and (5) carbon–heteroatom bond forming reactions (**Figure 1.18**).

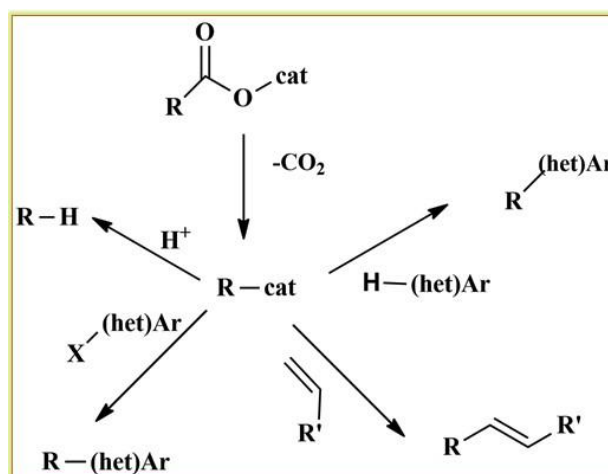


Figure 1.18 Overview of decarboxylation reaction

The C–COOH group undergoes C–C bond breaking to liberate one equivalent of carbon dioxide along with the formation of an active carbon species (e.g., a C–M species or carbon radical). Palladium [159,160] copper,[161] silver [162] gold [163] and rhodium [164] are efficient of inducing the decarboxylation of the benzoic acids to form the corresponding aryl-metal species. Considerable progresses of transition metal-catalyzed decarboxylative C–C bond formation have been established over the past few years [165] including those involving

C–H bond functionalization [166]. The second approach is the C–C bond cleavage for producing various types of organic species. One of the most important is decarboxylative halogenation or the halo-decarboxylation reaction [167]. Improving the decarboxylation activity of the catalyst system, it is often decisive when aiming at lower reaction temperatures that allow converting a broader scope of carboxylic acids, including sensitive, functionalized derivatives.

1.3.2 Use of lanthanide-MOF in catalysis

Rare-earth (RE)/ lanthanide (Ln) elements are referred to the 15 lanthanide elements including scandium (Sc) and yttrium (Y) elements. They have very similar properties and exhibit common valance of +3. Most of them can form stable compounds. The RE³⁺ ions are featured by a gradually filling of their 4f orbitals (from La^{III} to Lu^{III}), possessing diversified electronic energy levels. The unfilled 4f orbits are insensitive to the external surrounding chemical environments with shielding effect of the filled 5s and 5p orbits, leading to well-defined electronic energy levels [168–171]. Due to their special structure, unlike transition metal-based MOFs, RE-MOFs or RE-doped MOFs are less studied but can show satisfactory performance for catalysis [172-174] (**Figure 1.19**). They have abundant Lewis's acid sites centered at the rare earth ions. Because of the large coordination sites of rare earth ions, the selection of ligands is more diverse for understanding different functionalized features, such as light adsorption, acid-base sites, and well-designed channel morphology. In particular, the RE-MOF networks are stable at a high temperature or even in harsh alkaline and acidic environment. Additionally, they can perform as a carrier to load metal species. The synergistic effect and/or electronic interaction between metal loadings and RE-MOFs are hopefully can be employed to modulate catalytic activity. The RE-MOFs are now used as a promising candidate in different catalytic field. Most important catalysis reactions are described very briefly.

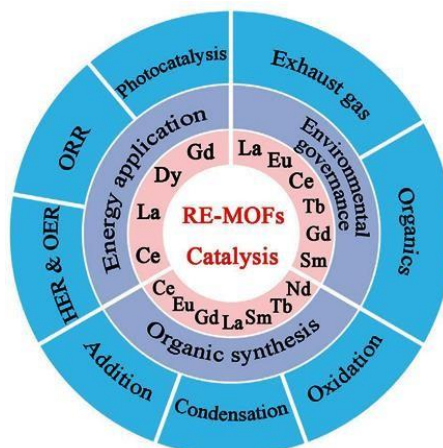


Figure 1.19 The application of Ln-MOF for catalytic conversion [174].

❖ Oxidation reaction by Ln-MOF

The rare-earth MOF-based materials perform as efficient catalysts for organic oxidation reactions. Lian and Yan [175] has synthesized an Eu-based MOF, used as a catalyst for the effective oxidation of α -phenethyl alcohol by ultraviolet light can be converted to acetophenone. Farha's group published that Ce-NU-1200 with tricarboxylic acid linkers and 8-connected hexanuclear nodes could catalyze the oxidation of 4-methoxybenzyl alcohol under 1×10^5 Pa O_2 at 105°C [176]. One of the well-known reactions in organic synthesis is the epoxidation reaction. High reaction turn-over efficiency largely depends on suitable catalysts using facile oxidants. Snecko's group has synthesized the LnPF-1 (Ln = La, Nd, Pr, Sm, Eu) by using 1,5-NDS (NDS = naphthalenedisulfonic acids) as connectors for the oxidation of linalool [177]. The catalyst of NdPF-1 led to the conversion of 76% yield using H_2O_2 as oxidant at 343K. Koner et al. reported a series of lanthanide-based compounds that exhibit excellent catalytic performance for the epoxidation of olefins with remarkable selectivity [178, 179]. Besides, they reported two novel lanthanide based three dimensional metal-organic frameworks, $[Nd(HCOO)_3]_n$ and

$[\text{Pr}(\text{HCOO})_3]_n$, which are efficient for preparation of various cyclic and linear olefinic epoxides using *tert*-BuOOH at 65-68°C [180]. The catalysts could be recycled easily without significant deactivation of catalytic activity and damage of MOF's networked structure.

❖ **Suzuki-Miyaura coupling reaction by Ln-MOF**

One of the most important C–C coupling reactions (**Figure 1.20**) is Suzuki-Miyaura coupling reaction, using a boronic acid and an organohalide catalyzed by palladium species, first reported by Miyaura et al. in 1979 [181]. Pd-graphite oxide and Pd-SiO₂ catalyst attracted immense attention due to its heterogeneity and recycling for C–C bond forming reaction. But the superiority of MOF-derived catalysts, especially Ln-MOF is that it can fix Pd by coordination. Sun et.al has synthesized a series of heterobimetallic porous Pd-Ln-MOFs (Ln = Nd, Sm, Dy, Eu, Pr, Gd, Tb) by hydrothermal method. They used 2,2'-bipyridine-4,40-dicarboxylic acid as linkers and bipyridine as ligand that coordinate to Pd(II) ions [182,183]. These catalysts exhibited excellent catalytic activities and recyclability in Suzuki–Miyaura reactions. Subsequently, they reported another Fe₃O₄@La-MOF-Schiff base-Pd catalyst with a novel core-shell structure generated by post-synthetic modification [184].

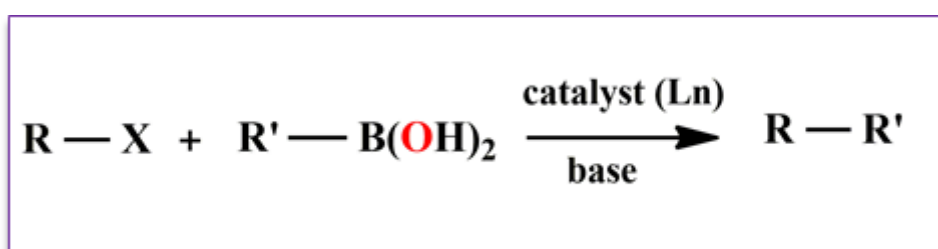


Figure 1.20 Schematic diagram of Suzuki-Miyaura coupling.

❖ Knoevenagel condensation by Ln-MOF

Knoevenagel condensation is another important C-C coupling reaction. In this reaction an active methylene group with electron withdrawing functional groups is added to carbonyl or aldehyde groups followed by a dehydration condensation (**Figure 1.21**). RE-MOF catalyst is one of the most important catalysts for Knoevenagel condensation as its metal nodes normally show Lewis acid activity and the nitrogenous heterocyclic groups present in the ligands serve as Lewis basic sites. Wang et al. have synthesized BIT-58 with Ce^{3+} as the metal node and BTB (BTB = 1,3,5-tris(4-carboxyphenyl) benzene) as the linker [185]. The size of the BIT-58 was controlled by using 1-methylimidazole by coordination modulation method and through competing the coordination sites with BTB. The nano-BIT-58 performed greater conversion efficacy towards Knoevenagel reaction of malonitrile and different benzaldehyde derivatives. Hu et.al used NH_2 -Tb-MOF possessing free amino group in framework structure that acts as active centers for Knoevenagel reaction under microwaved condition [186]. The catalytic activity was also influenced by the sizes of aldehydes. In the reaction of ethyl cyanoacetate and benzaldehyde, NH_2 -Tb-MOF showed comparable activity to the homogeneous catalyst with 86% yield of aniline at 40°C .

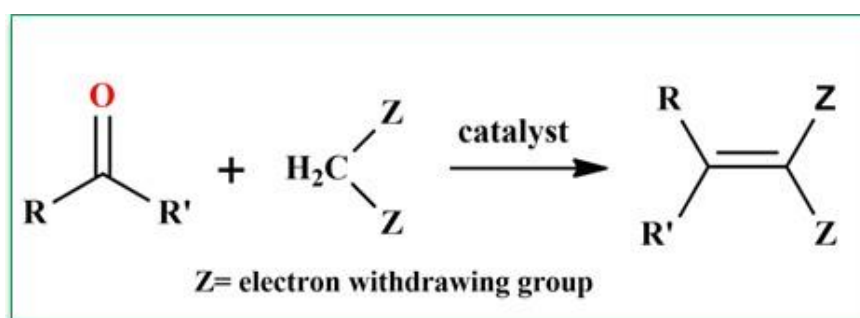


Figure 1.21 Schematic representation of Knoevenagel condensation.

❖ Cycloaddition of epoxy compounds by Ln-MOF

Carbon dioxide fixation to generate chemical and fuels [187, 188] are now a great demand for the maintenance of clean and sustainable environment as excessive CO₂ emission from fuel causes global warming as well as greenhouse effect. One of the most effective methods to fix greenhouse gas such as CO₂ is cycloaddition of CO₂ in epoxides. The product of cycloaddition, cyclic carbonate (**Figure 1.22**) has been widely used in different areas such as aprotic solvents, electrolytes for lithium ion batteries, and chemical intermediates for organic synthesis. Numerous Ln-MOFs have been employed as catalysts for the fixation of CO₂ with epoxides because the porous structure of MOFs can effectively absorb CO₂ and subsequently rich Lewis acidic sites from Ln³⁺ ions can interact with epoxide species leading to ring opening reaction with co-catalysts. Zhao's group had synthesized the [Eu(BTB)(phen)]·4.5DMF·2H₂O {H₃BTB=1,3,5-tris(4-carboxyphenyl) benzene} one dimensional channel with the total potential volume of 56.1%, which contributed to promote CO₂ adsorption [189]. The Eu-MOF along with tetrabutylammonium bromide as the co-catalyst showed high catalytic activity towards cycloaddition of CO₂ with styrene oxide at 1×10⁵ Pa. The yield of the corresponding cyclic carbonate was over 99% at 70°C. The cycloaddition of amines with epoxides was also investigated by Tehrani et al. using Tb-MOFs as the catalysts assisted with ultrasonic irradiation [190]. The Tb-MOFs exhibited highest yield of 95% in the reaction of styrene oxide and aniline at ambient temperature. Recently, Morsali et al. has synthesized a Lewis acid-base bi-functional and amine-functionalized Dy-MOF that can act as heterogeneous catalyst for the conversion CO₂ to cyclic carbonate in absence of solvent and under mild condition [191].

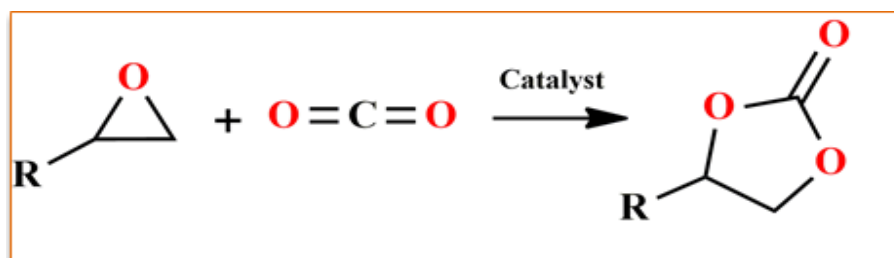


Figure 1.22 Schematic diagram for cycloaddition reaction.

Along with these catalytic reaction, other numerous catalysis reactions are carried out using lanthanide metal-organic framework such as acid-catalyzed Michael addition reaction, cyanosilylation reaction, reduction reaction, photocatalytic reaction, hydrogen production [192,193] etc.

1.3.3 Gas adsorption and separation studies

Possible applications with MOFs have been extensively studied in the area of gas separation, gas storage and purification [194]. Several MOFs responded for guest-induced breathing effect and these materials are used to produce the functional materials for gas separation.

In 1998, Yaghi *et al.* [195] synthesized a microporous material, MOF-2, $Zn(BDC)(H_2O)$ [BDC = 1,4-benzenedicarboxylate], which is the first report of creating microporosity in MOF. It was verified by surface area and pore volume measurements. Structural integrity and porosity of the structure are sustained in presence of solvent molecules or guest molecules [196-198]. The structure of MOF-2, a polynuclear metal cluster, $Zn_2(COO)_4(H_2O)_2$ paddle-wheel like secondary building units (SBUs) linked through BDC linkers (**Figure 1.23a,b**) revealed typical reversible type-1 gas sorption isotherms, such as zeolites, indicating that MOF-2 is permanently microporous, as demonstrated by nitrogen (at 77K) (**Figure 1.23c**) and carbon dioxide (at 195K) sorption. However, the

Langmuir surface areas for this particular MOF were calculated to be 270 and 310 m^2g^{-1} for N_2 and CO_2 , respectively, which was smaller than conventional zeolite molecules. This finding on MOF-2 was a crucial point in progress of 3D structures of MOF materials and subsequently creating a plethora of opportunities of combination of SBUs with organic linkers.

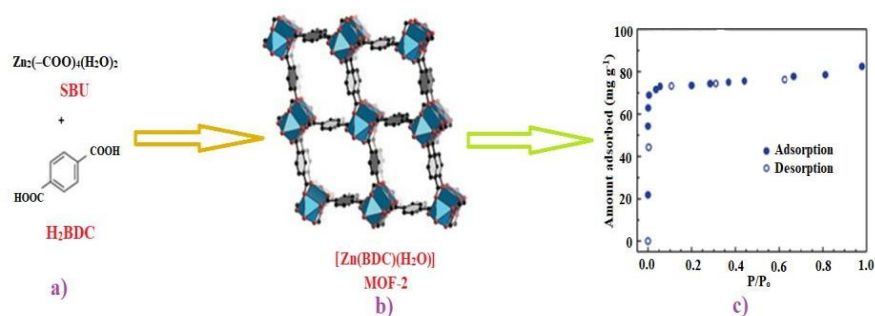


Figure 1.23 a) $\text{Zn}_2(\text{COO})_4(\text{H}_2\text{O})_2$ secondary building units (SBUs) are linked through BDC linkers to form MOF-2; b) View of MOF-2 along the crystallographic [001] direction, the rectangular channels are clearly visible (hydrogen atoms are omitted for better clarity). Color encryption: black, C atoms; red, O atoms; blue polyhedra, Zn metal centers; c) N_2 sorption [196].

It was first demonstrated in $\text{Mn}_3[(\text{Mn}_4\text{Cl})_3(\text{BTT})_8]_2$, (BTT=1,3,5-benzenetristetrazolate) that open metal sites on the framework surface can increase the capacity of H_2 adsorption. $\text{Mn}_3[(\text{Mn}_4\text{Cl})_3(\text{BTT})_8]_2$ contains open Mn^{2+} coordination sites and exhibits an isosteric heat of H_2 adsorption of 10.1 kJ/mol at zero coverage [199]. Most notably, however, at 90 bar and 298 K, a capacity of 12.1 g/L was observed. This is 77% greater than the density of compressed H_2 gas under these conditions, and represents the current record of hydrogen sorption onto a metal–organic framework.

Hydrogen is gravimetrically energy condensed and harmless, and its oxidation product is water. Hydrogen is best fuel option not only due to massive energy content (33.3 kWhkg^{-1}) [200], but because it is a carbon-neutral energy

system. Consequently, it is of importance to find substances that adsorb hydrogen with a H_2 density greater than the density of liquid H_2 [201]. Further, elimination of CO_2 from sources of anthropogenic emission is now a topmost importance, since CO_2 emission has close relevance to climate change.

Koner *et al.* reported a 2D layered alkaline earth metal based MOF compound, $\{[Mg_2(pzdc)_2(H_2O)_4] \cdot H_2O\}_n$ (pzdc = pyrazole-3,5-dicarboxylate). This MOF displayed significantly selective hydrogen (H_2) sorption (*ca.* 63 $cc\ g^{-1}$) over N_2 at 1 atm and 77K (**Figure 1.24**). Such a favored hydrogen uptake over nitrogen might be ascribed to the slight inter layer separations which allows only H_2 molecules to enter into the layers, hindering the entry for the N_2 molecules wherein kinetic diameters of H_2 is around 2.89 Å, smaller than the kinetic diameters of N_2 which is 3.64 Å [202].

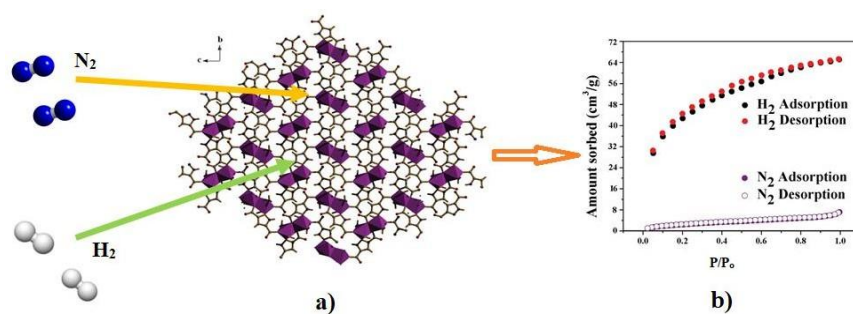


Figure 1.24 a) 2D network of compound $\{[Mg_2(pzdc)_2(H_2O)_4] \cdot H_2O\}_n$ along to bc plane; b) H_2 and N_2 sorption isotherm at 77 K [202].

1.3.4 MOF in photoluminescence sensing

Due to tunable porosity, stability, selectivity, and sensitivity, MOFs have drawn much attention in luminescence properties [203]. These properties are especially important for several potential as well as challenging sensing applications [204, 205]. Properties of MOFs can be tuned with respect to the desired application by altering metal nodes and/or organic linkers. Metal centered luminescence solely

depends on the nature of metal ions, geometry, and coordination environment comparison to traditional transition metal-based MOFs because of the superior luminescence properties of Ln^{3+} ions. Due to the presence of f-block, Ln^{3+} ions can produce a wider coordination sphere with a variety of coordination numbers and connectivity, Ln-MOFs engaged in superior luminescence characteristics such as large Stokes shifts, long lifetime, high color purity, sharp emissions, and high quantum yields that is observed in the visible and near-infrared region [206]. On the basis of hard-soft acid-base theory, Ln^{3+} ions tend to coordinate with oxygen with much preference compared to that happens in transition metal-based MOFs [207]. Therefore, unlike transition metal ions, Ln^{3+} has tremendous potential to build a promising platform to explore MOF-based sensors. The presence of electronic configurations of $[\text{Xe}] 4f^n$ ($n = 0$ to 14) provides lanthanides large number of electronic levels in inner orbital $14!/n!(14-n)!$ turning out unique optical properties [208,209]. Excepting for La^{3+} ($4f^0$) and Lu^{3+} ($4f^{14}$), other Ln ions exhibit f-f emission, which happens mainly in the visible (for Tb^{3+} , Sm^{3+} , Eu^{3+} , and Tm^{3+}) and NIR (for Pr^{3+} , Sm^{3+} , Nd^{3+} , Dy^{3+} , Ho^{3+} , Er^{3+} , Tm^{3+} , and Yb^{3+}) region [208, 210].

Luminescence in Ln-MOFs usually occurs via antenna effect due to the shielding effect of $5s^25p^6$ subshells and Laporte forbidden 4f-4f transition, (**Figure 1.25**) [211]. Other two types of allowed transitions occur with broader 4f-5d transition and LMCT (ligand-to-metal) or MLCT (metal-to-ligand) charge transfer transitions. There is always a probability mixing of electronic state due to ligand field influences by which the transitions occur although the 4f-4f transition is not allowed according to Laporte's parity selection rule [210, 212–213]. Therefore, now-a-days, Ln-MOF based compounds are widely used as successful candidate for sensing vast number of molecules such as organo-molecule, toxic organic molecules, pharmaceutical molecule sensing along with explosive nitro-aromatic sensing application [214].

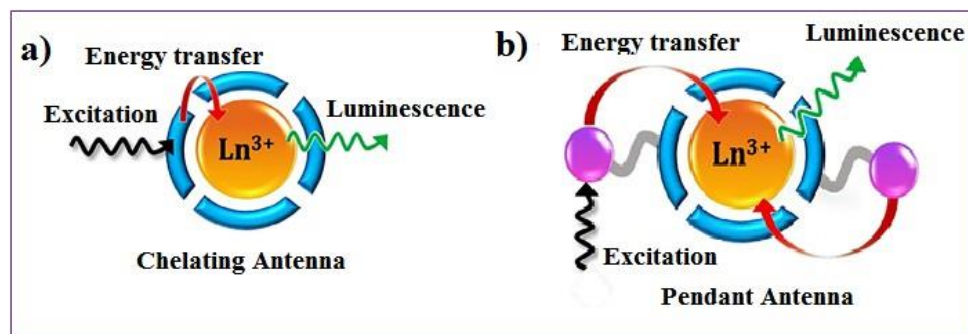


Figure 1.25 Illustration for the antenna effect of Ln^{3+} sensitization; using a) chromophoric chelate linker and b) chromophoric pendant ligand [211].

1.3.5 Proton conductivity in MOFs

During the past two decades, porous coordination polymers (PCPs) or porous crystalline metal–organic frameworks (MOFs) have been intensively studied in search of various applications. Compared with other traditional solid-state proton-conductive materials, MOFs, in particular, can be the suitable material for better understanding of proton conductivity and the mechanism of conducting pathways. MOFs have high tunability in structure and property with various design strategies. In addition, the high crystallinity and void space of MOFs are advantageous for understanding the conducting path and conception of proton-conducting media such as water [215, 216] non-volatile acid [217, 218] and protic organic molecules [219].

In 1950, Ubbelohde and Reger first proposed proton conduction in a solid through the hydrogen bonding (H-bonding) network [220] and its acid–base nature is a critical and fundamental principle in H^+ transport [221]. H^+ conductors exhibit a higher conductivity at room temperature (RT) than other ionic species like Li^+ or Na^+ as the covalent character of H-bonds lowers the Coulomb potential

of the H^+ pathway with a decrease in the net charge. In particular, the proton (H^+) transfer membrane, solid-state electrolyte is a significant component for acquiring safety and high performance in fuel cells that converts chemical into electrical energy through carbon-neutral mechanism. Further, it has vast potential in applications of electrochemical devices such as chemical sensors, batteries, and super capacitors [221-222]. So, typical designs for proton-conductive MOFs are concentrated on the effective H-bonding formation and increase of mobile protons (charge carrier density).

For achieving proton-conductive strategies in MOFs, they can be classified into five types depending on the proton source and hopping site (**Figure 1.26**) [223]. This figure briefly explains all the types of proton-conductive MOFs. In type 1, inclusion of counter ion such as hydronium (H_3O^+), ammonium (NH_4^+ , $Me_2NH_2^+$), or anion (SO_4^{2-}), is simultaneously produced during the MOF synthesis, resulting in the construction of charged frameworks [224, 225–227]. The counter ions that are generated by inclusion form the H-bonding with the guest water or the framework, forming the continuous H-bond network with efficient proton conduction. Recently, Kitagawa et al. published the super-protonic conduction of a Pt dimer based MOF, $[Pt_2(MPC)_4Cl_2Co-(DMA)(HDMA)\cdot guest]$ (6-mercaptopyridine-3-carboxylic acid=MPC); DMA, dimethylamine). The impregnated protic dimethylammonium cation ($HDMA^+$), trapped in the framework structure forms effective proton transport pathways upon hydration by changing its relative position, resulting in more than 10^5 times higher proton conductivity with respect to the dehydrated form [228]. Types 2 and 3 are the functionalized structural components such as non-coordinated functional groups in organic ligands (e.g., $-NH_2$, $-OH$, $-COOH$, $-SO_3H$, and $-PO_3H_2$) or insertion of coordinative functional molecules in metal centers (H_2O , $EtOH$, and imidazole).

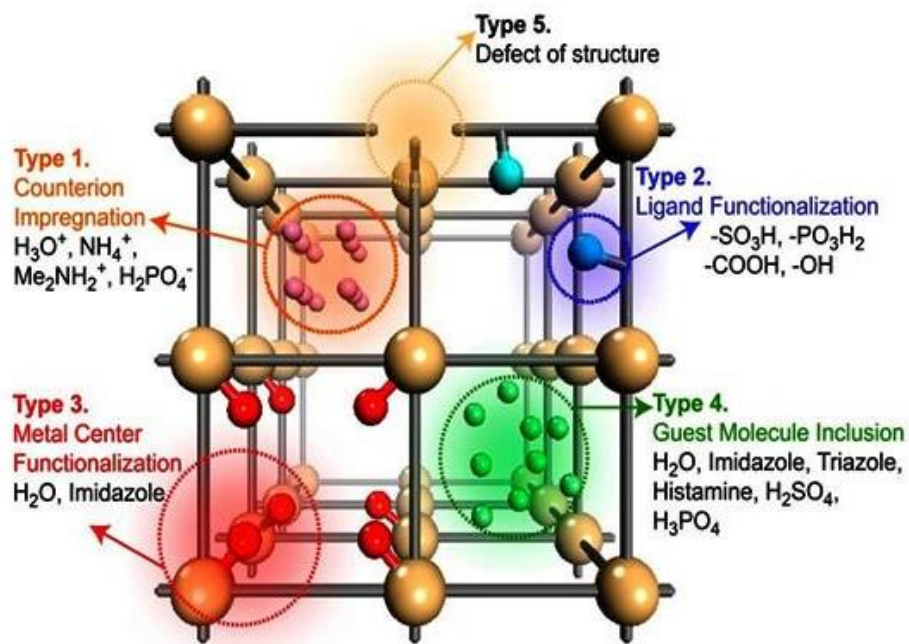


Figure 1.26. Classification of the types of proton-conductive MOFs [223].

In type 4, the insertion of functional guest molecules such as protic organic molecules, acid molecules, polyoxometalate (POM), or metal–organic polyhedra (MOP) molecules, forms the simplest method of using MOF porosity [229, 230, 231–233]. However, extraordinary structural stability is required for their high performance. Type 5 consists of the extrinsic and intrinsic defective MOFs for proton conduction [234–236]. The defect sites increase proton diffusion by producing an additional conducting pathway. Although the proton-conductive MOFs are classified simply into five types, in fact the published proton-conductive MOFs are more complexed and cannot be grouped into only a single type because the additional components act simultaneously for greater proton conductivity with a synergistic effect.

1.4 Scope and objective of the present thesis

Porous coordination polymers or metal organic frameworks (MOFs), are three-dimensional materials assembled by either cluster of metal or ions as nodes and organic ligands as linkers. These materials have relevance in the fundamental and applied point of view for liquid phase homogeneous and heterogeneous catalysis, enantioselective transformations. Their stable porous structures can successfully increase the enrichment of substrate molecules and active sites to enhance catalytic activity. The size of MOF pores can also be tuned by altering the length of organic ligands to realize steric selectivity of substrates and/or products. Most of the MOF catalysts are chemically robust and can be easily reused like conventional heterogeneous catalysts. Apart from traditional transition-metal based MOF, Ln-MOFs are becoming the emerging candidate for heterogeneous catalyst as well. Unlike, transition metal, lanthanide ions have abundant coordination geometry and large coordination number that in principle facilitates Ln-MOFs to be active in catalysis. Also, from literature survey, it was noticed that the rare-earth containing complexes can be used as potential catalysts in various organic reaction transformations, such as, in carbon-carbon bond forming reactions, cyano-silation, oxidation-reduction reaction and so on. It is also investigated that copper containing MOF can be used as potential catalysts in various organic reaction transformations, especially in carbon-carbon or carbon-heteroatom bond forming reactions. Till date, C-heteroatom bond formation reaction by Ln-MOF is not much explored. In this thesis attempt was made to synthesis such systems for the study of some specific carbon-heteroatom bond forming reactions by rare-earth based MOF. Catalysis by MOFs has just started to intrigue the scientific community and has an enormous scope for development of new materials with structure directing catalysis. There are increasing reports about catalytic applications of RE-MOFs towards pollution treatment, chemical synthesis, and energy transformation. With the development of RE-MOF

materials, significant breakthroughs in catalysis are expected in the future days. Many unique and exciting catalytic applications will be reported in the years to come.

To complete the study following objectives were taken:

- ❖ Lanthanide MOFs are synthesized by direct hydrothermal or solvothermal synthesis method and characterize them by different physico-chemical methods such as single-crystal-X-ray diffraction (SC-XRD), powder-X-ray diffraction (PXRD), FT-IR, elemental analysis (C, H, N), UV-Vis spectral analysis, TG-DTA (Thermogravimetric analysis) etc.
- ❖ To know the surface property of the MOF, Hirshfeld surface analysis has been carried out.
- ❖ To evaluate the catalytic activity of these materials in different organic reactions. The influence of different reaction parameters such as temperature, solvent, base effect *etc.* on the catalytic reaction was also studied to optimize the reaction condition.
- ❖ Finally, to examine the recyclability and heterogeneity nature of the catalyst. Therefore, it is convincing that research on Ln-MOFs continues to become more interdisciplinary, and the goal in the upcoming years will be to convert the acquired knowledge into technical applications.

1.5 Summary

The thesis contains of five (5) chapters as follows:

Chapter 1 introduces the general discussion on the diverse features of metal-organic frameworks (MOFs), numerous synthetic procedure to design diverse functional MOFs, key role of the different carboxylate linkers in the adaptability

of MOFs, involvement of transition metals to design carboxylate based MOFs while a variety of spacer has been used; application of MOFs in catalysis and the role of MOF solids in catalytic reactions such as C-heteroatom, C-N bond forming reactions; selective gas adsorption studies, luminescence properties, proton conductivity etc. Apart from transition metal based MOFs, vast application of different lanthanide or rare-earth based MOFs (Ln/RE-MOFs) in catalysis has been briefly discussed. Scope of the current research and the summary of the research works have also been presented shortly.

Chapter 2 discloses synthesis of a robust and thermally stable three dimensional Gd-MOF, $\{[\text{Gd}_4(\text{NDC})_6(\text{H}_2\text{O})_6] \cdot 2\text{H}_2\text{O}\}_n$ (MOF-1). This 3D Gd-MOF has been synthesized by hydrothermal route and different physical characterization have been described. Attractively, this $\{[\text{Gd}_4(\text{NDC})_6(\text{H}_2\text{O})_6] \cdot 2\text{H}_2\text{O}\}_n$ is capable of catalyzing the O-arylation reaction efficiently between substituted phenol and bromoarene under heterogeneous condition at 80°C to afford unsymmetrical diary ethers. In addition, thermogravimetric analysis demonstrates that the mass of MOF-1 remains constant until ~530°C after its dehydration under nitrogen atmosphere which is in agreement with the robust character of this Gd-MOF.

Chapter 3 reports the synthesis of novel lanthanide based two-dimensional metal-organic framework (MOF) compound $[\text{Dy}(\text{NDC})(\text{NO}_3)(\text{DMA})_2]_n$ (MOF-2) [H_2NDC =2,6-naphthalenedicarboxylic acid and DMA = N,N-dimethylacetamide]. MOF-2 has been synthesized by solvothermal route and the structure has been solved through single-crystal X-ray diffraction study. Structural analysis reveals that MOF-2 possesses a two-dimensional framework system. A “Paddle-wheel” like unit represents the core of the 2D network structure. Such type Paddle-wheel core unit is scarcely found amongst rare-earth MOFs. The morphology of the MOFs as well as different types of weak interactions possessed by the framework have been assessed using Hirshfeld surface analysis and fingerprint plots have been drawn to understand various interactions. Notably,

[Dy(NDC)(NO₃)(DMA)₂]_n (MOF-2) catalyzes C–N coupling reaction between aryl-halides and amines under heterogeneous condition.

Chapter 4 deals with the synthesis of two novel lanthanide MOFs with formula [Tb(NDC)(NO₃)(DMA)₂]_n (MOF-3) and [Ho(NDC)(NO₃)(DMA)₂]_n (MOF-4) [where, NDC= dinegative 2,6-naphthalenedicarboxylate ligand and DMA = N,N-dimethylacetamide]. Both of these two MOFs have been synthesized by solvothermal process with subtle change in synthesis procedure. SC-XRD analysis reveals that structure of these two MOFs are largely the same and morphology of the two and different types of weak interactions possessed by the framework have been confirmed using Hirshfeld surface analysis (HS) and subsequent supplementary pseudo-mirror 2D fingerprint plot. MOF-3 and MOF-4 have been tested as heterogeneous catalysts for O-arylation reaction that affords unsymmetrical diarylethers. Both of them are capable of catalyzing O-arylation reaction efficiently between substituted phenols and different substituted bromobenzene under heterogeneous condition at 95°C. The product yield obtained for MOF-3 is higher than MOF-4 catalyst.

Chapter 5 describes an unprecedented in situ decarboxylation-hydroxylation reaction of 3-hydroxy-2-quinoxalinecarboxylic acid catalyzed by lanthanide metal in hydrothermal condition under autogenous pressure in teflon lined Parr-acid digestion bomb. 3-hydroxy-2-quinoxalinecarboxylic acid is converted into 1,4-dihydroquinoxaline-2,3-dione (DQD). Apart from spectral characterization like IR and NMR spectroscopic and HRMS analysis the authenticity of hydroxylated derivative has been established by single crystal X-ray structure solution of the ligand. Besides, *in-situ* generated hydroxylated ligand affords lanthanide metal-organic framework compounds of Gd, Ho, Er and Yb (MOF-5, MOF-6, MOF-7 and MOF-8 respectively). All these four MOFs have been characterized by single-crystal X-ray diffraction and their structures have been established. Notably, this

work represents an unusual reaction (decarboxylation-hydroxylation catalyzed by lanthanides) and this is the first example of Ln-catalyzed decarboxylation hydroxylation.

1.6 References

- [1] J. J. Perry IV, J. A. Perman, M. J. Zaworotko, *Chem. Soc. Rev.* 38 (2009) 1400.
- [2] R.R. Salunkhe, Y.V. Kaneti, J. Kim, J. H. Kim, Y. Yamauchi, *Acc. Chem. Res.* 49 (2016) 2796.
- [3] H.C. Zhou, J.R. Long, O.M. Yaghi, *Chem. Rev.* 112 (2012) 673.
- [4] A. Schoedel, M. Li, D. Li, M. O’Keeffe, O.M. Yaghi, *Chem. Rev.* 116 (2016) 12466.
- [5] A. Sanora, I. Senkowska, S. Kaskel, P. K. Bharadwaj, *Inorg. Chem.* 52 (2013) 7358.
- [6] H. Sato, W. Kosaka, R. Matsuda, A. Hori, Y. Hijikata, R. V. Belosludov, S. Sakaki, M. Takata, S. Kitagawa, *Science*, 343 (2014) 167.
- [7] A. Wolf, L. Diestel, F. Lübke, T. Kodanek, T. Mohamed, J. Caro D. Dorfs, *Chem. Mater.* 28 (2016) 7511.
- [8] D. Lim, H. Kitagawa, *Chem. Rev.* 120 (2020) 8416.
- [9] S. Biswas, A. K. Mondal, S. Konar, *Inorg. Chem.* 55 (2016) 2085.
- [10] R. J. Marshall, Y. Kalinovsky, S. L. Griffin, C. Wilson, B. A. Blight, R. S. J. Forgan, *J. Am. Chem. Soc.* 139 (2017) 6253.
- [11] E. Linnane, S. Haddad, F. Melle, Z. Mei, D.F. Jimenez, *Chem. Soc. Rev.* 51 (2022) 6065.

- [12] J. Guo, Y. Qin, Y. Zhu, X. Zhang, C. Long, M. Zhao, Z. Tang, *Chem. Soc. Rev.* 50 (2021) 5366.
- [13] K. K. Sharma, A. Anan, R. P. Buckley, W. Ouellette, T. Asefa, *J. Am. Chem. Soc.* 130 (2008) 218.
- [14] M. J. Rosseinsky, *Micropor. Mesopor. Mater.* 73 (2004) 15.
- [15] B. F. Hoskins, R. Robson, *J. Am. Chem. Soc.* 112 (1990) 1546.
- [16] H. Li, M. Eddaoudi, M. O'Keeffe, O. M. Yaghi, *Nature* 402 (1999) 276.
- [17] Y. Shibata, *Journal of the College of Science*, 37(1916) 1.
- [18] J. F. Keggin, F. D. Miles, *Nature* 137 (1936) 577.
- [19] S. L. James, *Chem. Soc. Rev.* 32 (2003) 276.
- [20] B. F. Abrahams, B. F. Hoskins, D. M. Michail, R. Robson, *Nature* 369 (1994) 727.
- [21] D. Venkataraman, G. B. Gardner, S. Lee, J. S. Moore, *J. Am. Chem. Soc.* 117 (1995) 11600.
- [22] O. M. Yaghi, G. M. Li, H. L. Li, *Nature* 378 (1995) 703.
- [23] S. Subramanian, M. J. Zaworotko, *Angew. Chem. Int. Ed.* 34 (1995) 2127.
- [24] A. F. Wells, *Three Dimensional Nets and Polyhedra*, Wiley, New York, 1977.
- [25] Z. F. Bian, J. Zhu, F. L. Cao, Y. F. Lu, H. X. Li, *Chem. Commun.* (2009) 3789.
- [26] R. I. Walton, *Chem. Soc. Rev.* 31 (2002) 230.

- [27] A. Rabenau, *Angew. Chem. Int. Ed.* 24 (1985) 1026.
- [28] P. J. Hagrman, D. Hagrman, J. Zubieta, *Angew. Chem. Int. Ed.* 38 (1999) 2638.
- [29] T. Jiang, A. Lough, G. A. Ozin, R. L. Bedard, *J. Mater. Chem.* 8 (1998) 733.
- [30] G. J. Demazeau, *J. Mater. Chem.* 9 (1999) 15.
- [31] X. X. Zhao, J. P. Ma, Y. B. Dong, R. Q. Huang, *Cryst. Growth Des.* 7 (2007) 1058.
- [32] J. S. O. Evans, R. J. Francis, D. Ohare, S. J. Price, S. M. Clark, J. Flaherty, J. Gordon, A. Nield, C. C. Tang, *Rev. Sci. Instrum.* 66 (1995) 2442.
- [33] A. K. Cheetham, G. Ferey, T. Loiseau, *Angew. Chem. Int. Ed.* 38 (1999) 3268.
- [34] X. M. Zhang, *Coord. Chem. Rev.* 249 (2005) 1201.
- [35] J. S. Choi, W. J. Son, J. Kim, W. S. Ahn, *Micropor. Mesopor. Mater.* 116 (2008) 727.
- [36] W. J. Son, J. Kim, J. Kim, W. S. Ahn, *Chem. Commun.* (2008) 6336.
- [37] D.W. Jung, D. A. Yang, J. Kim, J. Kim, W. S. Ahn, *Dalton Trans.* 39 (2010) 2883.
- [38] J. Kim, S.T. Yang, S.B. Choi, J. Sim, J. Kim, W. S. Ahn, *J. Mater. Chem.* 21 (2011) 3070.

- [39] U. Mueller, M. Schubert, F. Teich, H. Puetter, K. Schierle-Arndt, J. Pastre, *J. Mater. Chem.* 16 (2006) 626.
- [40] Y. R. Lee, J. Kim, W. S. Ahn, *Korean J. Chem. Eng.* 30 (2013) 1667.
- [41] T. Friš, D.G. Reid, I. Halasz, R. S. Stein, R. E. Dinnebier, M. J. Duer, *Angew. Chem. Int. Ed.* 49 (2010) 724.
- [42] H.Y. Cho, J. Kim, S. N. Kim, W. S. Ahn, *Micropor. Mesopor. Mater.* 169 (2013) 180.
- [43] J. L. C. Rowsell, O. M. Yaghi, *Micropor. Mesopor. Mater.* 73 (2004) 3.
- [44] M. Eddaoudi, D. B. Moler, H. Li, B. Chen, T. M. Reineke, M. O'Keeffe, O. M. Yaghi, *Acc. Chem. Res.* 34 (2001) 319.
- [45] S. Kitagawa, R. Kitaura, S. Noro, *Angew. Chem. Int. Ed.* 43 (2004) 2334.
- [46] P. Pachfule, T. Panda, C. Dey, R. Banerjee, *CrystEngComm* 12 (2010) 2381.
- [47] J. J. Perry IV, J. A. Perman, M. J. Zaworotko, *Chem. Soc. Rev.* 38 (2009) 1400.
- [48] G. J. E. Davidson, S. J. Loeb, *Angew. Chem. Int. Ed.* 42 (2003) 74.
- [49] B. Moulton, M. J. Zaworotko, *Chem. Rev.* 101 (2001) 1629.
- [50] J. L. C. Rowsell, O. M. Yaghi, *Micropor. Mesopor. Mater.* 73 (2004) 3.
- [51] H. Li, M. Eddaoudi, M. O'Keeffe, O. M. Yaghi, *Nature* 402 (1999) 276.
- [52] J. J. Perry IV, J. A. Perman, M. J. Zaworotko, *Chem. Soc. Rev.* 38 (2009) 1400.

- [53] T. Chalati, P. Horcajada, R. Gref, P. Couvreur, C. Serre, *J. Mater. Chem.* 21 (2011) 2220.
- [54] A. Rabenau, *Angew. Chem. Int. Ed. Eng.* 24 (1985) 1026.
- [55] S. Kaskel, *Porous Metal-Organic Frameworks*, (Eds.) F. Schüth, K. S. W. Sing, J. Weitkamp, Vol. 2, 2002, pp. 1190.
- [56] H. Li, M. Eddaoudi, M. O'Keeffe, O. M. Yaghi, *Nature* 402 (1999) 276.
- [57] K. Barthelet, J. Marrot, D. Riou, G. Férey, *Angew. Chem. Int. Ed.* 41 (2006) 281.
- [58] K. Barthelet, J. Marrot, G. Férey, D. Riou, *Chem. Commun.* (2004) 520.
- [59] G. Férey, C. Serre, C. Mellot-Draznieks, F. Millange, S. Surble, J. Dutour, I. Margiolaki, *Angew. Chem. Int. Ed.* 43 (2004) 6296.
- [60] G. Férey, C. M. Draznieks, C. Serre, F. Millange, J. Dutour, S. Surble, I. Margiolaki, *Science* 309 (2005) 2040.
- [61] M. Eddaoudi, J. Kim, N. Rosi, D. Vodak, J. Wachter, M. O. Keeffe, O. M. Yaghi, *Science* 295 (2002) 469.
- [62] S. S. Y. Chui, S. M. F. Lo, J. P. H. Charmant, A. G. Orpen, I. D. Williams, *Science* 283 (1999) 1148.
- [63] P. D. C. Dietzel, Y. Morita, R. Blom, H. Fjellvag, *Angew. Chem. Int. Ed.* 44 (2005) 6354.
- [64] P. D. C. Dietzel, B. Panella, M. Hirscher, R. Blom, H. Fjellvag, *Chem. Commun.* (2006) 959.
- [65] N. L. Rosi, J. Kim, M. Eddaoudi, B. Chen, M. O'Keefe, O. M. Yaghi, J.

Am. Chem. Soc. 127 (2005) 1504.

- [66] E. Biemmi, T. Bein, N. Stock, *Solid State Sci.* 8 (2006) 363.
- [67] K. S. Park, Z. Ni, A. P. Cote, J. Y. Choi, R. Huang, F. J. Uribe-Romo, H. K. Chae, M. O'Keefe, O. M. Yaghi, *Proc. Natl. Acad. Sci. USA* 103 (2006) 10186.
- [68] J. A. Groves, S. R. Miller, S. J. Warrender, C. Mellot-Draznieks, P. Lightfoot, P. A. Wright, *Chem. Commun.* (2006) 3305.
- [69] J. Zhang, Y. Tan, W. J. Song, *Microchim. Acta.* 187 (2020) 234.
- [70] K.H. Goh, A.S.M.A. Haseeb, Y.H. Wong, *Mater. Sci. Semicond. Process.* 68 (2017) 302.
- [71] S.V. Eliseeva, J.C. Bunzli, *Chem. Soc. Rev.* 39 (2010) 189.
- [72] A. M. Ullman, J. W. Brown, M. E. Foster, F. Leonard, K. Leong, V. Stavila, M. D. Allendorf, *Inorg. Chem.* 55 (2016) 7233.
- [73] T. I. Kostelnik, C. Orvig, *Chem. Rev.* 119 (2019) 902.
- [74] H. Liu, M. S. Eisen, *Synthesis* 52 (2020) 629.
- [75] C. Daignebonne, N. Kerbellec, O. Guillou, *Inorg. Chem.* 47 (2008) 700.
- [76] F. Luo, S. R. Batten, Y. Che, *Chem. Eur. J.* 13 (2007) 4948.
- [77] Y. G. Huang, F. L. Jiang, M. C. Hong, *Coord. Chem. Rev.* 253 (2009) 2814.
- [78] A. D. G. Firmino, F. Figueira, J. P.C. Tome, F. A. A. Paz, J. Rocha, *Coord. Chem. Rev.* 355 (2018) 133.

- [79] A. Dhakshinamoorthy, A. M. Asiri, H. Garcia, *Chem. Eur. J.* 22 (2016) 8012.
- [80] J. Jacobsen, A. Ienco, R. D'Amato, F. Costantino, N. Stock, *Dalton Trans.* 49 (2020) 16551.
- [81] Y. Zhang, S. Liu, Z. S. Zhao, Z. Wang, R. Zhang, L. Liu, Z. Bo. Han, *Inorg. Chem. Front.* 8 (2021) 590.
- [82] R. G. Pearson, *Coord. Chem. Rev.* 100 (1990) 403.
- [83] Z. Huang, F. Zhao, L. Fan, W. Zhao, B. Chen, X. Chen, S.-F. Zhou, J. Xiao, G. Zhan, *Mater. Des.* 194 (2020) 108881.
- [84] S. Kitagawa, S. I. Noro, T. Nakamura, *Chem. Commun.* (2006) 701.
- [85] Y. Zhang, S. Liu, Z. S. Zhao, Z. Wang, R. Zhang, L. Liu, Z. Bo. Han, *Inorg. Chem. Front.* 8 (2021) 590.
- [86] S. M. Islam, N. Salama, P. Mondal, A. S. Roy, K. Ghosh, K. Tuhina, J. *Mol. Catal. A: Chem.* 387 (2014) 7.
- [87] F.X. Llabres i Xamena, A. Abad, A. Corma, H. Garcia, *J. Catal.* 250 (2007) 294.
- [88] A.K. Sharma, F. Lloret, R. Mukherjee, *Inorg. Chem.* 52 (2013) 4825.
- [89] B. Cristóvão, B. Mirosław, J. Kłak, M. Rams, *Polyhedron* 85 (2015) 697.
- [90] R. Sen, D. Mal, S. Bhunia, S. Koner, Y. Miyashita, K. Okamoto, *Langmuir* 25 (2009) 13667.
- [91] F. Ding, Y. Li, P. Yan, Y. Deng, D. Wang, Y. Zhang, I. Dragutan, V. Dragutan, K. Wang, *Molecules* 23 (2018) 2435.

- [92] T. Chen, Q. Huang, Y. Luo, Y. Huc, W. Lu, *Tetrahedron Lett.* 54 (2013) 1401.
- [93] F. Ullmann, *Ber. Dtsch. Chem. Ges.* 36 (1903) 2382.
- [94] F. Ullmann, *Ber. Dtsch. Chem. Ges.* 37 (1904) 853.
- [95] I. Goldberg, *Ber. Dtsch. Chem. Ges.* 39 (1906) 1691.
- [96] W. R. H. Hurtley, *J. Chem. Soc.* (1929) 1870.
- [97] A. Bruggink, A. McKillop, *Angew. Chem., Int. Ed. Engl.* 13 (1974) 340.
- [98] D. Ma, Y. Zhang, J. Yao, S. Wu, F. Tao, *J. Am. Chem. Soc.* 120 (1998) 12459.
- [99] S. L. Buchwald, A. Klapars, J. C. Antilla, G. E. Job, M. Wolter, F. Y. Kwong, G. Nordmann, E. J. Hennessy, WO02/085838 (priority number US0286268, 2001)
- [100] J. Chen, L. Dai, J. Li, M. Mohammadnia. *Appl. Organomet. Chem.* 34 (2020) 5708.
- [101] Y. Sun, M. Mohammadnia. *Inorg. Chem. Commun.*, 118 (2020)107993.
- [102] L. Danqing, J. Ming, L. Li, M. Mohammadnia. *Appl. Organomet. Chem.* 34 (2020) 5820.
- [103] S. Guin, S.K. Rout, A. Banerjee, S. Nandi, B.K. Patel. *Org. Lett.* 14 (2012) 5294.
- [104] X. Zhang, F. Liu, Z. Wei. Z. Wang. *Lett. Org. Chem.* 10 (2013) 31.
- [105] N. Iranpoor, H. Firouzabadi, A. Rostami. *Appl. Organometal. Chem.* 27

(2013) 501.

- [106] K.C. Nicolaou, S. Natarajan, H. Li, N.F. Jain, R. Hughes, M.E. Solomon, J.M. Ramanjulu, C.N.C. Boddy, M. Takayanagi. *Angew. Chem. Int. Ed.* 37 (1998) 2708.
- [107] Q. Zhang, D.P. Wang, X.Y. Wang, K. Ding. *J. Org. Chem.* 74 (2009) 7187.
- [108] G. Evano, N. Blanchard, M. Toumi. *Chem. Rev.* 108 (2008) 3054.
- [109] A.Y. Cheng, J.C. Hsieh. *Tetrahedron Lett.* 53 (2012) 71.
- [110] J. Lindley. *Tetrahedron* 40 (1984) 1433.
- [111] H. Liu, M. Liu, M. Kiasadegh, *J. Coord. Chem.* 74 (2021) 2873.
- [112] K. S. Egorova, V. P. Ananikov, *Organometallics* 36 (2017) 4071.
- [113] J. D. White, S. Shaw, *Org. Lett.* 14 (2012) 6270.
- [114] T. Arai, M. Watanabe, A. Yanagisawa, *Org. Lett.* 9 (2007) 3595.
- [115] Q. T. Nguyen, J. H. Jeong, *Polyhedron* 25 (2006) 1787.
- [116] M. Tobisu, N. Chatani, *Acc. Chem. Res.* 48 (2015) 1717.
- [117] M. E. Van der Boom, S.Y. Liou, Y. Ben-David, L. J. W. Shimon, D. J. Milstein, *J. Am. Chem. Soc.* 120 (1998) 6531.
- [118] M. Abyazisani, V. Jayalatharachchi, J. MacLeod, *Comprehensive Nanoscience and Nanotechnology Academic Press: Oxford, UK, 2019*, pp. 299.

- [119] F. Ullmann, J. Bielecki, Ber. Dtsch. Chem. Ges. 34 (1901) 2174.
- [120] X. Gong, J. Wu, Y. Meng, Y. Zhang, L.-W. Ye, C. J. G. C. Zhu, Green Chem. 21 (2019) 995.
- [121] J. Jiang, L. Du, Y. Ding, Catalyst. Mini Rev. Org. Chem. 17 (2020) 26.
- [122] K. K. Gurjar, R. K. J. H. Sharma, Heliyon 6 (2020) 3233.
- [123] M. Rovira, M. Soler, I. Guell, M. Z. Wang, L. Gomez, X. Ribas, J. Org. Chem. 81 (2016) 7315.
- [124] D. M. T. Chan, K. L. Monaco, R. P. Wang, M. P. Winters, Tetrahedron Lett. 39 (1998) 2933.
- [125] P. Y. S. Lam, C. G. Clark, S. Saubern, J. Adams, M. P. Winters, M. T. Chan, A. Combs, Tetrahedron Lett. 39 (1998) 2941.
- [126] D. A. Evans, J. L. Katz, T. R. West, Tetrahedron Lett. 39 (1998) 2937.
- [127] G. Prabusankar, C. N. Babu, G. Raju, N. J. Sampath, Chem. Sci. 129 (2017) 553.
- [128] B. M. Rosen, K.W. Quasdorf, D. A. Wilson, N. Zhang, A. M. Resmerita, N. K. Garg, V. Percec, Chem. Rev. 111 (2011) 1346.
- [129] F. Khan, M. Dlugosch, X. Liu, M. G. Banwell, Acc. Chem. Res. 51 (2018) 1784.
- [130] K. S. Egorova, V. P. Ananikov, Organometallics 36 (2017) 4071.
- [131] N. Tepale, V.V.A. Fernández-Escamilla, C. Carreon-Alvarez, V. J. González-Coronel, A. Luna-Flores, Crystals 9 (2019) 612.

- [132] Van der Boom, M.E. Liou, S. Y. Ben-David, Y. Shimon, L. J.W. Milstein, D. J. Am. Chem. Soc. 120 (1998) 6531.
- [133] S. Sadeghi, M. Jafarzadeh, A. R. Abbasi, K. Daasbjerg, New J. Chem. 41 (2017) 12014.
- [134] H. Q. Ha, H. T. D. Nguyen, T. H. M. Pham, V. T. Pham, T. Truong, Catal. Commun. 117 (2018) 79.
- [135] J. Bariwal, E. Van Der Eycken, Chem. Soc. Rev. 42 (2013) 9283.
- [136] M. R. Biscoe, B. P. Fors, S.L. Buchwald, J. Am. Chem. Soc. 130 (2008) 6686.
- [137] T. Ogata, J. F. Hartwig, J. Am. Chem. Soc. 130 (2008) 13848.
- [138] M. Kosugi, M. Kameyama, T. Migita, Chem. Lett. 12 (1983) 927.
- [139] A. W. Thomas, S. V. Ley, Angew. Chem., Int. Ed. 42 (2003) 5400.
- [140] P. A. Forero-Cortés, A. M. Haydl, Org. Process Res. Dev. 23 (2019) 1478.
- [141] D.S. Surry, S.L. Buchwald, Chem. Sci. 2 (2011) 27.
- [142] H. Hammoud, M. Schmitt, F. Bihel, C. Antheaume, J.-J. Bourguignon J. Org. Chem. 77 (2012) 417.
- [143] A. Klapars, J.C. Antilla, X. Huang, S.L. Buchwald, J. Am. Chem. Soc. 123 (2001) 7727.
- [144] F.Y. Kwong, A. Klapars, S.L. Buchwald, Org. Lett. 4 (2002) 581.
- [145] Z. Lu, R. J. Twieg, Tetrahedron 61 (2005) 903.
- [146] J.W. Tye, Z. Weng, A.M. Johns, C.D. Incarvito, J.F. Hartwig, J. Am.

Chem. Soc. 130 (2008) 9971.

- [147] R.K. Gujadhur, C.G. Bates, D. Venkataraman, *Org. Lett.* 3 (2001) 4315.
- [148] W. Long, W. Qiu, C. Guo, C. Li, L. Song, G. Bai, G. Zhang, H. He, M.L. Kuznetsov, *Molecules* 20 (2015) 21178.
- [149] T. Truong, C.V. Nguyen, N.T. Truong, N.T.S. Phan, *RSC Adv.* 5 (2015) 107547.
- [150] Z. Li, F. Meng, J. Zhang, J. Xie, B. Dai, Zhang Jie, *Org. Biomol. Chem.* 14 (2016) 10861.
- [151] P. Ma, F. Meng, N. Wang, J. Zhang, J. Xie, B. Dai, *ChemistrySelect* 3 (2018) 10694.
- [152] D. Saha, S. Koner, *ChemCatChem.* 6 (2014) 2373.
- [153] O.M. Yaghi, M. O’Keeffe, N.W. Ockwig, H.K. Chae, M. Eddaoudi, J. Kim, *Nature* 423 (2003) 705.
- [154] K. P. C. Vollhardt, N. E. Schore, *Organische Chemie*, (2000) 893.
- [155] K. P. C. Vollhardt, N. E. Schore, *Organische Chemie* (2000) 1081.
- [156] L. J. Goossen, N. Rodriguez, K. Goossen, *Angew. Chem.* 120 (2008) 3144.
- [157] L. J. Gooßen, N. Rodríguez, K. Gooßen, *Angew. Chem. Int. Ed.* 47 (2008) 3100.
- [158] N. Rodríguez, L. J. Goossen, *Chem. Soc. Rev.* 40 (2011) 5030.
- [159] A. G. Myers, D. Tanaka, M. R. J. Mannion, *J. Am. Chem. Soc.* 124 (2002)

- 11250.
- [160] D. Tanaka, S. P. Romeril, A. G. Myers, *J. Am. Chem. Soc.* 127 (2005) 10323.
- [161] Y. Wei, P. Hu, M. Zhang, W. Su, *Chem. Rev.* 117 (2017) 8864.
- [162] L. J. Gooßen, G. Deng, L. M. Levy, *Science* 313 (2006) 662.
- [163] J. Cornella, M. Rosillo-Lopez, I. Larrosa, *Adv. Synth. Catal.* 353 (2011) 1359.
- [164] Z.-M. Sun, P. Zhao, *Angew. Chem., Int. Ed.* 48 (2009) 6726.
- [165] J. D. Weaver, A. Recio, A. J. Grenning, Tunge, *Chem. Rev.* 111 (2011) 1846.
- [166] J. Miao, H. Ge, *Synlett* 25 (2014) 911.
- [167] A. Varenikov, E. Shapiro, M. Gandelman, *Chem. Rev.* 121 (2021) 412.
- [168] Z. Zeng, Y. Xu, Z. Zhang, Z. Gao, M. Luo, Z. Yin, C. Zhang, J. Xu, B. Huang, F. Luo, Y. Du, C. Yan, *Chem. Soc. Rev.* 49 (2020) 1109.
- [169] J. Xu, X. Chen, Y. Xu, Y. Du, C. Yan, *Adv. Mater.* 32 (2020) 1806461.
- [170] S. Ji, Y. Qu, T. Wang, Y. Chen, G. Wang, X. Li, J. Dong, Q. Chen, W. Zhang, Z. Zhang, S. Liang, R. Yu, Y. Wang, D. Wang, Y. Li, *Angew. Chem., Int. Ed.* 59 (2020) 10651.
- [171] B. L. Ramirez, C. C. Lu, *J. Am. Chem. Soc.* 142 (2020) 5396.
- [172] C. Pagis, M. Ferbinteanu, G. Rothenberg, S. Tanase, *ACS Catal.* 6 (2016) 6063.

- [173] T. Zhang, X. Wu, Y. Fan, C. Shan, B. Wang, H. Xu, Y. Tang, *Chem-Nano. Mat* 6 (2020) 1119.
- [174] X. Shi, B. Cao, J. Liu, J. Zhang, Y. Du, *Small* 17 (2021) 2005371.
- [175] X. Lian, B. Yan, *Inorg. Chem.* 55 (2016) 11831.
- [176] X. J. Wang, X. Zhang, P. Li, K.-I. Otake, Y. X. Cui, J. F. Lyu, *J. Am. Chem. Soc.* 141 (2019) 8306.
- [177] F. Gandara, A. Garcia-Cortes, C. Cascales, B. Gomez-Lor, E. Gutierrez-Puebla, M. Iglesias, *Inorg. Chem.* 46 (2007) 3475.
- [178] R. Sen, D. K. Hazra, M. Helliwell, M. Mukherjee S. Koner, *Eur. J. Inorg. Chem.* 2011, 241.
- [179] R. Sen, D. K. Hazra, M. Helliwell, M. Mukherjee, A. Bhattacharjee, S. Koner, *Polyhedron* 29 (2010) 3183.
- [180] R. Sen, D. Saha, S. Koner, *Catal. Lett.* 142 (2011) 124.
- [181] N. Miyaura, K. Yamada, A. Suzuki *Tetrahedron Lett.* 20 (1979) 3437.
- [182] L. X. You, W.H. Zong, G. Xiong, F. Ding, S. J. Wang, B. Y. Ren, *Appl Catal A.* 511 (2016) 1.
- [183] L. X. You, W. L. Zhu, S. J. Wang, G. Xiong, F. Ding, B. Y. Ren, *Polyhedron.* 115 (2016) 47.
- [184] G. Xiong, X. L. Chen, L. X. You, B. Y. Ren, F. Ding, I. Dragutan, V. Dragutan, Y. G. Sun, *J. Catal.* 361 (2018) 116.
- [185] Y. Chen, S. Zhang, F. Chen, S. Cao, Y. Cai, S. Li, H. Ma, X. Ma, P. Li, X. Huang, W. Wang, *J. Mater. Chem. A.* 6 (2018) 342.

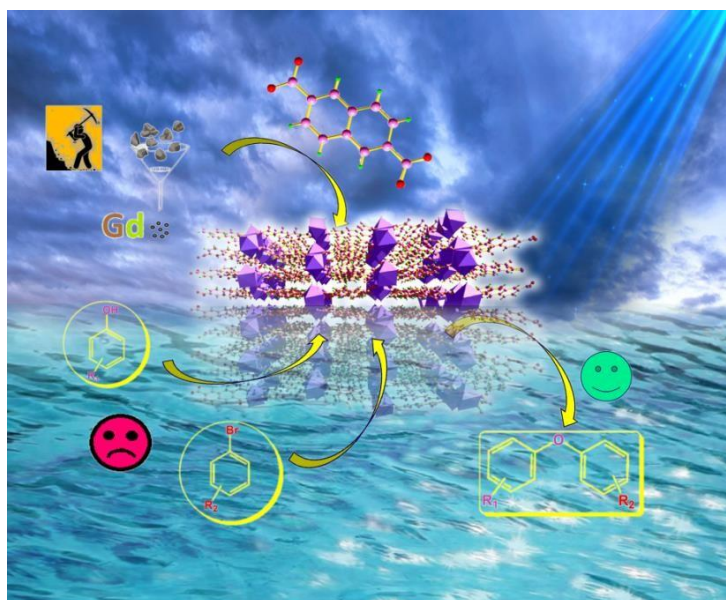
- [186] J. P. Huang, C. M. Li, L.L. Tao, H. L. Zhu, G. J. Hu, *J. Mol. Struct.* 114 (2017) 853.
- [187] Y. Matsubara, D. C. Grills, Y. Kuwahara, *ACS Catal.* 5 (2015) 6440.
- [188] S. Roy, A. Cherevotan, S. C. Peter, *ACS Energy Lett.* 3 (2018) 1938.
- [189] H. Xu, B. Zhai, C. S. Cao, B. Zhao, *Inorg. Chem.* 55 (2016) 9671.
- [190] M. Karimi, T. Hajiashrafi, A. Heydari, A. A. Tehrani, *Appl. Organometal. Chem.* 31 (2017) 3866.
- [191] R. Abazari, S. Sanati, A. Morsali, A. M. Kirillov, A. M. Z. Slawin, C. L. C. Warren, *Inorg. Chem.* 60 (2021) 2056.
- [192] X. Sun, K. Yuan, Y. Zhang, *J. Rare Earths* 38 (2020) 801.
- [193] X. Shi, B. Cao, J. Liu, J. Zhang, Y. Du, *Small* 17 (2021) 2005371.
- [194] R. B. Lin, S. Xiang, H. Xing, W. Zhou, B. Chen, *Coord. Chem. Rev.* 378 (2019) 87.
- [195] H. Li, M. Eddaoudi, T. L. Groy, O. M. Yaghi, *J. Am. Chem. Soc.* 120 (1998) 8571.
- [196] O. M. Yaghi, H. Li, *J. Am. Chem. Soc.* 118 (1996) 295.
- [197] O. M. Yaghi, C. E. Davis, G. Li, H. Li, *J. Am. Chem. Soc.* 119 (1997) 2861.
- [198] H. Li, C. E. Davis, T. L. Groy, D. G. Kelley, O. M. Yaghi, *J. Am. Chem. Soc.* 120 (1998) 2186.
- [199] M. Dincă, A. Dailly, Y. Liu, C. M. Brown, D. A. Neumann, J. R. Long, J.

- Am. Chem. Soc. 128 (2006) 16876.
- [200] L. Schlapbach, A. Züttel, *Nature* 414 (2001) 353.
- [201] M. P. Suh, H. J. Park, T. K. Prasad, D.-W. Lim, *Chem. Rev.* 112 (2012) 782.
- [202] D. Saha, T. Maity, S. Das, S. Koner, *Dalton Trans.* 42 (2013) 13912.
- [203] R. Sahoo, M.C. Das, *Coord. Chem. Rev.* 442 (2021) 213998.
- [204] D.J. Tranchemontagne, J.L. Mendoza-Cortés, M. O’Keeffe, O.M. Yaghi, *Chem. Soc. Rev.* 38 (2009) 1257.
- [205] M. Eddaoudi, D.B. Moler, H. Li, B. Chen, T.M. Reineke, M. O. Keeffe, O.M. Yaghi, *Acc. Chem. Res.* 34 (2001) 319.
- [206] S. N. Zhao, G. Wang, D. Poelman, P. Van Der Voort, *Materials* 11 (2018) 572.
- [207] B. Yan, *Inorg. Chem. Front.* 8 (2021) 201.
- [208] K. Binnemans, *Chem. Rev.* 109 (2009) 4283.
- [209] J.C. Bünzli, *Chem. Rev.* 110 (2010) 2729.
- [210] A.K. Das, M. Das, CBS Publishers and Distributors Pvt. Ltd., New Delhi, 2014.
- [211] J.C. Bünzli, C. Piguet, *Chem. Soc. Rev.* 34 (2005) 1048.
- [212] S. Eliseeva, J. Bünzli, *New J Chem.* 35 (2011) 1165.
- [213] E.G. Moore, A.P. Samuel, K.N. Raymond, *Acc. Chem. Res.* 42 (2009) 542.

- [214] T. Gorai, W. Schmitt, T. Gummlaugsson, *Dalton Trans.* 50 (2021) 770.
- [215] M. Sadakiyo, T. Yamada, H. Kitagawa, *J. Am. Chem. Soc.* 131(2009) 9906.
- [216] M. Sadakiyo, T. Yamada, H. Kitagawa, *ChemPlusChem* 81 (2016) 691.
- [217] V. G. Ponomareva, K. A. Kovalenko, A. P. Chupakhin, D. N. Dybtsev, E. S. Shutova, V. P. Fedin, *J. Am. Chem. Soc.* 134 (2012) 15640.
- [218] W. J. Phang, W. R. Lee, K. Yoo, D. W. Ryu, B. Kim, C. S. Hong, *Angew. Chem. Int. Ed.* 53 (2014) 8383.
- [219] F. Yang, G. Xu, Y. Dou, B. Wang, H. Zhang, H. Wu, W. Zhou, J. R. Li, B. Chen, *Nat. Energy* 2 (2017) 877.
- [220] S. E. Rogers, A. R. Ubbelohde, *Trans. Faraday Soc.* 46 (1950) 1051.
- [221] K. D. Kreuer, *Chem. Mater.* 8 (1996) 610.
- [222] H. Iwahara, *Solid State Ion.* 9 (1996) 86.
- [223] D. W. Lim, H. Kitagawa, *Chem. Rev.* 120 (2020) 8416.
- [224] M. Sadakiyo, T. Yamada, H. Kitagawa, *J. Am. Chem. Soc.* 131 (2009) 9906.
- [225] Y. S. Wei, X. P. Hu, Z. Han, X. Y. Dong, S. Q. Zang, T. C. W. Mak, *J. Am. Chem. Soc.* 139 (2017) 3505.
- [226] N. T. T. Nguyen, H. Furukawa, F. Gandara, C. A. Trickett, H. M. Jeong, K. E. Cordova, O. M. Yaghi, *J. Am. Chem. Soc.* 137 (2015) 15394.
- [227] S. S. Nagarkar, S. M. Unni, A. Sharma, S. Kurungot, S. K. Ghosh, *Angew.*

- Chem. Int. Ed. 53 (2014) 2638.
- [228] K. Otsubo, S. Nagayama, S. Kawaguchi, K. Sugimoto, H. Kitagawa, J. Am. Chem. Soc. 2 (2022) 109.
- [229] V. G. Ponomareva, K. A. Kovalenko, A. P. Chupakhin, D. N. Dybtsev, E. S. Shutova, V. P. Fedin, J. Am. Chem. Soc. 134 (2012) 15640.
- [230] W. J. Phang, W. R. Lee, K. Yoo, D. W. Ryu, B. Kim, C. S. Hong, Angew. Chem. Int. Ed. 53 (2014) 8383.
- [231] D. Umeyama, S. Horike, M. Inukai, Y. Hijikata, S. Kitagawa, Angew. Chem. Int. Ed. 50 (2011) 11706.
- [232] W. Chen, S. Horike, D. Umeyama, N. Ogiwara, T. Itakura, C. Tassel, Y. Goto, H. Kageyama, S. Kitagawa, Angew. Chem., Int. Ed. 55 (2016) 5195.
- [233] J. Lee, D. W. Lim, S. Dekura, H. Kitagawa, W. Choe, ACS Appl. Mater. Interfaces 11 (2019) 12639.
- [234] J. M. Taylor, S. Dekura, R. Ikeda, H. Kitagawa, Chem. Mater. 27 (2015) 2286.
- [235] J. M. Taylor, T. Komatsu, S. Dekura, K. Otsubo, M. Takata, H. Kitagawa, J. Am. Chem. Soc. 137 (2015) 11498.
- [236] M. Inukai, S. Horike, T. Itakura, R. Shinozaki, N. Ogiwara, D. Umeyama, S. Nagarkar, Y. Nishiyama, M. Malon, A. Hayashi, J. Am. Chem. Soc. 138 (2016) 8505.

Chapter 2



**Robust Gd-MOF for
heterogeneous catalytic
O-arylation reaction**

2.1 Introduction

Diarylethers are very important structural motifs in a large number of natural biologically active compounds, for example, K13, perrottetin, teicoplanin and vancomycin, as well as in polymer industries [1]. Traditionally, diaryl ethers are synthesized employing copper (I) catalyzed Ullmann type cross-coupling reactions from aryl iodide or bromide and phenols. However, drastic reaction condition such as very high temperature (125-200°C), requirement of stoichiometric amount of catalyst, purification problem and low to moderate yields limits its utility [2]. Therefore, search of new methods for the synthesis of diaryl ethers under milder condition are of interest [3, 4]. Later Buchwald, Hartwig and Beller have developed several palladium catalyzed processes for C–O cross–coupling reactions under mild condition [5]. Despite being highly efficient, palladium catalyzed methods have limited prospect due to high cost and toxicity of palladium and also requirement of suitable ligands in the process [6]. Under continuing investigation, it was observed that MOF, a porous solid material particularly demonstrates excellent catalytic efficacy [7, 8].

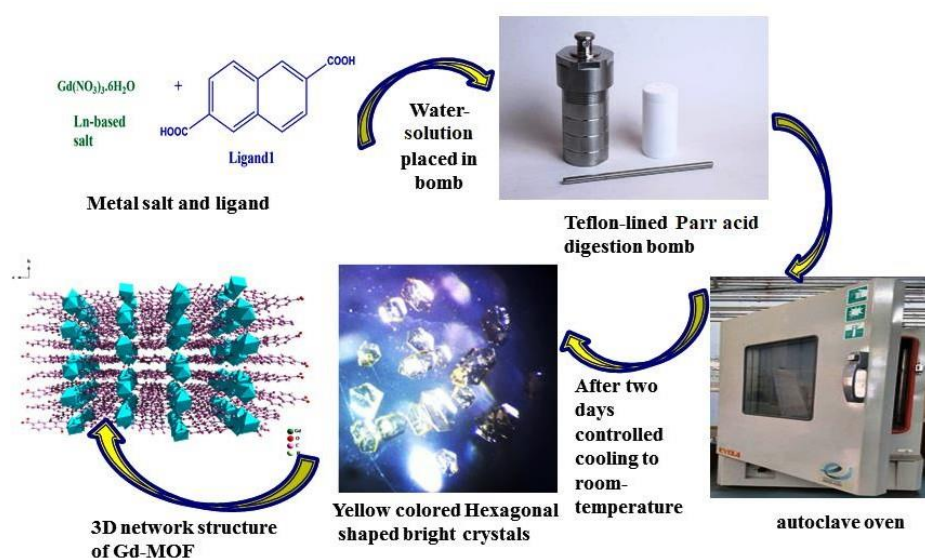
In last two decades MOFs attracted immense attention in heterogeneous catalysis research. Metal centers of the network, especially, coordinatively unsaturated metal centers present in the catalyst or such center generated *in situ* in reaction condition act as active site in catalysis [9]. It is also reported the use of porous MOFs as heterogeneous catalysts in a variety of catalyzed organic reactions such as C–C, C–N, C–O coupling reactions, aldol condensation, hydrogenation, epoxidation [10–13] etc. Many lanthanide-based metal-organic framework compounds have been synthesized mainly to study their magnetic and photo-luminescence property; however, their catalytic efficacy is not so well explored till date [14].

Few years ago, a fascinating Gd₂₆ cluster-based 3D framework compound, possessing spherical “CO₃@Gd₂₆” shell efficiently catalyzes heterogeneous

Chapter 2 Robust Gd-MOF for heterogeneous catalytic O-arylation reaction

epoxidation of olefinic substrates including α , β -unsaturated ketones [15–17]. Further exploration of gadolinium (III) carboxylate system availing hydrothermal synthetic route has afforded a structurally robust and thermally stable new three-dimensional MOF compound.

Hence in this study attempt has been made to synthesize a Gd–MOF (Scheme-2.1) based heterogeneous catalyst that can be used in catalytic O-arylation reaction. Notably, the catalyst efficiently catalyzed O-arylation reaction between substituted phenols and bromoarenes.



Scheme-2.1 Synthetic route for the preparation of Gd-MOF.

2.2 Experimental

2.2.1 Materials

Gadolinium (III) nitrate hexahydrate (99.9% pure), 2,6-naphthalenedicarboxylic acid (H₂NDC) (99%) were purchased from Sigma-Aldrich and used as received without further purification. Cesium carbonate (99%), substituted phenols, other chemicals and solvents

Chapter 2 **Robust Gd-MOF for heterogeneous catalytic O-arylation reaction**

(analytical grade) were procured from Merck (India). Solvents were distilled and dried before use.

2.2.2 Physical Measurements

IR spectra were recorded in KBr pellet (4000-400 cm^{-1}) on a Perkin-Elmer Spectrum II FTIR spectrometer. Elemental analysis was performed using a Vario-Micro V2.0.11 elemental (CHNSO) analyzer. Thermo-gravimetric (TGA) analysis was done on a Perkin-Elmer Pyris Diamond TG unit. The heating rate was programmed at $10^\circ\text{C}/\text{min}$ with a protecting stream of N_2 flow 20 mL/min. Powder X-ray diffraction (PXRD) pattern of samples were recorded with Bruker D8 Conquest X-ray diffractometer using $\text{Cu-K}\alpha$ radiation ($\lambda = 1.54056 \text{ \AA}$) at room temperature. Diffraction lines were measured in $2\theta = 5\text{-}50^\circ$ range with scanning speed of $0.1^\circ/\text{step}/\text{sec}$. Mass spectra were measured on a Waters XEVO-G2QTOF#YCA351 high resolution mass spectrometer. $^1\text{H-NMR}$ spectra were measured on a 300 MHz Bruker Advance DPX-300 NMR spectrometer.

2.2.3 Synthesis of $\{[\text{Gd}_4(\text{NDC})_6(\text{H}_2\text{O})_6]\cdot 2\text{H}_2\text{O}\}_n$ (MOF-1)

A salt of gadolinium nitrate hexahydrate (0.25 mmol, 0.112g) was dissolved in 2 ml of water and separately a 3 ml solution of 2,6-naphthalenedicarboxylic acid (0.25 mmol, 0.027g) in water was prepared. After mixing these two solutions properly, the resulting mixture was then placed in a 15 mL teflon-lined Parr acid digestion bomb and kept at 170°C for two days. After two days, the solution was allowed to cool down slowly at the rate of $10^\circ\text{C}/\text{h}$ to room temperature. Hexagonal-shaped yellow colored crystals were collected and washed with distilled water and dried in air (yield 60% based on metal). Phase purity was verified through elemental analysis and X-ray powder diffraction analysis. Anal. Calcd. for $\text{C}_{72}\text{H}_{48}\text{O}_{32}\text{Gd}_4$ (FW= 2054.17), C, 42.06, H, 2.33%, Found C, 42.5, H, 2.3%. Selected IR peaks (KBr pellet, ν , cm^{-1}) (**Figure 2.1**) 1600, 1527 [$\nu_{as}(\text{CO}_2^-)$],

1406 [$\nu_s(\text{CO}^2)$], 1334 [$\nu_s(\text{C-O})$], 1100-785 [$\nu(\text{C-H aromatic in plane bending})$], 3300 s.br [$\nu(\text{O-H})$].

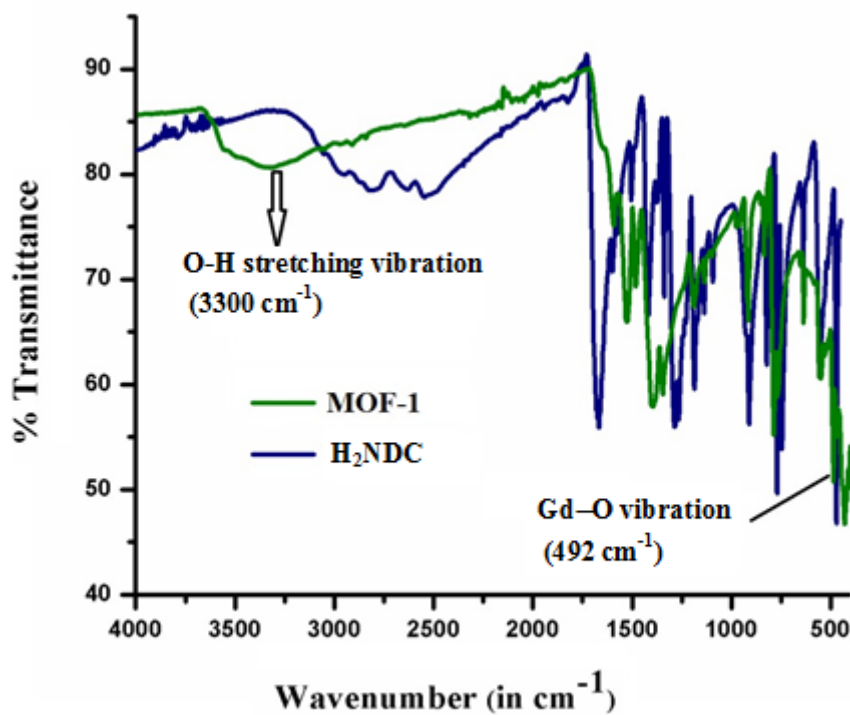


Figure 2.1 FT-IR spectra of the ligand (H₂NDC) and the MOF-1.

2.2.4 X-ray crystallography

A single crystal suitable for X-ray diffraction was selected from bulk under a microscope and carefully glued to a thin glass fiber. X-ray diffraction data of MOF-1 was collected on Microfocus Bruker D8 Conquest X-ray single crystal diffractometer using graphite-monochromated Mo-K α radiation ($\lambda = 0.71073 \text{ \AA}$). Cell refinement and determination of the integrated intensities were performed with the SAINT [18] software package using a narrow frame integration algorithm. An empirical absorption correction (SADABS) [18] was applied. The structure was solved by direct methods and refined by full-matrix least squares on

Chapter 2 **Robust Gd-MOF for heterogeneous catalytic O-arylation reaction**

F^2 using the SHELXL-2014 package [19], SHELXL 2018 [20] and Olex2 program [21]. Non-hydrogen atoms were refined with anisotropic thermal parameters. All other hydrogen atoms were placed in their geometrically idealized positions, except for the hydrogen atoms of the coordinated water molecules (O18 and O25) in MOF-1 which could not be located in the Fourier map. Successful convergence was indicated by the maximum shift/error of 0.001 for the last cycle of the least squares refinement. All calculation and molecular graphics were performed with WinGX [22], Diamond [23], Mercury [24] and PLATON [25]. A summary of the crystallographic data and the relevant structural refinement parameters for MOF-1 is given in Table 2.1. CCDC-2013484 contains the supplementary crystallographic data for this paper. These data can be obtained free of charge from Cambridge Crystallographic Data Centre via www.ccdc.cam.ac.uk/data_request/cif.

Table 2.1 Crystal data and refinement parameters of MOF-1

Formula	$C_{72}H_{52}O_{32}Gd_4$
Formula Weight	2058.17
Crystal System	Monoclinic
Space Group	$P2_1/n$
a (Å)	17.0880(13)
b (Å)	15.2662(12)
c (Å)	25.0888(19)
α (°)	90
β (°)	106.260(2)
γ (°)	90
V (Å ³)	6283.1(8)
Z	4
D_{calc} (gcm ⁻³)	2.171
μ (mm ⁻¹)	4.271
θ Range (°)	1.8-27.1

Chapter 2 **Robust Gd-MOF for heterogeneous catalytic O-arylation reaction**

Intervals of reflection indices	-21<=h<=21, -19<=k<=19, -32<=l<=32
Reflections measured	89844
R_{int}	0.056
Unique data	13844
R indices (all data)	$R_1 = 0.056$, $wR_2 = 0.0872$
Final R indices [$I > 2\sigma(I)$]	0.0385
Data with $I > 2\sigma(I)$	10704
R_I ($I > 2\sigma(I)$)	0.0385
$wR_2(I > 2\sigma(I))$	0.0872
$F(000)$	3968
Goodness-of-Fit on F^2	1.072

$$RI = \sum ||F_o| - |F_c|| / \sum |F_o|, wR2 = \{ \sum [w(F_o^2 - F_c^2)^2] / \sum w(F_o^2) \}$$

2.2.5 General procedure for catalytic reactions

0.151 g (1 mmol) of *p*-nitrobromobenzene and 0.103 g (1 mmol) of *p*-cresol added with 0.487 g (1.5 mmol) solid cesium carbonate in 3 mL dehydrated dimethylformamide (DMF) solvent in a 15 mL round-bottom flask. 0.005 g of MOF-1 was added to the reaction medium and stirred under continuous heating at 80°C for seven hours. The conversion of the reaction was monitored by thin layered chromatography (TLC) method. After completion of the reaction mixture, it was cooled to room temperature and purged on ice cold water. The aqueous layer was extracted three times with ethylacetate (6 mL). Combined organic layer thus collected was washed with brine solution, dried over anhydrous sodium sulfate and concentrated in vacuum. The residue thus collected was further purified by column chromatography on silica-gel (60-120 mesh) and was eluted with n-hexane/ethyl acetate mixture to get the desired product. The product analyzed through ¹H-NMR, elemental analysis and compared with the literature data.

2.3 Results and discussion

2.3.1 Description of the X-ray crystal structure of MOF-1

Single-crystal X-ray structure analysis reveals that MOF-1 is crystallized in monoclinic $P2_1/n$ space group with $Z=4$. Molecular structure of MOF-1 consists of tetra-nuclear homometallic gadolinium moieties. Molecular structure of the tetra-nuclear unit with atom numbering scheme of $\{[\text{Gd}_4(\text{NDC})_6(\text{H}_2\text{O})_6] \cdot 2\text{H}_2\text{O}\}_n$ (MOF-1) is shown in **Figure 2.2**. (thermal ellipsoid structure with 50% probability is given in **Figure 2.3**). The selected bond distances and angles and Gd-Gd bond distances are summarized in **Table 2.2** and **Table 2.3** respectively. The structure contains four Gd-metal centers of which Gd1, Gd4 (nine coordination) and Gd2, Gd3 (eight-coordinated) are same in coordination mode.

Table 2.2 Bond distances (Å) and angles (°) in MOF-1

Atoms	Distance	Atoms	Distance
Gd1 - O12	2.386(4)	Gd2 - O7	2.444(5)
Gd1 - O14	2.461(4)	Gd2 - O8	2.360(4)
Gd1 - O16	2.370(4)	Gd2 - O18	2.852(9)
Gd1 - O20	2.344(4)	Gd2 - O10 ^a	2.382(4)
Gd1 - O23	2.328(3)	Gd2 - O29 ^a	2.394(4)
Gd1 - O24	2.477(5)	Gd3 - O9	2.443(4)
Gd1 - O25	2.695(4)	Gd3 - O11	2.383(4)
Gd1-O17	2.911(4)	Gd3 - O22	2.367(4)
Gd1 - O26	2.360(4)	Gd3 - O25	2.718(4)
Gd2 - O1	2.353(4)	Gd3 - O27	2.322(4)
Gd2 - O3	2.362(4)	Gd3 - O28	2.381(4)
Gd2 - O6	2.303(4)	Gd4 - O15	2.361(4)
Gd3 - O30	2.529(5)	Gd4 - O17	2.325(4)
Gd3 - O4 ^b	2.325(4)	Gd4 - O19	2.499(5)
Gd4 - O2	2.341(4)	Gd4 - O21	2.369(4)
Gd4 - O5	2.335(4)	Gd4-O20	2.887(4)
Gd4 - O13	2.414(4)	Gd4-O18	2.907(9)

Atoms	Angle	Atoms	Angle
O12 - Gd1 - O14	129.63(14)	O3 - Gd2 - O6	128.96(14)
O12 - Gd1 - O16	81.21(14)	O3 - Gd2 - O7	139.93(14)
O12 - Gd1 - O20	75.78(14)	O3 - Gd2 - O8	79.13(14)
O12 - Gd1 - O23	136.77(12)	O3 - Gd2 - O18	61.82(18)
O12 - Gd1 - O24	138.90(13)	O3 - Gd2 - O10 ^a	127.08(14)
O12 - Gd1 - O25	66.70(12)	O3 - Gd2 - O29 ^a	80.94(14)
O12 - Gd1 - O26	78.65(14)	O6 - Gd2 - O7	74.29(14)
O14 - Gd1 - O16	76.77(14)	O6 - Gd2 - O8	80.31(15)
O14 - Gd1 - O20	81.38(12)	O6 - Gd2 - O18	67.22(19)
O14 - Gd1 - O23	81.32(12)	O6 - Gd2 - O10 ^a	91.28(13)
O14 - Gd1 - O24	71.54(14)	O6 - Gd2 - O29 ^a	144.22(16)
O14 - Gd1 - O25	136.57(11)	O7 - Gd2 - O8	140.87(14)
O14 - Gd1 - O26	144.50(15)	O7 - Gd2 - O18	124.6(2)
O16 - Gd1 - O20	125.65(14)	O7 - Gd2 - O10 ^a	75.75(14)
O16 - Gd1 - O23	78.02(13)	O7 - Gd2 - O29 ^a	69.94(14)
O16 - Gd1 - O24	139.52(14)	O8 - Gd2 - O18	68.65(19)
O16 - Gd1 - O25	65.90(12)	O8 - Gd2 - O10 ^a	75.57(14)
O16 - Gd1 - O26	135.08(13)	O8 - Gd2 - O29 ^a	130.11(14)
O20 - Gd1 - O23	145.87(14)	O10 ^a - Gd2 - O18	140.56(18)
O20 - Gd1 - O24	73.76(14)	O18 - Gd2 - O29 ^a	135.35(17)
O20 - Gd1 - O25	138.64(13)	O10 ^a - Gd2 - O29 ^a	81.16(12)
O20 - Gd1 - O26	87.25(13)	O9 - Gd3 - O11	75.14(14)
O23 - Gd1 - O24	72.93(12)	O9 - Gd3 - O22	148.60(15)
O23 - Gd1 - O25	70.25(12)	O9 - Gd3 - O25	135.43(12)
O23 - Gd1 - O26	90.04(13)	O9 - Gd3 - O27	83.96(13)
Atoms	Angle	Atoms	Angle
O22 - Gd3 - O27	90.63(13)	O24 - Gd1 - O25	126.23(13)
O22 - Gd3 - O28	75.83(14)	O24 - Gd1 - O26	73.00(14)
O22 - Gd3 - O30	75.20(16)	O25 - Gd1 - O26	69.29(12)
O4 ^b - Gd3 - O22	85.88(13)	O1 - Gd2 - O3	76.40(14)
O25 - Gd3 - O27	70.50(13)	O1 - Gd2 - O6	84.27(13)
O25 - Gd3 - O28	64.37(12)	O1 - Gd2 - O7	74.33(14)
O25 - Gd3 - O30	128.88(15)	O1 - Gd2 - O8	132.36(14)
O11 - Gd3 - O30	140.06(15)	O1 - Gd2 - O18	63.8(2)
O4 ^b - Gd3 - O11	126.45(14)	O1 - Gd2 - O10 ^a	149.85(15)
O22 - Gd3 - O25	69.64(12)	O1 - Gd2 - O29 ^a	85.18(13)
O11 - Gd3 - O22	134.01(13)	O9 - Gd3 - O28	128.21(14)
O11 - Gd3 - O25	64.59(12)	O9 - Gd3 - O30	73.58(16)
O11 - Gd3 - O27	78.54(14)	O4 ^b - Gd3 - O9	81.70(13)
O11 - Gd3 - O28	80.85(14)	O4 ^b - Gd3 - O25	137.85(13)

O2 - Gd4 - O5	87.10(13)	O27 - Gd3 - O28	134.84(13)
O2 - Gd4 - O13	149.89(15)	O27 - Gd3 - O30	74.08(16)
O2 - Gd4 - O15	75.91(15)	O4 ^b - Gd3 - O27	145.93(16)
O2 - Gd4 - O17	91.42(13)	O28 - Gd3 - O30	138.69(15)
O2 - Gd4 - O19	75.28(16)	O4 ^b - Gd3 - O28	76.89(14)
O2 - Gd4 - O21	127.15(14)	O4 ^b - Gd3 - O30	72.26(16)
O5 - Gd4 - O13	84.94(13)	O13 - Gd4 - O15	129.24(14)

Symmetry element ^a= -1+x,y,z, ^b= 1/2+x,3/2-y,1/2+z

Table 2.3 Gd-Gd distances (Å) in the MOF-1

Atoms	Gd2-Gd3	Gd3-Gd1	Gd1-Gd4	Gd4-Gd2
Distance	4.0897(6)	4.8112(6)	4.0752(6)	5.0805(7)

Along with this, six coordinated water molecules and two lattice water molecules are present in crystal structure. Two different types of geometries like tricapped-trigonal prism and bicapped-trigonal prismatic polyhedron are observed in MOF-1. Among four different Gd metal centers, Gd1 center (**Figure 2.4a**) is coordinated by five carboxylato oxygen atom (O14, O23, O26, O12, O20) of five 2,6-naphthalenedicarboxylate (NDC²⁻) ligand in monodentate μ_1 (O) mode (**Figure 2.5a**), two oxygen atoms (O16 and O17) in chelate- bidentate μ_1 (O,O) mode (**Figure 2.5b**), another two oxygen atoms from coordinated water molecules (O24 and O25) while ninth position is satisfied by an oxygen (O17) atom from carboxylato group through semi-coordination (long Gd–O bond = 2.911Å) [26]. Similarly, all coordination positions of Gd4 center are occupied by nine oxygen atoms (**Figure 2.4b**). Of which, five are occupied by oxygen atoms (O5, O13, O17, O15 and O2) from five 2,6-naphthalenedicarboxylate (NDC²⁻) ligand in monodentate mode (**Figure 2.5a**) another two oxygen atoms (O20 and O21) from one 2,6-naphthalenedicarboxylate (NDC²⁻) in a bidentate-chelate mode (**Figure 2.5b**) and rest two coordination positions are occupied by oxygen atoms of water molecule. However, Gd4–O18 (2.907Å) and Gd4–O20 (2.887Å) bond lengths are

Chapter 2 Robust Gd-MOF for heterogeneous catalytic O-arylation reaction

rather longer than normal Gd–O coordination bond [26]. Gd1 is situated between Gd4 and Gd3 centers, where Gd1 and Gd4 are bridged by *syn-syn* μ_2 - (O,O') and *syn-anti* μ_2 - (O,O') bridging fashion through NDC²⁻ ligand (Figure 2.5c, d) and Gd1 is connected to Gd3 center by bridging carboxylate (O22, O23, O26, O27) and water oxygen (O25) atoms. Both Gd1 and Gd4 displayed distorted tricapped-trigonal prism geometry (Figure 2.6a, e and 2.6b, f).

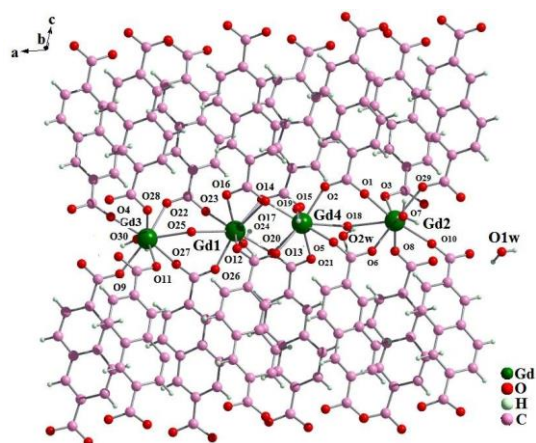


Figure 2.2 Tetra-nuclear unit of MOF-1 with atom numbering scheme.

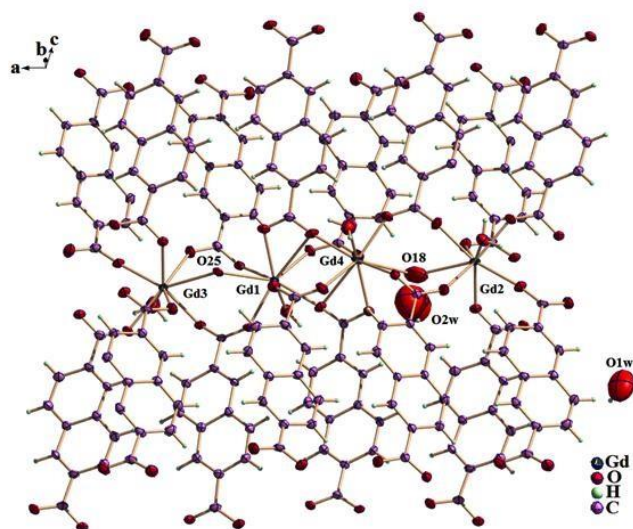


Figure 2.3 Thermal ellipsoid structure of MOF-1 with 50% probability level.

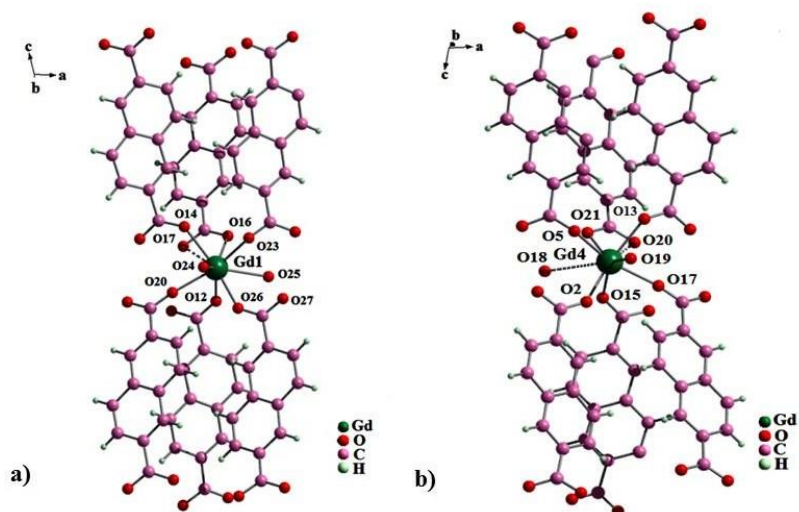


Figure 2.4 Coordination environment around a) Gd1 and b) Gd4 (nine coordination).

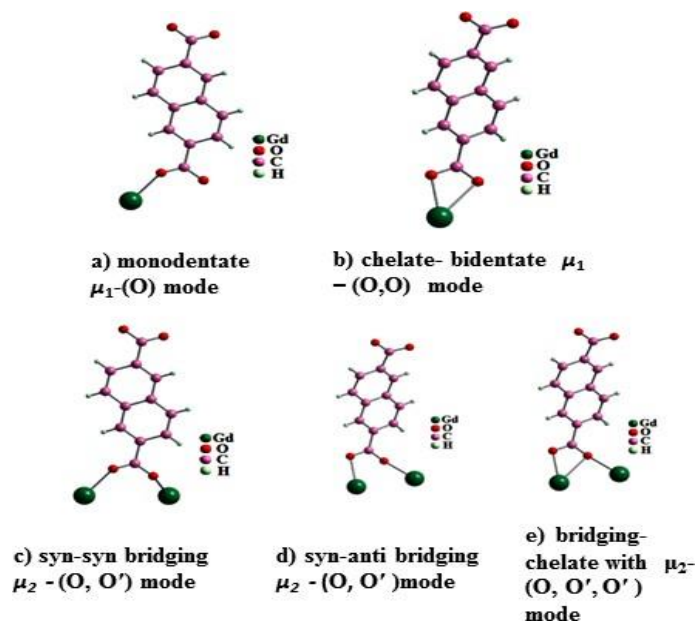


Figure 2.5 Various coordination modes of 2,6-naphthalenedicarboxylate(NDC²⁻) ligand.

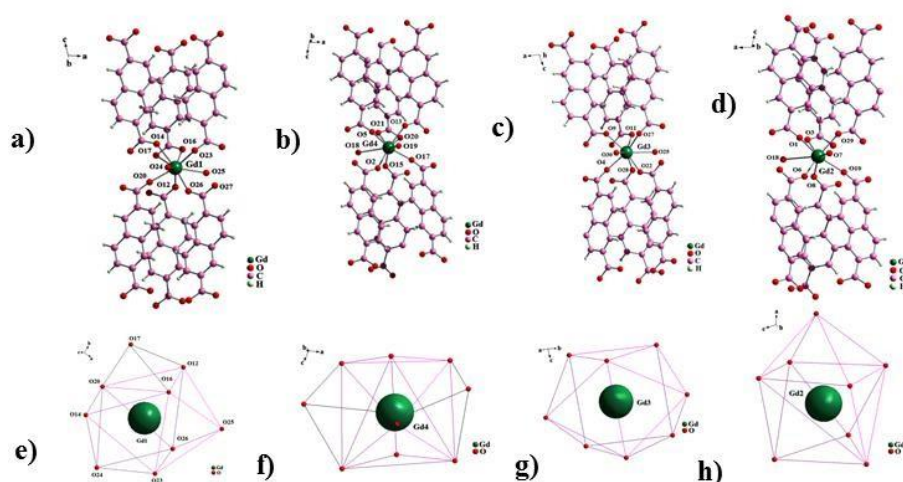


Figure 2.6 Coordination mode of different Gd-moieties; a) Gd1 b) Gd4 c) Gd3 and d) Gd2. Distorted tricapped trigonal prismatic geometry of e) Gd1 and f) Gd4 and distorted bicapped trigonal prism geometry of g) Gd3 and h) Gd2.

Coordination positions of Gd2 and Gd3 are satisfied by six oxygen atoms (O1, O3, O29, O10, O8, O6 for Gd2 and O9, O11, O27, O22, O28, O4 for Gd3 respectively) of six NDC²⁻ in monodentate fashion and one from coordinated water molecule (O7 for Gd2 and O30 for Gd3) and another oxygen from bridging water molecule (O18 and O25 for Gd2 and Gd3, respectively) which form distorted bicapped-trigonal prismatic polyhedrons (**Figure 2.6c, g** and **Figure 2.6d, h**). Both Gd2 and Gd3 are eight-coordinated and feature [GdO₈] chromophores (**Figure 2.7a, b**).

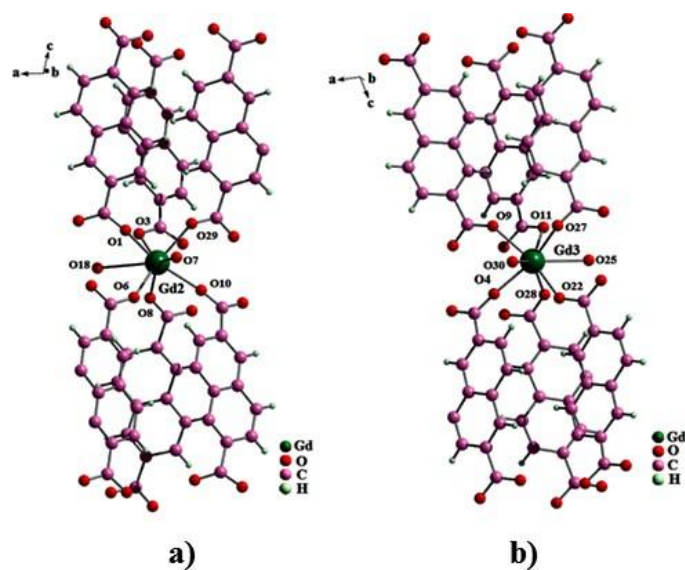


Figure 2.7 Coordination environments around a) Gd2 and b) Gd3 (8-coordination).

Gadolinium ions are inter-connected with each other through bridging carboxylato groups in *syn-syn*, *syn-anti* fashion and chelation in $\mu_2-(O,O',O')$ bridging mode (Figure 2.5), and alternate bridging water molecule to form a secondary building unit. Tetra-nuclear units are connected through oxygen atoms of NDC^{2-} ligand to form 1D chain along the crystallographic *a*-axis (Figure 2.8a). 1D chain is further connected by NDC^{2-} to construct 2D layers along crystallographic *ac*-plane (Figure 2.8b). Finally, 2D layers are again pillared 2,6-naphthalenedicarboxylate ligand (NDC^{2-}) to give rise to a 3D network structure (Figure 2.9a, b).

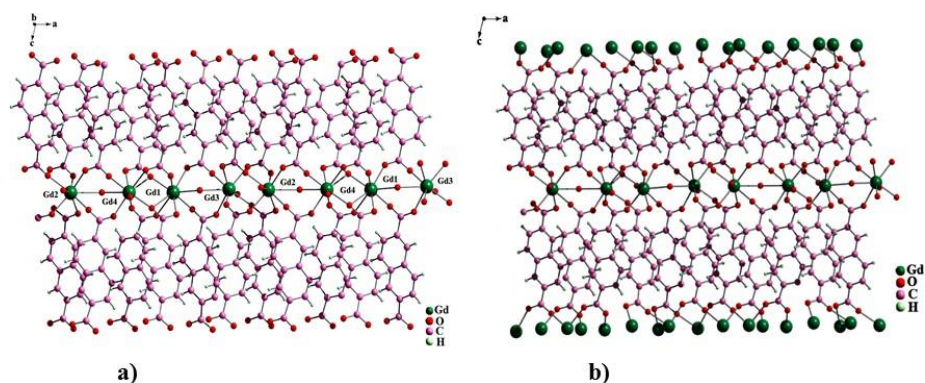


Figure 2.8 Two-dimensional connectivity of MOF-1.

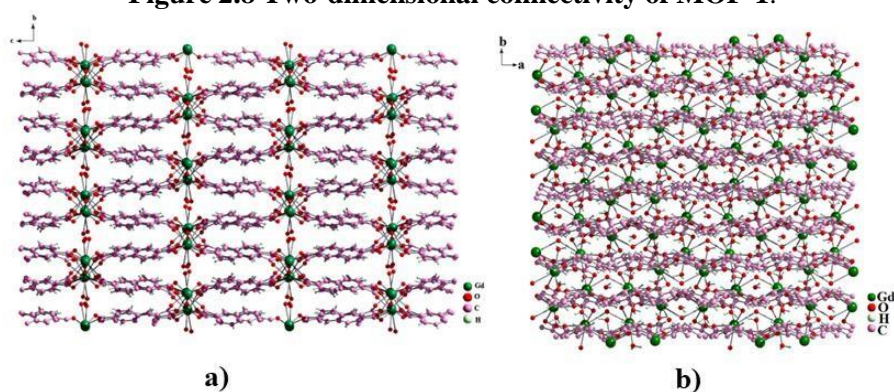


Figure 2.9 3D network structure of MOF-1; a) along crystallographic a -axis; b) along b -axis.

2.3.2 PXRD study

To confirm the phase purity of the bulk material of MOF-1, powder X-ray diffraction (PXRD) measurements were carried out. Comparison of experimental and simulated (from single crystal data) PXRD patterns (**Figure 2.10**) showed that all the major diffraction lines of experimental PXRD of MOF-1 matched well with those of simulated ones, indicating its reasonable crystalline phase purity. PXRD patterns of the metal organic framework are retained upon prolonged storage (at least 6 months). No significant changes in the PXRD patterns are observed upon

Chapter 2 *Robust Gd-MOF for heterogeneous catalytic O-arylation reaction*

exposure to various solvents such as water, methanol, ethanol, DMF and DMA (Figure 2.11). To study this, MOF-1 was kept deep solvents as suspension and PXRD had been recorded. All these suggest the robustness of the framework of MOF-1.

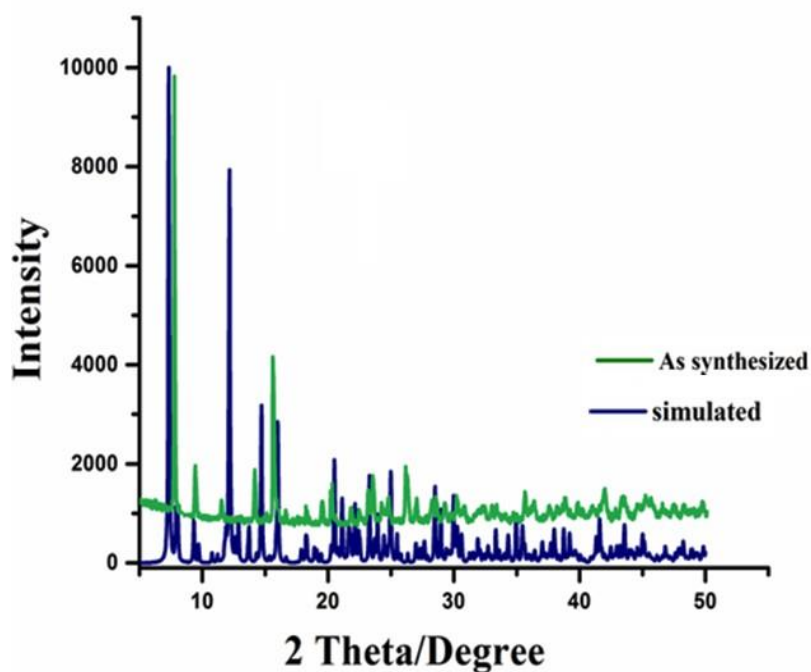


Figure 2.10 Powder X-ray diffraction pattern of MOF-1 simulated (blue) and measured (green).

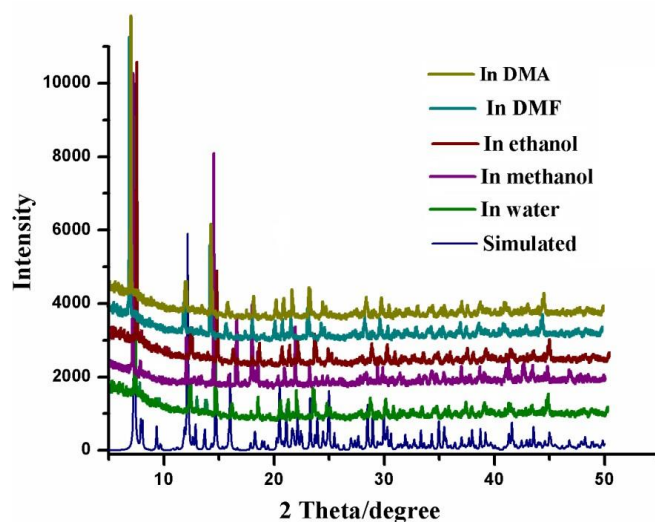


Figure 2.11 PXRD patterns check in different solvents. (Bruker D8 Conquest PXRD, scanning speed of 0.1° step /sec, temperature- 298 K).

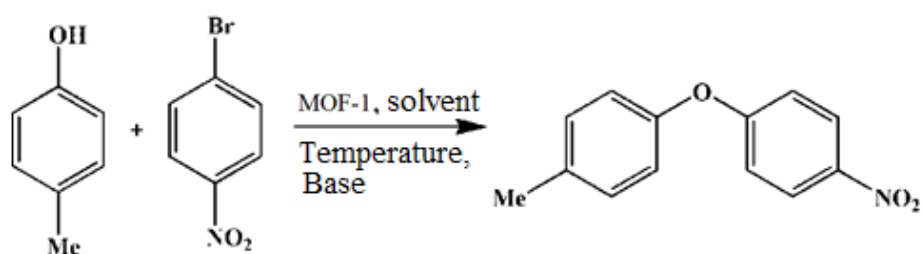
2.3.3 Catalytic activity study

To start with, optimization of O-arylation reactions was undertaken using *p*-cresol and *p*-nitrobromobenzene as substrate under various reaction conditions catalyzed by MOF-1 (Table 2.4). It has been explored the effect of solvents, since solvent plays important role in O-arylation reactions. Among various solvents used (entries 1-7), highest yield of desired product is obtained in DMF (entry 14). Generally, O-arylation reactions show better reactivity with Cs_2CO_3 (base) than with K_2CO_3 or Na_2CO_3 due to higher solubility and fine powder form of Cs_2CO_3 . In present case also Cs_2CO_3 becomes the best choice as a base among others (entries 8-12, 14). Isolated yield increases sharply with the increase of reaction temperature (entries 14, 15-17), however, do not significantly improve beyond 80°C . Catalyst concentration of a catalytic reaction is another very important factor to investigate. Accordingly, the O-arylation reaction was carried out in the presence of 0.01, 0.02, 0.025 and 0.05 mol% of the catalyst (entries 18-21). 0.025

Chapter 2 Robust Gd-MOF for heterogeneous catalytic O-arylation reaction

mol% of catalyst has shown maximum conversion in 7 hours. Besides, increasing of catalyst concentration beyond 0.05 mol% no noticeable increase in yield was observed. No reaction was occurred in the absence of catalyst in 7 hours (entry 13). In addition, a mixture of gadolinium nitrate salt and 2,6-naphthalenedicarboxylic acid (as mixture in stoichiometric ratio 4:7), and neat gadolinium nitrate salt have been tested as catalyst but only moderate to low conversion was observed (entry 22 and 23). Thus, the optimum condition of the catalytic reaction was as follows: Cs_2CO_3 (base), DMF (solvent), 0.025 mol% catalyst and reaction temperature 80 °C.

Table 2.4 Optimization of reaction condition^a



Entry	Catalyst	Base	Solvent	Isolated Yield ^b (%)
1	MOF-1	Cs_2CO_3	Ethanol	39
2	MOF-1	Cs_2CO_3	DMSO	79
3	MOF-1	Cs_2CO_3	Toluene	18
4	MOF-1	Cs_2CO_3	Acetonitrile	36
5	MOF-1	Cs_2CO_3	Methanol	64
6	MOF-1	Cs_2CO_3	Ethyleneglycol	58
7	MOF-1	Cs_2CO_3	Dioxane	42
8	MOF-1	K_2CO_3	DMF	87
9	MOF-1	Na_2CO_3	DMF	84
10	MOF-1	CH_3COONa	DMF	trace
11	MOF-1	t-BuOK	DMF	38
12	MOF-1	DABCO	DMF	29

13	–	Cs ₂ CO ₃	DMF	-
14	MOF-1	Cs ₂ CO ₃	DMF	94
15	MOF-1	Cs ₂ CO ₃	DMF	27 ^c
16	MOF-1	Cs ₂ CO ₃	DMF	69 ^d
17	MOF-1	Cs ₂ CO ₃	DMF	95 ^e
18	MOF-1	Cs ₂ CO ₃	DMF	49 ^f
19	MOF-1	Cs ₂ CO ₃	DMF	88 ^g
20	MOF-1	Cs ₂ CO ₃	DMF	94 ^h
21	MOF-1	Cs ₂ CO ₃	DMF	94 ⁱ
22	Gd(NO ₃) ₃ ·xH ₂ O + NDC	Cs ₂ CO ₃	DMF	41
23	Gd(NO ₃) ₃ ·xH ₂ O	Cs ₂ CO ₃	DMF	29

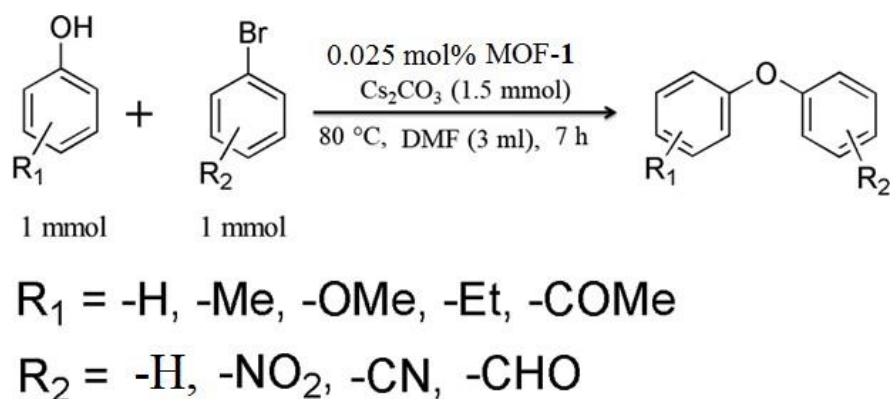
^aReaction conditions, *p*-cresol (1 mmol), *p*-nitrobromobenzene (1 mmol), catalyst (0.025mol%), base (1.5mmol), solvent (3mL) and temperature 80 °C. ^b Isolated yield. ^c Reaction temperature 40 °C. ^d Temperature of the reaction 60 °C. ^eReaction temperature 100 °C. ^f0.01 Mol% MOF-1. ^g0.02 Mol% MOF-1. ^h0.025 Mol% MOF-1. ⁱ0.05Mol% MOF-1.

Under the optimized reaction conditions, the scope and applicability of the coupling reaction using various bromoarenes with substituted phenol to unsymmetrical diaryl ethers were examined (Table 2.5). At first, investigation was carried out using various substitutions (electron donating or withdrawing) on phenol moiety (Table 2.5, entries 1, 2, 5, 10 and 11). Electron donating methyl group containing phenols yield higher quantity of products in comparison to simple phenol. The yield of diaryl ether products is decreased in the order *p*-> *o*->*m*-cresol. It may be realized that methyl substituent at *ortho/para* position affords positive inductive effect and hyper-conjugation effect which increases nucleophilicity of phenolate oxygen atoms, whereas substitution at the *meta* position affords only the positive inductive effect. Between *para* and *ortho* cresol, more steric crowding at *ortho* position might lead to lower yield. Interestingly in case of *p*-methoxyphenol yield is lower compared to *p*-cresol (entries 10 and 16). Though methoxy group has very strong positive resonance effect but it also has

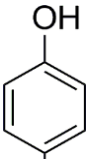
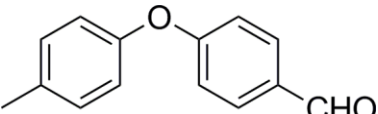
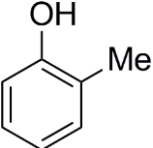
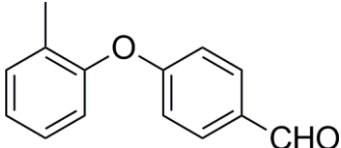
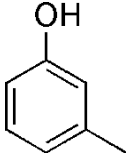
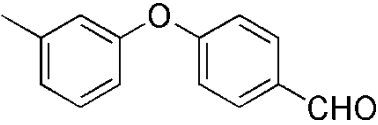
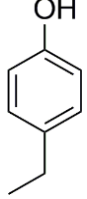
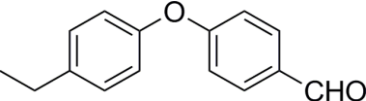
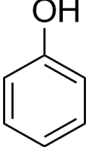
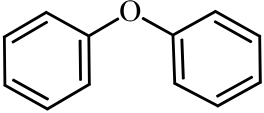
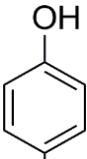
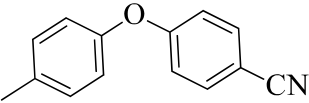
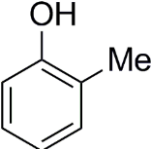
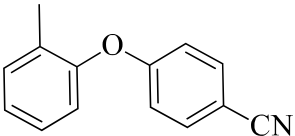
Chapter 2 Robust Gd-MOF for heterogeneous catalytic O-arylation reaction

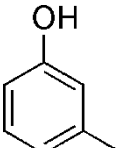
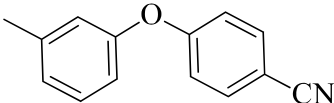
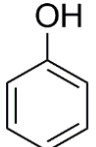
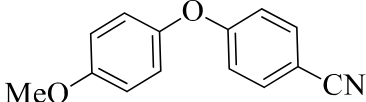
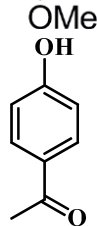
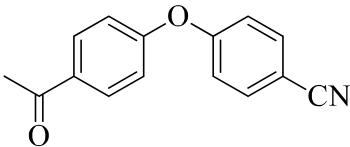
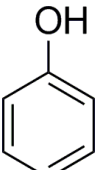
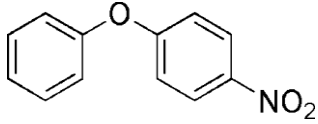
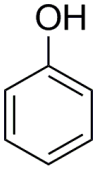
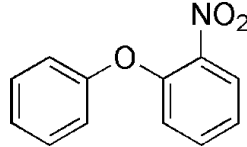
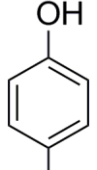
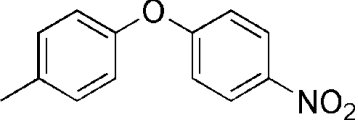
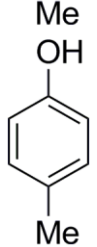
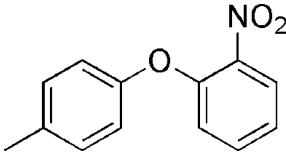
the ability to interact with metal centers [27]. May be due to this reason methoxy group loses its power to increase the nucleophilicity at phenolate oxygen atom. Moreover, the coupling reactions of electron-deficient phenols with aryl halides have been challenging as the corresponding phenolates are weak nucleophile [28]. MOF-1 also activates its catalytic efficiency towards weak nucleophile *e.g.* *p*-hydroxyacetophenone (entry 11). Apart from bromonitrobenzene, bromobenzonitrile and bromobenzaldehyde were also used as electrophile and corresponding products had been obtained in good yield. A representative plot of progress of catalytic reaction is shown in (Figure 2.12).

Table 2.5 O-arylation between substituted bromobenzene with phenols^a

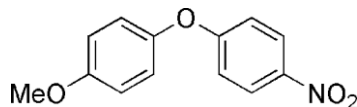
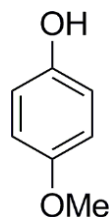


Entry	Aryl alcohol	Product	Isolated Yield ^b (wt%)	TOF ^c (h ⁻¹)
1			84	12.5

2			90	13.4
3			90	13.4
4			85	12.5
5			90	13.4
6			31	4.61
7			91	13.5
8			90	13.4

9			83	12.3
10			84	12.5
11 ^d			39	5.8
12			83	12.35
13			79	11.8
14			93	13.8
15			87	12.9

16



81

12.1

^aReaction condition: Nitroarene (1 mmol), aryl alcohol (1 mmol), Cs₂CO₃ (1.5mmol), MOF-1 as catalyst (0.025 mol %), DMF (3 mL) at 80 °C for 7 h.

^bIsolated yield. ^cMol. diaryl ether/mol. Gd/ h. ^d10 h.

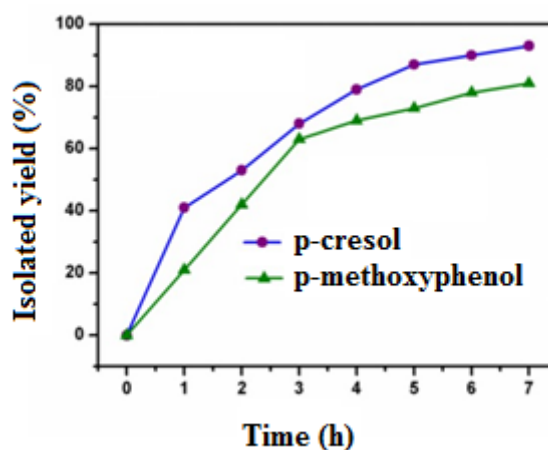


Figure 2.12 Isolated yield (%) of products corresponding to reactions *p*-nitro bromobenzene (1 mmol); *p*-cresol /*p*-methoxy phenol (1 mmol); Cs₂CO₃ (1.5 mmol); MOF-1 (0.025 mol %); DMF (3 mL) at 80 °C for 7 h.

2.3.4 Separation, catalyst reuse and heterogeneity test

As gadolinium(III) ions in water is toxic and it is a costly metal also, hence, reusability and heterogeneity is an important criteria to use MOF-1 as a catalyst. To ascertain that the catalysis is indeed heterogeneous, hot filtration test has been carried out. The solid catalyst is filtered hot after 2 hours of reaction and the residual activity of the supernatant solution after separation of the catalyst is studied. The supernatant solution is kept in reaction condition for another 7 h and

the composition of the solution is analyzed time to time. No progress of reaction is observed during this period, which excludes the presence of active species in the solution. This experiment clearly demonstrates that there was no leaching of gadolinium (III) ions from the solid catalyst during reactions (**Figure 2.13**).

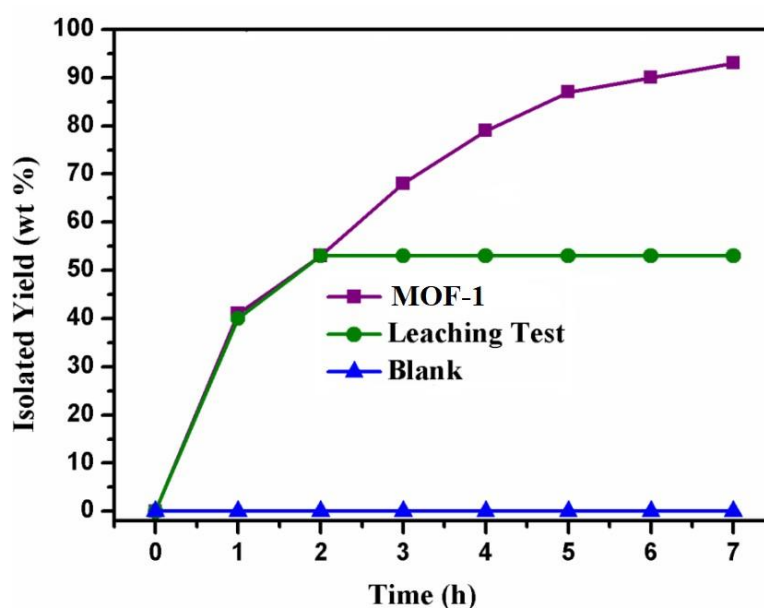


Figure 2.13 Leaching test of the catalyst using the reaction condition *p*-nitro bromobenzene (1mmol); *p*-cresol (1 mmol); Cs₂CO₃ (1.5 mmol); MOF-1 (0.025 mol%); DMF (3 mL) at 80 °C for 7 h. Blue line with triangular point signifies for blank; green line with solid sphere means isolated yield after hot filtration of the catalyst after 2 h. Purple line with square signifies isolated yield by using MOF-1 as catalyst.

In order to check the stability of the catalyst (MOF-1), It requires to characterize the recovered material. After the catalytic reactions are over, solid catalyst is recovered by centrifugation, washed thoroughly with dichloromethane and dried under vacuum at 100°C. The recovered catalyst is then subjected to X-ray powder diffraction analysis and IR spectral measurement. Comparison of

PXRD patterns (Figure 2.14) and IR spectra (Figure 2.15) with the pristine MOF and recovered catalyst convincingly demonstrated that the structural integrity of the MOF-1 is unaltered after the reaction.

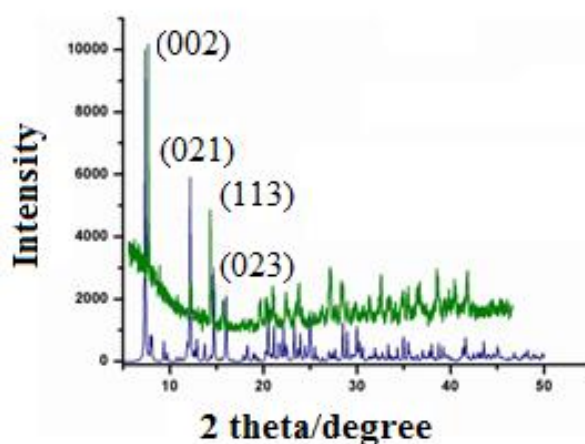


Figure 2.14 PXRD study after using MOF-1 as catalyst using the reaction condition *p*-nitro bromobenzene (1 mmol); *p*-cresol (1 mmol), Cs₂CO₃ (1.5 mmol); MOF-1 (0.025 mol %); DMF (3 mL) at 80 °C for 7 h.

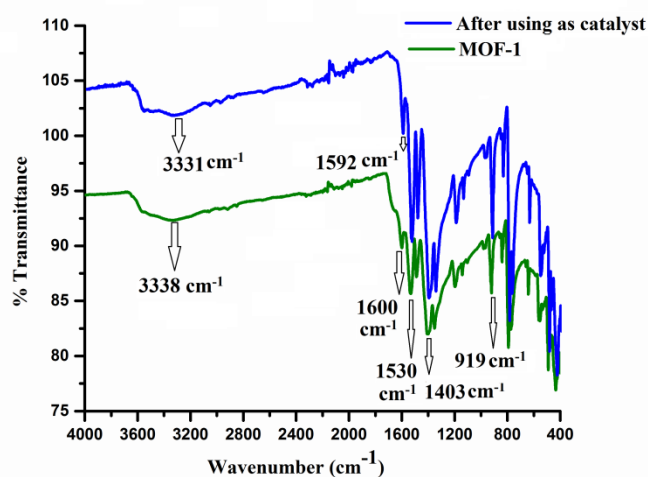


Figure 2.15 FT-IR spectra of MOF-1 before (green) and after (blue) using in catalytic reaction condition *p*-nitro bromobenzene (1 mmol); *p*-cresol (1 mmol); Cs₂CO₃ (1.5 mmol); MOF-1 (0.025 mol %), DMF (3 mL) at 80 °C for 7 h.

Chapter 2 Robust Gd-MOF for heterogeneous catalytic O-arylation reaction

For the recycling study, O-arylation reaction is performed using *p*-cresol with *p*-nitrobromobenzene. After the first cycle of reaction, the catalyst is recovered as mentioned earlier. The performance of the recycled catalyst is studied up to five successive runs (Figure 2.16). The catalytic efficacy of the recovered catalyst remained almost same in each run.

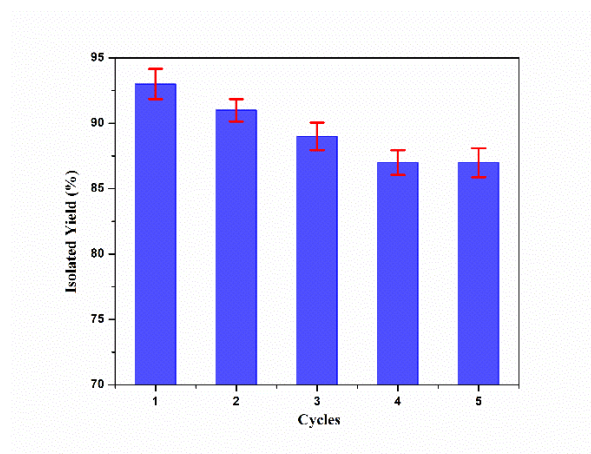


Figure 2.16 Recycling of the catalyst up to five catalytic cycles using the reaction condition *p*-nitro bromobenzene (1mmol); *p*-cresol (1 mmol); Cs₂CO₃ (1.5 mmol); MOF-1 (0.025 mol%); DMF (3 mL) at 80°C for 7 h. Error bars: standard deviation (n = 3)

2.4 Conclusion

In essence, a thermally stable and robust tetra-nuclear Gd-carboxylate based three dimensional metal-organic framework compound, {[Gd₄(NDC)₆(H₂O)₆]·2H₂O}_n have successfully synthesized *via* hydrothermal route. Structure of the MOF is established by X-ray diffraction analysis. Dehydrated compound is thermally stable upto 530 °C under nitrogen atmosphere and it can withstand treatment of various organic solvents including water. {[Gd₄(NDC)₆(H₂O)₆]·2H₂O}_n showed good catalytic efficacy towards O-arylation reaction under heterogeneous condition to yield unsymmetrical aryl ethers. The catalyst efficiently activates

Chapter 2 *Robust Gd-MOF for heterogeneous catalytic O-arylation reaction*

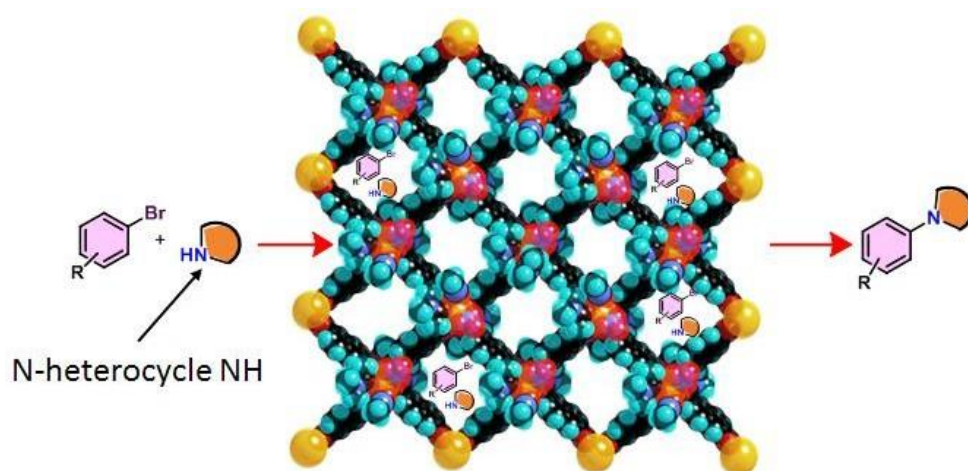
phenols containing wide range of functional groups including electron donating group. In accordance with the literature, lanthanide-based metal-organic framework system has rarely been tested as a catalyst in O-arylation reaction.

2.5 References

- [1] N. T. S. Phan, T. T. Nguyen, C. V. Nguyen, T. T. Nguyen, *Appl. Catal. A: Gen.* 457 (2013) 69.
- [2] J. W. Tye, Z. Weng, R. Giri, J. F. Hartwig, *Angew. Chem. Int. Ed.* 49 (2010) 2185.
- [3] S. Benyahya, F. Monnier, M. W. C. Man, C. Bied, F. Ouazzani, M. Taillefer, *Green Chem.* 11 (2009) 1121.
- [4] G. Mann, J. F. Hartwig, *Tetrahedron Lett.* 38 (1997) 8005.
- [5] L. Salvi, N. R. Davis, S. Z. Ali, S. L. Buchwald, *Org. Lett.* 14 (2012) 170.
- [6] L. Yin, J. Liebscher, *Chem. Rev.* 107 (2007) 133.
- [7] R. Sen, D. Saha, S. Koner, *Catal. Lett.* 142 (2012) 124.
- [8] S. Haldar, S. Koner, *J. Org. Chem.* 75 (2010) 6005.
- [9] D. Saha, T. Maity, S. Das, S. Koner, *Dalton Trans.* 42 (2013) 13912.
- [10] T. Maity, D. Saha, S. Das, S. Koner, *Eur. J. Inorg. Chem.* (2012) 4914.
- [11] T. Maity, D. Saha, S. Koner, *ChemCatChem* 6 (2014) 2373.
- [12] D. Saha, T. Maity, S. Das, S. Koner, *Dalton Trans.* 42 (2013) 13912.
- [13] T. Maity, D. Saha, S. Das, S. Bhunia, S. Koner, *Catal. Commun.* 58 (2015) 141.
- [14] A. D. G. Firmino, F. Figueira, J. P.C. Tome, F. A. A. Paz, J. Rocha, *Coord. Chem. Rev.* 355 (2018) 133.
- [15] R. Sen, S. Koner, D. K. Hazra, M. Helliwell, M. Mukherjee, *Eur. J. Inorg. Chem.* (2011) 241.
- [16] R. Sen, D. K. Hazra, M. Mukherjee, S. Koner, *Eur. J. Inorg. Chem.*

- (2011) 2826.
- [17] R. Sen, D. K. Hazra, S. Koner, M. Helliwell, M. Mukherjee, A. Bhattacharjee, *Polyhedron* 29 (2010) 3183.
- [18] SAINT and SADABS, version 6.02 and version 2.03; BrukerAXS, Inc.: Madison, WI, 2002.
- [19] G. M. Sheldrick, A short history of SHELX. *Acta Crystallogr. Sect. A: Found. Crystallogr.* 64 (2008) 112.
- [20] I. Usón, G.M. Sheldrick, *Acta Crystallogr. Sect. D* 74 (2018) 106.
- [21] O. V. Dolomanov, L. J. Bourhis, R. J. Gildea, J. A. K. Howard, H. Puschmann, OLEX2: a complete structure solution, refinement and analysis program. *J. Appl. Crystallogr.* 42 (2009) 339.
- [22] L. Farrugia, *J. Appl. Crystallogr.* 32 (1999) 837.
- [23] K. Brandenburg, DIAMOND, version 3.1 e; Crystal Impact Gbr: Bonn, Germany, 2007.
- [24] C. F. Macrae, I. J. Bruno, J. A. Chisholm, P. R. Edgington, P. McCabe, E. Pidcock, L. Rodriguez-Monge, R. Taylor, J. van de Streek, P. A. Wood, Mercury CSD 2.0 – New Features for the Visualization and Investigation of Crystal Structures. *J. Appl. Crystallogr.* 41 (2008) 466.
- [25] A.L. Spek, *J. Appl. Crystallogr.* 36 (2003) 7.
- [26] P. Caravan, J. J. Ellison, T. J. McMurry, R. B. Lauffer, *Chem. Rev.* 99 (1999) 2293.
- [27] R. Fernandez-Lopez, J. Kofoed, M. Machuqueiro, T. Darbre, *Eur. J. Org. Chem.* (2005) 5268.
- [28] C. H. Burgos, T. E. Barder, X. Huang, S. L. Buchwald, *Angew. Chem. Int. Ed.* 45 (2006) 4321.

Chapter 3

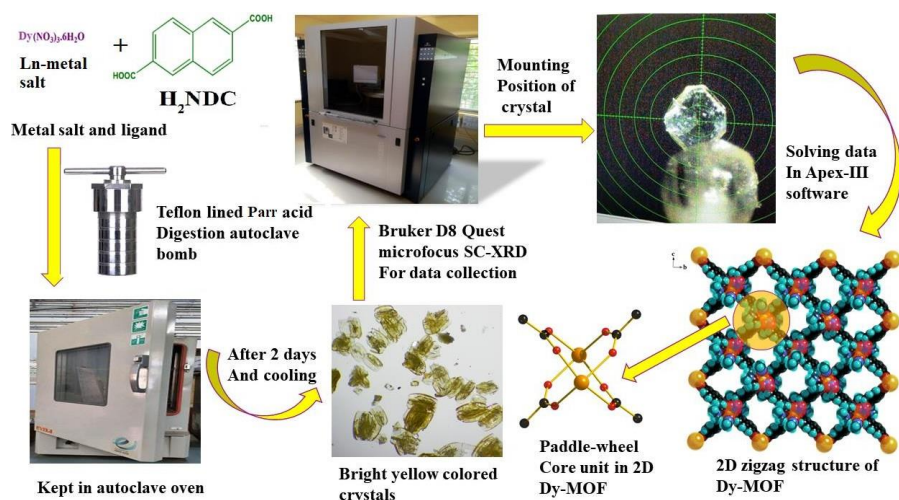


**Aromatic N-arylation reaction
catalyzed by 2D paddle-wheel
Dy-MOF under heterogeneous
condition**

3.1 Introduction

The C–N bond forming reaction for obtaining N-arylated products are of great interest by virtue of their presence in natural products, drugs and other organic materials [1, 2]. Various pharmaceutical compounds such as midazolam, celecoxib, nilotinib and insecticide or fungicide e.g. pyraclofos, pyraclostrobin are registered as important structural motifs of natural products and biologically active natural pharmaceutical agents [3]. Traditionally, these N-arylated products are synthesized by nucleophilic aromatic substitution (S_NAr) of N–H bond containing π -electron-rich nitrogen heterocycles with aryl halides or by classical Ullmann type coupling reactions [4-9]. In general, palladium [10, 11] and copper [12-14] catalysts have been extensively used in C–N cross-coupling reactions. Nevertheless, exploration of efficient metal catalyzed synthetic process for the construction of C–N bond is still in demand.

MOFs have attracted great attention and displayed their potential applications in heterogeneous catalysis that have been discussed in **Chapter 1**. Recently, Ln-MOFs are becoming the promising candidate for heterogeneous catalyst as discussed in **Chapter 1** as well as briefly in **Chapter 2**. Motivated by recent surge of research on Ln-MOFs including catalytic studies, further exploration of lanthanide carboxylate system has afforded a novel 2D MOF, containing lanthanide “paddle-wheel (PW)” as secondary building unit (SBU). Paddle-wheel cores are common in transition metal coordination polymers, however, reports of lanthanide PW structure are limited [15, 16, 17]. Recently, cadmium(II) acetate in combination with ethylene glycol catalyzes efficiently the C–N cross-coupling of amines with aryl iodides [18]. With all these facts in mind, C–N cross coupling reactions have been explored by employing the newly synthesized lanthanide-based MOF that acts as heterogeneous catalyst. A brief synthetic route which affords Dy-MOF (MOF-2) is presented in **Scheme-3.1**.



Scheme-3.1 Synthetic route for the preparation and data collection of Dy-MOF.

3.2 Experimental

3.2.1 Materials

Dysprosium(III) nitrate pentahydrate (99.9%), 2,6-naphthalenedicarboxylic acid (H_2NDC) (99%) were purchased from Sigma-Aldrich and used as received without further purification. Cesium carbonate (99%), imidazole (99.5%), pyrazole (98%), other chemicals and solvents (analytical grade) were procured from Merck (India). Solvents were distilled and dried before use.

3.2.2 Physical measurements

All the physical measurements were performed by using the same instruments already discussed in **Section 2.2.2, Chapter 2**.

3.2.3 Synthesis of $[\text{Dy}(\text{NDC})(\text{NO}_3)(\text{DMA})_2]_n$ (MOF- 2)

Dysprosium nitrate pentahydrate (0.25 mmol, 0.109g) was dissolved in 3 mL of dimethyl acetamide (DMA) and separately a 3 mL solution of 2,6-naphthalenedicarboxylic acid (0.125 mmol, 0.027g) in DMA was prepared. The two solutions were mixed and the resulting mixture was then placed in a 15 mL teflon-lined Parr acid digestion bomb and kept at 100°C for five days. After five days, the solution was allowed to cool down slowly at the rate of ~5°C/h to room temperature. Hexagon-shaped yellow-colored crystals were obtained from teflon-lined Parr acid digestion bomb and washed with DMA. Finally, the crystals are dried in air (yield 70% based on metal). X-ray quality hexagon-shaped crystals were chosen for the crystallography. Phase purity was verified through elemental analysis and X-ray powder diffraction analysis (**Figure 3.1**). Anal. Calcd. value for $\text{C}_{20}\text{H}_{24}\text{N}_3\text{O}_9\text{Dy}$ (FW= 612.92), C, 39.15%, H, 3.91%, N, 6.85 %, Found C, 39.2%, H,3.6%, N, 6.7 %. Selected IR peaks (KBr pellet, ν , cm^{-1}) (**Figure 3.2**): 1674 (w), 1603 (s), [$\nu_{as}(\text{CO}^-)$], 1470 (m), 1406 (s) [$\nu_s(\text{CO}^-)$], 1357 (w), 1307 (m) [$\nu_s(\text{C}-\text{O})$], 1031 (m) [$\nu(\text{C}-\text{N})$].

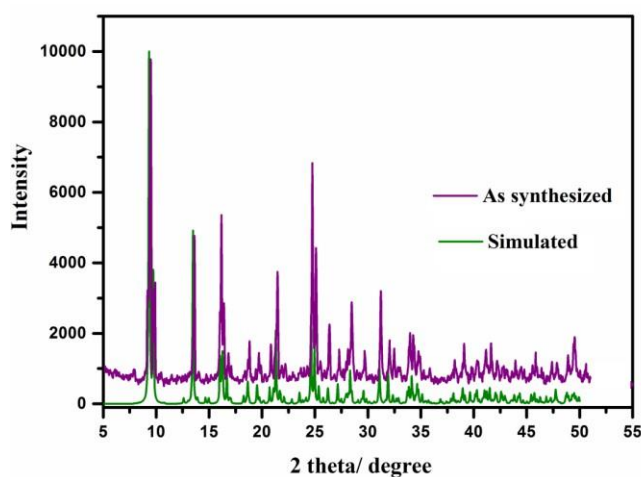


Figure 3.1 PXRD pattern of MOF-2 (scanning speed of 0.1° step /sec, temperature- 298 K).

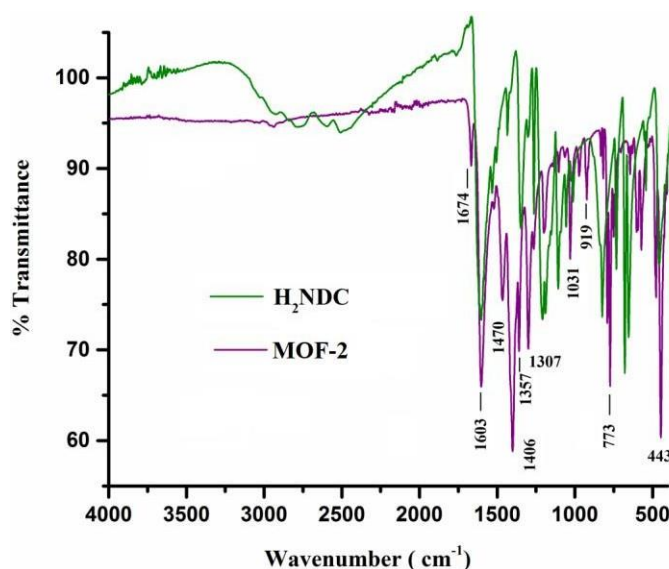


Figure 3.2 FT-IR spectra of MOF-2 and H₂NDC ligand.

3.2.4 X-ray crystallography

All the description about the procedure of data collection by single crystal X-ray diffraction and structure solution by using different software program have already been discussed in **Section 2.2.4, Chapter 2**. A summary of the crystallographic data and the relevant structural refinement parameters for MOF-2 are given in Table 3.1. CCDC-2107481 contains the supplementary crystallographic data for the MOF-2. These data can be obtained free of charge from Cambridge Crystallographic Data Centre via www.ccdc.cam.ac.uk/data_request/cif.

Table 3.1 Crystal data and refinement parameters of MOF-2

Formula	C ₂₀ H ₂₄ DyN ₃ O ₉
Formula Weight	612.92
Crystal System	Orthorhombic

Space Group	<i>Pbca</i> (no.61)
<i>a</i> (Å)	13.5940(11)
<i>b</i> (Å)	18.1676(15)
<i>c</i> (Å)	19.0043(15)
α (°)	90.00
β (°)	90.00
γ (°)	90.00
<i>V</i> (Å ³)	4693.5(7)
<i>Z</i>	8
<i>D</i> _{calc} (gcm ⁻³)	1.735
μ (mm ⁻¹)	3.238
<i>F</i> (000)	2424
θ Range (°)	2.2-27.1
Intervals of reflection indices	-17<= <i>h</i> <=17, -23<= <i>k</i> <=23, - 24<= <i>l</i> <=24
Reflections measured	157929
<i>R</i> _{int}	0.034
Unique data	5162
<i>R</i> indices (all data)	<i>R</i> 1 = 0.0289, <i>wR</i> 2 = 0.0901
Final <i>R</i> indices [<i>I</i> > 2 σ (<i>I</i>)]	<i>R</i> 1 = 0.0225, <i>wR</i> 2 = 0.0700
Data with <i>I</i> > 2(<i>I</i>)	4761
<i>R</i> ₁ (<i>I</i> > 2(<i>I</i>))	0.0225
<i>wR</i> ₂ (<i>I</i> > 2(<i>I</i>))	0.0700
(GOF) on <i>F</i> ²	1.223

$$R1 = \frac{\sum ||F_o| - |F_c||}{\sum |F_o|}, wR2 = \left\{ \frac{\sum [w(F_o^2 - F_c^2)^2]}{\sum w(F_o^2)^2} \right\}^{1/2}$$

3.2.5 General procedure for catalytic reactions

0.151 g (1 mmol) of *p*-nitrobromobenzene and 0.068g (1 mmol) of imidazole added with 0.487 g (1.5 mmol) solid cesium carbonate in 3 mL dehydrated dimethylformamide (DMF) solvent in a 15 mL round-bottom flask. 0.010 g of MOF-2 was added to the reaction medium and stirred under continuous heating at 95°C for sixteen hours. The conversion of the reaction was monitored by thin layered chromatography (TLC) method. After completion of the reaction, mixture was cooled to room temperature and purged on ice cold water. The aqueous layer was extracted three times with diethyl ether (2×15 mL). Combined organic layer thus collected was washed with brine solution, dried over anhydrous sodium sulfate and concentrated in vacuum. The collected residue was further purified by column chromatography on silica-gel (60-120 mesh) and was eluted with n-hexane/ethyl acetate mixture to get the desired product. The product analyzed through ¹H-NMR, elemental analysis and compared with the literature data.

3.3 Results and discussion

3.3.1 Description of crystal structure of MOF-2

It is revealed from single-crystal X-ray analysis that MOF-2 crystallizes in the orthorhombic *Pbca* (No.61) space group with a *Z* value 8. The asymmetric unit consists of one crystallographically independent Dy(III) ion, one 2,6-naphthalenedicarboxylate (NDC²⁻) linker, one coordinated nitrate anion and two coordinated dimethyl acetamide (DMA) molecules. The ORTEP diagram with atom numbering is given in **Figure 3.3**. **Figure 3.4a** shows the molecular structure of MOF-2, where Dy(III) is coordinated with eight oxygen atoms (DyO8) which adopts a distorted triangular-dodecahedral geometry (**Figure 3.4b**). The coordination mode of central metal ion is completed by four different oxygen atoms of monodentate COO⁻ group (O1, O4, O2, O3) from four different NDC²⁻

ligand, two oxygen atoms (O5, O6) from coordinated nitrate anion and other two oxygen (O8, O9) from two coordinated DMA molecules (**Figure 3.4**). The measured bond distances of Dy–O are found to be in the range of 2.279(2)–2.542(4) Å, and the angles of O–Dy–O vary from 50.15(12) to 152.56(10)° (**Table 3.2**), which all correspond well with other reported Dy(III) complexes containing aromatic carboxylic acid ligands [19, 20].

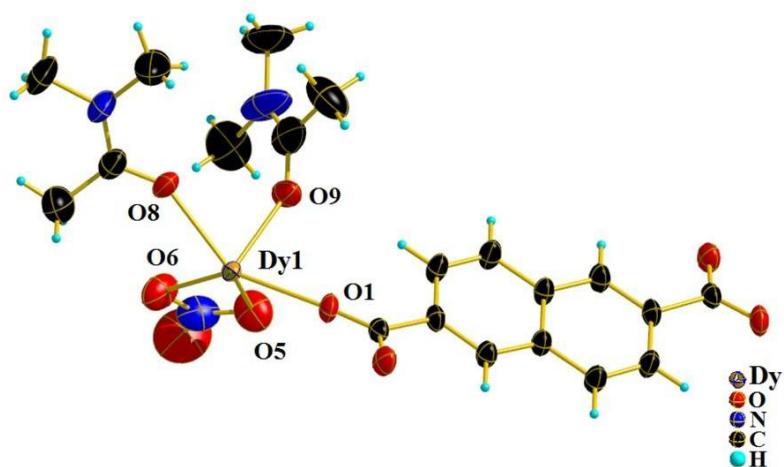


Figure 3.3 Ortep diagram of MOF-2 with 50% thermal ellipsoid probability.

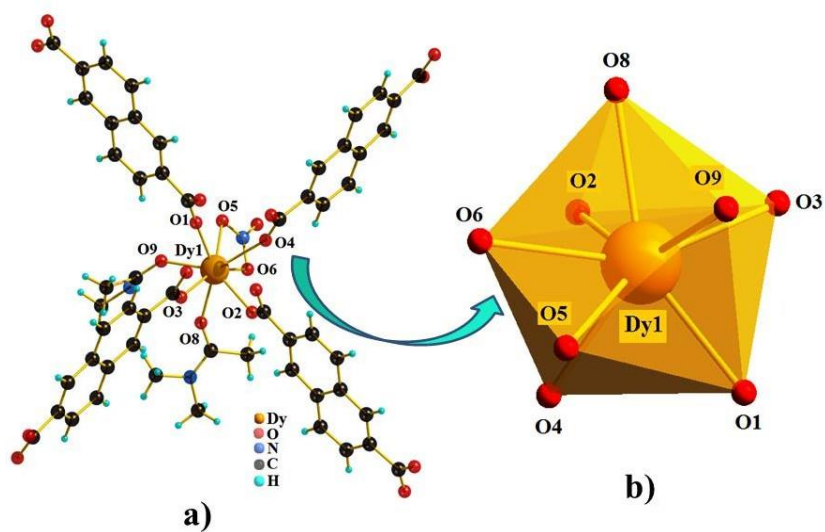


Figure 3.4 a) Coordination environment of Dy(III) center; b) Distorted triangular-dodecahedral geometry around Dy(III).

Table 3.2 Selected bond-length (Å) and angle (°) for MOF-2

Atoms	Distance (Å)
Dy1-O1	2.279(2)
Dy1-O5	2.542(4)
Dy1-O6	2.476(3)
Dy1-O8	2.359(3)
Dy1-O9	2.347(3)
Dy1- ^a O4	2.332(2)
Dy1- ^c O2	2.338(2)
Dy1- ^e O3	2.328(2)

Atoms	Angle(°)	Atoms	Angle(°)
O1-Dy1-O5	79.71(10)	^a O4-Dy1-O5	71.55(10)
O1-Dy1-O6	127.90(10)	^c O2-Dy1-O5	132.35(10)
O1-Dy1-O8	147.70(9)	^e O3-Dy1-O5	149.22(10)
O1-Dy1-O9	80.43(9)	O6-Dy1-O8	74.14(10)
O1-Dy1- ^a O4	77.78(8)	O6-Dy1-O9	95.27(10)
O1-Dy1- ^c O2	123.72(8)	^a O4-Dy1-O6	74.05(9)
O1-Dy1- ^e O3	78.75(8)	^c O2-Dy1-O6	89.13(9)
O5-Dy1-O6	50.15(12)	^e O3-Dy1-O6	152.56(10)
O5-Dy1-O8	109.77(11)	O8-Dy1-O9	73.54(9)
O5-Dy1-O9	73.13(11)	^a O4-Dy1-O8	134.42(9)
^c O2-Dy1-O8	73.47(8)	^e O3-Dy1-O8	78.90(9)
^a O4-Dy1-O9	141.11(9)	^c O2-Dy1-O9	144.05(9)
^e O3-Dy1-O9	81.79(9)	^c O2-Dy1- ^a O4	74.27(8)
^e O3-Dy1- ^a O4	124.17(8)	^c O2-Dy1- ^e O3	78.26(8)

Symmetry code; a = 1-x,-1/2+y,1/2-z, c = 1-x,1-y,1-z, e = x,3/2-y,1/2+z,

The 2,6-naphthalenedicarboxylate (NDC²⁻) ligand features *syn-syn* bridging μ -1,3 coordination mode. Two equivalent Dy(III) ions are connected by two carboxylate (COO⁻) groups from two different NDC²⁻ to generate a lanthanide paddle-wheel secondary building unit (SBU) {Dy₂(COO)₄} core (**Figure 3.5**). The secondary building units are linked each other through the ligand NDC²⁻ to construct an infinite 1D chain (**Figure 3.6a**). The chains are further connected via a pair of carboxylate groups of two different 2,6-naphthalenedicarboxylate (NDC²⁻) that afforded a 2D square grid network structure (**Figure 3.6b**). Two-dimensional framework structure of MOF-2 is also clearly viewed by polyhedral drawing of central metal coordination environment and by space-filled mode (**Figure 3.7** and **Figures 3.8a and 3.8b**).

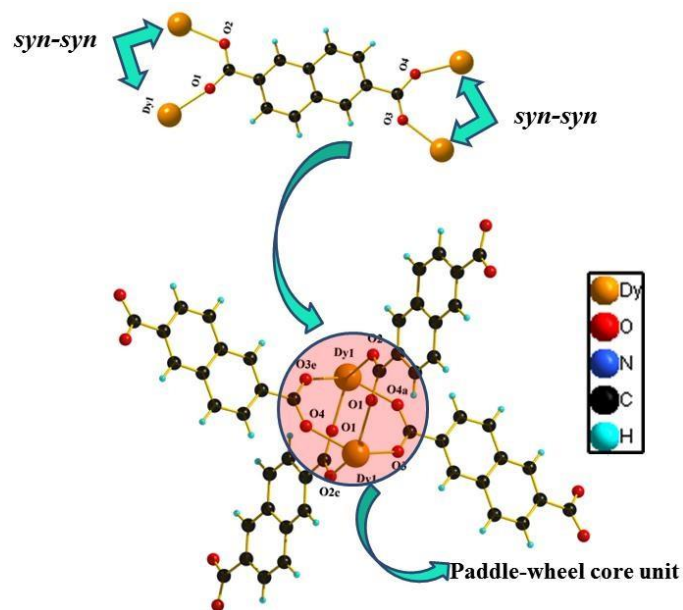


Figure 3.5 Coordination modes of the carboxylato ligand and “paddle-wheel” centered SBU.

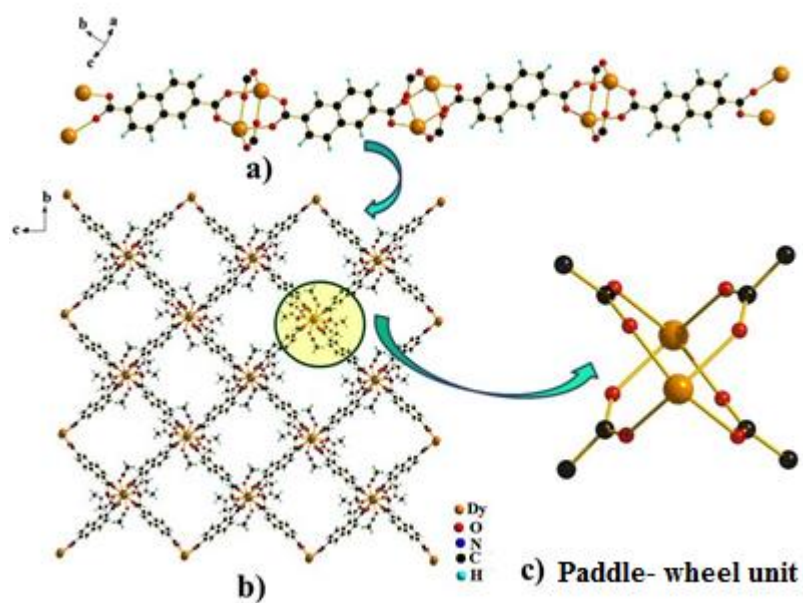


Figure 3.6 a) 1D chain propagation parallel to crystallographic *b*-axis; b) 2D network of MOF-2; c) Paddle-wheel core unit in the framework.

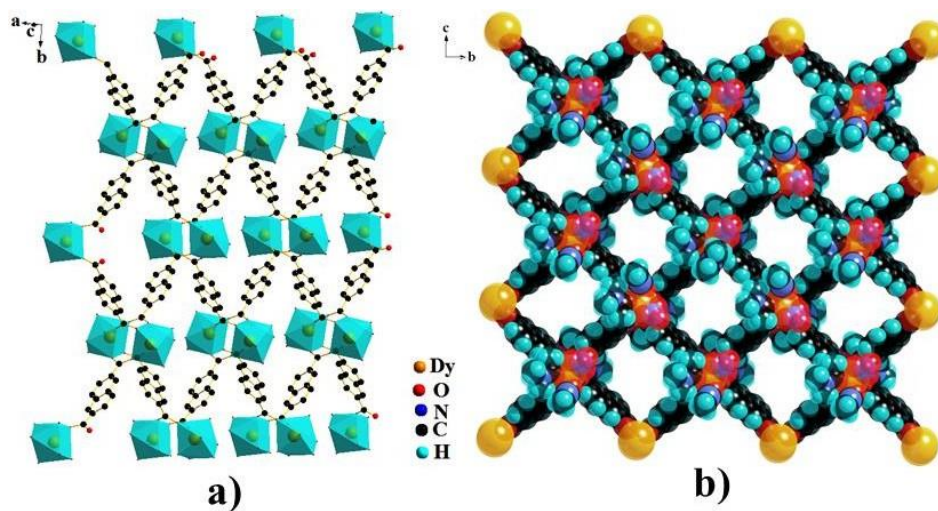


Figure 3.7 a) Polyhedral drawing MOF-2; b) Two-dimensional framework of MOF-2 in space-filled mode.

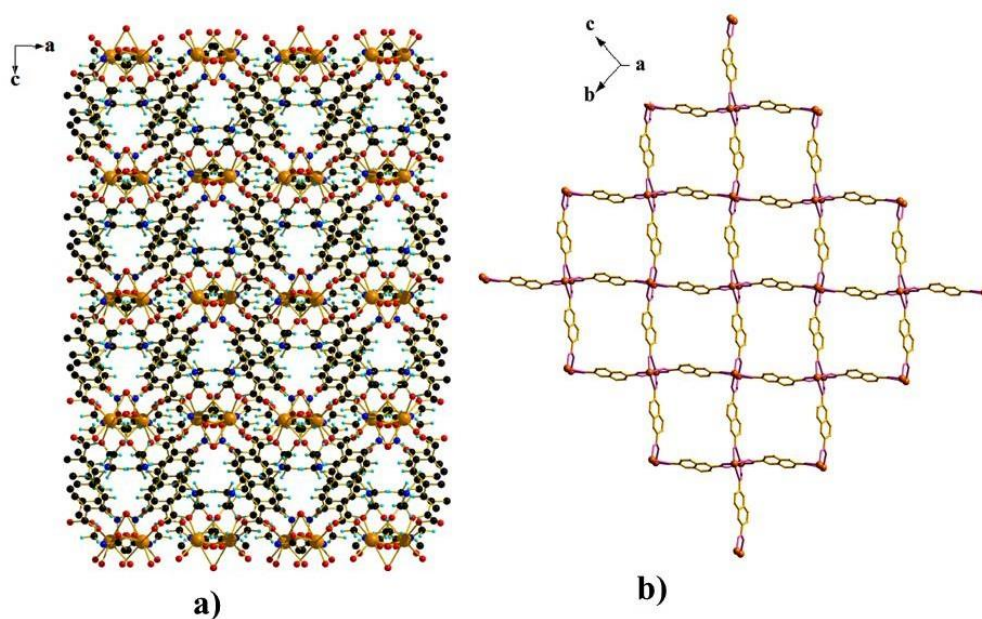


Figure 3.8 a) 2D network of MOF-2 propagates parallel to ac -plane; b) 2D drawing of MOF-2 (H atoms and DMA molecules are omitted for clarity).

To represent a simplified square grid 2D structure of MOF-2, OCO^- of NDC^{2-} moieties are depicted as pink colored connector for one layer and with a green colored connector for the next layer. The yellow colored Dy(III) centers are networked by those connectors resulting in a square grid network structure which propagates parallel to bc -plane (**Figure 3.9a**). Stacking of 2D layers along crystallographic a -axis is also clear in the figure (**Figure 3.9b**).

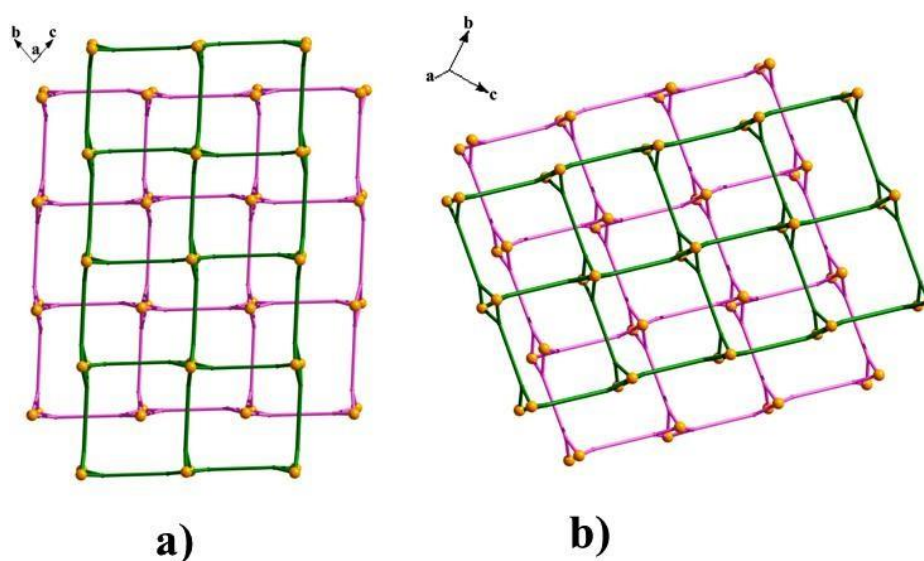


Figure 3.9 a) Simplified network structure of MOF-2 along bc -plane; b) stacking of 2D layers of MOF-2 along crystallographic a -axis.

3.3.2 Hirshfeld surface analysis for MOF-2

The analysis of molecular structures using Hirshfeld surfaces methods are increasingly gained of popularity in recent time. This approach represents an effort to venture beyond the current paradigm. Inter-nuclear distances and angles, crystal packing diagram with molecules are represented via various models, and the identification of close contacts are considered to be important, and to view molecules as “organic wholes”, thereby fundamentally altering the discussion of

intermolecular interactions through an unbiased identification of close contacts. In order to clarify the strength of weak interactions between the groups and relationship between the degree of aggregation of aromatic group Hirshfeld surface (HS) and 2D fingerprint analysis [21, 22] of the MOF-2 has been performed using CrystalExplorer 3.1 [23]. Hirshfeld surface plotted over d_{norm} (normalized distance) have been constructed between -0.670 and 1.698\AA for MOF-2 and it can be employed to display intermolecular interactions by color coding [24] as shown in **Figure 3.10**. Deep red circular depressions suggest the existence of strong interactions in the MOF-2. Blue and white regions on this HS give an indication for weak interactions and the interatomic distance is greater and equal to the sum of the Van der Waal radii of atoms respectively. Along with d_{norm} plots, the total as well as decomposed fingerprint plots have been employed for the quantitative description of individual interatomic interactions. In these plots, d_e designate the distance from the HS to the nearest nucleus outside the HS and d_i represents the distance from the surface to nearest nucleus inside the HS.

2D fingerprint plot for overall interactions are represented in **Figure 3.11**. The results show that H \cdots H interatomic contact (defined as Van der Waals interactions between the related H-atoms) are the most important contributor in the crystal packing with contribution 38.2% for MOF-2. In MOF-2 other interatomic contacts such as O \cdots H/ H \cdots O and C \cdots H/H \cdots C interactions contribute 24.6% and 21.9% respectively. The O \cdots O, Dy \cdots O, C \cdots O interatomic contacts have less contribution in crystal packing for the MOF-2 (8.0%, 4.7%, and 0.7%), (**Figure 3.11**). The shape index and curvedness plot are given in **Figure 3.11**. Blue triangle like pieces and orange/red on curvedness map give information about the van der Waals, (**Figures 3.10b** and **3.10c**) valance bond and $\pi\cdots\pi$ interactions.

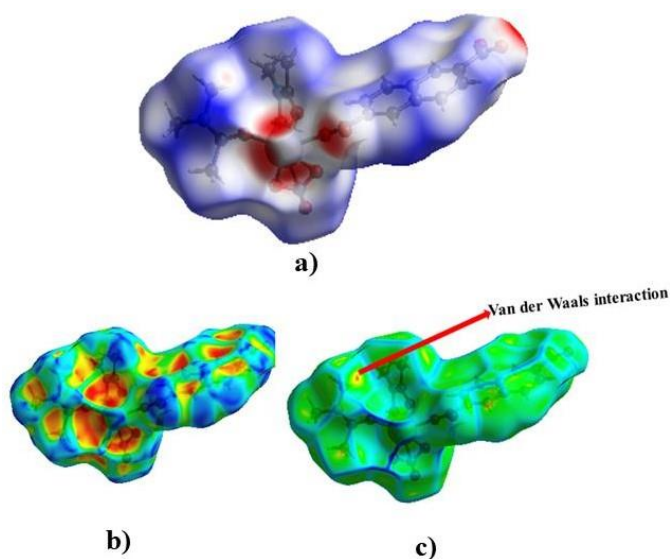


Figure 3.10 a) View of Hirshfeld surface of MOF-2 plotted over d_{norm} ; b) Hirshfeld surface of shape index plot; c) curvedness plot of MOF-2 (red arrow showing the van der Waals interaction).

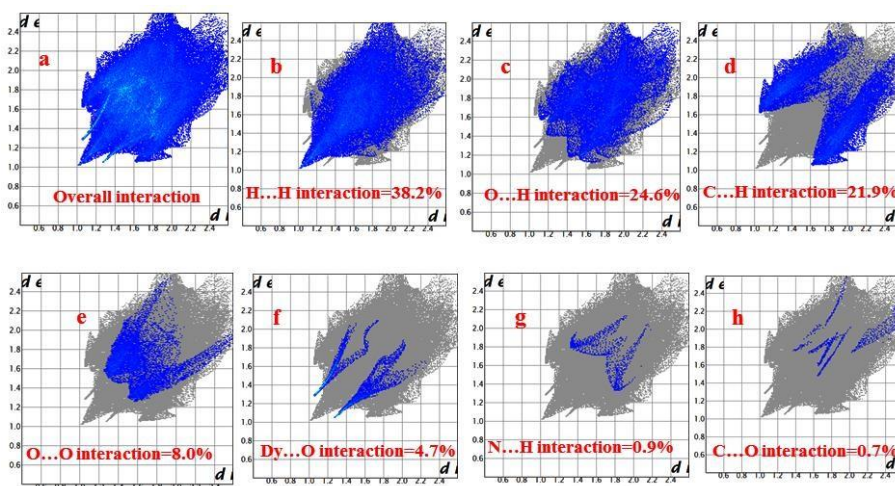


Figure 3.11 2D fingerprint plot of MOF-2; (a) overall interaction; (b-h) individual interatomic (major and weak) contacts including reciprocal contacts.

3.3.3 Thermal study of MOF-2

To understand the thermal stability of the framework in the solid state, thermogravimetric analysis was carried out for MOF-2. Thermal analysis of the MOF was undertaken from room temperature to 700° C under N₂ atmosphere using powdered sample (**Figure 3.12**). Upon heating MOF-2 starts to lose weight at *ca.* 176° C and displayed a total mass loss of ~ 27.1% in two stages which completes at *ca.* 340° C. This corresponds well with the theoretical value of ~ 28.3% mass losses due to release of two coordinated dimethylacetamide (DMA) molecules. Upon further heating, the desolvated MOF exhibits an additional mass loss of ~ 42.5% (theoretical ~ 45.1%) in the temperature range 410 – 570° C which can be corroborated with the decomposition of organic ligand and nitrate ion. Finally, the MOF converted to metal oxide after thermal decomposition.

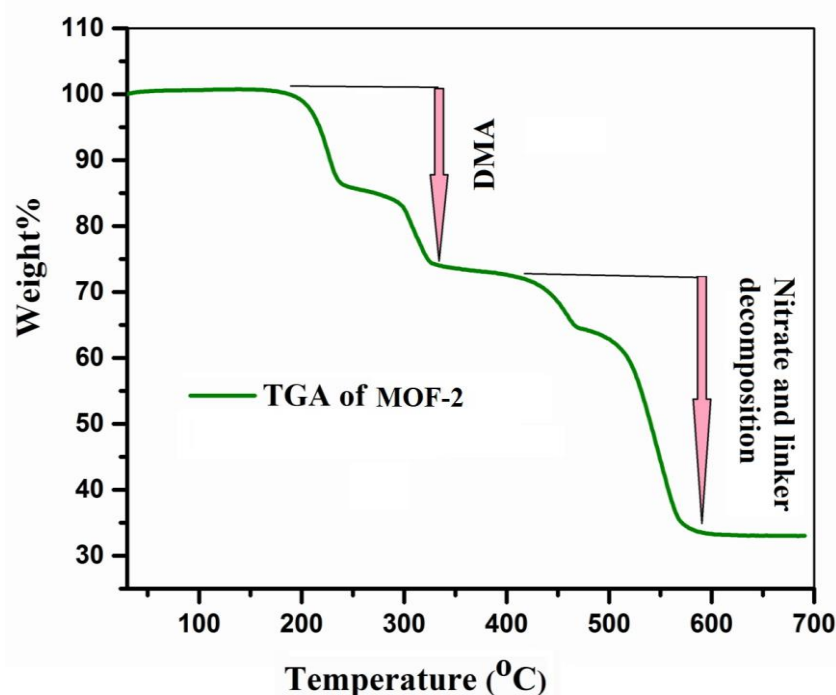


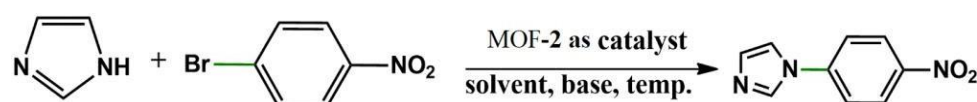
Figure 3.12 Thermogravimetric analysis plot of MOF-2.

3.3.4 Catalytic activity studies

Initial optimization condition of N-arylation reactions were examined by varying different parameters such as solvents, bases, reaction temperature and reaction time etc. because these parameters are found to impact the progress of the N-arylation reaction [25]. To illustrate the catalytic activity, different reaction conditions have been tested between imidazole and 1-bromo-4-nitrobenzene and the results are collated in Table 3.3. For selection of the best solvent, various solvents were tested in the C–N coupling reaction. Amongst them, DMF was found to be best suited for the catalytic reaction and products were obtained in good yield in this solvent (Table 3.3, entry 1). To find out the suitable base for the catalysis, a series of reactions were performed with different bases. It is revealed that solid inorganic bases like K_2CO_3 , Na_2CO_3 , K_3PO_4 , Na_3PO_4 , Cs_2CO_3 are much more efficient than the soluble organic base such as Et_3N (Table 3.3, entries 5–10). K_2CO_3 and Na_2CO_3 exhibits good reactivity in C–N coupling reaction but Cs_2CO_3 was chosen due to its high solubility, enhanced basicity in fine powder form and it becomes the best choice as a base among others (Table 3.3, entries 1). The catalyst was inactive in absence of base (Table 3.3, entry 12) and inert atmosphere was not employed as the catalyst is air stable. The stability of MOF-2 has been checked keeping the sample in open atmosphere for several days (Figure 3.1). Besides, reaction temperature and time play crucial role in C–N coupling reaction and showed noticeable impact on N-arylation of imidazole. Isolated yield was low at $60^\circ C$ even after 28 hours (Table 3.3, entry 14) and also not up to the mark at high temperature, $110^\circ C$. However, at $95^\circ C$ product yield improved up to 70% and it is chosen as optimized temperature for the coupling reaction. To ascertain catalytic efficacy of Dy-MOF (MOF-2), dysprosium nitrate salt (Table 3.3, entry 17) and a mixture of dysprosium nitrate and ligand 2,6-naphthalenedicarboxylic acid (Table 3.3, entry 18) have been tested as catalyst but only low to trace conversion was observed. Hence, the optimized reaction

conditions of the catalytic reaction to acquire highest yield of targeted product were found to be DMF as solvent, Cs₂CO₃ as base, 95 °C as reaction temperature under air using MOF-2 as the catalyst.

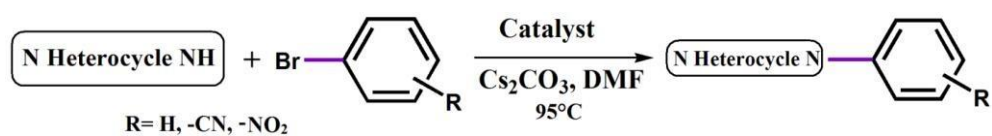
Table 3.3 Optimization of reaction conditions for N-arylation of imidazole with *p*-bromonitrobenzene



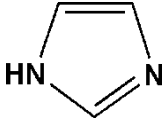
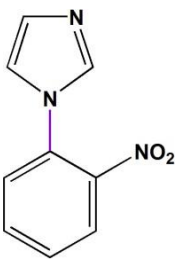
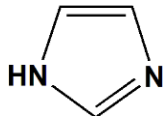
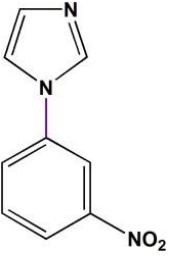
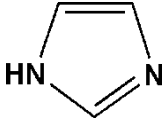
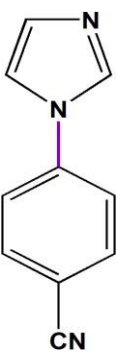
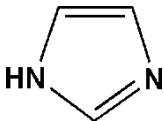
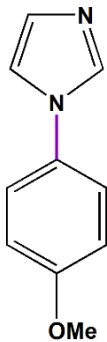
Entry ^a	Catalyst	Base	Solvent	Isolated Yield ^b (%)
1	MOF-2	Cs ₂ CO ₃	DMF	70
2	MOF-2	Cs ₂ CO ₃	Toluene	-
3	MOF-2	Cs ₂ CO ₃	Acetonitrile	-
4	MOF-2	Cs ₂ CO ₃	Methanol	-
5	MOF-2	Cs ₂ CO ₃	DMSO	61
6	MOF-2	Et ₃ N	DMF	34
7	MOF-2	K ₂ CO ₃	DMF	65
8	MOF-2	Na ₂ CO ₃	DMF	60
9	MOF-2	K ₃ PO ₄	DMF	40
10	MOF-2	Na ₃ PO ₄	DMF	38
11	-	Cs ₂ CO ₃	DMF	trace
12	MOF-2	-	DMF	0
13	MOF-2	Cs ₂ CO ₃	DMF	27 ^c
14	MOF-2	Cs ₂ CO ₃	DMF	40 ^d
15	MOF-2	Cs ₂ CO ₃	DMF	70 ^e
16	MOF-2	Cs ₂ CO ₃	DMF	65 ^f
17	Dy(NO ₃) ₃ ·xH ₂ O	Cs ₂ CO ₃	DMF	trace
18	Dy(NO ₃) ₃ ·xH ₂ O + NDC	Cs ₂ CO ₃	DMF	35

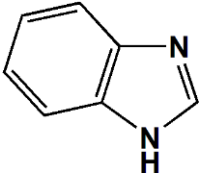
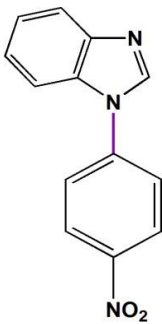
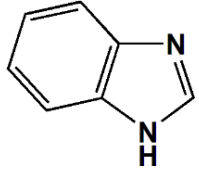

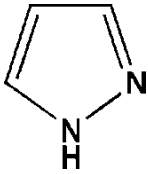
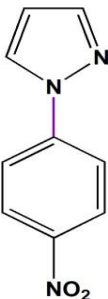
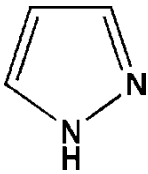
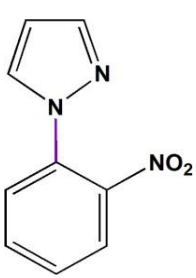
^a**Reaction conditions:** *p*-bromonitrobenzene (1 mmol), imidazole (1 mmol), MOF-2 as catalyst (10mg, 0.0016 mol %), base (1.5 mmol), solvent (3 mL) and temperature 95 °C. ^bIsolated yield. Reaction temperature: ^c40 °C, ^d60 °C, ^e95 °C and ^f110 °C.

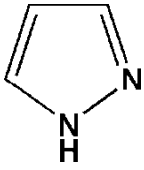
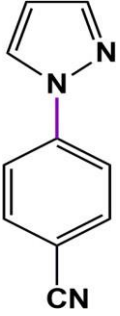
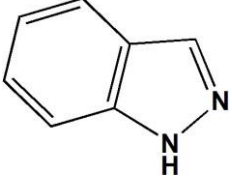
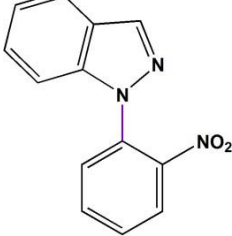
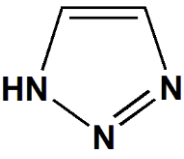
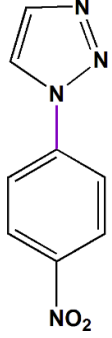
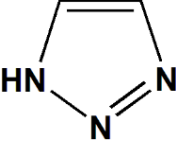
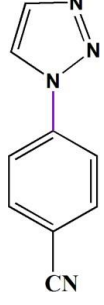
Under the optimized reaction conditions, the scope and applicability of N-arylation reaction using bromobenzene containing diverse functional groups with different N-heterocyclic amines were investigated (Table 3). Expected products were obtained in moderate yield in this catalytic reaction. The N-arylation reaction to imidazole, pyrazole, 1,2,3-triazole and 1,2,4-triazole have been performed with substituted bromoarenes. It was noticed that bromobenzenes containing electron withdrawing groups provided good yield (Table 3.4, entries 2, 3, 4, 5, 11, 12) than the corresponding electron donating group (Table 3.4, entry 6). Isolated products obtained at higher yield for the reaction between imidazole and substituted bromobenzene than the pyrazole with substituted bromoarenes. Presence of electron withdrawing $-\text{NO}_2$ group at *para*-position activity of bromobenzene ring is being elevated in the catalysis reaction and hence, maximum yield was obtained for the N-heterocycle, imidazole (Table 3.4, entry 2). But pyrazole showed sluggish reaction with 1-bromo-4-nitrobenzene and provided less isolated yield than imidazole (Table 3.4, entry 9). 1-bromo-2-nitro-bromobenzene gave lower yield compared to 1-bromo-4-nitrobenzene (Table 3.4, entries 3, 10). The reason may be the steric effect which has control over the reaction. The catalyst can also activate the substrates containing the other functional groups such as, cyano, methoxy group (Table 3.4, entries, 6, 11). The reaction was also tested for benzimidazole and benzpyrazole with substituted bromoarenes (Table 3.4, entries, 7, 8, 12) Besides, the scope of N-arylation reactions have been extended between 1,2,3-triazole and 1,2,4-triazole as N-containing heterocycles to couple with substituted aryl bromide (Table 3.4, entries 13, 14, 15, 16). It was observed that 1,2,4-triazole provided comparatively better isolated yield than 1,2,3-triazole. Kinetic plot displaying progress of the catalytic reaction is given in **Figure 3.13**. Aryl bromides were converted smoothly from the beginning of the reactions without showing any induction period.

Table 3.4 N-arylation between substituted bromobenzene with N-containing heterocycles^a

Entry ^a	R	Amine	Product	Time (h)	Yield ^b (wt%)
1	H			16	51
2	<i>p</i> -NO ₂			16	71

3	<i>o</i> - NO ₂			16	56
4	<i>m</i> - NO ₂			16	61
5	<i>p</i> - CN			16	69
6	<i>p</i> - OMe			16	50

7	<i>p</i> - NO ₂			16	66
8	<i>o</i> - NO ₂			16	54
9	<i>p</i> - NO ₂			16	59
10	<i>o</i> - NO ₂			16	49

11	<i>p</i> - CN			16	61
12	<i>o</i> - NO ₂			16	45
13	<i>p</i> - NO ₂			16	50
14	<i>p</i> - CN			16	47

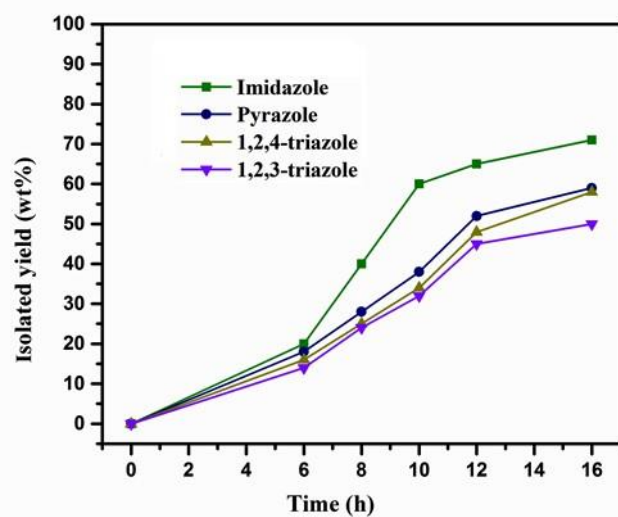
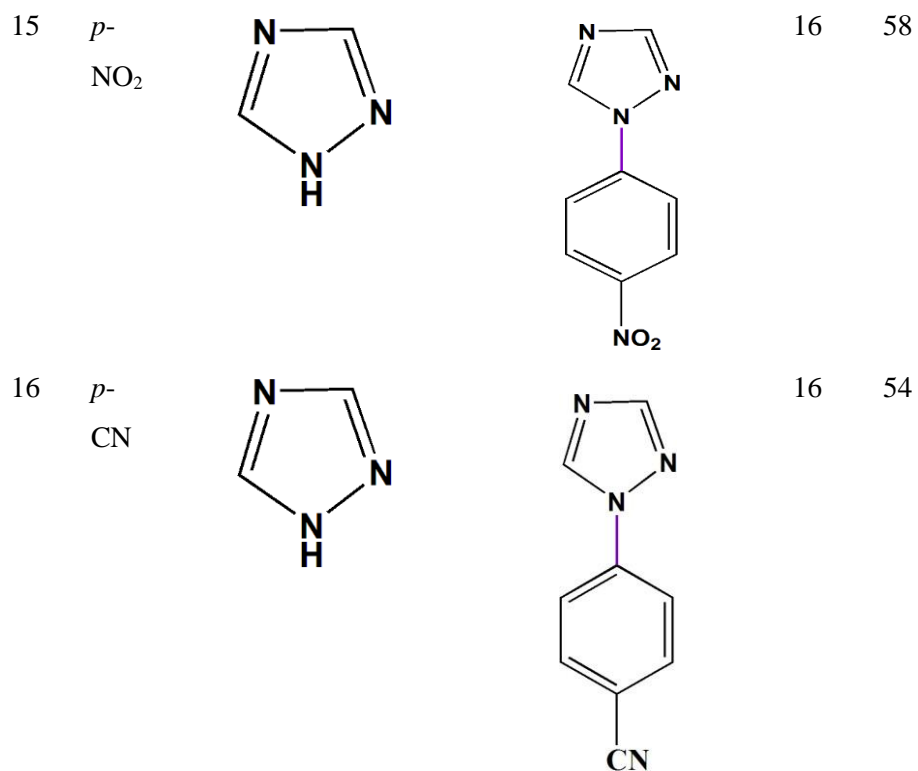


Figure 3.13 Plot showing progress of N-arylation reaction.

3.3.5 Separation, stability and recycling of the catalyst (MOF-2)

For the recycling study, N-arylation reaction were performed using imidazole, *p*-bromo-nitrobenzene and Cs_2CO_3 maintaining the optimized condition. After the catalysis reaction is over, the catalyst (MOF-2) was separated by centrifugation and washed with water and acetonitrile mixture thoroughly. Then, it was dried in air. In order to check the stability of the catalyst after reaction, it was subjected to powder X-ray diffraction analysis and IR spectral measurement. Comparison of PXRD data (Figure 3.14) and IR spectra (Figure 3.15) with the pristine MOF-2 and recovered catalyst convincingly demonstrated that the structural integrity of the MOF is unaltered after the reaction.

To check the performance of the recycled catalyst, the catalysis reaction was carried out up to four cycles under identical condition. Catalytic efficiency remains almost same after the four cycles and the performance of the recycled catalyst in these cycles was shown in Figure 3.16. Therefore, the catalyst can be reused several times without any effective loss of catalytic efficiency.

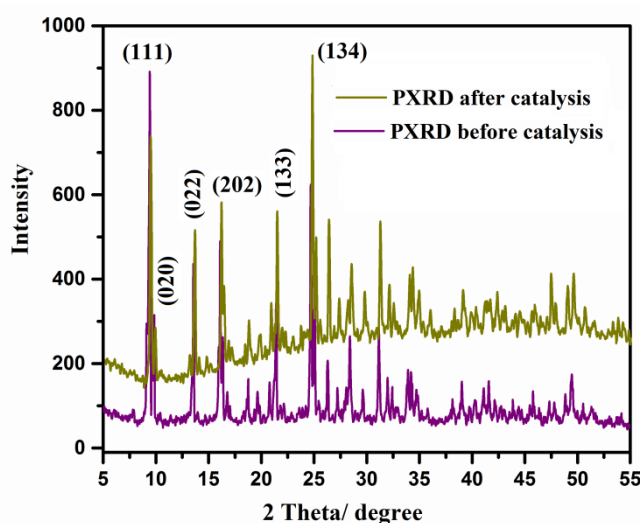


Figure 3.14 Powder X-ray diffraction patterns of MOF-2 (purple color) and solid recovered after catalytic reaction is over (greenish yellow color).

Reaction conditions: *p*-bromonitrobenzene (1mmol); imidazole (1 mmol); Cs_2CO_3 (1.5 mmol); MOF-2 (0.0016 mol %); DMF (3 mL) at 95 °C for 16

h.

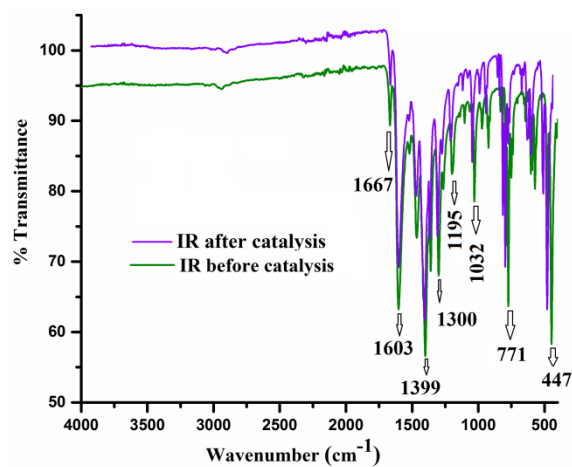


Figure 3.15 FT-IR spectra of catalyst (MOF-2); before catalysis (green); after catalysis (violet). Reaction conditions: *p*-bromonitrobenzene (1 mmol); imidazole (1 mmol); Cs₂CO₃ (1.5 mmol); MOF-2 (0.0016 mol %); DMF (3 mL) at 95 °C for 16 h.

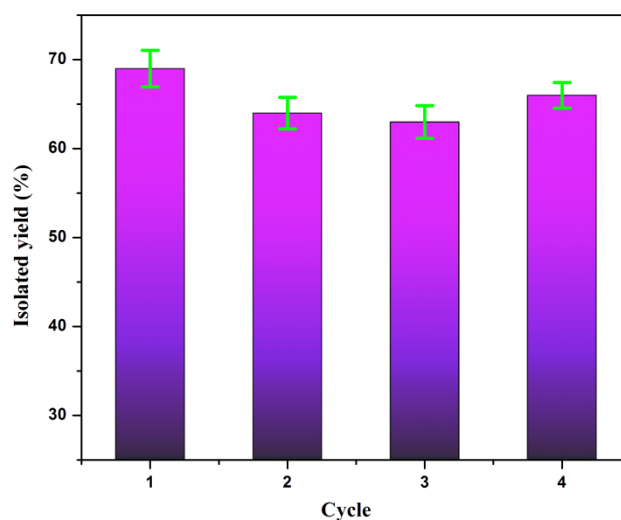


Figure 3.16 Plot showing efficiency of catalyst on recycling (upto four cycles).

Reaction conditions: *p*-bromonitrobenzene (1mmol), imidazole (1 mmol); Cs₂CO₃ (1.5 mmol); MOF-2 (0.0016 mol %); DMF (3 mL) at 95 °C for 16 h.

Error Bars: standard deviation (n = 3).

3.3.6. Heterogeneity of the catalyst

To ascertain the catalytic reaction is heterogeneous hot filtration test have been performed. The solid catalyst (MOF-2) was filtered in hot condition and the activity of the residual solution without the catalyst was studied [25]. The solution was kept in reaction condition for another ten hours and composition of the reaction was analyzed time to time. It was observed that the reaction was not progressed without the active species in the solution during this period. This experiment evidently explains that there was no leaching of dysprosium (III) ions from the solid catalyst during the catalysis reaction.

3.4 Conclusion

In summary, a two-dimensional paddle-wheel Ln-based MOF [Dy(NDC)(NO₃)(DMA)₂]_n (MOF-2) have been successfully isolated using solvothermal method. Structure of the MOF was established by X-ray diffraction analysis and interatomic interactions were mapped through Hirshfeld surface analysis. [Dy(NDC)(NO₃)(DMA)₂]_n (MOF-2) exhibited excellent catalytic efficacy towards N-arylation reaction under heterogeneous condition in N-arylation reaction between substituted bromobenzene and N-containing heterocycles. The catalyst activates various nitrogen containing heterocycles such as imidazole, pyrazole, 1,2,3-triazole and 1,2,4-triazole. Notably, this is one of the rarest examples of paddle-wheel core based two-dimensional Ln-MOF.

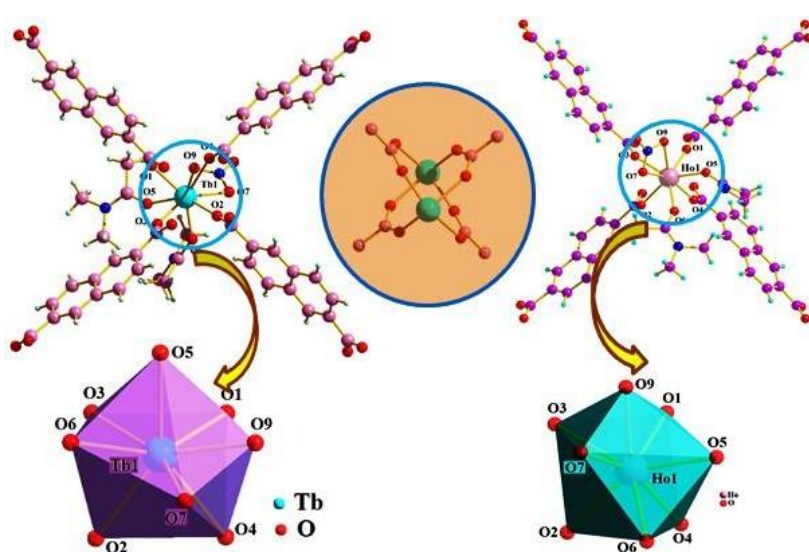
3.5 References

- [1] L. Rout, S. Jammi, T. Punniyamurthy, *Org. Lett.* 9 (2007) 3397.
- [2] G. Evano, N. Blanchard, M. Toumi, *Chem. Rev.* 108 (2008) 3054.
- [3] D. Kundu, S. Bhadra, N. Mukherjee, B. Sreedhar, B. C. Ranu, *Chem. Eur. J.* 19 (2013) 15759.
- [4] M. C. Venuti, R. A. Stephenson, R. Alvarez, J. J. Bruno, A. M.

- Strosberg, J. *Med. Chem.* 31 (1988) 2136.
- [5] G. R. Martinez, K. A. M. Walker, D. R. Hirschfeld, J. J. Bruno, D. S. Yang, P. J. Maloney, *J. Med. Chem.* 35 (1992) 620.
- [6] P. Cozzi, G. Carganico, D. Fusar, M. Grossoni, M. Menichincheri, V. Pinciroli, R. Tonani, F. Vaghi, P. Salvati, *J. Med. Chem.* 36 (1993) 2964.
- [7] J. Ohmori, M. S. Sasamata, M. Okada, S. Sakamoto, *J. Med. Chem.* 39 (1996) 3971.
- [8] R. Bambal, R. B. Haznlik, *J. Org. Chem.* 59 (1994) 729.
- [9] C. Jacobs, M. Frotscher, G. Dannhardt, R. W. Hartmann, *J. Med. Chem.* 43 (2000) 1841.
- [10] S. Zhang, Y. Wang, X. Feng, M. Bao, *J. Am. Chem. Soc.* 134 (2012) 5492.
- [11] R. M. Stolley, W. Guo, J. Louie, *Org. Lett.* 14 (2012) 322.
- [12] T. Maejima, Y. Shimoda, K. Nozaki, S. Mori, Y. Sawama, Y. Monguchi, H. Sajiki, *Tetrahedron* 68 (2012) 1712.
- [13] A. B. Sheremetev, N. V. Palysaeva, M. I. Struchkova, K. Y. Saponitsky, M. Y. Antipin, *Eur. J. Org. Chem.* (2012) 2266.
- [14] R. Berrino, S. Cacchi, G. Fabrizi, A. Goggiamani, *J. Org. Chem.* 77 (2012) 2537.
- [15] D. Liu, B. Liu, C. Wang, W. Jin, Q. Zha, G. Shi, D. Wang, X. Sang, *ACS Sustainable Chem. Eng.* 8 (2020) 2167.
- [16] J. Nicks, K. Sasitharan, R. R. R. Prasad, D. J. Ashworth, J. A. Foster, *Adv. Funct. Mater.* 31 (2021) 2103723.
- [17] Y. Zhang, S. Liu, Z. S. Zhao, Z. Wang, R. Zhang, L. Liu, Z. Bo. Han, *Inorg. Chem. Front.* 8 (2021) 590.
- [18] L. Rout, P. Saha, S. Jammi, T. Punniyamurthy, *Adv. Synth. Catal.* 350 (2008) 395.
- [19] R. Rajak, M. Saraf, S. K. Verma, R. Kumar, S. M. Mobin, *Inorg. Chem.* 58 (2019) 16065.

- [20] A. A. G. Valdivia, A. Z. Lekuona, A. G. Cardenas, B. Fernandez, J. A. Garcia, J. F. Q. d. Moral, J. Cepeda, A. R. Dieguez, *Inorganica Chim. Acta.* 509 (2020) 119687.
- [21] N. Shen, J. Li, Z. Wu, B. Hu, C. Cheng, Z. Wang, L. Gong, X. Huang, *Chem. Eur. J.* 23 (2017) 15795.
- [22] R. Arulraj, S. Sivakumar, K. Rajkumar, J. P. Jasinski, M. Kaurand A. Thiruvalluvar, *J. Chem. Crystallogr.* 50 (2019) 41.
- [23] S. K. Wolff, D. J. Grimwood, J. J. McKinnon, D. Jayatilaka, M. A. Spackman, *Crystal Explorer 2.0*; University of Western Australia: Perth, Australia, 2007. <http://hirshfeldsurfacenet.blogspot.com/>.
- [24] M.A. Spackman, D. Jayatilaka, *Hirshfeld surface analysis*, *Cryst. Eng. Comm.* 11 (2009) 19.
- [25] S. Das, T. Maity, S. Koner, *Appl. Catal. A. Gen* 513 (2016) 53.

Chapter 4



Synthesis of two isostructural lanthanide paddle-wheel based 2D MOF and exploration of catalytic O-arylation reaction

4.1 Introduction

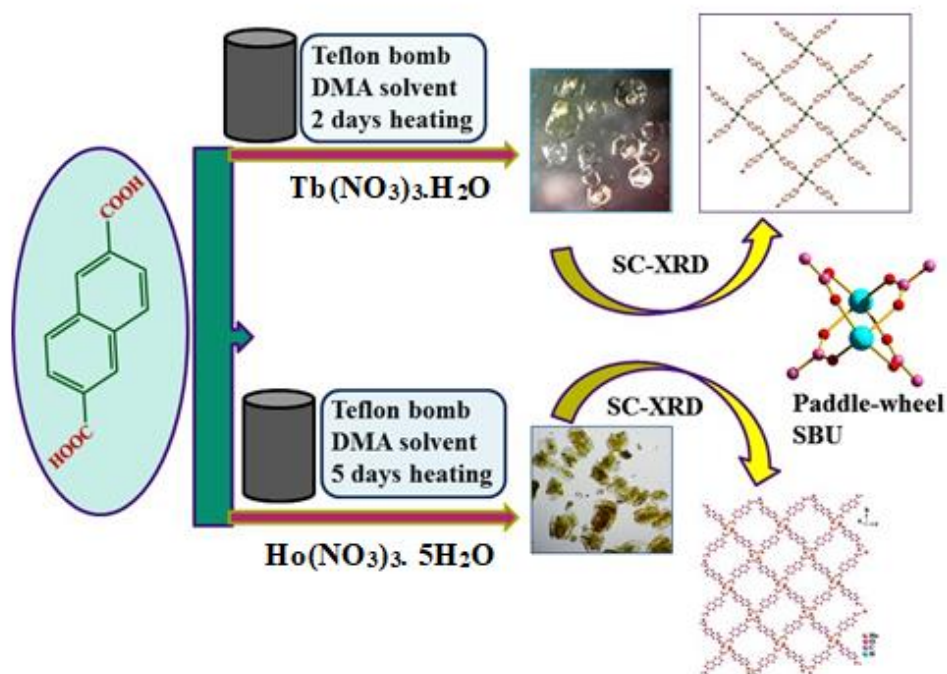
Cross-coupling methods are believed as an important synthetic strategy that involves catalytic reaction of aryl halides electrophile with an organometallic nucleophile [1-4]. In 1940s, first catalytic cross-coupling reactions were investigated using simple metal salts of first row transition series like CoCl_2 , NiCl_2 , CuCl_2 , FeCl_3 as catalysts. Later on, because of excellent catalytic efficacy and high stability, palladium-based catalysts have attracted huge attention in the field of organic synthesis and catalysis. Cross-coupling reactions are involved in the development of facile synthetic routes for the production of organic compounds in small and large scale at industry level.

Among different types of cross-coupling reactions, Suzuki reaction and O-arylation of phenols are very much important C-C and C-O coupling reaction. O-arylation reactions are particularly important because this reaction involves in the formation of diaryl ethers and it is used to produce such ether functionality during the synthesis of several biologically active compounds and natural products [5-6]. The remarkable importance of diaryl ethers in natural products and bio-active compounds has already been described in **Chapter 2**. Besides, many Schiff-base transition metal complexes catalyzed C-O coupling reactions have been studied at length [7-10]. Those include both heterogeneous and homogeneous reaction media [11-14, 15-19].

Recently, naphthalene containing compounds have gained significant attention in clinical, biological and analytical fields due to their structural diversity [20-22]. Metal complexes containing naphthalene ring in the ligand are well known for showing interesting fluorescent sensing for the detection of various analytes [23-26]. A large number of symmetrical and unsymmetrical multidentate imine-based metal complexes are known that exhibit interesting catalytic properties [27]. Very recently, a naphthalene core based Pd-Schiff base complexes

have been reported that can efficiently catalyze O-arylation reaction [28]. Though a significant efforts have been employed on catalytic C-O coupling reactions by using transition metal compound as catalyst, but naphthalene core based lanthanide MOF for O-arylation are rarely known in literature [29].

Considering these facts, C-O cross coupling reactions have been explored by employing the newly synthesized lanthanide-based MOFs (Tb and Ho-MOF containing “Paddle-wheel” core unit with naphthalene based ligand) that acts as heterogeneous catalyst. A brief synthetic procedure is given in **Scheme 4.1**.



Scheme-4.1 Synthetic route for the preparation of Ln-MOF (Tb and Ho)

4.2 Experimental**4.2.1 Materials**

Terbium(III) nitrate hydrate (99.9%), holmium(III) nitrate pentahydrate (99.99%), 2,6-naphthalenedicarboxylic acid (H₂NDC) (99%) were purchased from Sigma-Aldrich and were used as received without further purification. Cesium carbonate (98%), substituted phenols, other chemicals and solvents (analytical grade) were purchased from Merck (India). Solvents were distilled and dried before use.

4.2.2 Physical measurements

All the physical measurements and details of instrumentation have been already discussed in **Section 2.2.2, Chapter 2**.

4.2.3 Synthesis of [Tb(NDC)(NO₃)(DMA)₂]_n (MOF-3)

A mixture of terbium nitrate hydrate (0.25 mmol, 0.109g), 2,6-naphthalenedicarboxylic acid (0.125 mmol, 0.027g) and dimethylacetamide (DMA, 6mL) were sealed in a 15 mL teflon-lined Parr acid digestion bomb and kept at 100°C for three days. After three days, the solution was allowed to cool down slowly at the rate of ~5°C/h to room temperature. Hexagon-shaped yellow colored crystals were obtained from teflon-lined Parr acid digestion bomb. Crystals were washed with DMA thoroughly. Finally, the crystals are dried in air (yield 70% based on metal). X-ray quality hexagon-shaped crystals were chosen for the crystallographic study. Anal. Calcd. value for C₂₀H₂₄N₃O₉Tb (FW= 609.35), C, 39.38%, H, 3.93%, N, 6.89 %, Found C, 39.3%, H, 3.85%, N, 6.72 %. Selected IR peaks (FT-IR, ATR ν , cm⁻¹) (**Figure 4.1a**): 1674 (w), 1603 (s), [ν_{as} (CO₂⁻)], 1470 (m), 1406 (s) [ν_s (CO₂⁻)], 1357 (w), 1307 (m) [ν_s (C-O)], 1031 (m) [ν (C-N)].

4.2.4 Synthesis of $[\text{Ho}(\text{NDC})(\text{NO}_3)(\text{DMA})_2]_n$ (MOF-4)

MOF-4 was synthesized following a similar procedure as in MOF-3, however, in this case longer solvothermal treatment is necessary to grow good quality crystalline product. Holmium nitrate pentahydrate (0.25 mmol, 0.1102g) and 2,6-naphthalenedicarboxylic acid (0.125 mmol, 0.027g) were dissolved separately in DMA solvent. Two solutions were then mixed in a teflon lined Parr acid digestion bomb and heated to 100°C for 5 days. After cooling, X-ray quality yellow-colored crystals of MOF-4 were obtained. Anal. Calcd. value for $\text{C}_{20}\text{H}_{24}\text{O}_9\text{N}_3\text{Ho}$ (FW= 615.35), C, 39.00, H, 3.90, N, 6.82%, Found C, 39.13, H, 3.95, N, 6.85%. Selected IR peaks (FT-IR, ATR ν , cm^{-1}) (Figure 4.1 b): 1674 (w), 1610 (s), [$\nu_{a2}(\text{CO}^-)$], 1470 (m), 1399 (s) [$\nu_s(\text{CO}^{2-})$], 1357 (w), 1294(s) [$\nu_s(\text{C-O})$].

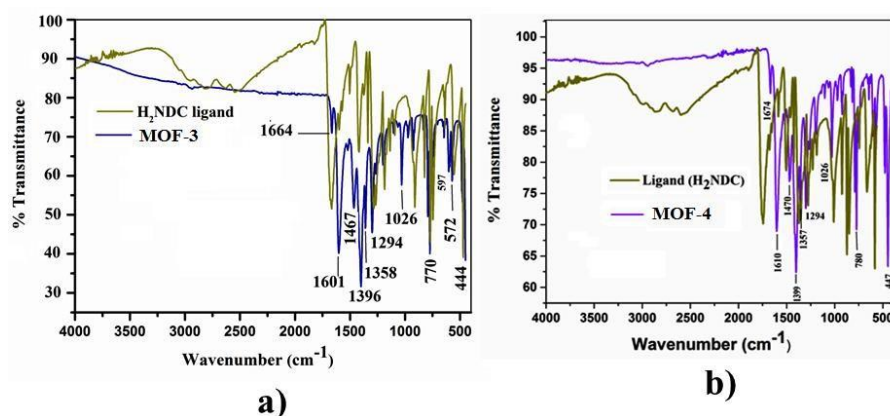


Figure 4.1 a) FT-IR spectra of MOF-3 and H_2NDC ligand; b) FT-IR spectra of MOF-4 and H_2NDC .

4.2.5 X-ray crystallography

All the description and the procedure of data collection by single crystal X-ray diffraction and structure solution by using different software programme have been already discussed in Section 2.2.4, Chapter 2. A summary of the

crystallographic data and the relevant structural refinement parameters for MOF-3 and MOF-4 are given in Table 4.1.

Table 4.1 Data collection, cell and refinement parameters obtained from single-crystal X-ray diffraction analysis. Experiments were carried out at temperature 298 K.

MOF	MOF-3	MOF-4
Formula	C ₂₀ H ₂₄ N ₃ O ₉ Tb	C ₂₀ H ₂₄ N ₃ O ₉ Ho
Formula Weight	609.35	615.35
Crystal System	Orthorhombic	Orthorhombic
Space Group	<i>Pbca</i> (no.61)	<i>Pbca</i> (no.61)
<i>a</i> (Å)	13.4259(15)	13.5941(12)
<i>b</i> (Å)	18.034(2)	18.1413(16)
<i>c</i> (Å)	19.129(2)	18.9853(17)
α (°)	90.00	90.00
β (°)	90.00	90.00
γ (°)	90.00	90.00
<i>V</i> (Å ³)	4631.6(9)	4682.1(7)
<i>Z</i>	8	8
<i>D</i> _{calc} (gcm ⁻³)	1.748	1.746
μ (mm ⁻¹)	3.108	3.434
<i>F</i> (000)	2416	2432
θ Range (°)	2.5-27.1	2.2-27.1
Intervals of reflection indices	-13<= <i>h</i> <=17, -23<= <i>k</i> <=23, -24<= <i>l</i> <=24	-17<= <i>h</i> <=17, -23<= <i>k</i> <=23, -24<= <i>l</i> <=24
Reflections measured	48630	132213
<i>R</i> _{int}	0.088	0.053
Unique data	5106	5163
<i>R</i> indices (all data)	<i>R</i> 1 = 0.0602, w <i>R</i> 2 = 0.1512	<i>R</i> 1 = 0.0392, w <i>R</i> 2 = 0.0700

Final R indices [$I > 2\sigma(I)$]	$RI = 0.0475$, $wR2 =$ 0.1264	$RI = 0.0257$, $wR2 = 0.0584$
Data with $I > 2(I)$	4122	4127
$R_1 (I > 2(I))$	0.0475	0.0257
$wR_2 (I > 2(I))$	0.1264	0.0584
(GOF) on F^2	1.071	1.104

$$RI = \frac{\sum ||F_o| - |F_c||}{\sum |F_o|}, wR2 = \left\{ \frac{\sum [w(F_o^2 - F_c^2)^2]}{\sum w(F_o^2)^2} \right\}^{1/2}$$

4.2.6 General procedure for catalytic O-arylation reactions

0.151 g (1 mmol) of *p*-nitrobromobenzene and 0.103 g (1 mmol) of *p*-cresol added with 0.487 g (1.5 mmol) solid cesium carbonate in 4 mL dehydrated dimethylformamide (DMF) solvent in a 15 mL round-bottom flask. 5mg of MOF-3 and 10 mg MOF-4 was added separately to the reaction medium and stirred under continuous heating at 95°C for eight hours. The conversion of the reaction was monitored by thin layered chromatography (TLC) method. After completion of the reaction, mixture was cooled to room temperature and purged on ice cold water. The aqueous layer was extracted three times with diethylether (50 mL). Combined organic layer thus collected was washed with brine solution, dried over anhydrous sodium sulfate and later concentrated in vacuum. Then the collected residue was further purified by column chromatography on silica-gel (60-120 mesh) and was eluted with petroleum ether /ethyl acetate mixture to get the desired product. The product analyzed through elemental analysis, ¹H-NMR, and compared with the literature data.

4.3 Results and discussion

4.3.1 X-ray structural description of [Tb(NDC)(NO₃)(DMA)₂]_n (MOF-3) and [Ho(NDC)(NO₃)(DMA)₂]_n (MOF-4)

Single-crystal X-ray diffraction analysis reveals that MOF-3 crystallizes in orthorhombic *Pbca* space group with *Z* value 8. The asymmetric unit of MOF-3 comprises of one crystallographically unique Tb(III) ion, one 2,6-naphthalenedicarboxylate (NDC²⁻) linker, two coordinated dimethyl acetamide (DMA) molecules and one coordinated nitrate anion. The ORTEP diagram with atom numbering is given in **Figure 4.2**. Each Tb(III) is surrounded by four oxygen atoms of monodentate COO⁻ group (O1, O2, O3, O4) from four different NDC²⁻ ligand, two oxygen (O5, O6) from two coordinated DMA molecules and other two oxygen atoms (O7, O9) from one coordinated nitrate anion (**Figure 4.3a**), adopting a distorted triangular-dodecahedral geometry (**Figure 4.3b**). The carboxylic Tb-O bond distances range 2.292(4)–2.541 (6) Å and the angles of O–Tb–O vary from 50.42(15) to 152.52(13) given in **Table 4.2** and **Table 4.3** respectively all of which are comparable to those for other Tb-O donor complexes with aromatic carboxylic acid ligands [30]

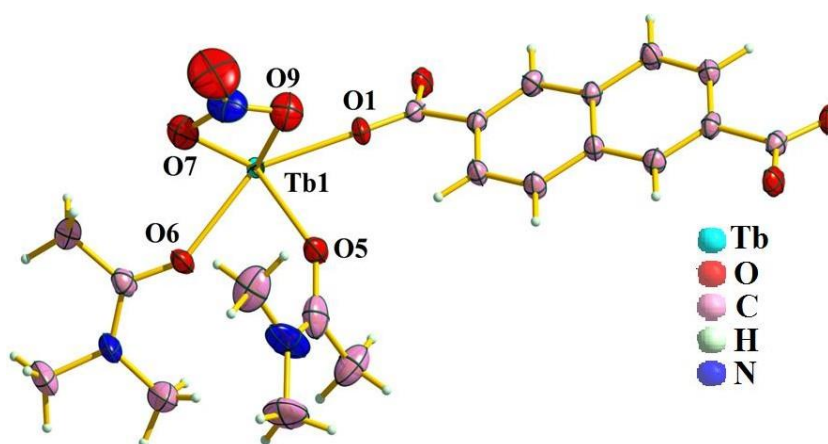


Figure 4.2 Ortep diagram of MOF-3 with 50% ellipsoid probability.

Table 4.2 Selected bond-lengths (Å) for MOF-3 and MOF-4.

Atoms	Distance (Å)	Atoms	Distance (Å)
Tb1–O1	2.292(4)	Ho1–O1	2.265(3)
Tb1–O5	2.352(4)	Ho1–O5	2.330(3)
Tb1–O6	2.377(4)	Ho1–O6	2.349(3)
Tb1–O7	2.486(5)	Ho1–O7	2.454(3)
Tb1–O9	2.541(6)	Ho1–O9	2.534(4)
Tb1– ^a O4	2.344(4)	Ho1– ^b O3	2.324(3)
Tb1– ^c O2	2.355(4)	Ho1– ^c O2	2.326(3)
Tb1– ^e O3	2.341(4)	Ho1– ^d O4	2.316(3)

Table 4.3 Selected angles (°) for MOF-3 and MOF-4.

Atoms	Angle	Atoms	Angle
O1–Tb1–O5	80.84(13)	O1–Ho1–O5	80.43(10)
O1–Tb1–O6	147.92(12)	O1–Ho1–O6	147.53(10)
O1–Tb1–O7	127.93(13)	O1–Ho1–O7	128.10(11)
O1–Tb1–O9	79.60(15)	O1–Ho1–O9	79.33(11)
O1–Tb1– ^a O4	77.75(12)	O1–Ho1– ^b O3	77.97(10)
O1–Tb1– ^c O2	123.66(14)	O1–Ho1– ^c O2	123.68(10)
O1–Tb1– ^e O3	78.86(13)	O1–Ho1– ^d O4	78.63(9)
O5–Tb1–O6	73.36(13)	O5–Ho1–O6	73.52(10)
O5–Tb1–O7	95.85(15)	O5–Ho1–O7	94.92(11)
O5–Tb1–O9	73.68(15)	O5–Ho1–O9	73.03(11)
^a O4–Tb1–O5	141.94(13)	^b O3–Ho1–O5	140.98(10)
^c O2–Tb1–O5	143.19(13)	^c O2–Ho1–O5	144.19(10)
^e O3–Tb1–O5	81.26(13)	^d O4–Ho1–O5	82.02(10)
O6–Tb1–O7	74.37(13)	O6–Ho1–O7	74.04(11)
O6–Tb1–O9	110.15(15)	O6–Ho1–O9	110.28(11)
^a O4–Tb1–O6	134.18(13)	^b O3–Ho1–O6	134.39(10)
^c O2–Tb1–O6	72.97(13)	^c O2–Ho1–O6	73.53(10)
^e O3–Tb1–O6	78.66(13)	^d O4–Ho1–O6	78.86(10)
O7–Tb1–O9	50.42(15)	O7–Ho1–O9	50.59(12)
^a O4–Tb1–O7	73.87(14)	^b O3–Ho1–O7	74.15(10)
^c O2–Tb1–O7	89.05(14)	^c O2–Ho1–O7	89.21(11)
^e O3–Tb1–O7	152.52(13)	^d O4–Ho1–O7	152.44(11)

^a O4–Tb1–O9	71.76(15)	^b O3–Ho1–O9	71.30(11)
^c O2–Tb1–O9	132.72(15)	^c O2–Ho1–O9	132.51(11)
^e O3–Tb1–O9	149.13(15)	^d O4–Ho1–O9	149.01(11)
^c O2–Tb1– ^a O4	74.34(12)	^c O2–Ho1– ^b O3	74.20(9)
^e O3–Tb1– ^a O4	124.09(14)	^b O3–Ho1– ^d O4	124.21(10)
^c O2–Tb1– ^e O3	78.00(12)	^c O2–Ho1– ^d O4	78.25(9)

Symmetry element ^a= 1-x,-1/2+y,1/2-z, ^c= 1-x,1-y,1-z, ^d= x,1/2-y,-1/2+z ^e=1/2+z,
^b=1-x,1/2+y,3/2-z

The ligand NDC²⁻ features *syn-syn* bridging μ -1,3 coordination mode (Figure 4.3c). Carboxylate oxygen atoms O1, O2 and O3, O4 of NDC²⁻ connects two Tb(III) metal centres through μ ₂-*syn,syn*-bridge binding mode and form dimeric Tb units (Figure 4.3d). In addition, two crystallographically equivalent Tb(III) ions are bridged by four bidentate carboxylate groups of four different NDC²⁻ in a di-monodentate fashion to generate a lanthanide paddle-wheel building block i.e {Tb₂(COO)₄} core as can be seen in Figure 4.3e.

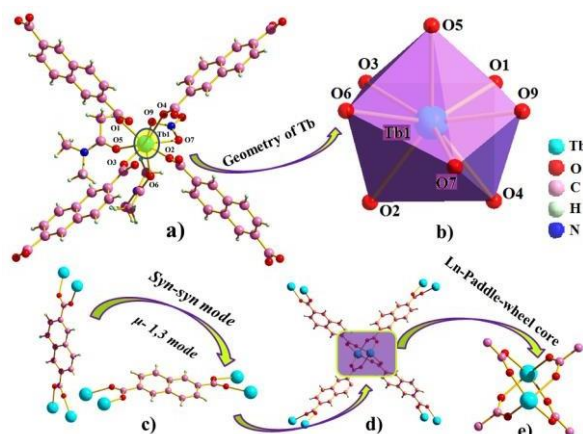


Figure 4.3 a) Coordination fashion for Tb(III) metal center; b) Distorted triangular-dodecahedral geometry around Tb(III); c) Coordination mode of 2,6-naphthalene dicarboxylate (NDC²⁻) ligand; d) Formation of Tb based paddle-wheel SBU core molecular structure; e) Clear representation of Tb based Paddle-wheel core.

The Tb···Tb distance in the paddle-wheel is 4.3053(6) Å. The paddle-wheel building blocks connects each other through two carboxylate groups of 2,6-naphthalene dicarboxylate (NDC²⁻) ligand along crystallographic c-axis to lead to a one dimensional (1D) infinite chain ···Tb–O–C–O–Tb··· (Figure 4.4 a). These paddle-wheel Tb dimer cluster may be visualized as secondary building units (SBUs), which are further interconnected by NDC²⁻ ligands to construct a infinite two-dimensional square grid network structure (Figure 4.4b). Representation of two-dimensional framework structure of MOF-3 is also clearly viewed by polyhedral drawing of central metal coordination environment and also by space-filled model (Figure 4.5a, b).

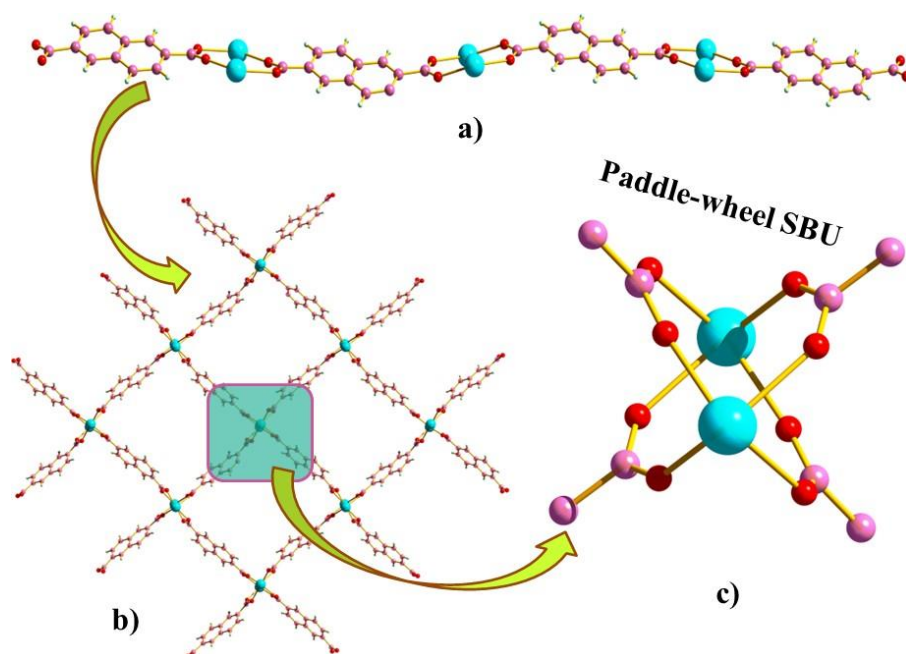


Figure 4.4 a) Construction of 1D chain by NDC²⁻ ligand for MOF-3; b) 2D square-grid network structure of MOF-3, coordinated nitrate and DMA molecules are omitted for clarity; c) Clear representation of Tb-based paddle-wheel SBU in 2D structure.

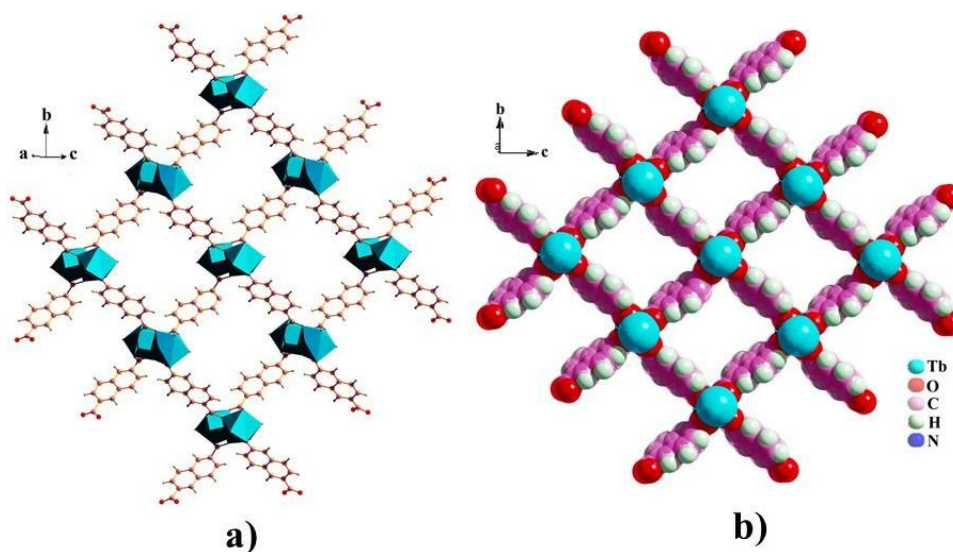


Figure 4.5 a) Polyhedral drawing MOF-3 b) Two-dimensional framework of MOF-3 in space-filled mode

MOF-4 crystallizes in the same crystal system (orthorhombic) with same space group (*Pbca*) as MOF-3. ORTEP diagram is given in **Figure 4.6**. The molecular structure of MOF-4 is represented in the following **Figure 4.7a** where holmium metal centre is eight coordinated with HoO_8 coordination polyhedron. The geometry of unique Ho1 is distorted tricapped dodecahedron as shown in **Figure 4.7b**. Bond distance of Ho–O are found to be in the range of 2.265(3)–2.538(4) Å where bond angles of O–Ho–O vary from 50.61(15) to 152.49(12)° (**Table 4.2** and **4.3** respectively). Construction of two-dimensional network structure of MOF-4 through so called “paddle-wheel” secondary building unit is given in **Figure 4.7c, d**. 2D square-grid network structure is also described by space-filled model as shown in **Figure 4.7e**. Polyhedral drawing around the metal centre and two-dimensional structure of MOF-4 along different planes are depicted in **Figure 4.8a, b**.

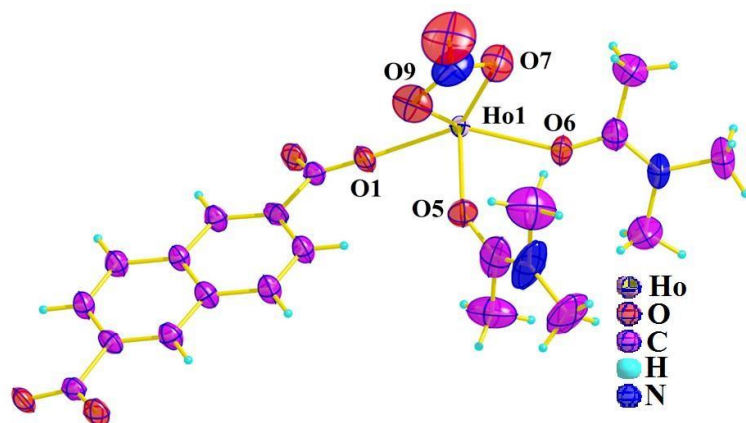


Figure 4.6 Ortepe diagram of MOF-4 with 50% ellipsoid probability.

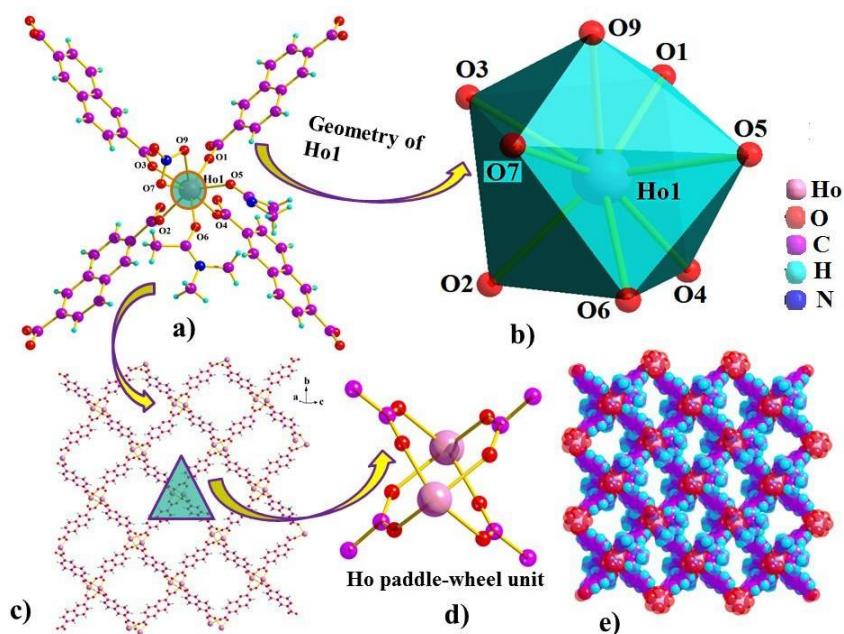


Figure 4.7 a) Coordination environment of MOF-4 with atom numbering around central metal Ho; b) Coordination fashion of ligand (distorted tricapped dodecahedral geometry); c) 2D square-grid array of MOF-4; d) Clear representation of Ho-based paddle-wheel into 2D structure; e) Space-filled model of MOF-4.

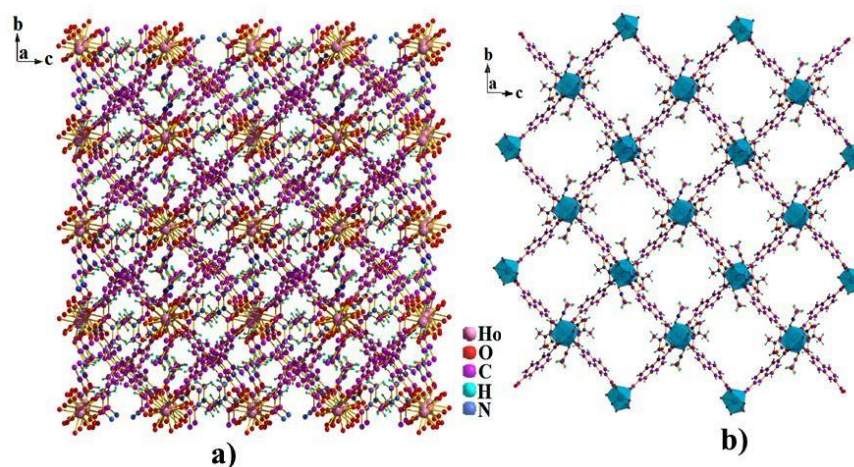


Figure 4.8 a) 2D picture of MOF-4 along *ac*-plane; b) 2D picture along *ab*-plane.

4.3.2 Phase identification for MOF-3 and MOF-4

Powder X-ray diffraction (PXRD) analysis of MOF-3 and MOF-4 was carried out to characterize the phase purity at room temperature (Figure 4.9a, b). The experimental results show sharp peaks with strong intensity and all the major peaks are present and matched well with the simulated PXRD pattern (major peaks are indexed and marked with Miller plane). This indicates the reasonable crystallinity of both the MOFs and purity of bulk phase of the as synthesized samples.

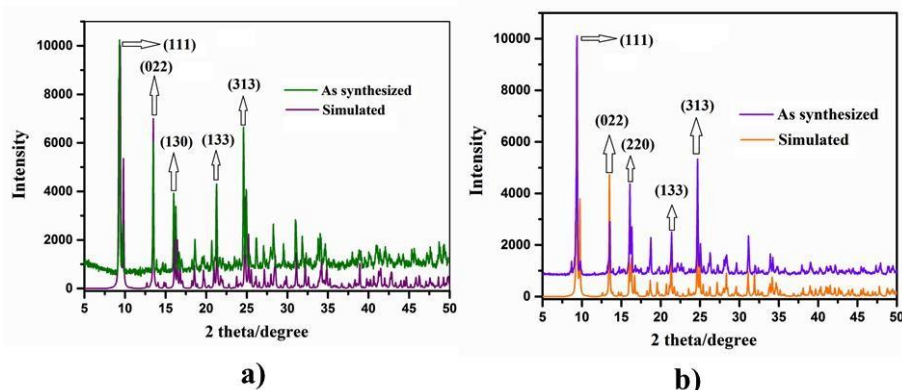


Figure 4.9 a) PXRD pattern of MOF-3; b) PXRD pattern of MOF-4

4.3.3 Hirshfeld surface analysis for MOF-3 and MOF-4

Hirshfeld surface analyses have increasingly gained in popularity in last few years. It is a useful tool with which intermolecular interaction of crystal structures can be studied well and can provide a detailed explanation of the immediate environment of a molecule in a crystal. The Hirshfeld surface analysis and consequent supplementary pseudo-mirror two-dimensional (2D) fingerprint plots over the surface have been performed and produced to recognise and quantify the nature of strong and weak intermolecular interactions within the crystal lattice of MOF-3 and MOF-4. In order to clarify the strength of weak interactions between the groups and relationship between the degrees of aggregation of aromatic group Hirshfeld surface (HS) and 2D fingerprint analysis of these two MOFs have been performed using Crystal Explorer 3.1. Hirshfeld surface of a particle is mapped utilizing the descriptor d_{norm} factor which is analyzed with respect to the d_i (internal) and d_e (external) distances to nearby atoms. The d_{norm} plot for MOF-3 and MOF-4 plotted between -0.6 to 1.6 Å display deep red circular depression marked on the blue surface mapped with fluctuating intensity demonstrate the presence of interactions which are shorter than or equivalent to the van der Waals

radii sum of the two interacting nuclei. In order to visualize the atoms, the surfaces are depicted transparently. The intensity of the red patch present on the blue surfaces suggests the strength of a short interaction. For MOF-3 and MOF-4, Hirshfeld surfaces are generated by fixing the iso-value 0.5, which gave Hirshfeld surface area 484.43 \AA^2 and 485.21 \AA^2 , Hirshfeld surface volume of 566.27 \AA^3 and 572.77 \AA^3 with globularity 0.683 and 0.687 and asphericity 0.299 and 0.296 respectively. The shape-index and curvedness plots are generated from -1.000 to 1.000 a.u. and from -4.000 to 4.000 a.u. for both the two MOFs. The shape index and curvedness plots are clearly depicted in **Figure 4.10**. Blue triangle like pieces and orange/red on curvedness map give information about the Van der Waals, (**Figure 4.10**) valance bond and $\pi \cdots \pi$ interactions.

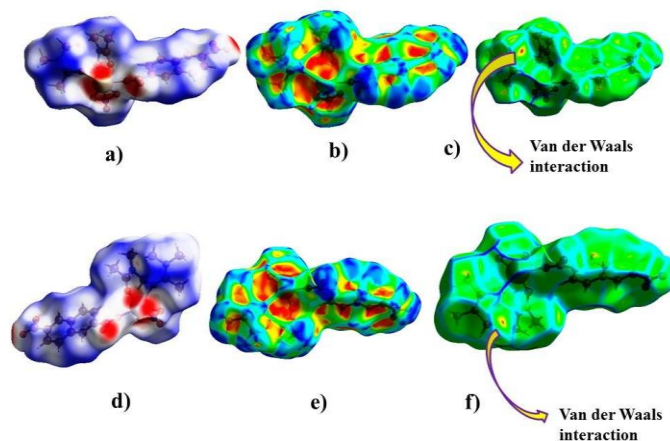


Figure 4.10 a) View of Hirshfeld surface of MOF-3 plotted over d_{norm} ; b) Shape index plot of MOF-3; c) Curvedness plot of MOF-3; d) d_{norm} Hirshfeld surface of MOF-4; e) Shape index plot of MOF-4; f) Curvedness plot of MOF-4.

Additionally, the total and decomposed fingerprint plots for MOF-3 and MOF-4 have been constructed. 2D fingerprint plot for overall interactions are represented in **Figure 4.11** and **Figure 4.12**. The results show that H \cdots H interatomic contact (defined as Van der Waals interactions between the related H-

atoms) are the most important contributor in the crystal packing with contribution 37.8% for MOF-3 and 38.3% for MOF-4. In MOF-3 other interatomic contacts such as O...H/ H...O and C...H/H...C interactions contribute 25.1% and 22% respectively while in MOF-4, O...H/ H...O and C...H/H...C engage in 24.4% and 21.9% percentage contribution to the HS. O...O, Tb...O/ Ho...O, C...O interatomic contacts have less contribution in crystal packing for both of the two MOFs (7.8%, 4.8%, and 0.7% for MOF-3 and 8.1%, 4.7% and 0.7% for MOF-4 respectively). 2D fingerprint plots of these short interatomic contacts show that the major contributions are from H...H, C...H and O...H compared to the other short interatomic contacts. So, from the inspection of total and split fingerprint plots, there is a very small variation in the respective contribution and also nearly similar in morphologies. This can be attributed the isostructural characteristics of the two MOFs.

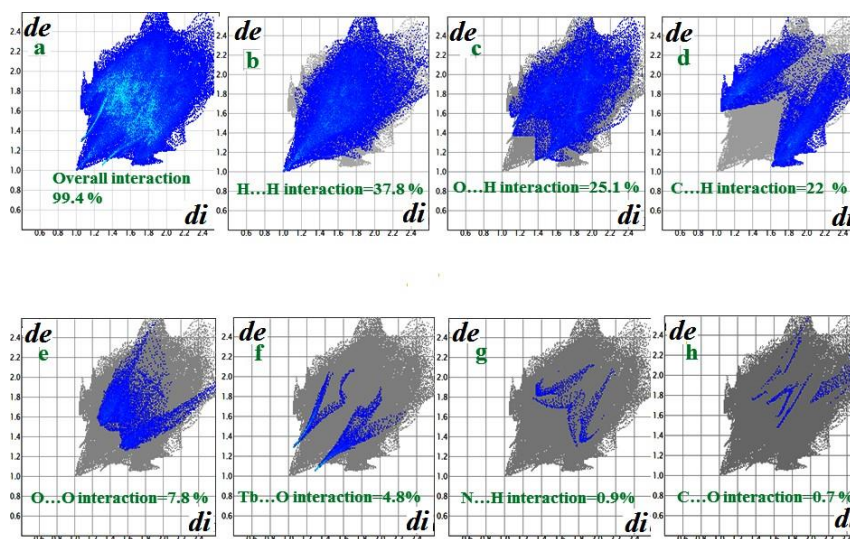


Figure 4.11 2D fingerprint plot of MOF-3: (a) Overall interaction; (b-h) Individual interatomic (major and weak) contacts including reciprocal contacts.

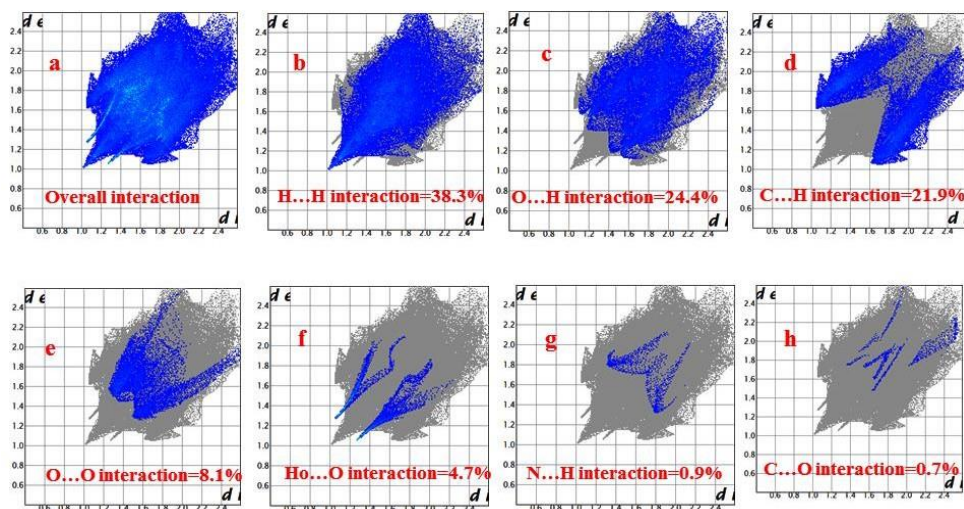


Figure 4.12 Fingerprint plot of MOF-4: (a) Overall interaction; (b-h) Individual interatomic contacts (major and weak) including reciprocal contacts.

4.3.4 Thermal study of MOF-3 and MOF-4

To study the thermal stability of the framework in the solid state, thermogravimetric analysis was carried out for MOF-3 and MOF-4. Thermal analysis of these two MOFs were analyzed by using powdered sample from room temperature to 800°C under N₂ atmosphere. **Figure 4.13a** showed the thermogram from the heating result of the two where it can be observed that there were desolvation and decomposition of the ligand. MOF-3 and MOF-4 showed mass loss in four stages. At the first step, upon heating, MOF-3 displayed mass loss of ~ 28.02% which is corroborated with the theoretical value of ~ 28.3% due to release of two coordinated dimethyl acetamide (DMA) molecules at a temperature range of 190-335° C whereas for MOF-4, a thermal mass loss of ~ 27.28% (theoretical value ~ 28.28%) occurred at a temperature of 173-348 °C owing to the loss of two coordinated DMA molecules from the metal centre as represented in **Figure**

4.13b. Upon further heating, the desolvated MOF-3 exhibits an additional mass loss of ~ 40.5% (theoretical ~ 45.1%) and MOF-4 shows mass loss ~ 40.5% (theoretical ~ 45.2%) in the temperature range 410–748°C which can be corroborated with the decomposition of organic ligand and nitrate ion. Finally, the MOF converted to metal oxide after thermal decomposition.

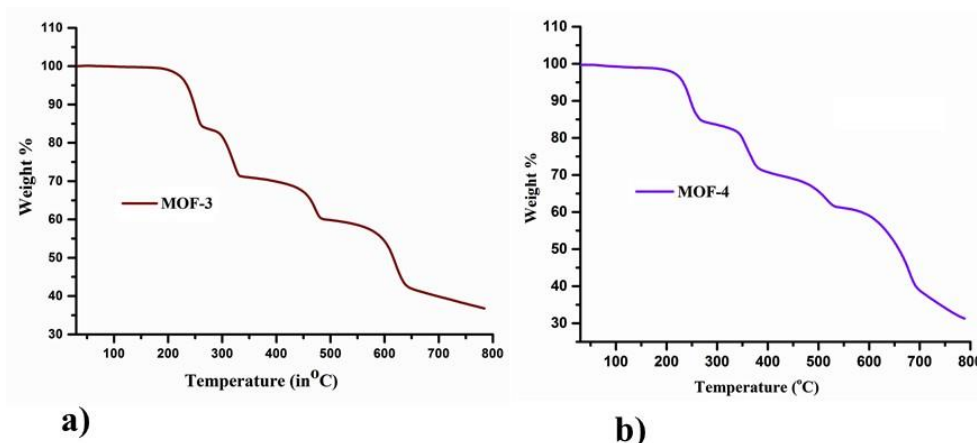
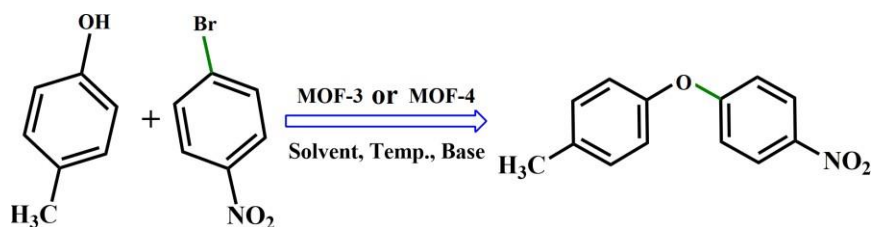


Figure 4.13 Thermogravimetric plot of a) MOF-3 and b) MOF-4

4.3.5 Catalytic activity studies

Initial optimization of O-arylation reactions were carried out using *p*-cresol and *p*-nitrobromobenzene as substrate under various reaction conditions catalyzed by MOF-3 or by MOF-4 (both can be used as catalyst) (Table 4.4). The catalytic O-arylation reaction have been carried out using different parameters such as solvents, bases, reaction temperature and reaction time etc. because these parameters are found to impact the progress of the O-arylation reaction [31]. For the selection of the best solvents, the catalysis reactions were carried out using different solvents (entries 1-8). Amongst them, highest yield of desired product is obtained in DMF (entry 6). Generally, O-arylation reactions show much better reactivity with Cs₂CO₃ (base) than with K₂CO₃ or Na₂CO₃ due to higher solubility, enhanced basicity and fine powder form. Obviously, Cs₂CO₃ becomes the best

choice as a base among others (entries 6–9). The catalyst does not show its activity in absence of base and inert atmosphere is not applied as the catalysts are stable in air (checked by PXRD pattern keeping several days in atmosphere (**Figure 5a, b**)). Besides, temperature and time of the reaction play an important role in O-arylation reaction. Hence, progress of the reaction has been checked by changing the reaction temperature from low to high. Isolated yield increases sharply with the increase of reaction temperature (entries 11–15). At 95°C product yield improved markedly and goes up to 90% for catalyst MOF-3 in O-arylation reactions, however, in case of catalyst MOF-4 the yield was 78%. Nevertheless, isolated yield of the product do not significantly improve beyond 110°C for both the catalysts. Trace to small yield was obtained in the absence of catalyst in 9 hours (entry 10). In addition, a mixture of terbium nitrate salt and 2,6-naphthalenedicarboxylic acid, and holmium nitrate and 2,6-naphthalenedicarboxylic acid, and neat terbium and holmium nitrate salt have been tested as catalyst but only low to trace conversion was observed (entry 16 and 17). Thus, the optimum condition of the catalytic O-arylation reaction for both catalysts was as follows: Cs₂CO₃ as base, DMF as solvent and 95°C as reaction temperature in open air condition.

Table 4.4 Optimization of reaction condition^a for the O-arylation reaction of p-cresol with p-bromonitrobenzene

Entry	Catalyst	Base	Solvent	Isolated Yield ^b (%) (MOF-3)	Isolated Yield ^b (%) (MOF-4)
1	MOF-3/MOF-4	Cs ₂ CO ₃	Methanol	–	–
2	MOF-3 /MOF-4	Cs ₂ CO ₃	Ethanol	29	19
3	MOF-3 /MOF-4	Cs ₂ CO ₃	Acetonitrile	21	–
4	MOF-3 /MOF-4	Cs ₂ CO ₃	DMSO	72	62
5	MOF-3 /MOF-4	Cs ₂ CO ₃	Ethylene-glycol	54	46
6	MOF-3 /MOF-4	Cs ₂ CO ₃	DMF	88	78
7	MOF-3 /MOF-4	K ₂ CO ₃	DMF	78	70
8	MOF-3 /MOF-4	Na ₂ CO ₃	DMF	74	73
9	MOF-3 /MOF-4	CH ₃ COONa	DMF	trace	–
10	–	Cs ₂ CO ₃	DMF	trace	trace
11	MOF-3 /MOF-4	Cs ₂ CO ₃	DMF	29 ^c	21 ^c
12	MOF-3 /MOF-4	Cs ₂ CO ₃	DMF	41 ^d	35 ^d
13	MOF-3 /MOF-4	Cs ₂ CO ₃	DMF	70 ^e	57 ^e
14	MOF-3 /MOF-4	Cs ₂ CO ₃	DMF	90 ^f	73 ^f
15	MOF-3 /MOF-4	Cs ₂ CO ₃	DMF	91 ^g	78 ^g
16	Tb(NO ₃) ₃ .xH ₂ O + 2,6-NDC / Ho(NO ₃) ₃ . xH ₂ O + 2,6-NDC	Cs ₂ CO ₃	DMF	29	18

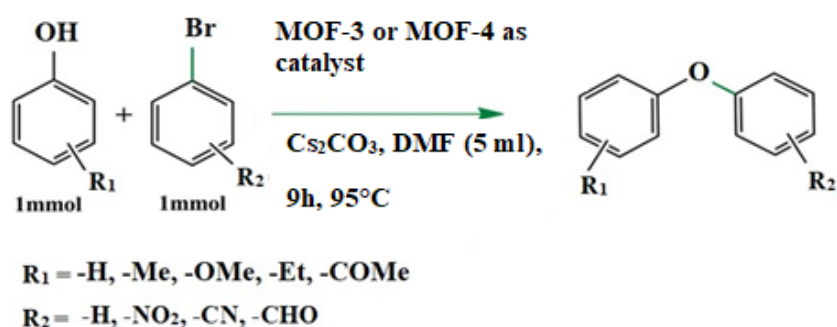
17	Tb(NO ₃) ₃ .xH ₂ O / Ho(NO ₃) ₃ . xH ₂ O	Cs ₂ CO ₃	DMF	trace	–
----	--	---------------------------------	-----	-------	---

^aReaction conditions: *p*-cresol (1 mmol), *p*-nitrobromobenzene (1 mmol), catalyst (5 mg MOF-3 and 10 mg MOF-4), base (1.5 mmol), solvent (5 mL) and temperature 95°C. ^bIsolated yield. ^cReaction temperature 30°C. ^dReaction temperature 50°C. ^eReaction temperature 70°C. ^fReaction temperature 95°C. ^gReaction temperature 110 °C.

Under the optimized reaction conditions, the applicability of the O-arylation reaction using substituted phenol with bromoarenes containing diverse functional groups using MOF-3 or MOF-4 as catalysts to unsymmetrical diaryl ethers were investigated (Table 4.5). The O-arylation reactions occurred smoothly with various substitutions (electron donating or withdrawing) on phenol moiety and bromoarenes with different functional groups (Table 4.5, entries 1, 2, 5, 10 and 11). Expected products were obtained with good yield in this catalysis reaction. Electron donating methyl group containing phenols yield higher quantity of products in comparison to other substituted phenol and it is noticed that MOF-3 shows comparatively better catalytic efficacy than MOF-4. (Table 3, entry 3, 4, 5, 10). The yield of diaryl ether products is decreased in the order *p*-> *o*- >*m*-cresol. It may be realized that methyl substituent at *ortho/para* position affords positive inductive effect and hyper-conjugation effect which increases nucleophilicity of phenolate oxygen atoms, whereas substitution at the *meta* position affords only the positive inductive effect. Between *para* and *ortho* cresol, more steric crowding at *ortho* position might lead to lower yield. Presence of electron withdrawing group (–NO₂, –CHO, –CN) at *para*-position activity of bromobenzene is being elevated in the catalysis reaction and hence, maximum yield was obtained for the unsymmetrical ethers (Table 4.5 entry 3, 5, 9). The coupling reactions of electron-deficient phenols with aryl halides have been challenging as the

corresponding phenolates are weak nucleophile [30]. Catalysis reaction has also been examined towards weak nucleophile such as *p*-hydroxyacetophenone (entry 14). Isolated yield for this reaction was low and MOF-3 exhibited comparatively good yield than MOF-4. Apart from *p*-hydroxyacetophenone, O-arylation reaction was carried out with *p*-methoxyphenol and the expected product with isolated yield is given in Table 4.5, entry 12.

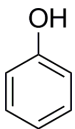
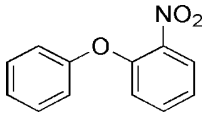
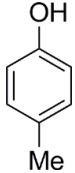
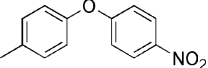
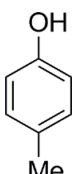
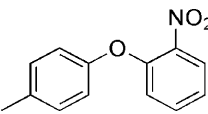
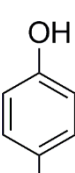
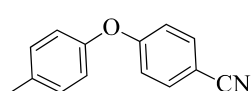
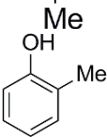
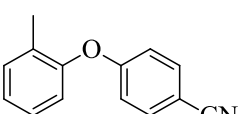
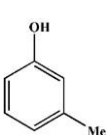
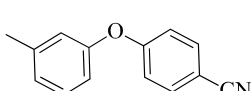
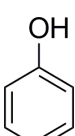
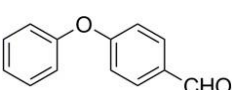
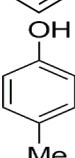
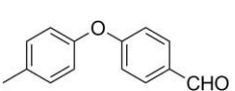
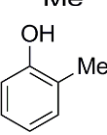
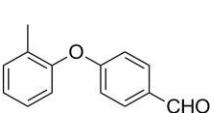
Table 4.5 O-arylation between substituted phenols with substituted bromobenzene^a

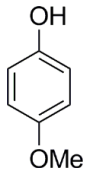
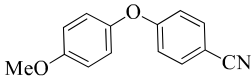
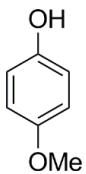
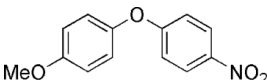

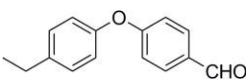
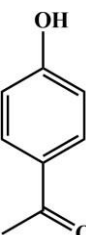
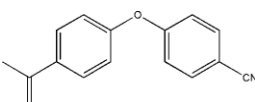


Entry	Aryl alcohol (Substituted phenol)	-R ₂	Product	Reaction time (h)	Isolated Yield ^b (wt%)	Isolated Yield ^b (wt%) for MOF-3 for MOF-4
1		- <i>p</i> NO ₂		9	77	64

Chapter 4

Catalytic O-arylation by PW-Ln-MOF

2		- <i>o</i> NO ₂		9	69	56
3		- <i>p</i> NO ₂		9	90	78
4		- <i>o</i> NO ₂		9	81	67
5		- <i>p</i> CN		9	88	76
6		- <i>p</i> CN		9	85	73
7		- <i>p</i> CN		9	81	68
8		- <i>p</i> CHO		9	79	63
9		- <i>p</i> CHO		9	86	70
10		- <i>p</i> CHO		9	80	62

11		-pCN		9	82	69
12		-pNO ₂		9	86	72
13		-pCHO		9	87	77
14		-pCN		9	40	32

4.3.6 Heterogeneity of the catalysts

Reusability and heterogeneity is an important criterion to use MOF-3 or MOF-4 as catalyst, because terbium and holmium are costly as well as toxic. We have performed hot filtration test to ascertain the catalytic reaction is indeed heterogeneous. The solid catalyst was filtered in hot condition after 4 hours and the activity of the residual solution without the catalyst was studied [30]. The solution was kept in reaction condition for another eleven hours and composition of the reaction mixture was analyzed time to time. It was noticed that the reaction does not proceed during this period. This experiment evidently demonstrates that

there was no leaching of terbium(III) and holmium(III) ions from the solid catalyst during the catalysis reaction.

4.3.7 Separation and stability of the two catalysts (MOF-3 and MOF-4)

After the catalysis reaction is over, the catalysts were separated by centrifugation and washed with water and dichloromethane mixture thoroughly and dried under vacuum. As, the amount recovered catalyst was very small amount in a single batch, catalyst collected upto seven batches to get considerable amount of sample that is suitable for PXRD and IR studies. In order to check the stability of the catalyst after reaction, powder X-ray diffraction analysis (PXRD) and IR spectral measurements were carried out. Comparison of PXRD data (**Figure 4.14 a, b**) and IR spectra (**Figure 4.15 a, b**) with the previous MOF and recovered catalyst clearly proved that the structural integrity of the MOF remain same after the catalysis reaction.

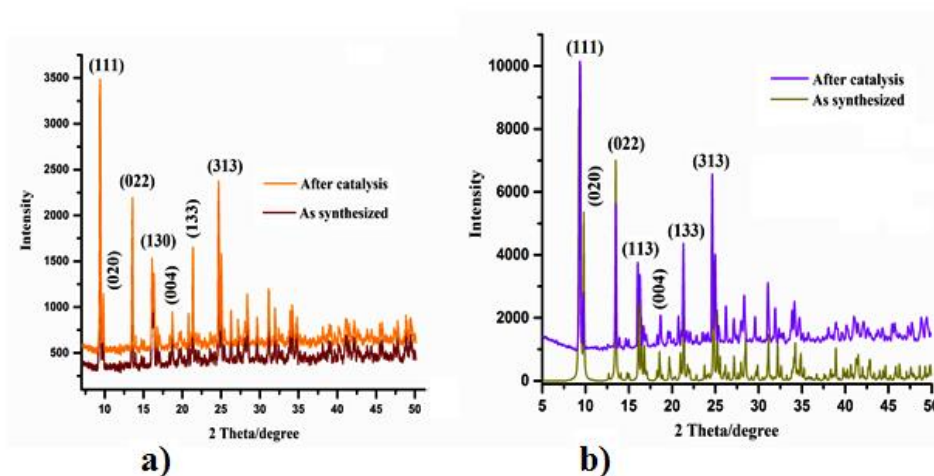


Figure 4.14 a) PXRD study after using MOF-3 or b) MOF-4 as catalyst under following reaction conditions; *p*-nitro bromobenzene (1mmol), *p*-cresol (1 mmol), Cs₂CO₃ (1.5 mmol), MOF-3 or MOF-4 (0.025 mol%), DMF (5 mL) at 95 °C for 9 h.

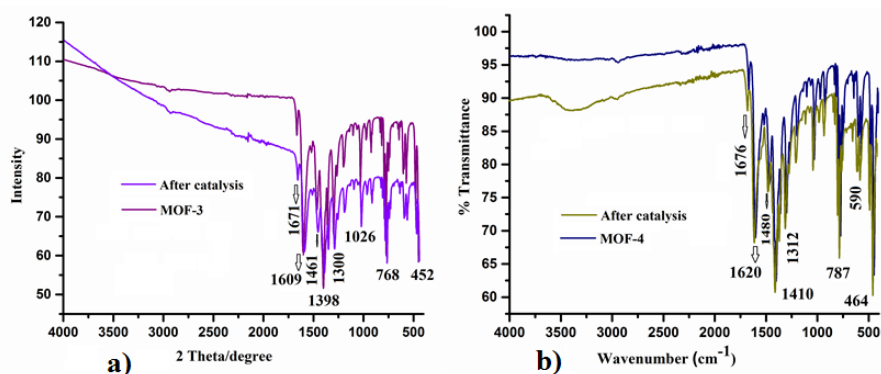


Figure 4.15 a) FT-IR spectra of MOF-3 or b) MOF-4 before and after using them in catalytic reaction. Reaction conditions: *p*-nitro bromobenzene (1mmol), *p*-cresol (1 mmol), Cs₂CO₃ (1.5 mmol), MOF-3 or MOF-4 (0.025 mol %), DMF (5 mL) at 95°C for 9 h.

4.4 Conclusion

In summary, synthesis of the two novel isostructural 2D paddle-wheel Ln-based MOFs, *viz.* [Tb(NDC)(NO₃)(DMA)₂]_n (MOF-3) and [Ho(NDC)(NO₃)(DMA)₂]_n (MOF-4) have been reported. Structure of the complex was established by single-crystal X-ray diffraction analysis. 2,6-naphthalenedicarboxylic acid (2,6-NDC²⁻), nitrate anion (NO₃⁻) and dimethyl formamide (DMF) serve as coordinating ligands for both MOF-3 and MOF-4. Both the MOFs are made of a rare “paddle-wheel” type secondary building unit (SBU) and 2,6-NDC²⁻ ligand play the key role to generate this paddle-wheel type building block, which ultimately generate two-dimensional (2D) network structure. MOF-3 and MOF-4 displayed distorted triangular dodecahedral geometry and different weak interatomic interactions were mapped through Hirshfeld surface analysis and 2D fingerprint plot. Besides, the isostructural nature of the MOFs can be confirmed by Hirshfeld surface analysis. Catalytic O-arylation reactions between substituted phenols and various

substituted bromobenzene have been explored using $[\text{Tb}(\text{NDC})(\text{NO}_3)(\text{DMA})_2]_n$ (MOF-3) and $[\text{Ho}(\text{NDC})(\text{NO}_3)(\text{DMA})_2]_n$ (MOF-4) as catalyst under heterogeneous condition. Both the MOFs have shown good catalytic efficiency towards O-arylation reaction. However, MOF-3 exhibits better catalytic efficacy in this catalytic reaction. Nevertheless, both the catalysts are active towards various phenol moieties containing electron donating functional groups to yield unsymmetrical diarylethers. As per the acquired information, it is one of the rarest examples of paddle-wheel core based two-dimensional Ln-MOF which are tested active in catalytic O-arylation reaction.

4.5 References

- [1] J. P. Corbet, G. Mignani, *Chem. Rev.* 106 (2006) 2651.
- [2] J. Magano, J. R. Dunetz, *Chem. Rev.* 111 (2011) 2177.
- [3] P.G. Gildner, T.J. Colacot, *Organometallics* 34 (2015) 5497.
- [4] P. R. Castillo, S.L. Buchwald, *Chem. Rev.* 116 (2016) 12564.
- [5] D.A. Evans, K.M. Devries, M. Decker, *Glycopeptides Antibiotics, Drugs and the Pharmaceutical Sciences*, Ramakris Nagarajan, New York, 1994, pp. 63.
- [6] G. Evano, N. Blanchard, M. Toumi, *Chem. Rev.* 108 (2008) 3054.
- [7] P.G. Cozzi, *Chem. Soc. Rev.* 33 (2004) 410.
- [8] K.C. Gupta, A.K. Sutar, *Coord. Chem. Rev.* 252 (2008) 1420.
- [9] B. Banik, A. Tairaia, P.K. Bhattacharyya, P. Das, *Appl. Organometal. Chem.* 30 (2016) 519.
- [10] N. Shahnaz, B. Banik, P. Das, *Tetrahedron Lett* 54 (2013) 2886.
- [11] S. Yamada, *Coord. Chem. Rev.* 191 (1999) 537.
- [12] Y. Jia, J. Li, *Chem. Rev.* 115 (2015) 1597.
- [13] I.P. Ejidike, P.A. Ajibade, *Rev. Inorg. Chem.* 35 (2015) 191.
- [14] S. Gaur, *Asian J. Chem.* 15 (2003) 250.

- [15] P. Oswal, A. Arora, S. Singh, D. Nautiyal, S. Kumar, G.K. Rao, A. Kumar, Dalton Trans 49 (2020) 12503.
- [16] P. Das, W. Linert, Coord. Chem. Rev. 311 (2016) 1.
- [17] A. Kumar, M. Agarwal, A.K. Singh, Polyhedron 27 (2008) 485.
- [18] P. Oswal, A. Arora, S. Gairola, A. Datta, A. Kumar, New J. Chem. 45 (2021) 21449.
- [19] A. Kumar, G.K. Rao, F. Saleem, R. Kumar, A.K. Singh, J. Hazard. Mater. 269 (2014) 9.
- [20] K. Maher, Asian J. Chem. 30 (2018) 1171.
- [21] S. Chahmana, S. Keraghel, F. Benghanem, R. Ruiz-Rosas, A. Ourari, E. Morallón, Int. J. Electrochem. Sci. 13 (2018) 175.
- [22] P.R. Reddy, A. Shilpa, Chem. Biodivers. 9 (2012) 2262.
- [23] H. Tian, X. Qiao, Z.-L. Zhang, C. Xie, Q.-Z. Li, J.-Y. Xu, Spectrochim. Acta A. 207 (2019) 31.
- [24] A. L. Berhanu, I. Gaurav, A. K. Mohiuddin, J. S. Malik, V. Kuma. Aulakh, K. H. Kim, Trends Anal. Chem. 116 (2019) 74.
- [25] B. K. Datta, C. Kar, G. Das, J. Chem. Sci. 127 (2015) 337.
- [26] T. B. Wei, G. Y. Gao, W. J. Qu, B. B. Shi, Q. Lin, H. Yao, Y. M. Zhang, Sens. Actuat. B 199 (2014) 142.
- [27] A. Kumar, M. Agarwal, A.K. Singh, J. Organomet. Chem. 693 (2008) 3533.
- [28] J. Kaushal, S. Singh, P. Oswal, A. Arora, D. Nautiyal, A. Kumar, J. Mol. Struct. 1253 (2022) 132099.
- [29] P. Ghosh, T. Maity, S. Biswas, R. Debnath, S. Koner, Polyhedron 194 (2021) 114934.
- [30] X. Yu, D. I. Pavlov, A. A. Ryadun, A. S. Potapov, V. P. Fedin, Molecules 27 (2022) 7849.

- [31] S. Das, T. Maity, S. Koner, Appl. Catal. A-Gen 513 (2016) 53.

Chapter 5



**In situ decarboxylation
hydroxylation of 3-hydroxy-2-
quinoline carboxylic acid
assisted by lanthanide metal in
autoclave**

5.1 Introduction

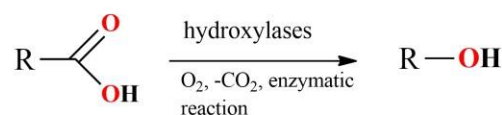
Carboxylic acids are among the most valuable starting materials for synthesis. They are commercially available in large structural diversities at low cost. They can be easily prepared by various well-established methods [1]. Many carboxylic acids can be synthesized directly from natural resources that can help to avoid the exploitation of fossil resources like gas or oil in the production of chemicals [2]. In addition, these compounds are generally stable to moisture and air, easy to handle and long shelf life. As a result, carboxylic acids are drawing immense attraction as starting materials for synthesis of numerous organic compounds. Carboxy groups can be contemplated as a regio- and chemo-selective leaving group which is excluded traceless as carbon dioxide (CO₂) from the reaction mixture. Interestingly, many naturally occurring carboxylic acids contains one or more centers of chirality that can be beneficial for the synthesis of enantiopure pharmaceuticals, if the decarboxylation reaction can be performed stereoselectively or retention of configuration [3].

Decarboxylative hydroxylation is a valuable transformation in organisms as well as in synthetic organic chemistry. In nature, this process is catalyzed in a highly efficient and specific way by various hydroxylases [4]. For example, salicylate hydroxylase (SALH) that was isolated from naturally occurring microorganism, *Pseudomonas Putida S-1* can break the C–COOH bond of a carboxylic acid and generate C–O bond for the transformation of salicylate to catechol by extruding CO₂ [5]. It gives one carbon shorter alcohol directly from highly stable and inexpensive carboxylic acid. A lot of direct decarboxylative hydroxylation methods have been devised [6]. Many rely on the direct use of stoichiometric high-valent metal ions such as Mn(III), Pb(IV), Ce(IV) that acts as oxidant in reaction medium (**Scheme 5.1**) [7,8]. Recently, Lu et al. developed decarboxylative hydroxylation photolytically using molecular oxygen as oxidant [9]. This elegant transformation is useful for its green and mild reaction condition.

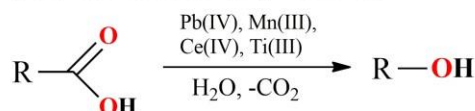
Chapter 5 *In situ* decarboxylation hydroxylation by Ln-salts in autoclave

In 2020, Sun et al. put forward a general and practical method for decarboxylative hydroxylation of carboxylic acid through visible light induced photocatalysis using O₂ as green oxidant [10]. Use of NaBH₄ reduced the in-situ generation of peroxy radical that facilitates much broadened and substrate scope. T. Ritter et al. first disclosed the decarboxylative hydroxylation of benzoic acid for the synthesis of phenol at mild reaction condition. The reaction proceeds via photoinduced LMCT (ligand-to-metal charge transfer) based radical decarboxylative carbometallation in presence of copper [11].

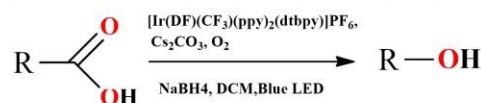
a) Enzymatic methods



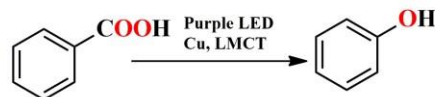
b) Chemical methods using high-valent metal



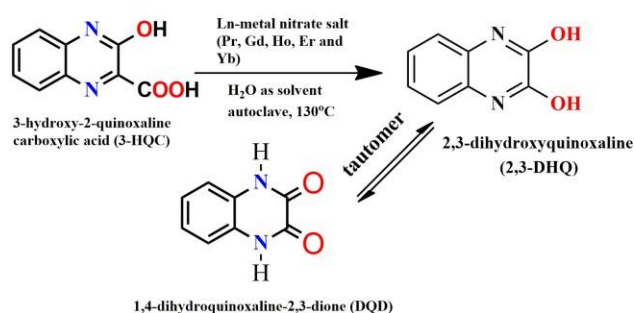
c) Decarboxylation hydroxylation photocatalytically



d) preparation of phenol from benzoic acid by decarboxylation hydroxylation



e) This work



Scheme 5.1 Decarboxylative hydroxylation of carboxylic acids.

Quinoxaline based compounds belong to important class of heterocycles known as diazanaphthalene. Derivatives of quinoxaline and their metal complexes have drawn immense attention due to their promising analytical, industrial and clinical applications [12-14]. These compounds also find application in chemosensors [15], corrosion inhibition [16] and catalysis [17]. One of the important benzoheterocyclic quinoxaline-based compounds is 2,3-dihydroxyquinoxaline. This compound can be prepared by conventional method reported in the literature [18]. It is well known that this compound can exist in another tautomeric form 1,4-dihydroquinoxaline-2,3-dione (DQD) [19] (tautomer forms are given in **Scheme 5.1e**). Nevertheless, decarboxylative hydroxylation reaction of aromatic heterocyclic compound assisted by lanthanide metal is not reported so far (**Figure 5.1**). Production of 1,4-dihydroquinoxaline-2,3-dione (DQD) from 3-hydroxy-2-quinoxaline carboxylic acid in green solvent (water) via decarboxylative hydroxylation might lead to a new horizon in chemical research.

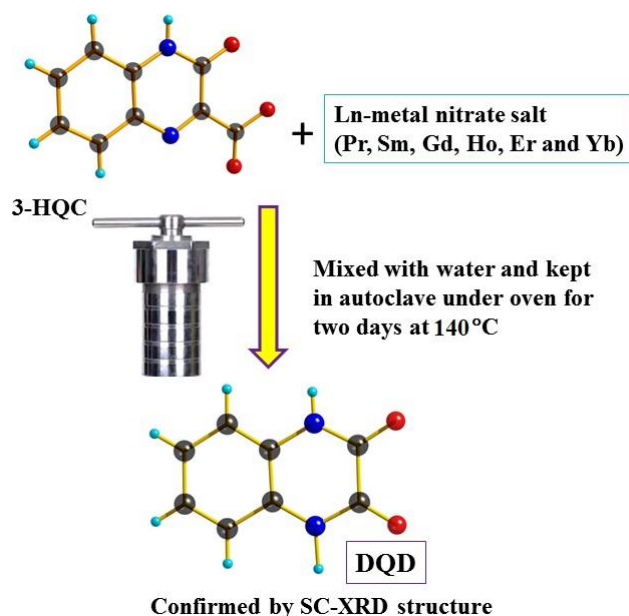


Figure 5.1 Synthesis of DQD from 3-HQC.

5.2 Experimental section

5.2.1 Materials

Praseodymium(III) nitrate hexahydrate (99.99%), gadolinium(III) nitrate hexahydrate (99.9%), holmium(III) nitrate pentahydrate (99.9%), erbium(III) nitrate pentahydrate (99.9%), ytterbium(III) nitrate pentahydrate(99.9%), 2,6-naphthalenedicarboxylic acid (H₂NDC) (99%), 3-hydroxy-2-quinoxaline carboxylic acid (3-HQC) (97%) were purchased from Sigma-Aldrich and were used as received without further purification. Other chemicals and solvents (analytical grade) were purchased from Merck (India). Solvents were distilled and dried before use.

5.2.2 Physical Measurements

All the physical measurements were performed by using the same instruments as discussed in **Section 2.2.2, Chapter 2**.

5.2.3 Synthesis of MOF-5 $\{[\text{Gd}(\text{NDC})_5(\text{DQD})]\cdot\text{H}_2\text{O}\}_n$, MOF-6 $\{[\text{Ho}(\text{NDC})_5(\text{DQD})]\cdot\text{H}_2\text{O}\}_n$, MOF-7 $\{[\text{Er}(\text{NDC})_5(\text{DQD})]\cdot\text{H}_2\text{O}\}_n$, MOF-8 $\{[\text{Yb}(\text{NDC})_5(\text{DQD})]\cdot\text{H}_2\text{O}\}_n$ and DQD

MOF-(**5-8**) were prepared by using lanthanide nitrate salt (Gd, Ho, Er, Yb) (0.25 mmol), 3-hydroxy-2-quinoxaline carboxylic acid (0.125 mmol) and 2,6-naphthalenedicarboxylic acid (0.125 mmol). A salt of lanthanide nitrate was dissolved in 2 mL of water and separately a 2 mL solution of 2,6-naphthalenedicarboxylic acid and 3-HQC in water was prepared. After mixing thoroughly, the resulting mixture was then placed in a four different 15 mL teflon-lined Parr acid digestion bomb and kept at 140°C for two days. After two days, the solution was allowed to cool down slowly at the rate of ~5°C/h to room temperature. Two different types of crystals were obtained from each Teflon bomb. One type is thin colorless rod shaped (with maximum yield) and another

type is block shaped with different color from different batch of autoclave (yield is 20-30% based on metal). Two different types of crystals were collected from different reaction mixture and washed with distilled water and dried in air. 1,4-dihydroquinoxaline-2,3-dione (DQD) was separated from the reaction mixture as thin crystalline substance. Details about this synthesis have been discussed in **Section 5.3.1**. Anal. Calcd. value for DQD: $C_8H_6N_2O_2$ (FW=162.15) C, 59.20, H, 1.23%, Found C, 59.12, H, 1.3%. Selected IR peaks of DQD (KBr pellet, ν , cm^{-1}) (**Figure 5.2 a**) 2860-3044 [ν_s (C-H aromatic stretching vibration)], 1670 [ν_s (C=O for cyclic imide)], 1100-785 [ν (C-H aromatic in plane bending)]. IR spectra of DQD obtained during the reaction of lanthanide MOF synthesis was compared with the pure DQD. It was observed that the spectra are well matched with the pure DQD one. Details IR spectra is given in **Figure 5.2b** and **Figure 5.2c**.

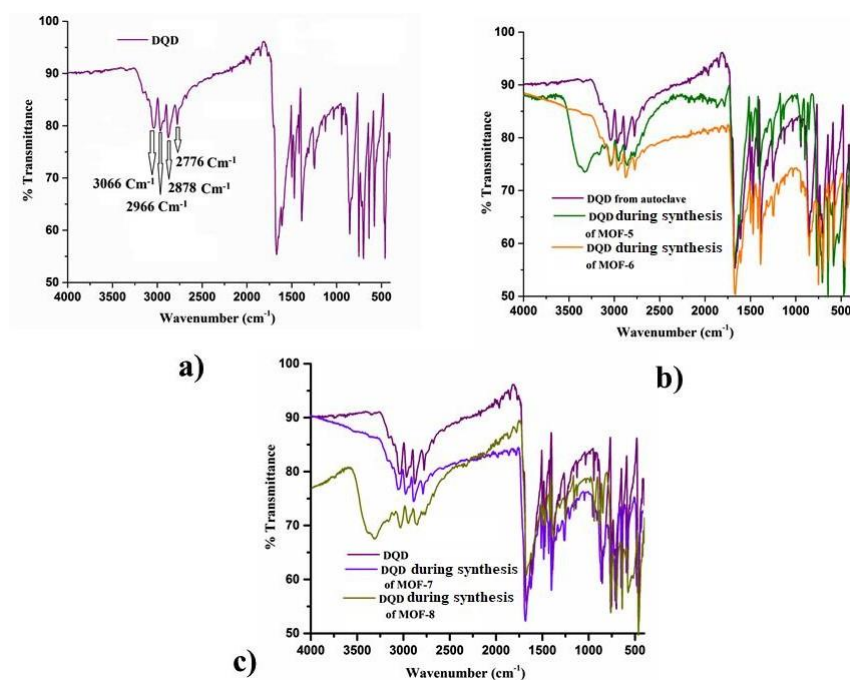


Figure 5.2 a) FT-IR spectra of DQD only; **b)** DQD during synthesis of MOF-5-6; **c)** DQD during synthesis of MOF-7-8.

5.2.4 X-ray crystallography

All the description about the procedure of data collection by single crystal X-ray diffraction and structure solvation by using different software program have already been discussed in **Section 2.2.4, Chapter 2**. A summary of the crystallographic data and the relevant structural refinement parameters for DQD and MOF-5-8 are given in **Table 5.1** and **5.2**.

Table 5.1 Crystal data and refinement parameters of DQD and MOF-5-6

Formula	DQD	MOF-5	MOF-6
	C ₈ H ₆ N ₂ O ₂	C ₂₆ H ₁₇ N ₂ O ₉ Gd	C ₂₆ H ₁₇ N ₂ O ₉ Ho
Formula Weight	162.15	658.67	664.33
Color	colorless	colorless	Yellowish pink
Crystal System	monoclinic	triclinic	triclinic
Space Group	<i>Pn</i> (no.7)	<i>P-1</i> (no.2)	<i>P-1</i> (no.2)
<i>a</i> (Å)	8.0671(10)	10.3520(15)	10.2708(11)
<i>b</i> (Å)	4.2822(5)	11.7120(18)	11.6108(12)
<i>c</i> (Å)	20.952(3)	12.3112(19)	12.3793(13)
α (°)	90.00	63.605(3)	64.203(3)
β (°)	100.400(4)	82.055(4)	82.408(3)
γ (°)	90.00	73.523(3)	73.770(3)
<i>V</i> (Å ³)	711.90(16)	1282.0(3)	1276.1(2)
<i>Z</i>	4	2	2
<i>D</i> _{calc} (gcm ⁻³)	1.513	1.660	1.729
μ (mm ⁻¹)	0.112		3.157
<i>F</i> (000)	336	626	648
θ Range (°)	2.0-27.2	2.0-27.2	1.8-27.1
Intervals of reflection indices	-10≤ <i>h</i> ≤10, -5≤ <i>k</i> ≤5,	-13≤ <i>h</i> ≤13, -15≤ <i>k</i> ≤15,	-13≤ <i>h</i> ≤13, -14≤ <i>k</i> ≤14,

	-26<= <i>l</i> <=26	-15<= <i>l</i> <=15	-15<= <i>l</i> <=15
Reflections measured	9657	29411	43821
R_{int}	0.036	0.057	0.094
Unique data	2810	5678	5637
Final R indices [$I > 2\sigma(I)$]	$R_1 = 0.0510,$ $wR_2 = 0.1506$	$R_1 = 0.0678,$ $wR_2 = 0.1890$	$R_1 = 0.0321,$ $wR_2 = 0.0747$
Data with $I > 2(I)$	1993	5045	5213
$R_1 (I > 2(I))$	0.0510	0.0678	0.0321
$wR_2(I > 2(I))$	0.1506	0.1890	0.0747
(GOF) on F^2	0.917	1.801	1.087

Table 5.2 Crystal data and refinement parameters of MOF-7 and MOF-8

Formula	MOF-7 (C ₂₆ H ₁₇ N ₂ O ₉ Er)	MOF-8 (C ₂₆ H ₁₇ N ₂ O ₉ Yb)
Formula	662.65	672.44
Weight		
Color	Golden yellow	Light yellow
Crystal System	triclinic	triclinic
Space Group	$P-1$ (no.2)	$P-1$ (no.2)
a (Å)	10.266(3)	10.2084(9)
b (Å)	11.607(3)	11.5736(11)
c (Å)	12.381(7)	12.3745(11)
α (°)	64.45(3)	64.298(2)
β (°)	82.47(4)	82.442(3)
γ (°)	73.62(2)	73.827(3)
V (Å ³)	1276.9(9)	1265.1(2)
Z	2	2

D_{calc} (gcm^{-3})	1.724	1.765
μ (mm^{-1})	3.340	3.753
$F(000)$	644	654
θ Range ($^{\circ}$)	1.8-27.1	1.8-27.1
Intervals of reflection indices	-12 \leq h \leq 13, -13 \leq k \leq 14, -15 \leq l \leq 15	-13 \leq h \leq 13, -14 \leq k \leq 14, -15 \leq l \leq 15
Reflections measured	20632	42040
R_{int}	0.037	0.083
Unique data	5564	5592
Final R indices	$R1 = 0.0428$, $wR2 =$	$R1 = 0.0257$, $wR2 = 0.0650$
$[I > 2\sigma(I)]$	0.1160	
Data with $I > 2(I)$	4975	5318
$R_1 (I > 2(I))$	0.0428	0.0257
$wR_2(I > 2(I))$	0.1160	0.0650
(GOF) on F^2	1.059	1.120

5.3 Results and discussion

5.3.1 Synthesis

For few highly activated carboxylic acids such as diphenyl acetic acid, β -oxoacids and polyfluorobenzoic acid decarboxylation reaction occur readily. A wide range of carboxylic acids including propiolic, heterocyclic, ortho and ortho-disubstituted carboxylic acid derivatives decarboxylated easily by using strong Brønsted acids [20]. Ionic liquids have been found to catalyze the decarboxylation of various aryl carboxylic acids and N-heteroaryl effectively with microwave irradiation under

aqueous conditions [21]. However, decarboxylative hydroxylation of the heterocyclic compound like quinoxaline based carboxylic acid is scarcely reported. An interesting and serendipitous decarboxylation hydroxylation of 3-HQC has been investigated in details and will be reported in this chapter.

In order to synthesize new lanthanide-based metal organic frameworks (MOF), a reaction was undertaken using 3-hydroxy-2-quinoxaline carboxylic acid (3-HQC), 2,6-naphthalenedicarboxylic (H_2NDC) acid and lanthanide metal nitrate salt as reagents in teflon-lined Parr-acid digestion bomb in an oven at $140^\circ C$. After two days of continuous heating the mixture was allowed to cool to room temperature. Upon verification of the product under microscope two type's crystals were observed. The crystals were collected under microscope and subjected for characterization through several methods. Structure of the crystals have been solved through single crystal X-ray diffraction (SC-XRD) measurement. Surprisingly, structure solution shows 3-HQC transforms to 1,4-dihydroquinoxaline-2,3-dione (DQD) under hydrothermal condition in presence of lanthanide salts. From structure analysis it also becomes clear that 3-hydroxy-2-quinoxalinecarboxylate does not coordinate to lanthanide ions before it transforms to 1,4-dihydroquinoxaline-2,3-dione. Clearly, 3-HQC first transformed to DQD upon *in situ* decarboxylation-hydroxylation reaction. The ligand (DQD) thus formed binds the Ln-metal center to afford the new types of Ln-MOF (**Figure 5.3**). Notably, the pH of the reaction medium which was initially acidic (pH=1-2), changed to neutral after completion of reaction. Structure of Ln-MOFs were also solved through single crystal X-diffraction analysis. DQD is conventionally synthesized from 1,2-diaminopheneline and oxalic acid in acidic medium [18]. Thus, this serendipitous *in-situ* decarboxylation-hydroxylation gives a new avenue for the conversion of 3-HQC to DQD in presence of lanthanide salts. Survey showed such type of decarboxylation-hydroxylation reaction is not reported in

Chapter 5 *In situ decarboxylation hydroxylation by Ln-salts in autoclave*

literature to date. Details of the optimization of reaction conditions are given in Table 5.3.

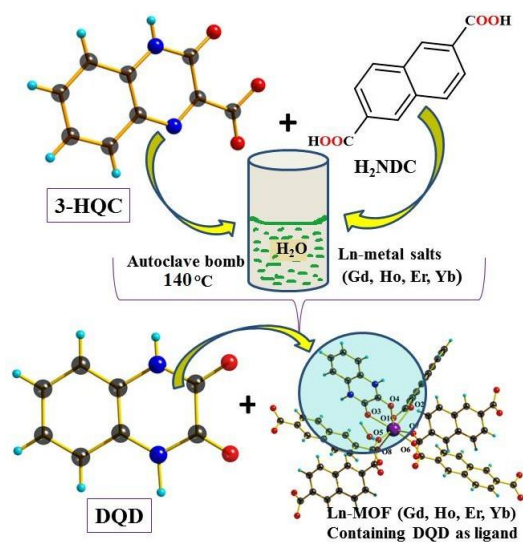


Figure 5.3 Details of reaction scheme for conversion of 3-HQC to DQD during synthesis of Ln-MOF in autoclave.

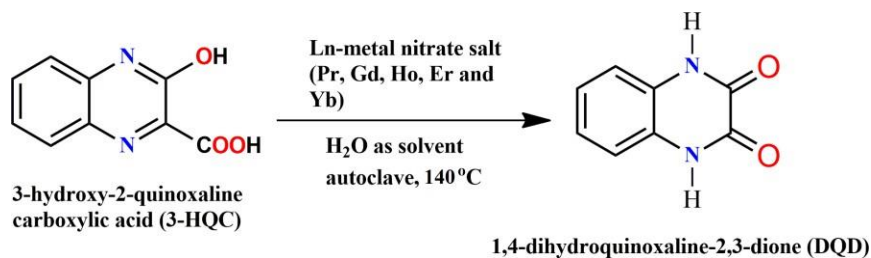


Table 5.3 Optimization of reaction conditions

^a Entry	Hetero-cyclic substrate	Ln-metal salt	Solvent	^b Autoclave (two days) (140 °C)	^c Yield (%) of DQD
1	3-HQC	Pr(NO ₃) ₃ ·6H ₂ O	H ₂ O	autoclave	55

Chapter 5***In situ decarboxylation hydroxylation by Ln-salts in autoclave***

2	3-HQC	Gd(NO ₃) ₃ .6H ₂ O	H ₂ O	autoclave	60
3	3-HQC	Ho(NO ₃) ₃ .6H ₂ O	H ₂ O	autoclave	62
4	3-HQC	Er(NO ₃) ₃ .6H ₂ O	H ₂ O	autoclave	65
5	3-HQC	Yb(NO ₃) ₃ .6H ₂ O	H ₂ O	autoclave	68
6	3-HQC	No Ln-metal salt	H ₂ O	autoclave	No reaction
7	3-HQC	Ln-metal salt	H ₂ O	in air	No expected product
8	3-HQC	Ln-metal salt	MeOH	autoclave	No reaction
9	3-HQC	Ln-metal salt	EtOH	autoclave	No reaction
10	3-HQC	Ln-metal salt	DMA	autoclave	No reaction
11	3-HQC	Ln-metal salt	DMF	autoclave	No reaction
12	3-HQC and H ₂ NDC	Ln-metal salt (Gd, Ho, Er and Yb)	H ₂ O	autoclave	30 (along with Ln-MOF)
13	3-HQC and H ₂ NDC	-	H ₂ O	autoclave	No reaction
14	3-HQC	-	Acidulated H ₂ O	autoclave	No expected product

15	3-HQC	Ln-metal salt	H ₂ O	autoclave (90-119°C)	^d Product not detected at temperature range 90- 110°C
----	-------	---------------	------------------	-------------------------	---

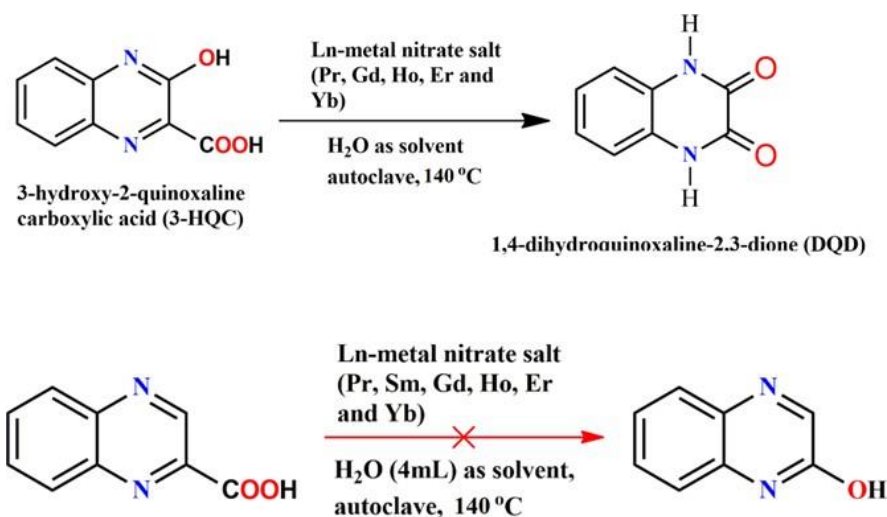
Reaction conditions: 3-HQC (0.20 mmol), Ln-metal salt (0.0125 mmol); water as solvent (4-6 mL); H₂NDC (0.12 mmol) (entry 12 and 13). ^bReaction temperature: 140°C. ^cYield (yield obtained from autoclave directly); ^dreaction temperature: 90-110°C. Pdt = product.

The optimized reaction conditions are given in **Table 5.3**. Condition of reactions are examined by varying various parameters such as solvents, reagents, reaction temperature and reaction time etc. because these parameters are found to impact the progress of the in-situ decarboxylation-hydroxylation reaction of 3-HQC. Solvents play vital roles in any chemical reaction. This particular reaction is occurred only when water is used as solvent medium and hydrothermal conditions are maintained (autoclave) in presence of lanthanide metal salts (**Table-5.1**, entry 1-6). Other solvents like methanol, ethanol, dimethylacetamide (DMA), dimethylformamide (DMF) do not afford the conversion of 3-HQC to DQD. Besides, the reaction proceeds only in presence of lanthanide metal salts and H₂NDC is used in water medium. In this case, expected product (DQD) is obtained along with Ln-MOF (Ln = Gd, Ho, Er and Yb) (**Table-5.1**, entry 12). This decarboxylation-hydroxylation reaction does not occur in open atmosphere (**Table-5.1**, entry 7). Hydrothermal treatment of mixture of H₂NDC in 3-HQC in absence of Ln salt did not afford any product (**Table-5.1**, entry 13). While pH of the medium itself has no role in decarboxylation-hydroxylation reaction (**Table-5.1**, entry 14), temperature plays crucial role for this reaction and showed noticeable impact on the reaction. The in-situ decarboxylation-hydroxylation is occurring particularly at 140°C in autoclave. At temperature 90-110°C, upto the

Chapter 5 *In situ decarboxylation hydroxylation by Ln-salts in autoclave*

mark yield was not obtained (Table-5.1, entry 15). However, reaction occurs above 140°C but yield was much less and maximum yield was obtained at 140°C.

In order to increase the scope of the reaction, attempts have been made to use other similar type of compounds also. However, this particular reaction is restricted to only for 3-hydroxy-2-quinoxalinecarboxylic acid (3-HQC). Decarboxylation-hydroxylation was also tested for 2-quinoxalinecarboxylic acid. But for 2-quinoxalinecarboxylic acid, -COOH group at 2-position is not converted to O-H group under identical reaction condition as applied in the case of 3-HQC (Scheme 5.2). Other carboxylic acids with similar structure of 3-HQC are not easy to come by.

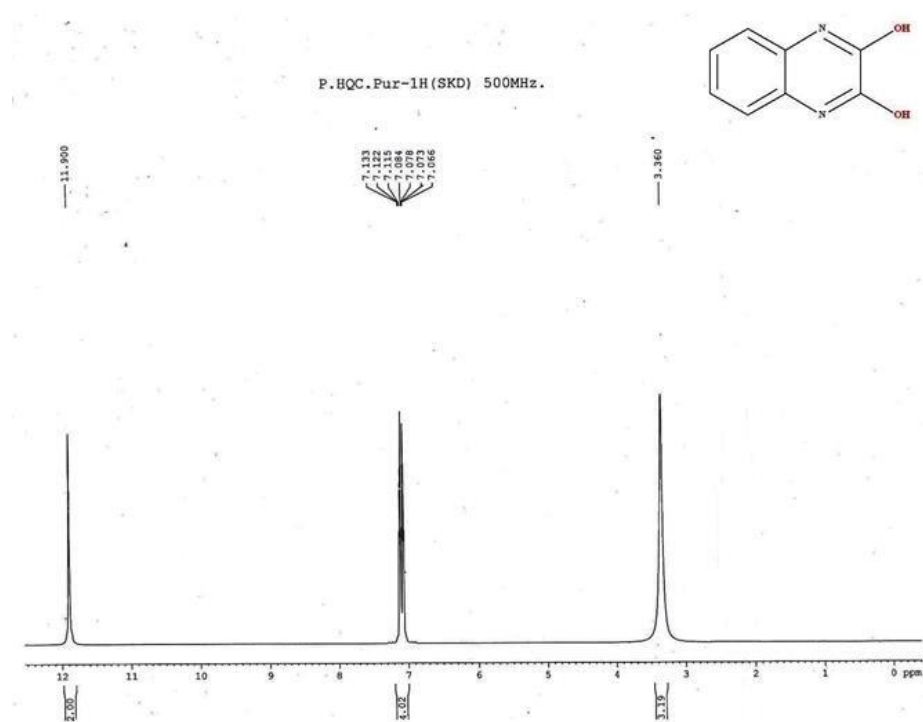


Scheme-5.2 Exploration of decarboxylation hydroxylation for two heterocyclic compounds.

5.3.2 Characterization

Proton NMR and Mass spectra of 1,4-dihydro-quinoxaline-2,3-dione (DQD)

δ_H (500 MHz; d^6 -DMSO) 7.133-7.066 (4H, m), 11.90 (2H, s); Elemental analysis: (found: C 59.12, H 1.3; for $C_8H_6N_2O_2$ requires: C 59.20, H 1.23%) (Figure 5.4). Mass spectra is given in Figure 5.5.

Figure 5.4 1H NMR spectra for DQD

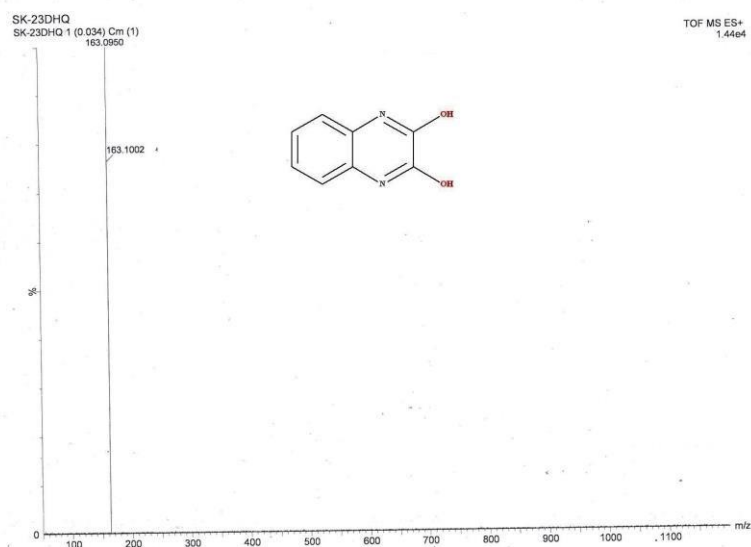


Figure 5.5 HRMS for DQD

5.3.3 Description of crystal structure of 1,4-dihydro-quinoxaline-2,3-dione (DQD)

Single crystal X-ray diffraction studies reveals that DQD crystallizes in the Pn space group of the monoclinic system with $Z = 4$. The molecular unit consist of two discrete molecules and the crystal is stabilized by supramolecular interaction like strong intermolecular H-bonding (Figure 5.6a and b respectively).

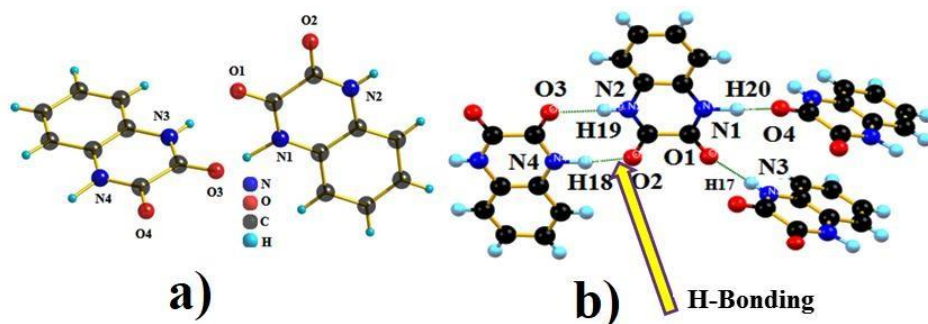


Figure 5.6 a) Molecular unit of DQD; b) H-bonded supramolecular structure.

5.3.4 Description of crystal structure of MOF-(5-8)

Single-crystal X-ray diffraction analysis established that MOF-(5-8) crystallizes in triclinic *P-1* space group with *Z* value 2. The crystal structure of MOF-5 as a representative example of this series of isomorphous MOFs is described in details. The molecular unit of MOF-5 consists of one crystallographically independent Gd(III) metal center, five coordinated 2,6-naphthalenedicarboxylate (NDC²⁻) and one 1,4-dihydroquinoxaline-2,3-dione (DQD) with one crystalline water molecule (**Figure 5.7a**). The unique metal center is surrounded by eight coordinated oxygen atoms. The geometry of octa-coordinated Gd, GdO₈ can be described as a distorted triangular-dodecahedral geometry (**Figure 5.7 b**). The eight coordination sites around central Gd(III) metal ion is satisfied by two oxygen atoms (O1, O2) from one DQD ligand and other six oxygen atoms (O3, O4, O5, O6, O7, O8) from five 2,6-naphthalenedicarboxylate (NDC²⁻) ligands leads to triangular dodecahedral geometry. The carboxylic Gd–O bond distances range 2.297(7)–2.475 (8) Å and the angles of O–Gd–O vary from 52.43(3) to 150.1(3). The selected bond distances and angles are summarized in **appendix** portion of the thesis.

The ligand NDC²⁻ can show various coordination modes, however, in this structure NDC²⁻ exhibits *syn-syn* bridging μ -1,3 coordination mode only. Carboxylate atoms O3, O4 and O7, O8 of NDC²⁻ connects two Gd(III) metal centers through μ ₂-*syn,syn*-bridge binding mode and form dimeric Gd units. Two crystallographically equivalent Gd(III) ions are bridged by four bidentate carboxylate groups of four different NDC²⁻ in a *syn-syn* bridging μ -1,3 fashion to generate a secondary building unit core leading to the formation of two-dimensional structure by linker NDC²⁻ (**Figure 5.7c**). Two-dimensional motifs are further interconnected by NDC²⁻ to generate a 3D network, where the DQD ligand is positioned interior of the MOFs (**Figure 5.7d**).

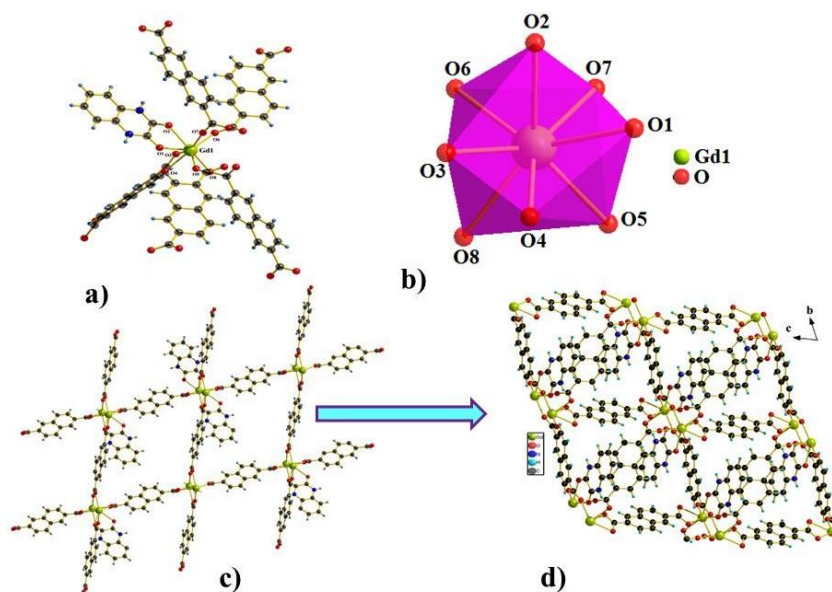


Figure 5.7 a) Molecular unit of MOF-5; b) geometry around Gd(III) metal center; c) simplified 2D structure; d) 3D network

The structure and geometry of other three MOFs is displayed in **Figure 5.8**. All of them are isostructural with the previously described MOF-5. Moreover, the 3D network structure of MOF-(6-8) is given in **Figure 5.9**. Details of bond length and bond angle of MOF-(6-8) are collated in the appendix section of this thesis.

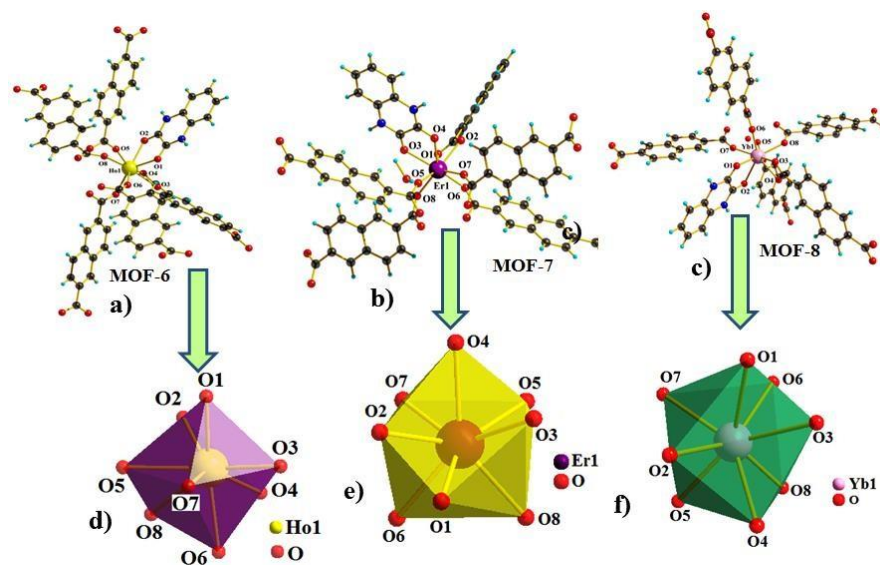


Figure 5.8 a, b, c) Molecular unit and coordination environment of MOF-6, MOF-7 and MOF-8 respectively; d, e, f) geometry of central metal ion of the respective MOFs.

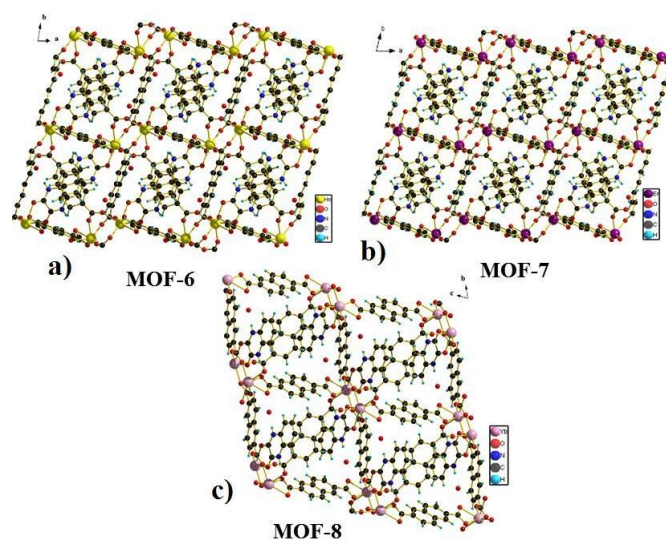


Figure 5.9 a) 3D network structure of MOF-6 along *ab*-plane; b) 3D MOF-7 along *ab*-plane; c) 3D MOF-8 along *bc*-plane.

5.4 Conclusion

In this study, lanthanide metal salt assisted decarboxylation hydroxylation of quinoxaline-based compound in hydrothermal condition has been discovered. The results obtained so far inferred that the reaction is specifically occurs only in 3-hydroxy-2-quinoxalinecarboxylic acid. 3-HQC is converted to 1,4-dihydro-quinoxaline-2,3-dione (DQD) in this reaction condition. Another quinoxaline-based compound, 2-quinoxalinecarboxylic acid is remained inactive towards decarboxylation hydroxylation under the similar conditions. Hence, it may be concluded that this reaction is regiospecific for 3-HQC ligand. Decarboxylation reaction for β -hydroxy-carboxylic acid is feasible due to formation of six-membered cyclic transition state which is typical not exception. But the next step i.e. the hydroxylation step is not understood fully. Evidently, water plays a crucial role for hydroxylation step as the reaction proceeds only in water not in other solvents like methanol, ethanol, DMA, DMF etc. Besides, the decarboxylative hydroxylation of 3-HQC is indeed proceed in reaction medium which is further evident in isolation of MOF-(5-8). Structural analysis of these MOFs reveals that 1,4-dihydro-quinoxaline-2,3-dione (DQD) is coordinated to Ln metal centers to afford MOFs through decarboxylative hydroxylation of 3-HQC. Lanthanide assisted decarboxylation hydroxylation of quinoxaline-based compound is not reported so far in the literature.

5.5 References

- [1] S. L. Hegedus, L. Wade, *Compendium of Organic Synthetic Methods*; John Wiley & Sons: Hoboken 3 (1977) 8.
- [2] E. Scott, F. Peter, J. Sanders, *Appl. Microbiol. Biotechnol.* 75 (2007) 751.
- [3] J. Schwarz, B. König, *Green Chem.* 20 (2018) 323.
- [4] R. A. Totah, R. P. Hanzlik, *J. Am. Chem. Soc.* 124 (2002) 10000.

Chapter 5 *In situ decarboxylation hydroxylation by Ln-salts in autoclave*

- [5] T. Uemura, A. Kita, Y. Watanabe, M. Adachi, R. Kuroki, Y. Morimoto, *Biochem. Biophys. Res. Commun.* 469 (2016) 158.
- [6] K. Okada, K. Okubo, M. Oda, *Tetrahedron Lett.* 33 (1992) 83.
- [7] P. Haldar, J. K. Ray, *Tetrahedron Lett.* 49 (2008) 3659.
- [8] Y. Sakakibara, P. Cooper, K. Murakami, K. Itami, *Chem. Asian J.* 13 (2018) 2410.
- [9] H. T. Song, W. Ding, Q. Q. Zhou, J. Liu, L.-Q. Lu, W.-J. J. Xiao, *J. Org. Chem.* 81 (2016) 7250.
- [10] S. N. Khan, M. K. Zaman, R. Li, Z. Sun, *J. Org. Chem.* 85 (2020) 5019.
- [11] W. Su, P. Xu, T. Ritter, *Angew. Chem.* 133 (2021) 24214.
- [12] C. Urquiola, D. Gambino, M. Cabrera, *J. Inorg. Biochem.* 102 (2008) 77.
- [13] N. C. Romero, G. Aguirre, P. Hernandez, *Bioorg. Med. Chem.* 17 (2009) 641.
- [14] P. Nobia, M. Vieites, M. H. Torre, *J. Inorg. Biochem.* 100 (2006) 281.
- [15] X. Fang, G. Zhao, Y. Xiao, *Tetrahedron Lett.* 54 (2013) 806.
- [16] A. Zarrouk, A. Dafali, B. Hammouti, *Int. J. Electrochem. Sci.* 5 (2010) 46.
- [17] S. Adewuyi, G. Li, S. Zhang, W. Wang, P. Hao, W. h. Sun, N. Tang, J. Yi, *J. Organomet. Chem.* 692 (2007) 3532.
- [18] P. Sukanya, Ch. V. R. Reddy, G. Bhargavi, *Crystallography Reports* 65 (2020) 72.

Chapter 5 *In situ decarboxylation hydroxylation by Ln-salts in autoclave*

- [19] J. Albering, M. A.M. Abu-Youssef, S. M. Soliman, J. Mol. Struct. 48 (2013) 1053.
- [20] R. W. Hay and M. J. Taylor, Chem. Commun. 525 (1966).
- [21] A. Sharma, R. Kumar, N. Sharma, V. Kumar and A. K. Sinha, Adv. Synth. Catal. 350 (2008) 2910.

Chapter 6



Highlights

6.1 Highlights

The main findings of the present investigation are collected in this chapter. The thesis represents a glimpse of recent advances in the field of heterogeneous catalysis by lanthanide-based metal organic frameworks. The major emphasis is given on the synthesis, structural characterization of framework compounds, and catalytic C–heteroatom bond forming reaction under heterogeneous condition.

The importance of framework compounds in industrial and fundamental research led to develop various lanthanide systems that have potential in heterogeneous catalysis study. To develop the catalytic system 2,6-naphthalenedicarboxylate linkers and different conditions have been applied. Various lanthanide-based metal organic frameworks have been employed in C–heteroatom bond forming reaction.

A new robust and thermally stable three-dimensional Gd-MOF $\{[\text{Gd}_4(\text{NDC})_6(\text{H}_2\text{O})_6] \cdot 2\text{H}_2\text{O}\}_n$ (MOF-1) has been synthesized and structurally characterized by single-crystal X-ray diffraction. The 3D Gd-MOF has been synthesized by hydrothermal process and subjected for various physico-chemical characterization. Interestingly, $\{[\text{Gd}_4(\text{NDC})_6(\text{H}_2\text{O})_6] \cdot 2\text{H}_2\text{O}\}_n$ is capable of catalyzing the O-arylation reaction efficiently between substituted phenol and bromoarene under heterogeneous condition at 80°C to afford unsymmetrical diaryl ethers. In addition, thermogravimetric analysis demonstrates that after dehydration the mass of MOF-1 remains constant until ~530°C under nitrogen atmosphere which attests the robust character of Gd-MOF.

A novel lanthanide based two-dimensional metal-organic framework compound $[\text{Dy}(\text{NDC})(\text{NO}_3)(\text{DMA})_2]_n$ (MOF-2) [H_2NDC = 2,6-naphthalenedicarboxylic acid and DMA = N,N-dimethylacetamide] has been synthesized by solvothermal process and structure of the MOF has been solved through single-crystal X-ray diffraction study. Structural analysis reveals that

MOF-2 is a two-dimensional coordination polymer. 2D network structure has been constructed by “Paddle-wheel” (PW) like core unit. Notably, such type of 2D MOF consists of PW units rarely reported in literature. The morphology of the MOFs as well as different types of weak interactions possessed by the framework have been assessed using Hirshfeld surface analysis and fingerprint plots have been drawn to understand various interactions. $[\text{Dy}(\text{NDC})(\text{NO}_3)(\text{DMA})_2]_n$ (MOF-2) efficiently catalyzes C–N coupling reaction between aryl-halides and amines under heterogeneous condition.

Two novel Ln-MOFs with formula $[\text{Tb}(\text{NDC})(\text{NO}_3)(\text{DMA})_2]_n$ (MOF-3) and $[\text{Ho}(\text{NDC})(\text{NO}_3)(\text{DMA})_2]_n$ (MOF-4) [where, NDC= dinegative 2,6-naphthalenedicarboxylate ligand and DMA = N,N-dimethylacetamide] have been synthesized by solvothermal process with subtle change in synthesis procedure. Various physico-chemical methods have been employed to characterize the MOFs. Single crystal XRD study reveals that structure of these two MOFs are almost the identical Morphology and different types of weak interactions possessed by the framework compound have been confirmed with the help of Hirshfeld surface analysis (HS) and consequent supplementary pseudo-mirror 2D fingerprint plot. MOF-3 and MOF-4 have been tested as heterogeneous catalysts for O–arylation reaction to afford unsymmetrical diarylethers. Both of them are capable of catalyzing O–arylation reaction efficiently between substituted phenols and different substituted bromobenzene under heterogeneous condition at 95°C.

An unprecedented *in situ* decarboxylation hydroxylation reaction in 3-hydroxy-2-quinoxaline carboxylic acid catalyzed by lanthanide metal has been discovered in this study. 3-hydroxy-2-quinoxaline carboxylic acid converts into 1,4-dihydroquinoxaline-2,3-dione (DQD) under high temperature and autogenous pressure in teflon lined Parr-acid digestion bomb. The molecular structure of 1,4-dihydroquinoxaline-2,3-dione (DQD) has been confirmed by single crystal XRD analysis and other spectral measurements such as IR, NMR and high-resolution

mass spectroscopy. Additionally, formation of hydroxylated compound has been proved through isolation of four lanthanide metal-organic framework compounds containing Gd, Ho, Er and Yb. All three MOFs have been characterized by single-crystal X-ray diffraction analysis that shows that MOFs possess three-dimensional network structure. Interestingly, this work represents an unprecedented decarboxylation hydroxylation reaction catalyzed by lanthanides.

Lanthanide based MOF materials in the area of catalytic conversion, such as C-heteroatom bond forming reaction may be attempted to develop efficient catalytic system. As a series of novel catalysts, the lanthanide-based MOFs have been developed that displayed comparable catalytic efficiency to the mature catalysts in several reactions. Benefiting from aid of porous MOF structures and lanthanide active sites, the lanthanide-based MOFs have immense potential for catalytic application in the future.

Appendix I

List of Publications

- [1] Tanmoy Maity, Debraj Saha, Soma Das, **Pameli Ghosh**, Subratanath Koner. Homo and hetero-bridged dinuclear copper(II) complex: Synthesis, X-ray structure and catalytic N-arylation. **Polyhedron** **173** (2019) **114127**.
- [2] **Pameli Ghosh**, Tanmoy Maity, Saptarshi Biswas, Rakesh Debnath, Subratanath Koner Thermally stable and robust gadolinium-based metal-organicframework: Synthesis, structure and heterogeneous catalytic O-arylation reaction. **Polyhedron** **194** (2021) **114934**.
- [3] Tanmoy Maity, **Pameli Ghosh**, Soma Das, Debraj Saha, Subratanath Koner. A post-synthetically modified metal–organic framework for copper catalyzed denitrative C–N coupling of nitroarenes under heterogeneous conditions. **New J. Chem.** **45** (2021) **5568**.
- [4] Mrinmoy Ghosh, Samik Biswas, Moumita Roy, Saptarshi Biswas, **Pameli Ghosh**, Subratanath Koner, Supratim Mandal and Sandip Saha. A trinuclear Zn(II) Schiff base azido compound: synthesis, structure and exploration of antimicrobial activity. **New J. Chem.** **45** (2021) **12296**.
- [5] Saikat Gayen, **Pameli Ghosh**, Hisashi Honda, Debraj Saha, Saptarshi Biswas, Rakesh Debnath, Subratanath Koner. Solvent mediated photoluminescence responses over mixed-linker cadmium (II) based metal–organic frameworks. **Polyhedron** **208** (2021) **115444**.
- [6] Birendra Nath Patra, **Pameli Ghosh**, Nayim Sepay, Saikat Gayen, Subratanath Koner, Paula Brandao, Zhi Lin, Rakesh Debnath, Jahar Lal Pratihari, Tanmay Maity, Dasarath Mal. Aerobic epoxidation of olefins by carboxylate ligand-based cobalt (II) compound: synthesis, X-ray

crystallography and catalytic exploration. **Appl Organomet Chem.** **2022.**

- [7] Rakesh Debnath, Rahul Bhowmick, **Pameli Ghosh**, Saptarshi Biswas and Subratanath Koner, Selective luminescent sensing of metal ions and nitroaromatics over a porous mixed-linker cadmium(II) based metal-organic framework. **New J. Chem.** **46 (2022) 8523.**
- [8] **Pameli Ghosh**, Tanmoy Maity, Nilufa Khatun, Rakesh Debnath, Subratanath Koner, 2D paddle wheel lanthanide metal-organic framework: Synthesis, structure and exploration of Catalytic N-arylation reaction. **Polyhedron** **219 (2022) 115789.**
- [9] Rakesh Debnath, **Pameli Ghosh**, Subratanath Koner, Preferential CO₂ adsorption over cadmium-based Porous Metal-organic Framework. **Journal of Porous Materials** (in press).

Appendix II

Selective $^1\text{H-NMR}$ spectra and bond-length, bond-angle data

Table-2.5, entry 1; δ_{H} (300 MHz; CDCl_3) 6.97-7.03 (4H, m), 7.13-7.19 (1H, m), 7.34 (2H, t, $J = 7.8$ Hz), 7.77 (2H, d, $J = 8.4$ Hz), 9.85 (1H, s); Yield ca. 93% based on amine; Elemental analysis (found: C 78.79, H 5.10; for $\text{C}_{13}\text{H}_{10}\text{O}_2$ requires: C 78.77, H 5.09%).

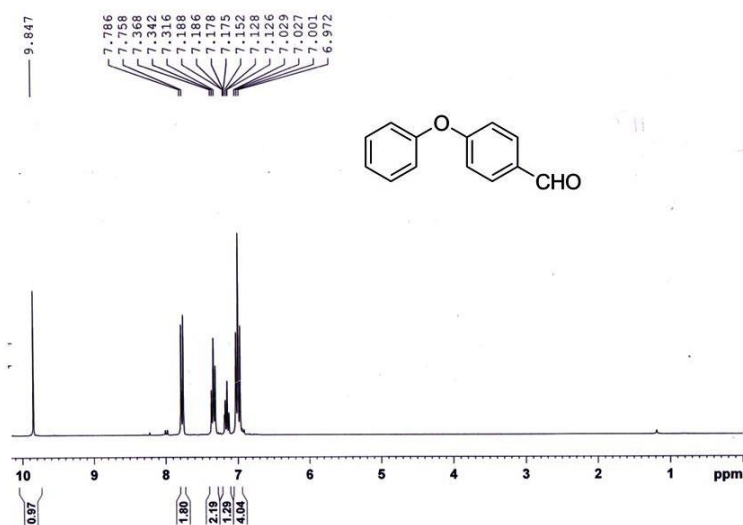


Table-2.5, entry-2; δ_{H} (300 MHz; CDCl_3) 2.37 (3H, s), 6.96-7.04 (4H, m), 7.21 (2H, d, $J = 8.2$ Hz), 7.82 (2H, d, $J = 8.6$ Hz), 9.90 (1H, s); Elemental analysis (found: C 79.25, H 5.72; for $\text{C}_{14}\text{H}_{12}\text{O}_2$ requires: C 79.22, H 5.70%).

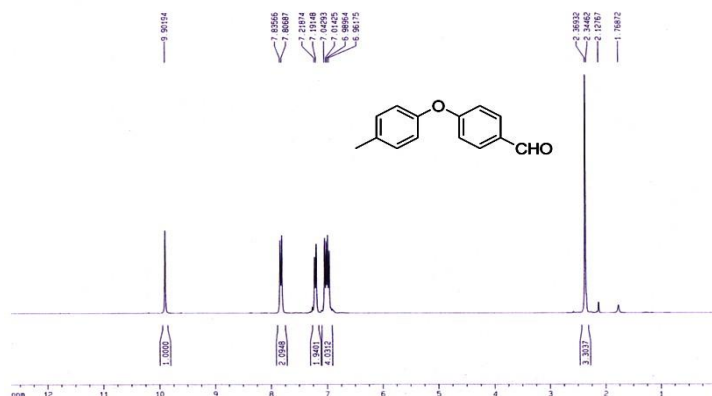


Table-2.5, entry-5; δ_H (600 MHz; CDCl_3 , TMS) 1.15-1.27 (3H, m), 2.59-2.68 (2H, m), 6.93-7.10 (4H, m), 7.22-7.23 (2H, m), 7.82 (2H, d, $J = 8.4$ Hz), 9.89 (1H, s); Elemental analysis (found: C 79.60, H 6.22; for $\text{C}_{15}\text{H}_{14}\text{O}_2$ requires: C 79.62, H 6.24%).

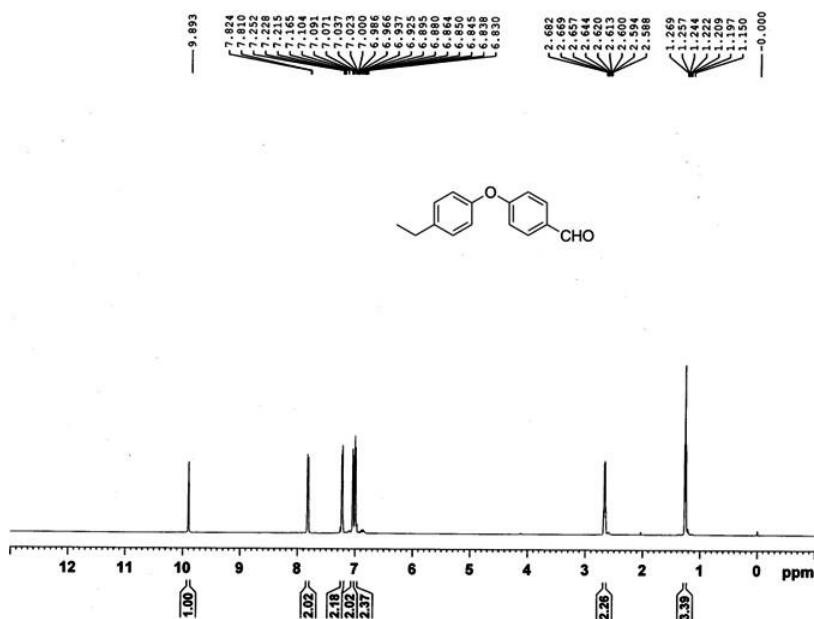


Table-2.5, entry-7; δ_H (300 MHz; CDCl_3) 2.37 (3H, s), 6.99-6.94 (4H, m), 7.21 (2H, d, $J = 7.8$ Hz), 7.56 (2H, d, $J = 8.4$ Hz); Elemental analysis (found: C 80.36, H 5.30, N 6.69; for $\text{C}_{14}\text{H}_{12}\text{O}_2$ requires: C 80.34, H 5.37, N 6.63%).

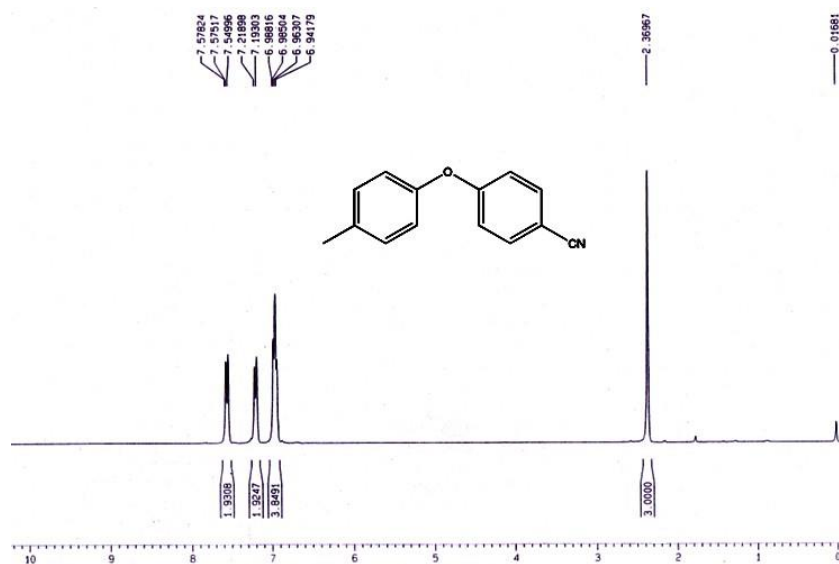


Table-2.5, entry-8; δ_H (300 MHz; CDCl_3) 2.17 (3H, s), 6.89-6.99 (3H, m), 7.17-7.30 (3H, m), 7.57 (2H, dd, $J = 1.9$ and $J = 6.8$ Hz); Elemental analysis (found: C 80.36, H 5.30, N 6.69; for $\text{C}_{14}\text{H}_{12}\text{O}_2$ requires: C 80.39, H 5.34, N 6.72%).

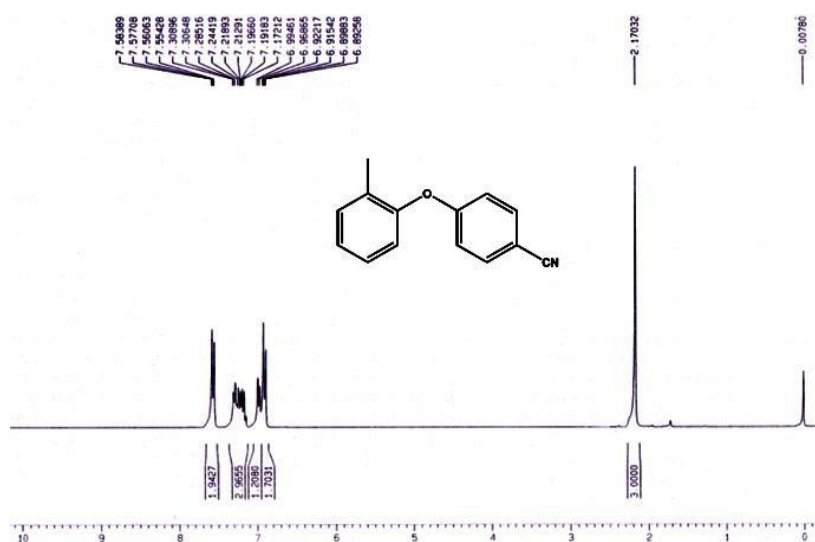


Table- 2.5 entry 14; δ_H (300 MHz, $CDCl_3$, ppm) 2.38 (s, 3H), 6.98 (d, $J = 9.2$ Hz, 4H), 7.22 (d, $J = 8.2$ Hz, 2H), 8.16–8.19 (m, 2H); Elemental analysis (found: C, 68.13; H, 4.86; N, 6.12. for $C_{13}H_{11}NO_3$ requires: C, 68.11; H, 4.84; N, 6.11%).

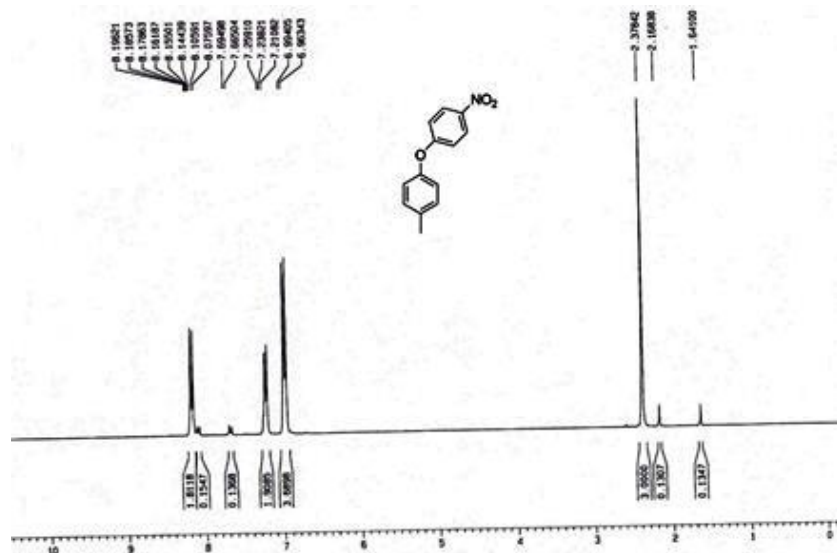


Table-2.5, entry 15; δ_H (300 MHz, $CDCl_3$, ppm) 2.35 (s, 3H), 6.94–6.98 (m, 3H), 7.13–7.19 (m, 3H), 7.47 (m, 1H), 7.93 (d, $J = 8.3$ Hz, 1H); Elemental analysis (found: C, 68.15; H, 4.85; N, 6.14. for $C_{13}H_{11}NO_3$ requires: C, 68.11; H, 4.84; N, 6.11%).

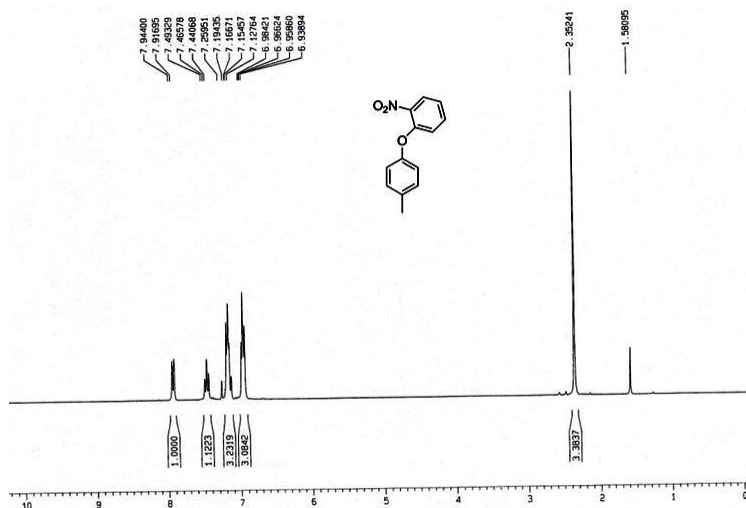


Table 3.4, entry 1 (1-Phenyl-1H-imidazole): ^1H NMR (300 MHz, CDCl_3): δ (ppm): 7.85 (s, 1H), 7.50-7.32 (m, 5H), 7.27 (s, 1H), 7.18 (s, 1H); Anal. Calcd. for $\text{C}_9\text{H}_8\text{N}_2$: Requires C, 74.98%; H, 5.59%; N, 19.43%. Found: C, 75%; H, 5.4%; N, 19%.

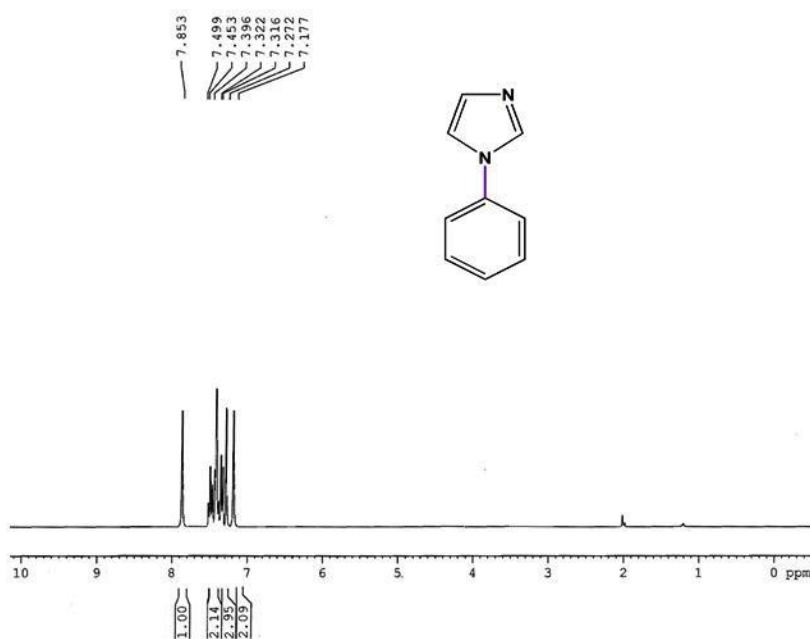


Table 3.4, entry 2 (Imidazole-*p*-nitrobenzene): ^1H -NMR (300 MHz, CDCl_3): δ (ppm): 8.42 (d, $J = 9$ Hz, 2H), 8.00 (s, 1H), 7.61 (d, $J = 6$ Hz, 2H), 7.40 (s, 1H), 7.30 (d, $J = 6$ Hz, 1H). Anal. Calcd. for $\text{C}_9\text{H}_7\text{N}_3\text{O}_2$: Requires C, 57.14%; H, 3.73%; N, 22.21%. Found: C, 57.2%; H, 3.8%; N, 22%.

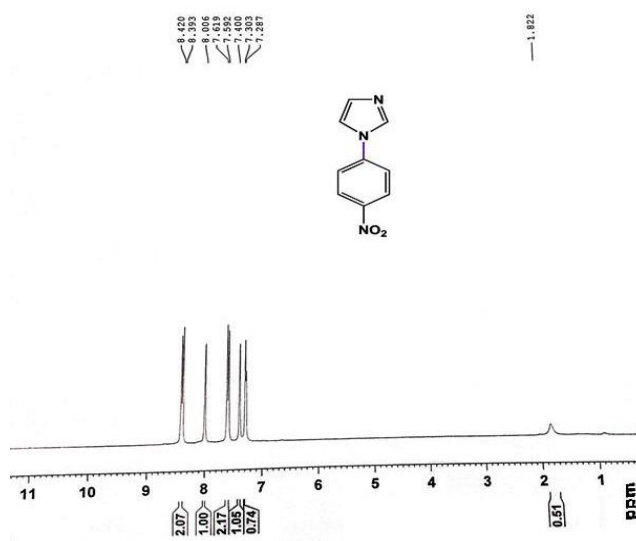
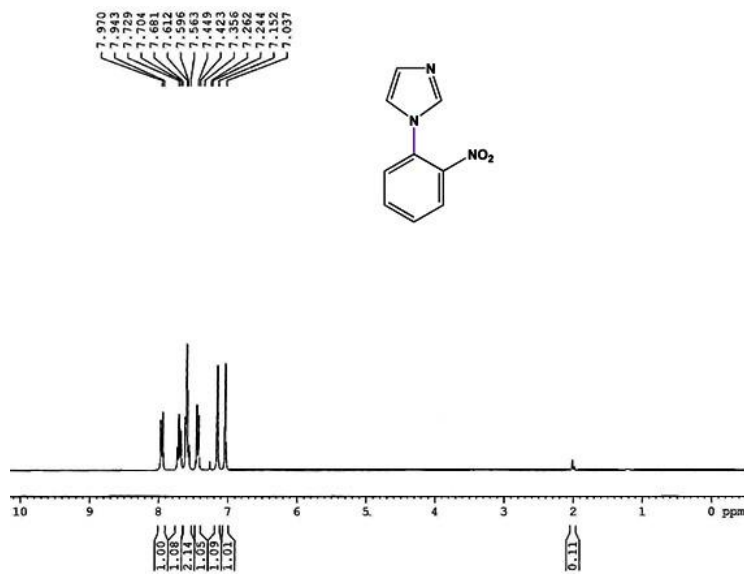


Table 3.4, entry 3 (Imidazole-*o*-nitrobenzene): ¹H-NMR (300 MHz, CDCl₃): δ (ppm): 7.97 (d, *J* = 9 Hz, 1H), 7.72 (d, *J* = 6 Hz, 1H), 7.61-7.56 (m, 2H), 7.44-7.35 (m, 1H), 7.15 (s, 1H), 7.03 (s, 1H); Anal. Calcd. for C₉H₇N₃O₂: Requires C, 57.14%; H, 3.73%; N, 22.21. Found: C, 57.17%; H, 3.76%; N, 22%.



(Table 3.4, entry 5) (Imidazole-*p*-benzonitrile): $^1\text{H-NMR}$ (300 MHz, CDCl_3): δ (ppm): 8.03-7.97 (m, 1H), 7.84-7.81 (m, 2H), 7.57-7.54 (m, 2H), 7.37 (s, 1H), 7.28 (s, 1H); Anal. Calcd. for $\text{C}_{10}\text{H}_7\text{N}_3$: Requires C, 70.99%; H, 4.17%; N, 24.84%. Found: C, 70.94%; H, 4.20%; N, 24.87%.

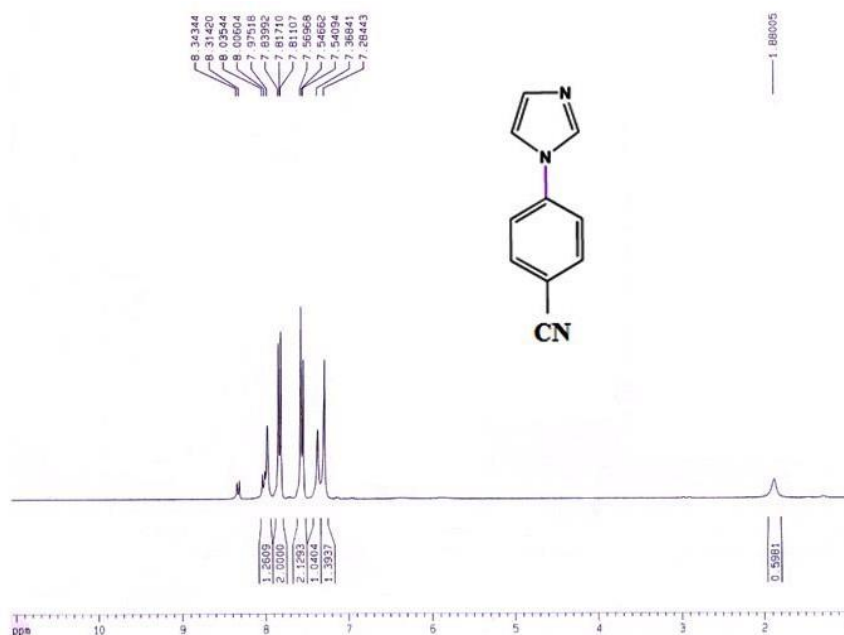


Table 3.4, entry 7 (Benzimidazole-*p*-nitrobenzene): $^1\text{H-NMR}$ (300 MHz, CDCl_3): δ (ppm): 8.45 (d, $J = 8.7$ Hz, 2H), 8.19 (s, 1H), 7.91-7.88 (m, 1H), 7.75 (d, $J = 8.89$ Hz, 2H), 7.62-7.59 (s, 1H), 7.38-7.41 (m, 2H); Anal. Calcd. for $\text{C}_{13}\text{H}_9\text{N}_3\text{O}_2$: Requires C, 65.27%; H, 3.79%; N, 17.56%. Found: C, 65.30%; H, 3.81%; N, 17.59%.

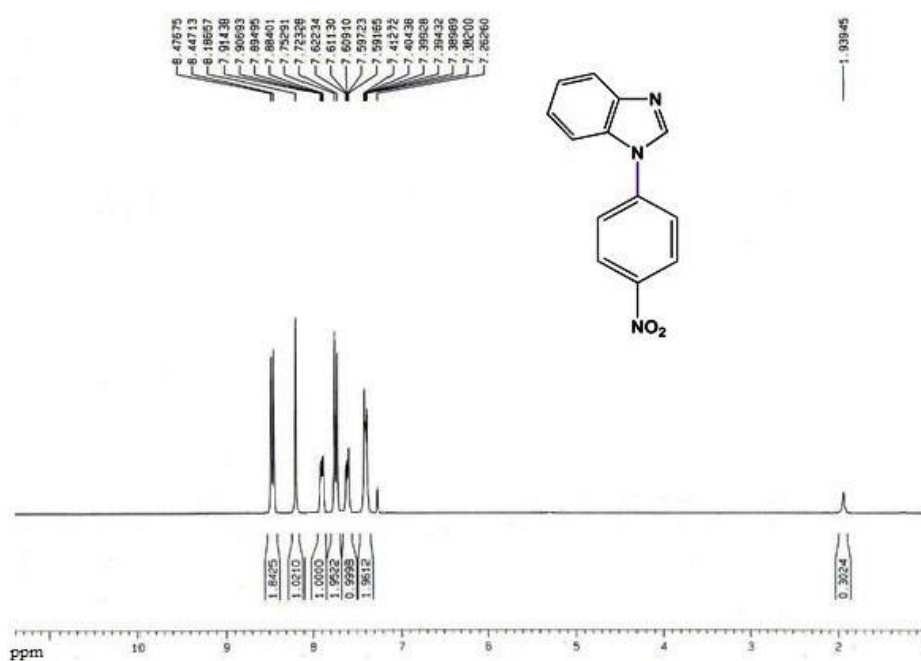


Table 3.4, entry 11 (Pyrazole-*p*-benzonitrile): ¹H-NMR (300 MHz, CDCl₃): δ (ppm): 7.97 (d, *J* = 2.52 Hz, 1H), 7.8 (d, *J* = 8.82 Hz, 2H), 7.67-7.74 (m, 3H), 6.5 (t, *J* = 1.8 Hz, 1H); Anal. Calcd. for C₁₀H₇N₃: C, 70.99%; H, 4.17%; N, 24.84%. Found: C, 70.97%; H, 4.15%; N, 24.82%.

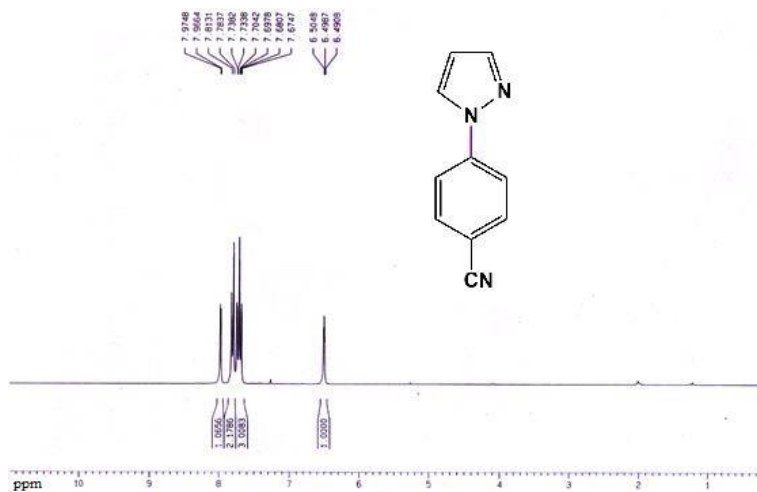


Table 3, entry 12 (benzpyrazole-*p*-nitrobenzene): $^1\text{H-NMR}$ (300 MHz, CDCl_3): $\delta(\text{ppm})$: 8.2 (s, 1H), 8.04 (d, $J = 8.1\text{Hz}$ 1H), 7.84 (d, $J = 9\text{ Hz}$ 1H), 7.8-7.78 (m, 2H), 7.64-7.61 (m, 1H), 7.60-7.55 (m, 2H), 7.34-7.25 (m, 1H). Anal. Calcd. for $\text{C}_{13}\text{H}_9\text{N}_3\text{O}_2$: Requires C, 65.27%; H, 3.79%; N, 17.56%. Found: C, 65%; H, 4 %; N, 17.6%.

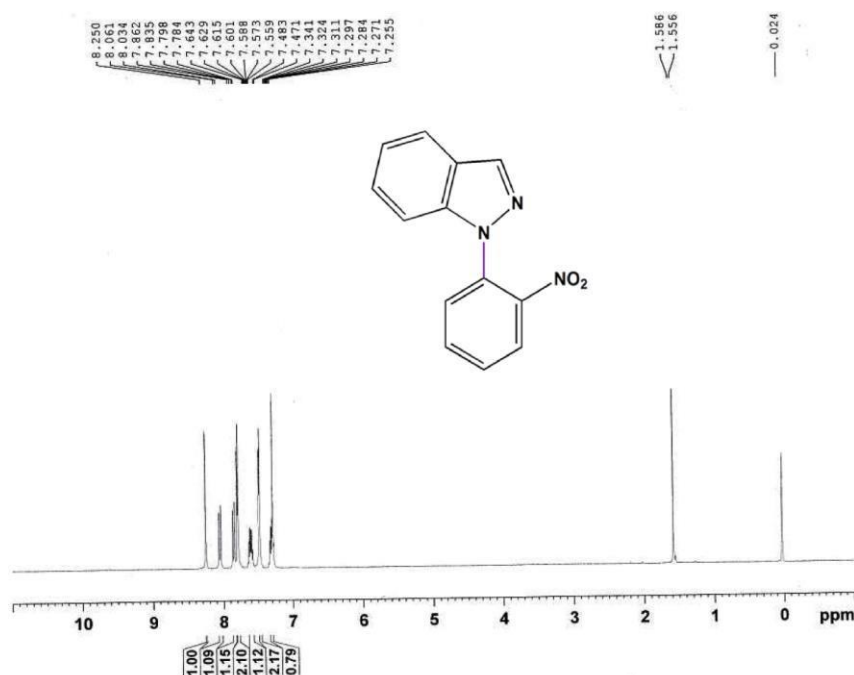


Table 3.4, entry 13 {1-(4-Nitrophenyl)-1H-1,2,3-triazole}: $^1\text{H-NMR}$ (300 MHz, CDCl_3): $\delta(\text{ppm})$: 8.40 (d, $J = 9\text{ Hz}$, 2H), 8.11 (s, 1H), 7.99 (d, $J = 9\text{ Hz}$, 2H), 7.92 (s, 1H). Anal. Calcd. for $\text{C}_8\text{H}_6\text{N}_4\text{O}_2$: Requires C, 50.53%; H, 3.18%; N, 29.46%. Found: C, 50.61%; H, 3.3%; N, 29.49%.

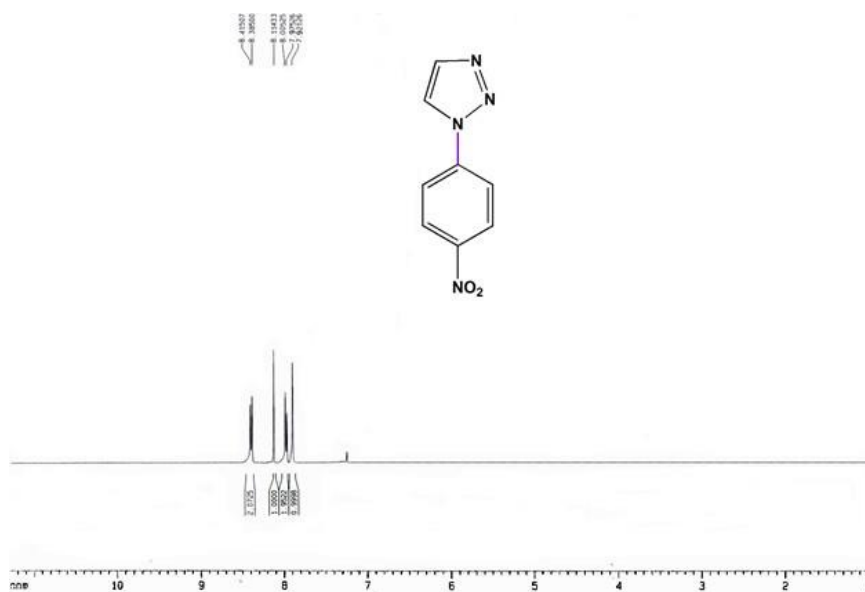


Table 3.4, entry 14 (1,2,3-triazole-*p*-benzonitrile): ¹H-NMR (300 MHz, CDCl₃): δ (ppm): 8.09 (s, 1H), 7.95-7.83 (m, 5H); Anal. Calcd. for C₉H₆N₄: Requires C, 63.52%; H, 3.55%; N, 32.92. Found: C, 63%; H, 3.60%, N, 32.81%.



Table 3.4, entry 15 {1-(4-Nitrophenyl)-1H-1,2,4-triazole}: ^1H NMR (300 MHz, CDCl_3): δ (ppm): 8.72 (s, 1H), 8.43-8.39 (m, 2H), 8.18 (s, 1H), 8.02-7.92 (m, 2H); Anal. Calcd. for $\text{C}_8\text{H}_6\text{N}_4\text{O}_2$: Requires C, 50.53%; H, 3.18%; N, 29.46%. Found: C, 51%; H, 3.25%; N, 29%.

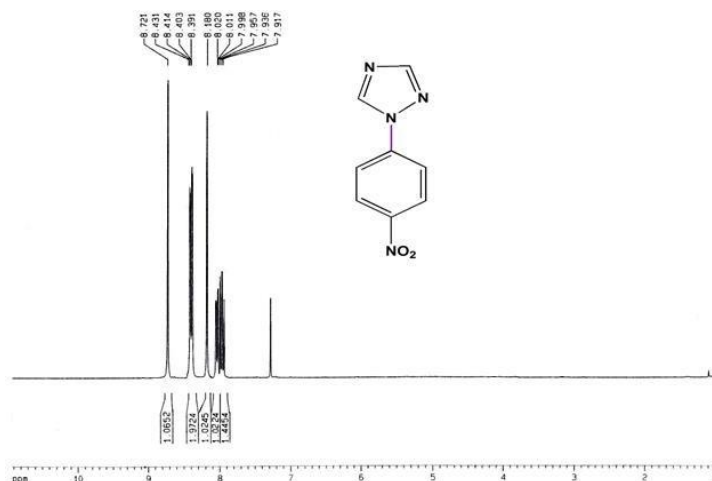


Table 3.4, entry 16 (1,2,4-triazole-*p*-benzonitrile): ^1H -NMR (300 MHz, CDCl_3): δ (ppm): 8.67 (s, 1H), 8.14 (s, 1H), 7.88-7.81 (m, 4H); Anal. Calcd. for $\text{C}_9\text{H}_6\text{N}_4$: Requires C, 63.52%; H, 3.55%; N, 32.92. Found: C, 63.58%; H, 3.59%, N, 32.94%.

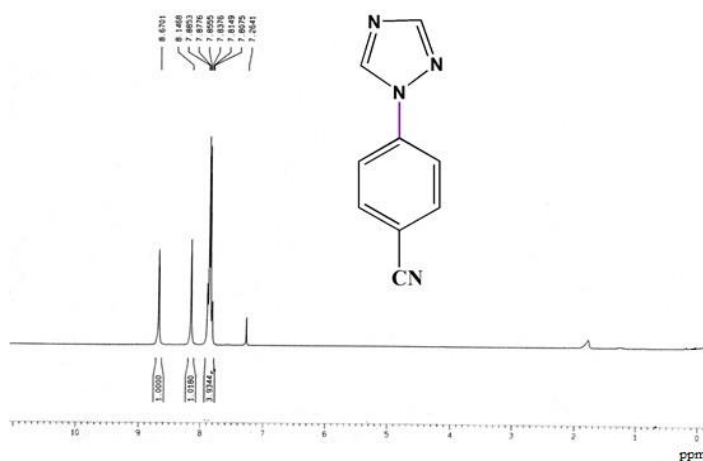


Table-4.5, entry 1; δ_{H} (300 MHz, CDCl_3 , ppm) 7.00–7.45 (m, 4H), 7.46–7.47 (m, 1H), 7.47–7.49 (m, 2H), 8.18–8.23 (m, 2H); Elemental analysis (found: C, 66.92; H, 4.22; N, 6.48. for $\text{C}_{12}\text{H}_9\text{NO}_3$ requires: C, 66.97; H, 4.22; N, 6.51%).

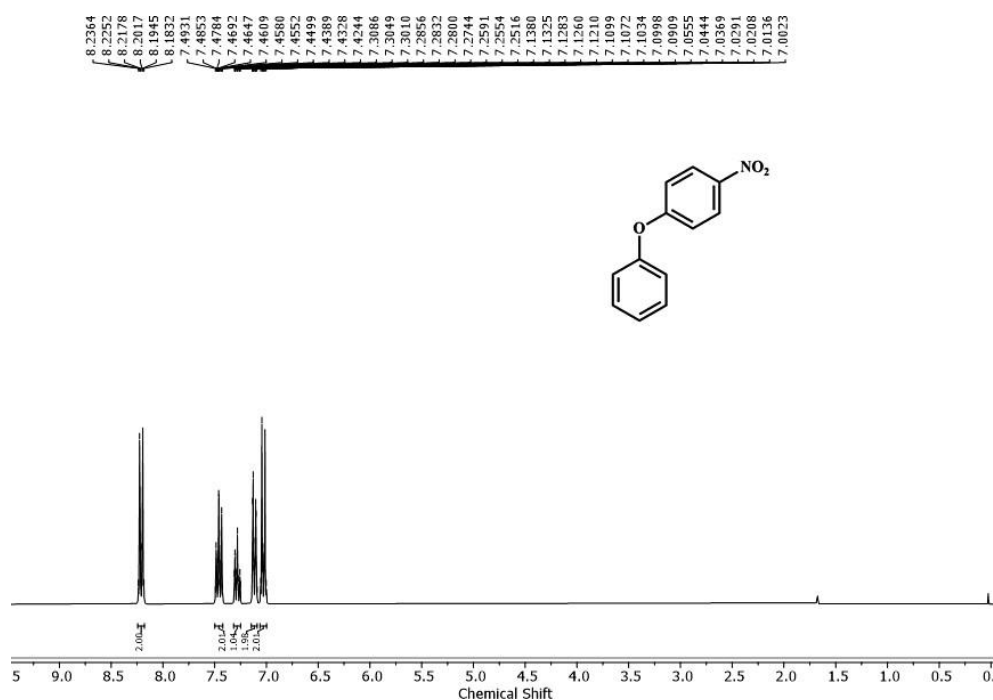


Table-4.5, entry 3; δ_{H} (300 MHz, CDCl_3 , ppm) 2.40 (s, 3H), 6.97–7.24 (m, 4H), 7.25–7.28 (m, 2H), 8.17–8.25 (m, 2H); Elemental analysis (found: C, 68.10; H, 4.82; N, 6.09. for $\text{C}_{13}\text{H}_{11}\text{NO}_3$ requires: C, 68.11; H, 4.84; N, 6.11%).

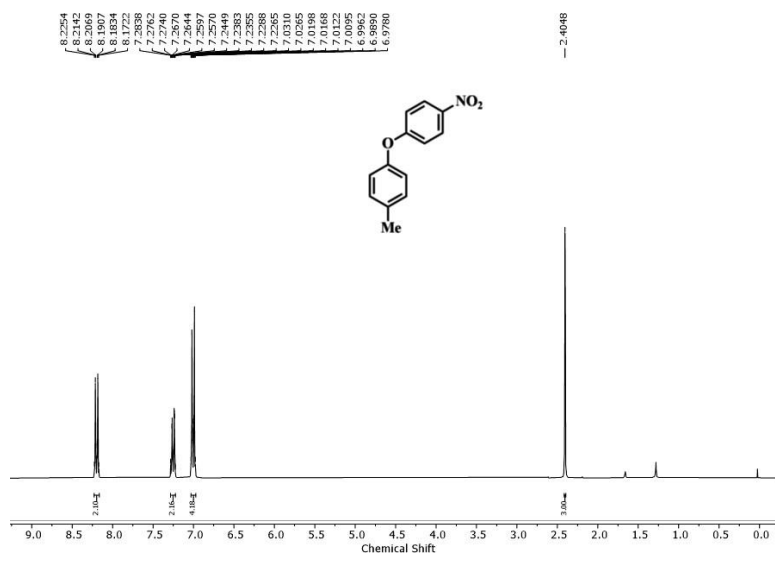


Table-4.5, entry-7; δ_H (300 MHz; CDCl_3) 2.42 (3H, s), 6.86-7.07 (5H, m), 7.28 (1H, t, $J = 9$ Hz), 7.59-7.62 (2H, m); Elemental analysis (found: C 80.30, H 5.29, N 6.61; for $\text{C}_{14}\text{H}_{12}\text{O}_2$ requires: C 80.32, H 5.28, N 6.62%).

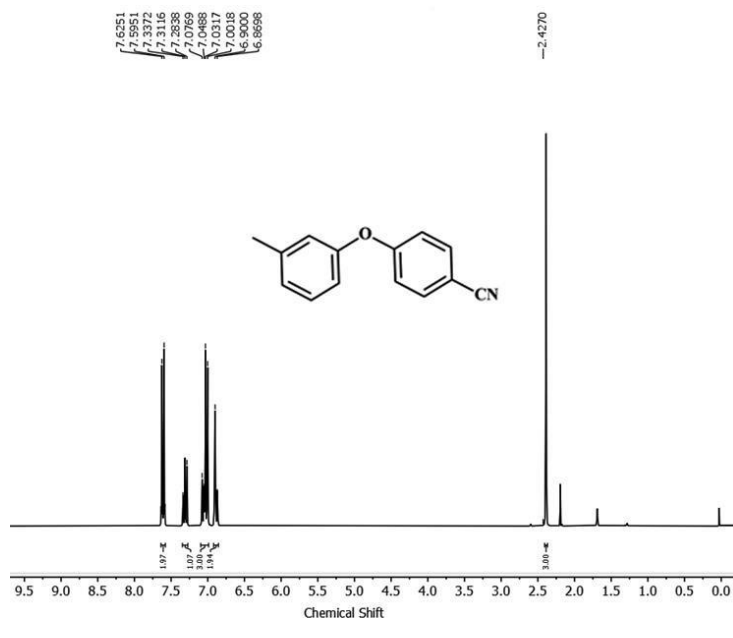


Table-4.5, entry 12; δ_{H} (300 MHz, CDCl_3 , ppm) 3.84 (s, 3H), 6.94–7.06 (m, 6H), 8.16 (d, $J = 9.3$ Hz, 2H); Elemental analysis (found: C, 63.62; H, 4.50; N, 5.69. for $\text{C}_{13}\text{H}_{11}\text{NO}_4$ requires: C, 63.67; H, 4.52; N, 5.71%).

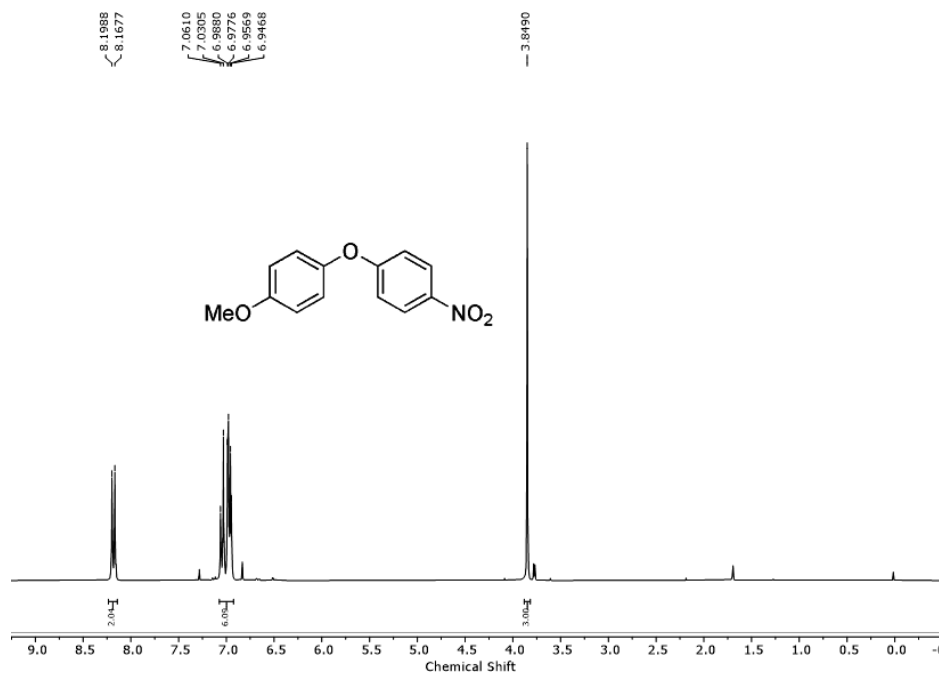


Table. Bond distances (\AA) and angle ($^\circ$) around the metal centre in MOF-(5-8)

MOF-5		MOF-6		MOF-7	
Atoms	Distance	Atoms	Distance	Atoms	Distance
Gd1-O1	2.474(7)	Ho1-O1	2.436(3)	Er1-O1	2.441(5)
Gd1-O2	2.463(7)	Ho1-O2	2.423(4)	Er1-O2	2.401(6)
Gd1-O3	2.475(8)	Ho1-O3	2.456(3)	Er1-O3	2.407(6)
Gd1-O4	2.455(7)	Ho1-O4	2.413(3)	Er1-O4	2.432(6)
Gd1-O5	2.297(7)	Ho1-O5	2.260(3)	Er1-O5	2.246(5)

Appendix I

Gd1-O7	2.301(7)	Ho1-O6	2.256(4)	Er1-O7	2.247(5)
Gd1- ^a O6	2.344(7)	Ho1-O7	2.328(4)	Er1- ^a O6	2.321(5)
Gd1- ^a O8	2.379(7)	Ho1-O8	2.315(3)	Er1- ^a O8	2.297(5)
MOF-8		MOF-5		MOF-6	
Atoms	Distance	Atoms	Angle(°)	Atoms	Angle(°)
Yb1-O1	2.382(4)	O1-Gd1-O2	65.5(2)	O1-Ho1-O2	66.63(12)
Yb1-O2	2.409(3)	O1-Gd1 -O3	103.7(2)	O1-Ho1-O3	105.03(11)
Yb1-O3	2.435(3)	O1-Gd1 -O4	71.4(2)	O1-Ho1-O4	71.47(11)
Yb1-O4	2.380(3)	O1-Gd1-O5	74.5(2)	O1-Ho1-O5	77.87(11)
Yb1-O5	2.230(3)	O1-Gd1-O7	79.0(3)	O1-Ho1 -O6	75.35(12)
Yb1-O7	2.229(2)	O1-Gd1- ^a O6	139.7(2)	O1-Ho1-O7	138.54(13)
Yb1- ^d O6	2.284(3)	O1-Gd1- ^a O8	138.5(3)	O1-Ho1-O8	140.47(12)
Yb1- ^d O8	2.288(3)	O2-Gd1-O3	72.6(2)	O2 -Ho1-O3	72.83(11)
MOF-5		O2 -Gd1-O4	95.4(2)	O2-Ho1-O4	96.21(12)
Atoms	Angle(°)	O2 -Gd1-O5	137.7(2)	O2-Ho1-O5	79.26(12)
O2-Gd1-O7	82.0(3)	O2-Gd1- ^a O6	80.0(2)	O2-Ho1-O6	139.04(12)
O2-Gd1- ^a O8	141.9(3)	O3 -Gd1-O4	52.4(3)	O2-Ho1-O7	142.87(12)
O3-Gd1-O5	132.4(3)	O3-Gd1 -O7	150.1(3)	O2-Ho1-O8	79.33(12)
O3-Gd1- ^a O6	83.9(2)	O3-Gd1- ^a O8	72.5(3)	O3-Ho1-O4	53.49(12)
O4-Gd1-O5	84.0(3)	O4-Gd1-O7	148.3(3)	O3-Ho1-O5	147.57(13)
O4-Gd1- ^a O6	134.7(2)	MOF-6		O3-Ho1-O6	133.96(12)
O5-Gd1-O7	77.4(3)	Atoms	Angle(°)	O3-Ho1-O7	73.56(12)
O5-Gd1- ^a O8	78.8(3)	O5-Ho1-O7	125.74(13)	O3-Ho1-O8	82.29(12)
O7-Gd1- ^a O8	125.2(3)	O5-Ho1-O8	76.52(12)	O4-Ho1-O5	148.07(12)
O4-Gd1- ^a O8	74.7(3)	O6-Ho1-O7	77.28(12)	O4-Ho1-O6	85.38(12)
O5-Gd1- ^a O6	128.6(2)	O6-Ho1-O8	127.13(12)	O4-Ho1-O7	75.85(13)
^a O6-Gd1-O7	76.2(3)	O7-Ho1-O8	80.98(13)	O4-Ho1-O8	134.17(12)
^a O6-Gd1- ^a O8	81.7(3)			O5-Ho1-O6	78.39(13)

MOF-7					
Atoms	Angle(°)				
		O4-Er1-O7	75.3(2)	O2-Yb1-O7	77.36(11)
		O4-Er1- ^a O6	138.8(2)	O2-Yb1- ^d O6	140.83(11)
O1-Er1-O2	53.7(2)	O4-Er1- ^a O8	140.64(19)	O2-Yb1- ^d O8	138.43(12)
O1-Er1-O3	73.14(19)	O5-Er1-O7	78.8(2)	O3-Yb1-O4	54.08(11)
O1-Er1-O4	105.50(19)	O5-Er1- ^a O6	126.0(2)	O3-Yb1-O5	134.42(10)
O1-Er1-O5	147.1(2)	O5-Er1- ^a O8	76.65(19)	O3-Yb1-O7	146.57(12)
O1-Er1-O7	134.05(18)	^a O6-Er1-O7	77.25(19)	O3-Yb1- ^d O6	81.75(11)
O1-Er1- ^a O6	73.54(19)	O7-Er1- ^a O8	127.0(2)	O3-Yb1- ^d O8	73.93(11)
O1-Er1- ^a O8	82.01(18)	^a O6-Er1- ^a O8	80.6(2)	O4-Yb1-O5	85.57(11)
O2-Er1-O3	95.9(2)	MOF-8		O4-Yb1-O7	147.64(11)
O2-Er1-O4	71.13(19)	Atoms	Angle(°)	O4-Yb1- ^d O6	134.30(10)
O2-Er1-O5	147.6(2)	O1-Yb1-O2	67.59(12)	O4-Yb1- ^d O8	76.57(10)
O2-Er1-O7	85.6(2)	O1-Yb1-O3	72.69(11)	O5-Yb1-O7	78.93(11)
O2-Er1- ^a O6	76.7(2)	O1-Yb1-O4	96.35(11)	O5-Yb1- ^d O6	126.89(12)
O2-Er1- ^a O8	134.28(19)	O1-Yb1-O5	139.55(11)	O5-Yb1- ^d O8	76.96(11)
O3-Er1-O4	66.7(2)	O1-Yb1-O7	78.34(12)	^d O6-Yb1-O7	76.55(10)
O3-Er1-O5	78.5(2)	O1-Yb1- ^d O6	78.87(11)	O7-Yb1- ^d O8	126.03(11)
O3-Er1-O7	138.96(19)	O1-Yb1- ^d O8	142.87(12)	^d O6-Yb1- ^d O8	80.74(11)
O3-Er1- ^a O6	143.1(2)	O2-Yb1-O3	105.79(11)		
O3-Er1- ^a O8	79.46(19)	O2-Yb1-O4	71.23(10)		
O4-Er1-O5	77.43(19)	O2-Yb1-O5	75.05(12)		

Symmetry element of MOF-(5-8): a = -x,1-y,1-z; d = 2-x,1-y,1-z